Gene and Stem Cell Therapy for Type 1 Diabetes Mellitus

Dario Gerace

Centre for Health Technologies, School of Life Sciences,

University of Technology Sydney, Australia

2017

Thesis submitted for the degree of Doctor of Philosophy (Faculty of Science)

Certificate of Authorship and Originality

I certify that this thesis has not been previously submitted for a degree nor has it been submitted as part of the requirements for a degree except as fully acknowledged within the text.

I also certify that the thesis has been written by me. Any help that I have received in my research work and the preparation of the thesis itself has been acknowledged. In addition, I certify that all information sources and literature used are indicated in the thesis. This research was supported by an Australian Government Research Training Program Scholarship.

Dario Gerace

Acknowledgements

First and foremost, I would like to thank my supervisors Prof Ann Simpson and Dr Rosetta Martiniello-Wilks for their assistance and support throughout the duration of my PhD studies. I am very grateful for the opportunity to develop my knowledge and skills in the field of gene and stem cell therapy under their tuition. I would also like to thank my fellow colleagues, staff and faculty members within the School of Life Sciences (UTS), in particular Dr Binhai Ren, Dr Najah Nassif and Dr Eileen McGowan who were always available and happy to consult with regards to lentiviral preparation, gene expression analysis and thesis preparation respectively. I must also thank the team at the Advanced Cytometry Facility (Centenary Institute, Sydney, Australia) who assisted with the sorting of transduced BMSCs. A special mention to Fiona Ryan and Lalit Overlunde who managed the maintenance and running of the Ernst Facility. Finally, I would like to thank my wife Angelica, my daughter Chelsea, and my family and friends for their support over the years.

This research was supported by research grants from the Australian Diabetes Society and the Rebecca L Cooper Foundation, and I was supported by an Arrow Bone Marrow Transplant Foundation/Hawkesbury Canoe Classic PhD Scholarship.

Abstract

Type 1 diabetes (T1D) results from the autoimmune destruction of the insulin-producing pancreatic β-cells. As a result, people with T1D suffer from high blood glucose which requires exogenous insulin therapy to maintain within the normal physiological range. However, exogenous insulin therapy does not mimic the tightly regulated function of the pancreas, and as a result does not prevent the development of diabetic complications. Currently, the only cure is either pancreas or islet transplantation; however these treatments are hampered by a shortage of donors. As a result, the generation of an alternative cell replacement therapy would overcome the aforementioned limitations with current treatments. Gene therapy as a means of generating "artificial" insulin-producing cells (IPCs) is being considered as a potential cure for T1D. Previous research has shown that the viral-mediated transfer of the pancreatic transcription factor *NeuroD1* and human furin-cleavable insulin (*INS-FUR*) genes to hepatocytes resulted in their transdifferentiation into pancreatic-like cells capable of synthesising, storing and secreting insulin in response to fluctuating glucose concentrations. Due to their ease of isolation, ease of genetic modification and immune-modulatory properties, the aim of this study was to evaluate the utility of *ex vivo* expanded murine bone marrow-derived mesenchymal stem cells (BMSCs) as gene therapy targets for the development of a T1D cell replacement therapy following the lentiviral over-expression of murine *NeuroD1* and *Pdx1*, and *INS-FUR*.

Non-invasive bioluminescence imaging (BLI) technology is an established and sensitive tool for accessing cell replacement therapy efficacy and treatment outcome in living preclinical small animal models. Furthermore, preclinical BLI results often serve as the decision point of

a cell replacement therapy's suitability (efficacy and safety) for clinical trial testing in humans. This study utilised the *Firefly luciferase* reporter protein *Luc2*, a *Luc2* specific light producing substrate D-luciferin and an IVIS Lumina II imaging system. First, a unique sub-population of BMSCs were isolated from the bone marrow of non-obese diabetic (NOD) mice. These BMSCs displayed potent clonogenicity and tri-lineage differentiation potential, hallmark characteristics of mesenchymal stem cells, when compared to the plastic adherent bone marrow stromal cell starting population. Second, BMSCs were nucleofected to express the yeast fusion cytosine deaminase uracil phosphoribosyltransferase (*CDUPRT*) and/or *Luc2* genes (BMSC-*Luc2/CDUPRT*; BMSC-*Luc2*). *Luc2* was utilised as a reporter protein for evaluating the *in vitro* and *in vivo* persistence of transgene expression in BMSCs and the *in vivo* persistence of gene-modified BMSCs in immune intact and immune-compromised mice. *CDUPRT* is a pro-drug converting enzyme, otherwise known as a suicide gene that was utilised as a cell therapy experimental 'off' switch. *CDUPRT* converts the non-toxic pro-drug 5-fluorocytosine (5-FC) into the toxic metabolite 5-fluorouracil (5-FU) that causes BMSC death. *In vitro* functional characterisation of *CDUPRT* using a *Luc2* based cytotoxicity assay showed that following exposure to 5-FC, BMSC-*Luc2/CDUPRT* demonstrated increased cell death when compared to BMSC-*Luc2* and parental BMSC controls. A subcutaneous transplant of *Luc2/CDUPRT*-expressing BMSCs in immune-intact (NOD; n=4) and immune-deficient (NOD/*Scid*; n=4) mice persisted for 2 weeks and 12 weeks respectively. These results show a BMSC transplant survival providing an experimental window of 12 weeks in NOD/*Scid* mice and the rapid immune-mediated destruction of BMSC carrying non-mammalian genes in NOD mice.

Ex vivo culture-expanded BMSCs were subsequently transduced with the HMD lentiviral vector (MOI=10) to express *INS-FUR*, and murine *NeuroD1* and *Pdx1* as mediators of β-cell differentiation. Pancreatic transdifferentiation was characterised via reverse transcriptase

polymerase chain reaction (RT-PCR), followed by the assessment of insulin storage and secretion. *INS-FUR*-expressing BMSCs lacked glucose-responsiveness and secreted large amounts of human insulin chronically, whereas *NeuroD1* and *Pdx1*-expressing BMSCs lacked glucose-responsiveness and insulin secretion capabilities. Furthermore, RT-PCR analysis showed that BMSC did not undergo pancreatic transdifferentiation when transduced with pancreatic transcription factors, and did not store insulin within secretory granules as determined by acid/ethanol extraction. A subcutaneous transplant of $1x10^7$ and $5x10^7$ *INS-FUR*-expressing BMSCs were assessed for their ability to reverse diabetes in STZ-NOD/*Scid* mice (n=5), which failed to do so upon transplantation.

This study showed *ex vivo* expanded BMSC multipotential differentiation into fat and bone diminishes with increasing passage, and therefore BMSC may be more useful as gene therapy targets prior to expansion. This correlates with other studies where *ex vivo* expansion of MSCs is associated with a loss of MSC characteristics (phenotype, proliferative capacity, self-renewal, immunomodulation) and negative T1D clinical outcomes.

Table of Contents

List of Figures and Tables

Figure **Page**

Table **Page**

List of Publications

1. **Gerace D**, Martiniello-Wilks R, Habib R, Ren B, Nassif NT, O'Brien BA *et al*. *Ex vivo* expansion impairs genetic engineering of murine MSC-derived pancreatic β-cells. 2017; *In preparation.*

2. **Gerace D**, Martiniello-Wilks R, Habib R, Simpson AM. *In vitro* luciferase-based validation of mesenchymal stem cell suicide gene therapy. 2017; *In preparation*.

3. **Gerace D**, Martiniello-Wilks R, Nassif NT, Lal S, Steptoe R, Simpson AM. CRISPR-targeted genome editing of mesenchymal stem cell-derived therapies for type 1 diabetes: a path to clinical success? *Stem Cell Research & Therapy* 2017; **8**(1)**:** 62.

4. **Gerace D**, Martiniello-Wilks R, Simpson AM. Viral-mediated gene therapy for the generation of artificial insulin-producing cells as a therapeutic treatment for type 1 diabetes mellitus. In: A. Hardikar A (ed) *Pancreatic Islet Biology*. Springer International Publishing: Cham, 2016, pp 241-255.

5. **Gerace D**, Martiniello-Wilks R, Simpson AM. Diabetes reversal via gene transfer: building on successes in animal models. *Research and Reports in Endocrine Disorders* 2015; 5: 15-29.

6. **Gerace D**, Martiniello-Wilks R, O'Brien BA, Simpson AM. The use of β-cell transcription factors in engineering artificial β-cells from non-pancreatic tissue. *Gene Ther* 2014; 22(1): 1-8.

7. **Gerace D**, Ren B, Hawthorne WJ, Byrne MR, Phillips PM, O'Brien BA *et al.* Pancreatic transdifferentiation in porcine liver following lentiviral delivery of human furin–cleavable insulin. *Transplantation Proceedings* 2013; 45(5): 1869-1874.

List of Presentations

1. **Gerace D**, Martiniello-Wilks R, Nassif NT, Ren B, Simpson AM. *Ex vivo* expanded murine mesenchymal stem cells as targets for the generation of a cell replacement therapy for type 1 diabetes. In: 77th American Diabetes Association (ADA) Scientific Sessions. San Diego, USA, 2017.

2. **Gerace D**, Martiniello-Wilks R, Simpson AM. Persistence of Luciferase Expressing Bone Marrow-Derived Mesenchymal Stem Cells (BMSCs) in Non-Obese Diabetic (NOD) and NOD/*Scid* Mice. In: *8th Islet Society – Australian Islet Study Group Meeting*. Sydney, Australia, 2015

3. **Gerace D**, Martiniello-Wilks R, Simpson AM. Bioluminescent Imaging of Mesenchymal Stem Cell Engraftment in Immune Competent and Immune Deficient Animal Models of Type 1 Diabetes. In: *9th Australasian Gene and Cell Therapy Society (AGCTS) Conference*. Melbourne, Australia, 2015

4. **Gerace D**, Martiniello-Wilks R, Simpson AM. Persistence of Luciferase Expressing Bone Marrow-Derived Mesenchymal Stem Cells (BMSCs) in Non-Obese Diabetic (NOD) and NOD/*Scid* Mice. In: *18th Meeting of the American Society of Gene & Cell Therapy (ASGCT)*. New Orleans, USA, 2015.

5. **Gerace D**, Ren B, Hawthorne WJ, Byrne MR, Phillips P, O'Brien BA *et al.* Reversal of Diabetes in a Porcine Model Following Liver-Directed Gene Therapy. In: *8th AGTS Meeting*. Sydney, Australia, 2013.

6. **Gerace D**, Ren B, Hawthorne WJ, Byrne MR, Phillips P, O'Brien BA *et al.* Reversal of Diabetes in a Pig Model Following Lentiviral Delivery of Human Furin-Cleavable Insulin (INS-FUR). In: *The Annual Scientific Meeting of the Australian Diabetes Society and the Australian Diabetes Educators Association*. Gold Coast, Australia, 2012.

7. **Gerace D**, Ren B, Hawthorne WJ, Byrne MR, Phillips P, O'Brien BA *et al.* Pancreatic Transdifferentiation in Porcine Liver Following Lentiviral Delivery of Human Furin-Cleavable Insulin. In: *The 24th International Congress of the Transplantation Society*. Berlin, Germany, 2012.

8. **Gerace D**, Ren B, Byrne MR, O'Brien BA, Swan A, Simpson AM. Pancreatic Transdifferentiation in the Livers of Non-Obese Diabetic (NOD) Mice Following Lentiviral Delivery of Furin-Cleavable Insulin. In: *RNSH/UTS/USYD/KIMR Annual Scientific Meeting*. Sydney, Australia, 2011.

Abbreviations

5-FC	5-fluorocytosine
5-FU	5-fluorouracil
AAV	Adeno-associated virus
AD-MSCs	Adipose-derived mesenchymal stem cells
ANOVA	Analysis of variance
APC	Antigen presenting cell
ATP	Adenosine triphosphate
BB	Biobreeding
bFGF	Basic fibroblast growth factor
BLI	Bioluminescence imaging
BMSCs	Bone marrow-derived mesenchymal stem cells
CD	Cluster of differentiation
CD	Cytosine deaminase
CDUPRT	Yeast cytosine deaminase uracil phosphoribosyltransferase fusion pro-drug converting enzyme
CLEC16A	C-type lectin domain containing 16A
CMV	Cytomegalovirus
CRISPR	Clustered regularly interspaced short palindromic repeat
CTLA-4	Cytotoxic lymphocyte antigen 4
DC	Dendritic cell
DMSO	Dimethyl sulfoxide
DPP-4	Dipeptidyl peptidase-4
EDTA	Ethylenediaminetetracetic acid

eGFP	Enhanced green fluorescent protein
EGR1	Early growth response-1
ER	Endoplasmic reticulum
ESCs	Embryonic stem cells
ESRF	End-stage renal failure
FACS	Fluorescence-assisted cytometric sorting
FCS	Foetal calf serum
Fcy::Fur	Yeast gene that encodes CDUPRT fusion protein
FoxA1/FoxA2	Forkhead box factors
G1RE	Glucose-responsive element
GD	Gestational diabetes
GFP	Green fluorescent protein
GLUT2	Glucose transporter 2
GSIS	Glucose-stimulated insulin secretion
GWAS	Genome-wide association study
HbA1C	Glycated haemoglobin
HBSS	Hanks buffered salt solution
HDAD	Helper-dependent adenovirus
Hes-1	Hairy and enhancer of split 1
hIPCs	Human islet-derived progenitor cells
HLA	Human leukocyte antigen
HNF	Hepatocyte nuclear factor
hTERT	Human telomerase reverse transcriptase
ICA	Islet cell-like aggregates
IDO	Indoleamime 2,3-dioxygenase
IDDM1	Insulin-dependent diabetes mellitus 1
IFN-γ	Interferon gamma

IL	Interleukin
IL2RA	Interleukin 2 receptor subunit alpha
INS-FUR	Furin-cleavable human insulin
IPCs	Insulin-producing cells
IPGTT	Intraperitoneal glucose tolerance test
iPSCs	Induced pluripotent stem cells
IRES	Internal ribosome entry site
ISG	Insulin secretory granules
Isl-1	LIM Homeobox 1
IVC	Individually ventilated cage
KCNJ11	ATP-sensitive potassium channel
LADA	Latent-onset autoimmune diabetes in adults
LB	Luria broth
LPK	L-type pyruvate kinase
Luc2	Firefly luciferase
mAb	Monoclonal antibody
MafA	v-maf musculoaponeurotic fibrosarcoma A
MAP	*Mycobacterium avium* paratuberculosis
MHC	Major histocompatibility complex
MOI	Multiplicity of infection
MODY	Mature-onset diabetes of the young
MSCs	Mesenchymal stem cells
NCBI	National Centre for Biotechnology Information
NeuroD1	Neuronal differentiation 1
Neurog3	Neurogenin 3
NK	Natural killer
Nkx2.2	NK2 homeobox 2

Nkx6.1	*NK6 homeobox 1*
P/S/G	Penicillin-Streptomycin-Glutamine
PANDER	Pancreatic derived factor
Pax4	Paired homeobox 4
Pax6	Paired homeobox 6
PBS	Phosphate buffered saline
PD-1	Programmed death 1
Pdx1	Pancreatic and duodenal homeobox 1
PGE2	Prostaglandin E2
PP	Pancreatic polypeptide
PPAR-γ	Peroxisome proliferator-activated receptor gamma
PTPN2	Protein tyrosine phosphatase, non-receptor type 2
PTPN22	Protein tyrosine phosphatase, non-receptor type 22
QTL	Quantitative trait loci
RLU	Relative light units
RO	Reverse osmosis
rSAP	Shrimp alkaline phosphatase
RT-PCR	Reverse transcription polymerase chain reaction
SCA-1	Stem cell antigen 1
Scid	Severe combined immunodeficiency
SSEA-1	Stage-specific embryonic antigen 1
STRO-1	Stromal cell antigen 1
STZ	Streptozotocin
SV40T	Simian virus 40 antigen
T1D	Type 1 diabetes
T2D	Type 2 diabetes
TBE	Tris/Borate/EDTA

TCF7L2	Transcription factor 7-like 2
TFF	Tangential flow filtration
TGF-β	Transforming growth factor beta
UC-MSCs	Umbilical cord mesenchymal stem cells
UPRT	Yeast uracil phosphoribosyltransferase pro-drug converting enzyme
UTR	Untranslated region
VNTR	Variable number tandem repeat
VSMCs	Vascular smooth muscle cells

Chapter 1

Gene and stem cell therapy for the treatment of Type 1 Diabetes Mellitus

1.1 The types of diabetes and their impact on society

Diabetes mellitus describes a range of conditions where the inability to produce insulin or utilise insulin effectively leads to elevated blood glucose levels known as hyperglycaemia[1]. The three main types of diabetes are Type 1 diabetes (T1D), Type 2 diabetes (T2D) and gestational diabetes (GD). T1D results from the autoimmune destruction of the insulin-producing pancreatic β-cells within the islets of Langerhans[1-3]. Consequently, insulin-responsive tissues lose the ability to take up glucose for normal cell functioning, resulting in elevated levels of unabsorbed glucose in the blood. People with T1D require multiple daily exogenous insulin injections to manage their glycaemia; however this does not prevent the long-term complications of hyperglycaemia[4, 5]. In Australia, people with T1D constitute ~10-15% of all cases of diabetes, with Australia boasting one of the highest rates of T1D incidence in the world (Figure 1.1). Although predominantly occurring in children and young adults between the ages of 0-14, diagnosis of latent-onset autoimmune diabetes in adults (LADA) is more frequently becoming reported. Currently, the only long-term treatments for T1D that reduce or eliminate the requirement for exogenous insulin injections are either whole pancreas transplantation, islet transplantation or closed-loop systems (artificial pancreas); however for pancreas and islet transplantation, these two treatments are hampered by a limited number of donors and the requirement for lifelong immunosuppression[6]. In the case of the artificial pancreas, studies have demonstrated heterogeneity in glycaemic benefit for people with T1D, where the system is hampered by the requirement for user interaction and the fact that it does not exquisitely mimic the function of the pancreas[7].

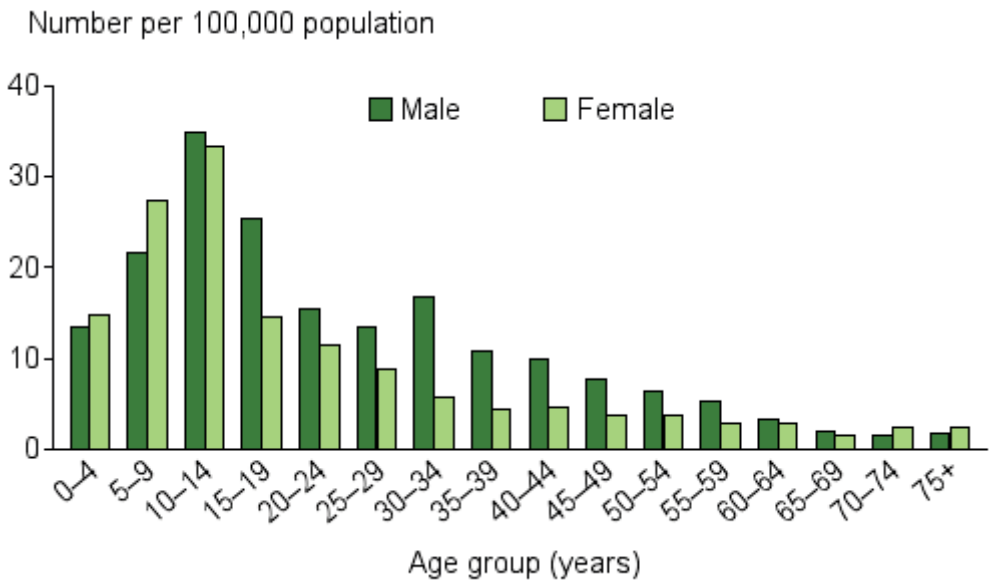

Figure 1.1: Incidence of T1D in the Australian population in 2014 Representation of the incidence of T1D in Australia according to age and sex. *Source:* AIHW analysis of 2014 National (insulin-treated) Diabetes Register (NDR).

T2D is the most common form of diabetes in Australia accounting for 85-90% of all cases of diabetes[1, 8, 9]. T2D results from either lower than normal insulin production or the body's inability to utilise insulin effectively (also known as insulin resistance)[9]. Insulin resistance leads to an accumulation of high levels of glucose in the blood, which in the case of many people with T2D goes unnoticed for many years. As a result, people are usually diagnosed with T2D once the effects of prolonged elevated blood glucose levels are manifested in the form of diabetic complications. The reason for the development of T2D is a complex combination of a number of predisposing risk factors including obesity, poor diet, physical inactivity, ageing, family history and ethnicity[10-13]. However, of these, genetics has been well studied and implicated in the development of T2D. The most well-recognised candidate gene loci associated with T2D include the nuclear receptor PPAR-γ (*PPARG*)[14], the ATP-sensitive potassium channel (*KCNJ11*)[15] and the transcription factor 7-like 2 (*TCF7L2*)[16]. Additionally, mutations in hepatocyte nuclear factor 1-alpha (*HNF1-α*), hepatocyte nuclear factor 4-alpha (*HNF4-α*), hepatocyte nuclear factor 1-beta (*HNF1-β*) and glucokinase are well characterised

in the development of the familial monogenic forms of diabetes known as mature-onset diabetes of the young (MODY). However, recent genome-wide association studies (GWAS) have identified numerous candidate gene loci in specific ethnic populations associated with the development of T2D, highlighting the broad and complex genetic nature of the disease[17, 18].

People with newly diagnosed T2D usually do not require exogenous insulin injections and are encouraged to adjust their lifestyle and dietary habits as a means of preventing chronic hyperglycaemia. However, many progress to a phase of beta-cell dysfunction and severe insulin resistance where exogenous insulin therapy is thereafter prescribed. In addition, healthcare practitioners prescribe the use of pharmaceuticals for lowering blood glucose levels for those with T2D who fail or are unable to maintain normoglycaemia. Currently there are five classes of blood glucose lowering tablets used in Australia for people with T2D. These are known as biguanides, sulphonylureas, thiazolidinediones (glitazones), alpha glucosidase inhibitors (acarbose) and dipeptidyl peptidase (DPP-4) inhibitors. The most commonly prescribed drugs are biguanides such as Metformin and sulphonylureas such as Glibenclamide. Metformin increases insulin sensitivity *in vivo* to improve the function of endogenously produced insulin, thereby increasing the uptake of glucose from the blood[19]. Glibenclamide lowers blood glucose by stimulating insulin production in the pancreas[20], and is commonly co-prescribed with Metformin in cases where endogenous insulin production is reduced. However, as a consequence of sulphonylurea-induced stimulation of insulin production, hypoglycaemic events are common in people with poor patient compliance in the form of over-dosage[21]. As a result, care must be taken when combining sulphonylureas with insulin-sensitising agents such as biguanides and glitazones. Since T2D is a progressive disease that leads to near-complete β-cell dysfunction, insulin injections are ultimately

required as an exogenous source of insulin in combination with sensitising agents such as Metformin as a life-long form of blood glucose regulation.

GD occurs in women during pregnancy due to an increase in insulin resistance that is thought to be associated with placental hormone production that blocks insulin function[9]. Normally, elevated blood glucose levels associated with GD disappear after birth, however if glycaemia is not maintained within normal physiological concentrations, pregnant women who have GD are at a significantly higher risk of developing T2D later in life and in subsequent pregnancies[22]. In addition, the unborn foetuses of pregnant women who have GD are at greater risk of developing obesity and T2D during their lifetime. Nonetheless, by engaging in a healthy lifestyle and moderate physical activity, uncomplicated pregnancies are the most likely outcome for women with gestational diabetes. In Australia, during 2009-2011, 5.8% of women who gave birth and did not have pre-existing diabetes were diagnosed with GD[8].

The impact of diabetes in Australia can be measured both quantitatively and qualitatively. Financial costs associated with T1D and T2D in Australia (Table 1.1) highlight the burden of diabetes on the Australian healthcare system. The total annual cost for Australians with T2D is up to $6 billion including healthcare costs, the cost of carers and Commonwealth government subsidies[23]. For T1D, the total annual cost is up to $570 million[24]. A reduction in the financial burden of T2D on the Australian healthcare system can be achieved by targeting early prevention of T2D in pre-diabetics with intensive lifestyle changes. However, such preventative measures currently do not exist for T1D. In addition to the financial impact on society, 41% of people with diabetes report poor psychological well-being with periods of stress, anxiety and depression associated with having to cope with diabetes[22]. Despite being one of the top ten causes of death in Australia, the prevalence of diabetes in Australia is growing steadily and it is expected that by 2025, three million Australians will be diagnosed

with diabetes[22]. As a result, the need for diabetes education, prevention, and treatment is of significant importance. The remainder of this thesis will focus on the development of a novel treatment for T1D.

Table 1.1: Annual patient healthcare costs associated with diabetic complications

	Type 1 diabetes	Type 2 diabetes
No complications of diabetes	$3,468	$4,025
Microvascular complications only	$8,122	$7,025
Macrovascular complications only	$12,105	$9,055
Micro and Macrovascular complications	$16,698	$9,645

Source: Colagiuri et al, *DiabCo$t Australia: Assessing the burden of Type 2 diabetes in Australia*, 2003.

1.2 T1D genetics and pathogenesis

1.2.1 Genetics

The genetic susceptibility of T1D has been studied for a number of decades due to the suspected hereditary transmission of the disease. Early studies by Eisenbarth stipulated that a genetic component was a primary mediator in the onset of T1D[25]. However, in the ensuing decades of research it became well accepted that T1D is a complex, multigenic disease that is mediated by a number of genetic and non-genetic factors, and that T1D development does not follow the previously suspected hereditary transmission pathway. In terms of genetic predisposition, a number of genes have been implicated in conferring susceptibility to T1D. The most recognised of these are the major histocompatibility complex (MHC) class II genes[3, 26, 27]. More recently, other susceptibility markers have been mapped to a variety of loci across a number of chromosomes (Table 1.2). However, they are not yet to be confirmed

as either major/minor markers of disease susceptibility. Of the susceptibility loci identified, a recent GWAS identified and reconfirmed a number of immune-related genes such as cytotoxic lymphocyte antigen-4 (*CTLA-4*), protein tyrosine phosphatase, non-receptor type 22 (*PTPN22*), interleukin 2 receptor subunit alpha (*IL2RA*), chromosome locations 12q13 and 12q24, C-type lectin domain containing 16A (*CLEC16A*), and protein tyrosine phosphatase, non-receptor type 2 (*PTPN2*) in T1D pathogenesis. In addition, it is likely that in reality, expression of T1D genetic susceptibility markers will vary from individual to individual, and that consequently, a broad and varying expression profile of these markers will be identified. However, due to the complex nature of the disease and our growing understanding of environmental stimuli that effect disease development, it is unlikely that a single genetic predictor will be identified.

1.2.1.1 Human leukocyte antigens

The MHC encodes for a number of highly polymorphic molecules that are involved in immune recognition known as the human leukocyte antigens (HLA)[1, 3, 26, 27]. The HLA molecules that predispose an individual to T1D are further characterised into quantitative trait loci (QTLs) that were originally believed to be located on chromosome six. However, research suggested that QTL could be traced to a number of different chromosomes, and that certain HLA expression profiles were either associated with susceptibility or protection from T1D[1]. It was believed that HLA class II molecules collectively known as insulin-dependent diabetes mellitus 1 (*IDDM1*) were the strongest genetic contributors to T1D susceptibility[28-30]. The HLA class II molecules are expressed on the surface of antigen presenting cells (APCs) and are involved in presenting antigenic peptides to $CD4^+$ T lymphocytes. Susceptible individuals commonly possess the DR3/4-DQ8 heterozygous haplotype (DR3 is DRB1*03-DQB1*0201, DR4 is DRB1*04-DQB1*0302, DQ8 is DQA1*0301, DQB1*0302).

However, despite expression of HLA class II molecules accounting for ~95% of T1D susceptibility, they are not determining factors in the development of T1D as ~50% of healthy individuals also express these antigens[31]. Conversely, the DRB1*1501-DQA1*0102-DQB1*0602 haplotype, found in 20% of the population but only 1% of patients, confers dominant protection against T1D.

Class I alleles have also been associated with genetic susceptibility, albeit to a lesser extent[32, 33]. Specifically, HLA-B and HLA-A genes, and most remarkably the HLA-B*39 allele was found to be a significant risk factor[33]. One of the most prevalent class I alleles (HLA-A*0201) has also been implicated with a frequency of 60% in T1D patients. Another study also suggested the involvement of HLA-A*02-restricted $CD8^+$ T cells in T1D progression[34], with the data further supported by a transgenic animal model expressing human HLA-A*02 molecules demonstrating accelerated islet destruction[35].

1.2.1.2 Insulin gene

IDDM2, a polymorphic, non-HLA associated variable number tandem repeat (VNTR) locus near the insulin gene has also been identified as contributing to T1D susceptibility and protection[36, 37]. Variations in the repeat number that occur in VNTR alleles either confer susceptibility or protection to T1D. The VNTR Type I polymorphism is characterised by shorter repeats and confers susceptibility, whereas the VNTR Type III polymorphism, characterised by longer repeats protects against T1D. The estimated contribution of IDDM2 to T1D genetic susceptibility is ~10%, yet collectively IDDM1 and IDDM2 do not cumulatively account for all genetic components of T1D[38]. Other genetic factors include the lymphoid protein tyrosine phosphatase gene, whose function as a negative regulator of T cell receptor signaling has only recently been identified as a risk factor in T1D susceptibility, and has also been implicated in the development of other autoimmune diseases[39, 40].

Table 1.2: Summary of all QTL associated with predisposition to T1D

Locus	Chromosome	Candidate Genes/Microsatellites
IDDM1	6p21.3*	HLA-DQ/DR
IDDM2	11p15*	INS VNTR
IDDM3	15q26	D15s107
IDDM4	11q13	MDU1, ZFM1, RT6, FADD/MORT1, LRP5
IDDM5	6q24-27	ESR, MnSOD
IDDM6	18q12-q21	D18s487, D18s64, JK (Kidd locus)
IDDM7	2q31	D2s152, IL-1, NEUROD, GALNT3
IDDM8	6q25-27	D6s264, D6s446, D6s281
IDDM9	3q21-25	D3s1303
IDDM10	10p11-q11	D10s193, D10s208, D10s588
IDDM11	14q24.3-q31	D14s67
IDDM12	2q33*	CTLA-4, CD28
IDDM13	2q34	D2s137, D2s164, IGFBP2, IGFBP5
IDDM14	?	NCBI# 3413
IDDM15	6q21	D6s283, D6s434, D6s1580
IDDM16	?	NCBI# 3415
IDDM17	10q25	D10s1750- D10s1773
2p12	EI*LUC2*AK3	-
5p11-q13	-	-
16p	-	D16s405- D16s207
16q22-q24	-	D16s515- D16s520
1q42	-	D1s1617
Xp11	-	DXS1068

1.2.2 Inductive events leading to autoimmunity

The period preceding clinical onset of T1D is characterised by elevated levels of autoantibodies against islet antigens that suggests a series of inductive events that lead to autoimmunity. The most well characterised islet-cell autoantigens associated with T1D are insulinoma-associated antigen-2, insulin autoantigen, glutamic acid decarboxylase 65 and zinc transporter 8 ZnT8[1, 41]. However, due to the variable periods of T1D initiation and detection amongst individuals, identification of inductive stimuli as a direct cause of T1D is challenging. It may be possible that stimuli vanish following activation of autoimmunity; or that multiple triggers initiate pathogenesis, with a variety of multiple triggers between individuals. Nonetheless, epidemiological data suggests that the rising incidence of T1D is due to environmental stimuli such as viral or bacterial infections that trigger the autoimmune response[42].

1.2.2.1 Viruses

Research that demonstrated the capacity of coxsackievirus B to infect β-cells and induce insulitis provided support for environmental stimuli as triggers of T1D autoimmunity[43]. Coxsackievirus B infection of β-cells generates cytokines and other inflammatory mediators that induce the expression of adhesion molecules in pancreatic islets[3]. By inducing the expression of adhesion molecules in the endothelium of the islets, circulating leukocytes are targeted towards the islets where β-cell antigens can be presented to lymphocytes by macrophages[3]. Consequently, studies to identify a causal relationship between viral infection and T1D by analysing islets for the presence of viral components were conducted[44, 45]. Surprisingly, data revealed the absence of viral proteins in islet extracts, contradicting prior assumptions on the relationship between viral infection and the development of T1D.

However, with the development of further optimised methods of viral detection, a study identified the presence of viral capsid proteins in analysed β-cells[46]. Not surprisingly, a consensus on the relationship between viral infection and T1D is yet to be realised. To complicate the argument further, a study has suggested that under particular experimental conditions, viral infection can protect against T1D[47]. Other viral infections such as rotavirus[48], cytomegalovirus (CMV)[49], parvovirus[50], and encephalomyocarditis virus [51] have also been associated with T1D; however a direct causal relationship has not been identified and further studies are required to verify their reported links.

1.2.2.2 Bacteria

Just as important as their viral counterparts, bacteria have been acknowledged as serving an important role in the development of T1D. Evidence suggests that an aggravated intestinal microbial community can lead to T1D, with conflicting views regarding the effect of antibiotic administration on this process[52, 53]. On the other hand, it has been shown that administration of probiotics can prevent islet cell autoimmunity under specific conditions[54]. Nonetheless, it appears that the administration of antibiotics and probiotics can influence the development of T1D by altering the intestinal microbial community. More recently a subspecies of *Mycobacterium avium* paratuberculosis (MAP) has been partially implicated with T1D due to humoral responses to MAP antigens being isolated from the blood of T1D patients[55].

1.2.2.3 Other environmental triggers

Considering the association of an unbalanced gut microbiota on the development of T1D, other environmental triggers that may disturb this balance have been implicated. For example, proteins found in cow's milk (specifically the albumin components) have been

shown to possess cross-reactivity with islet-cell autoantigen-1 (a β-cell surface protein) thereby stimulating islet autoimmunity[56]. To a lesser extent, wheat proteins such as gluten have also been implicated in islet autoimmunity, with some individuals presenting with increased peripheral blood T cell reactivity to gluten[57]. In addition, links between early infant exposure to cereals and subsequent islet autoimmunity have been suggested[58]. Additionally, although a number of other compounds have been associated with autoimmunity, further evidence is required to support those claims.

1.2.3 Autoimmune process

The exact mechanisms involved in the initiation and destruction of β-cells has been studied extensively[2, 3, 59] yet remain unclear. It is believed that initially the presentation of β-cell specific autoantigens by APCs such as macrophages or dendritic cells (DC) to $CD4^+$ helper T cells in association with MHC class II molecules is the first step in the initiation phase (Figure 1.2). Macrophages subsequently secrete interleukin (IL)-12, stimulating $CD4^+$ T cells to release interferon gamma (IFN-γ) and IL-2. IFN-γ induced secretion of cytokines such as IL-1β, tumour necrosis factor alpha (TNF-α) and free radicals by other macrophages results in the destruction of β-cells. Additionally, IFN-γ and IL-2 induce the migration of specific $CD8^+$ cytotoxic T cells to the islets, and specifically the β-cells expressing autoantigens. Following migration, and in association with class II molecules, $CD8^+$ cytotoxic T cells cause β-cell damage by releasing perforin, granzyme and superoxides. Continued destruction of the β-cells by Fas-mediated apoptosis subsequently results in the onset of diabetes[60, 61].

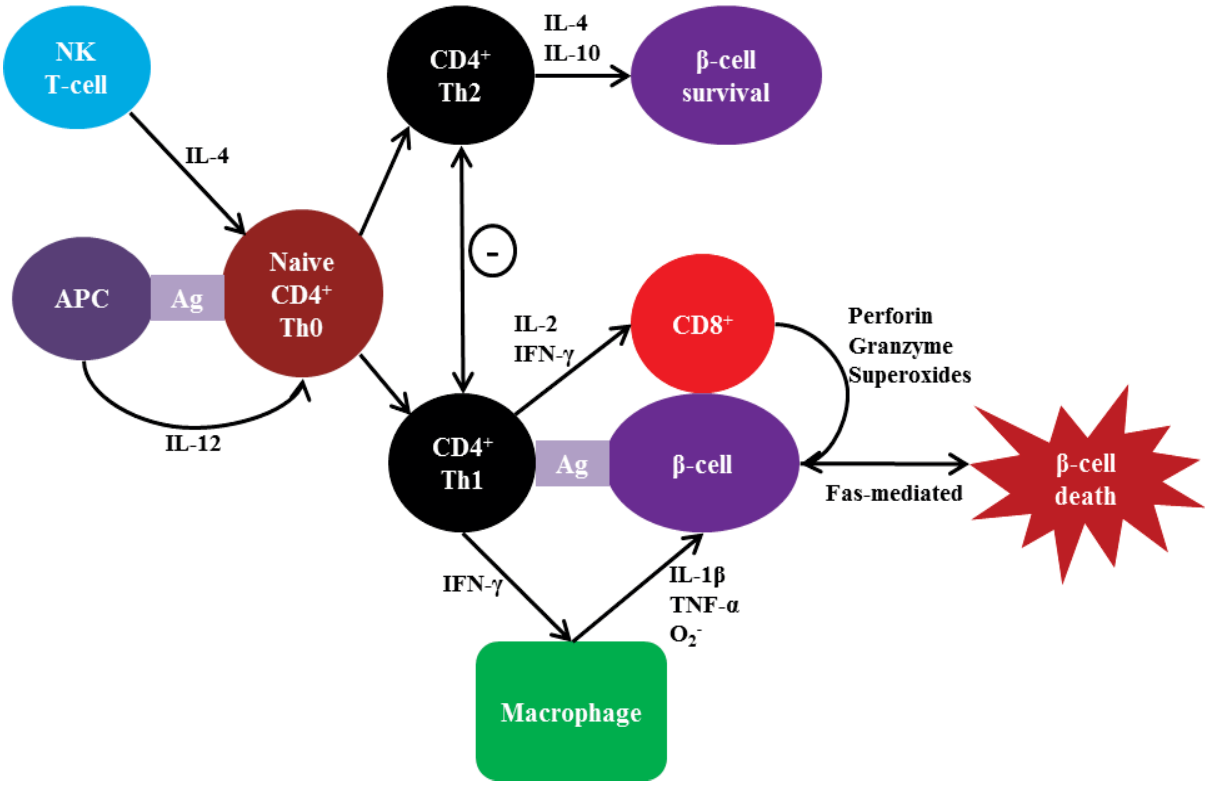

Figure 1.2: Mechanism of T1D autoimmunity APCs secrete interleukin IL-12 stimulating $CD4^+$ T cells, to secrete interferon IFN-γ and IL-2. IFN-γ stimulates other resting macrophages to release, in turn, other cytokines such as IL-1β, tumour necrosis factor (TNF)-α, and free radicals, which are toxic to pancreatic β-cells. During this process, cytokines induce the migration of β-cell autoantigen specific $CD8^+$ cytotoxic T cells. On recognising specific autoantigens on β-cells in association with class II molecules, the $CD8^+$ cytotoxic T cells cause β-cell damage by releasing perforin and granzyme and by Fas-mediated apoptosis of the β-cells.

1.3 Diabetic complications

Upon diagnosis with diabetes, physicians most commonly recommend lifestyle or pharmaceutical interventions through which prevention and control of hyperglycaemia can be achieved. This not only ensures an adequate distribution of glucose throughout the body, it reduces the risk of diabetic complications as a result of uncontrolled glycaemia. Ultimately, the risk of developing diabetic complications is directly related to the severity and duration of hyperglycaemia. Consequently, routine follow-up and measurements of percentage glycated haemoglobin (% HbA1C) become fundamental in assessing long-term glycaemic control and the development of management plans in order to reduce the likelihood of the development of diabetic complications[62]. Immediate (acute) complications of diabetes such as hyperglycaemia, hypoglycaemia and diabetic ketoacidosis are potentially life-threatening if intervention is delayed. However, most people with diabetes become increasingly aware of the symptoms of acute complications, and as such develop an intrinsic capacity to intervene appropriately without severe consequences. Of more concern are the chronic complications arising from long-term, unregulated glycaemic control, the symptoms of which can go undetected until the diabetic situation has deteriorated. These complications can be divided in to two major categories: microvascular and macrovascular complications[4, 63]. Whilst good glycaemic control can reduce the risk of these complications, it does not prevent them.

The most common manifestation of diabetic microvascular complications is retinopathy. Most people with T1D develop evidence of retinopathy within 20yrs of diagnosis, with early symptoms of retinopathy correlating with poor glycaemic control following diagnosis[64]. Mechanisms by which diabetes leads to retinopathy include osmotic stress as a consequence of increases in intracellular sorbitol concentration[65], the formation of advanced glycosylated end products[66], oxidative stress as a consequence of the production of free radicals and

reactive oxygen species[66], and the production of growth factors such as vascular endothelial growth factor and transforming growth factor-β[67]. These mechanisms are believed to also be associated with diabetic nephropathy. When left untreated, people with diabetes will develop microalbuminuria that progressively deteriorates to renal failure[68]. In extreme cases, end-stage renal failure (ESRF) results and patients who do not receive a kidney transplant are subsequently dependent upon dialysis. Ironically, patients with ESRF are more likely to receive a pancreas transplant (in combination with kidney transplantation) than those who have good glycaemic control, yet are also in need of a donor pancreas. This highlights the significance of donor shortages, limiting eligibility for pancreas transplantation to those who have poor quality of life due to their diabetic complications.

In addition, a person with T1D is susceptible to diabetic neuropathy that is most commonly manifested as peripheral loss of sensation. Development of diabetic neuropathy, like other microvascular complications, is closely linked to degree and duration of hyperglycaemia, and similarly triggered by the same mechanisms[69]. Management of the symptoms of microvascular complications is typically through pharmaceutical intervention, although many are associated with adverse side effects and carry a significant financial burden. With respect to diabetic macrovascular complications, cardiovascular disease is the leading cause of death in people with T1D[63, 70]. In comparison to the general population, those with T1D are at an increased risk of suffering from heart disease and stroke[70]. However, intensive glycaemic treatment was shown to reduce the risk by 57%[71]. Due to the development of diabetic complications and their impact on quality of life, a long-term cure for T1D is required.

1.4 Current and future treatments for T1D

Treatments for T1D can be categorised into the management of acute and chronic complications, and therapeutic interventions to permanently cure people with T1D. Currently, patients with T1D control their blood glucose levels using several daily injections of exogenous insulin[1], however this does not mimic the exquisite metabolic responsiveness of the β-cell. Insulin therapy delays, but does not eliminate hyperglycaemic episodes and chronic complications associated with extended periods of hyperglycaemia[4, 5]. Of equal, if not more, concern to the patient are the life-threatening hypoglycaemic episodes that are exacerbated due to hypoglycaemia unawareness, a phenomenon which worsens with both disease duration and maintenance of blood glucose levels close to normal values[5].

Currently whole pancreas or islet transplantation are the only clinically viable treatments for T1D. However, they are limited by a shortage of pancreas donors and the requirement for lifelong immunosuppression, which carries adverse side effects and can compromise the survival of transplanted tissue[6]. Although islet transplantation can provide insulin-independence for a number of years, the transplanted islets lose function over time[72]. Further exacerbating this is the requirement for 2-4 donors to isolate sufficient quantities of islets to confer insulin-independence. To overcome the challenge of donor shortages, the sourcing of porcine islets due to their physiological similarity and function to human islets has been pursued, however the risk of human infection with porcine endogenous retroviruses is a deterrent for xenotransplantation[73]. Although successful reversal of diabetes has been achieved utilising porcine islets, xenotransplantation is at a greater threat of strong xeno responses, therefore requiring extensive immunosuppression to permit survival of the graft[74]. As a result, developing autologous cell and gene therapy strategies as alternative therapies

could potentially avoid both the requirement for immunosuppression or encapsulation, and represent an unlimited source of cells for *ex vivo* gene modification.

Over the past decade, there have been several attempts to generate "artificial" β-cells that produce insulin in response to glucose in a regulated manner. Several approaches have been explored including: (i) the dedifferentiation and directed transdifferentiation of autologous cells[75-78] *ex vivo* followed by transplantation, (ii) *in vivo* transdifferentiation via the direct delivery of viral vectors to target organs; and (iii) the genetic modification and expansion of various stem cells *ex vivo* that can then be transplanted. The production of a functional "artificial" β-cell, via genetic manipulation, requires a comprehensive understanding of the pancreatic developmental process. The temporal expression of the various pancreatic transcription factors, their role in determining endocrine cell fate, and their involvement in mature β-cell function are key factors for consideration in the design of an artificial β-cell. The types of vectors used for gene delivery and the selection of an ideal candidate cell type for differentiation towards a β-cell phenotype are key considerations for achieving this objective. The ultimate goal for the cell and gene therapy of T1D is to produce a surrogate cell that has the ability to process, store and secrete insulin, and maintain normal glucose tolerance in response to fluctuating blood glucose concentrations, whilst avoiding autoimmune attack. This remainder of this chapter will compare putative non-pancreatic target cells, viral vectors and pancreatic transcription factors for gene modification to achieve this goal. In addition, I will comment on the utility of mesenchymal stem cells (MSCs) in pre-clinical and clinical trials of T1D, and propose their use as target cells for T1D combinatorial cell and gene therapy.

1.5 Gene therapy

Due to the destruction of pancreatic β-cells, people with T1D who suffer severe complications require whole pancreas or islet-cell transplantation and consequent immunosuppression. Evasion of the immune process by genetically engineering other cell types in the body to produce insulin is an alternative. However, this is limited by the absence of various unique characteristics of pancreatic β-cells such as a glucose-sensing system, proinsulin processing enzymes, a glucose-regulatable promoter and an exocytosis system in many cell types. Issues concerning the production of biologically active insulin, glucose-responsiveness and the assembly of secretory granules have all been addressed with respect to identifying candidate target cells for gene therapy.

1.5.1 Animals models of T1D

The use of animal models in diabetes research has been pursued extensively. Most studies are performed in small animal models (Table 1.3) such as rodents and mice to provide proof of concept for the development of a Phase I clinical trial. However, large animal models of diabetes in pigs, dogs and monkeys are becoming increasingly popular due to criticism that rodents do not adequately represent the human condition of diabetes.

In the past, one of the most popular methods for inducing diabetes in animals was by complete pancreatectomy[79]. However, this does not correctly represent the clinical manifestation of diabetes due to the loss of potential feedback mechanisms as a consequence of the absence of pancreatic hormone-producing cells, which are still present in people with diabetes. As a result, non-surgical methods of inducing a diabetic state in animal models via the administration of toxins such as streptozotocin (STZ) and alloxan are now routinely

utilised. STZ is a nitrosurea derivative isolated from *Streptomyces achromogenes*[80], with either a single high dose or multiple low dose administrations. A single high dose in mice ranges from 100-200mg/kg, with complete destruction of β-cells and the development of hyperglycaemia[81]. Whereas with multiple low dose administrations, the dose per day ranges from 20-40mg/kg over a 5 day period, which leads to insulitis in mice[82]. Alloxan, which is commonly administered in mice at a dose of 50-200mg/kg, generates superoxide free radicals that destroy β-cells as they do not possess any defence mechanisms against the chemical[83, 84]. These models are particularly useful in studying the success of transplantation of pancreatic tissue or putative artificial β-cells, and cytokine-targeted therapies. However, some of the limitations of chemically inducing diabetes is potential toxicity to other organs and the report of β-cell regeneration after high dose STZ administration[85].

Currently, the most popular choices of T1D animal model are the spontaneous non-obese diabetic (NOD) mouse and the biobreeding (BB) rat. These models manifest with a similar autoimmune diabetes that is present in the human condition, and currently dominate the literature. The NOD mouse was developed at the Shionogi Research Laboratories in Osaka, Japan in 1974[86]. NOD mice typically develop insulitis at around 3–4 weeks of age, during which the pancreatic islets are infiltrated by $CD4^+$ and $CD8^+$ lymphocytes, and to a lesser degree by B cells and natural killer (NK) cells[87]. They develop typical diabetes between 12-30 weeks of age. Due to the parallel in T1D clinical manifestation between NOD mice and humans, they have been useful in identifying pathways that lead to T1D, and are also suitable for testing of therapies which modulate the autoimmune response[88]. More recently, NOD mice are being used to study the success of cell therapies to either modulate the autoimmune response[89-91] or directly control hyperglycaemia by the artificial β-cells[92-94]. Nonetheless, some major differences do exist, such as the fact that due to being an inbred model of diabetes, the genetic susceptibility to the development of diabetes in NOD mice can be easily

traced, and is evident by the fact that female mice are susceptible, whereas males are not[95]. In humans, susceptibility to the development of T1D is governed by a much more complex interaction of genetic and environmental stimuli. In addition, there is evidence that NOD mice develop lymphopenia, a characteristic not seen in the human situation[96]. An isolated genetic contamination of the NOD mouse outcrossed with a C57BL/6 mouse produced an insulitis-resistant and diabetes-free strain named the non-obese resistant mouse which is now routinely used as an MHC-matched control mouse for studies utilising NOD mice[97]. The BB rat which spontaneously develops autoimmune diabetes was derived from outbred Wistar rats in 1974[98]. They develop diabetes between 8-16 weeks of age, and similarly to NOD mice, they display insulitis with the infiltration of T cells, B cells, macrophages and NK cells. However, like NOD mice, these animals develop lymphopenia and therefore are not as routinely utilised as NOD mice[96, 99]. Other animal models of spontaneous autoimmune diabetes include the LEW.1AR1/-iddm rats[100], the keeshond dog[101], and the celebes black ape (*Macaca nigra*)[102].

In addition to these main animal models of T1D, genetically-induced and virally-induced models are available for research purposes. The AKITA mouse was derived in Akita, Japan from a C57BL/6NSlc mouse with a spontaneous mutation in the insulin 2 gene which results in a severe insulin-dependent diabetes beginning at 3-4 weeks of age, and are used to study the success of islet transplantation[103]. Since the implication of viruses in the pathogenesis of T1D, viruses have been used to induce diabetes in animal models. These include coxsackie B virus[104], encephalomyocarditis virus[105] and Kilham rat virus[106].

Table 1.3: Animal models of T1D

Mechanism of Induction	Model	Uses/Studies
Chemically-induced	High-dose STZ	Drug discovery Models of transplantation Preventatives of β-cell destruction
	Multiple-dose STZ	
	Alloxan	
Spontaneous diabetes	NOD mice	T1D genetics and pathogenesis analyses Preventatives of β-cell destruction Immunomodulation studies Restoration of normoglycemia
	BB rats	
	LEW.1AR1/IDDM rats	
	Keeshond dog	
	Celebes black ape (*Macacca nigra*)	
Breeding/genetically selected	AKITA mice	Drug discovery Models of transplantation Preventatives of β-cell destruction
	LETL (Long-Evans Tokushima Lean)	
	NZ white rabbit	
	Chinese hamster	
Pancreatectomized	Westran pigs	Restoration of normoglycemia β-cell regeneration
	Dogs	
Virally-induced	Coxsackie B virus	Role of viruses in the induction of T1D
	Encephalomyocarditis virus	
	Kilham rat virus	

1.5.2 Selecting an ideal target cell

The first trials of T1D gene therapy were performed using somatic cells, such as monkey kidney cells and fibroblasts[107, 108]. However, these cells were unable to produce biologically active insulin, as they did not express proinsulin-processing enzymes. As a result, attention turned to autologous cells that are derived from an endodermal origin and possess characteristics similar to those of β-cells[109] (Table 1.4). The ideal surrogate for β-cell engineering would be able to sense minute changes in glucose, process proinsulin to insulin and C-peptide and store this mature insulin for later secretion.

Endocrine cells have been examined, in particular, pituitary cells which contain both proinsulin-processing enzymes and secretory granules. A murine pituitary cell line (AtT20MtIns-1.4) transfected *in vitro* with a recombinant plasmid containing human preproinsulin cDNA produced biologically active insulin, however, glucose-responsiveness was absent in these cells[110]. After transfection with both the glucose transporter 2 (Slc2a2) and glucokinase (Gck) genes, the AtT20ins cells became glucose-responsive, at sub-physiological levels. Also, the *in vivo* secretion of adenocorticotropic hormone stimulated glucocorticoid synthesis, inhibiting insulin function and therefore limiting their therapeutic efficacy[111].

Muscle cells have been only sparingly studied due to their lack of insulin proconvertases and storage vesicles. As a result, they require intensive genetic manipulation to produce functional β-cells, which is not optimal for therapeutic applications. Nonetheless, muscle targeted gene therapy for the treatment of T1D has been explored. Implantation of vascular smooth muscle cells transduced with furin-cleavable human insulin (*INS-FUR*) under the control of a glucose-regulatable promoter into spontaneously diabetic congenic BB rats has been attempted. This resulted in the reduction of blood glucose levels in two of the eight rats

for a period of 6 weeks, however insulin therapy was still required[112]. Regulated insulin secretion resulted in markedly lower exogenous insulin requirements to sustain normal growth without any hypoglycaemic episodes. Another study indicated that it was possible to reverse diabetes in STZ-mice for greater than 4 months following the dual expression of insulin and glucokinase in muscle[113]. A synergenic action in the skeletal muscle between the insulin produced and the increased phosphorylation of glucokinase was established, preventing hyperglycaemia.

Liver cells are derived from the same endodermal origin as the pancreas and consequently are more amenable to pancreatic transdifferentiation when compared to other cell types[114]. Like pancreatic β-cells, they express the key glucose-responsive elements glucose transporter 2 (GLUT2) and glucokinase, making hepatocytes an attractive target cell for engineering artificial β-cells. Although hepatocytes do not contain proinsulin-processing enzymes and lack secretory granules, this function may be induced via expression of insulin analogues cleaved by furin in the liver[76, 77]. However, truly regulated secretion to a glucose stimulus requires the presence of insulin storage granules. Within seconds of being exposed to glucose, the cell transports glucose across the membrane and metabolises it. The secretory granule migrates to the surface of the cell, fuses with the membrane and secretes its contents, thus regulating blood glucose levels. The result in many studies that have simply expressed either insulin or insulin analogues in liver cell lines or animal livers[115-117] has been the synthesis and constitutive release of insulin, but not its storage or regulated secretion. By comparison, our laboratory has shown that the expression of insulin in a liver cell line (Huh7ins) that had endogenous expression of β-cell transcription factors led to pancreatic transdifferentiation, formation of secretory granules and a regulated response to glucose with reversal of diabetes[76]. However, glucose stimulated insulin secretion (GSIS) was at sub-physiological levels, but further engineering to express human islet glucokinase in the cells,

led to the development of Melligen cells, which secrete insulin in the normal physiological range and have shown reversal of diabetes in NOD/*Scid* mice without the development of hypoglycaemia[118].

Table 1.4: Summary of target cells and degree of β-cell similarity

Characteristics	Target Cell				
	Liver	**Pituitary**	**Muscle**	**K cells**	**MSC**
Endodermal Origin	+	-	-	-	+
Possession of β-cell Transcription Factors	-	-	-	-	+
Glucose-Sensing System	+	-	-	+	-
Processing Enzymes	-	+	-	+	-
Glucose-Regulatable Promoter	+	-	-	+	-
Exocytosis System	-	+	-	+	-
Autologous Use	+	+	+	+	+
Allogeneic Use	-	-	-	-	+

The presence/absence of β-cell characteristics is denoted by "+/-".

1.5.3 Vector choice for gene therapy

By exploiting the natural ability of viruses to infect and deliver genes into cells, engineered viral vectors that do not replicate and efficiently transduce genes into infected target cells have been developed. Their suitability for gene transfer into target cells is determined by whether they are integrating or non-integrating, the target cell-type and the nature of gene expression required (Table 1.5). Ideally, β-cell engineering would employ integrating viral

vectors to provide sustained gene transfer in daughter cells over the life of the patient resulting in a sustained therapeutic benefit.

1.5.3.1 Retroviral

Retroviral vectors are the most widely used gene delivery vector, and are derived from disabled murine viruses[119]. The advantage of integration into the host's genome is however overshadowed by the risk of insertional mutagenesis[120]. This was first recognised in 1999 following the treatment of nine severe combined immunodeficiency (*Scid*) patients with a retroviral vector, which resulted in the development of leukaemia in four of the nine patients[121]. This study showed that retroviruses in general have site specific integration preferences in close proximity to the transcriptional regulatory sequences of proto-oncogenes[122]. Retroviral gene transfer is also limited by their ability to only transduce dividing cells, and can therefore only be targeted towards selected cell or tissue types. This ultimately becomes a challenge when the target tissue is composed predominantly of non-dividing cells, such as the liver. Xu *et al*,[123] studied the retroviral transduction of bone marrow-derived mesenchymal stem cells (BMSCs) with an insulin gene under the control of the CMV promoter; and the ability of these transduced cells to restore normoglycaemia in STZ-diabetic mice.

1.5.3.2 Adenoviral

Adenoviral vectors were initially studied due to their ability to transduce non-dividing cells with high efficiency. However, these vectors transfer their genes episomally and subsequently provide only transient gene expression[119, 124]. In addition, immune responses against the viral proteins and in some cases the transgene itself have been reported[125, 126]. To overcome the immunogenicity of the viral capsid proteins, a "gutless" adenovirus was

developed, in which the majority of the viral genes were removed[127]. Although reduced immunogenicity was observed with the new generation adenoviral vectors, immunosuppression was required to manage immune responses activated following treatment[128]. The prevalence of pre-existing immunity to adenoviruses in humans would also limit the multiple administrations of vector required to maintain long-term therapeutic effects. These characteristics actively work against choosing adenoviral vectors to produce an artificial β-cell.

1.5.3.3 Adeno-associated

Adeno-associated viral (AAV) vectors are replication-defective parvoviruses able to transduce both dividing and non-dividing cells. Although they show a limited gene cargo capacity (<5kb), they preferentially integrate into the host genome at a specific site on chromosome 19[129]. This renders AAV a safe and attractive gene delivery candidate as their insertion sites can be predicted and potentially oncogenic consequences avoided. AAV vectors have been utilised in the treatment of T1D, specifically to directly deliver the preproinsulin gene to livers of chemically STZ-mice[130], where proinsulin was produced in the liver and blood glucose levels were transiently reduced. This study supports the utility of AAV for insulin gene transfer to non-dividing hepatocytes.

1.5.3.4 Lentiviral

Lentiviral vectors are retroviruses with the ability to transduce non-dividing cells as well as dividing cells, which makes them attractive candidates for the transduction of a variety of cell lineages[131]. They are derived from the human immunodeficiency virus (HIV), and, accordingly, biosafety was initially a concern surrounding their suitability as human therapeutics. Construction of self-inactivating HIV-derived vectors, with deletions in the long

terminal repeat promoter, decreases the likelihood of generating a replication competent virus[132], and subsequently provides greater safety for clinical application. As a result, lentiviral vectors have shown promise for corrective gene therapy and are currently the gene transfer vector of choice within our laboratory. We have successfully used a lentiviral vector (HMD) to deliver *INS-FUR* to the livers of STZ-diabetic rats[77], NOD-mice[133] and pancreatectomized Westran pigs[134]. In these animal models we have seen spontaneous expression of an array of β-cell transcription factors, formation of granules and regulated and permanent correction of diabetes in a number of animal models[77, 133, 134]. Liver to pancreas transdifferentiation is relatively common in other situations[135], especially when the liver is insulted. The pancreatic transdifferentiation in our studies was undoubtedly related to the combination of the surgical procedure employed, which isolates the liver from the circulation, the lentiviral vector and the microenvironment of diabetic hyperglycaemia, which collectively insulted the liver cells. By comparison the simple injection of insulin into the portal circulation led to unregulated constitutive insulin release, no pancreatic transdifferentiation and an abnormal glucose response[133] as seen in a similar study by Elsner *et al*[116]. Whilst lentiviral expression of insulin has become a popular choice for gene therapy in some rodent models showing amelioration of hyperglycaemia, normal glucose tolerance was not achieved due to an absence of β-cell transcription factor expression and resultant pancreatic transdifferentiation[136, 137].

Table 1.5: Summary of viral vectors for gene delivery

Viral Vector	Packaging Capacity	Advantages	Disadvantages
Retroviral	8-10kb	Integrates into host genome No expression of viral proteins Long-term expression	Only transduces dividing cells. Limited insertion capacity Random integration into host genome
Adenoviral	<8kb	Transduces dividing and non-dividing cells Produces high titres of virus High levels of expression	Immune response to viral proteins No integration into host genome Short-term expression
Adeno-associated	<5kb	Transduces dividing and non-dividing cells Non-pathogenic and low immunogenicity Long-term expression Broad host range	Requires helper virus Can generate neutralising antibodies Limited insertion size
Lentiviral	<10kb	Transduces dividing and non-dividing cells Stable, long-term expression Can be generated into a self-inactivating vector	Possible toxicity due to viral proteins in packaging construct Random integration into host genome

1.5.4 Mechanism of glucose-responsive insulin secretion

Ultimately, T1D gene therapy approaches aim to create "artificial" β-cells that reproduce the mechanism of insulin secretion that occurs normally within β-cells (Figure 1.3). Normally, insulin is initially translated as a proinsulin precursor in the endoplasmic reticulum (ER), it is then transported from the ER to the Golgi Apparatus, and crosses the Golgi Network before being sorted into clathrin-coated immature insulin secretory granules (ISGs)[138]. Various biochemical modifications trigger the maturation of ISGs, and following glucose stimulation the mature ISGs secrete their insulin content into the extracellular space. GLUT2 transporters carry glucose into the pancreatic β-cell where it is immediately converted to glucose-6-phosphase by hexokinase IV and enters glycolysis. An increase in adenosine triphosphate (ATP) concentration causes ATP-gated K^+ channels to close, resulting in the depolarisation of the membrane. Consequently, voltage-gated Ca^{2+} channels open, thereby increasing cytosolic [Ca^{2+}]. Release of insulin from mature ISGs via exocytosis due to the increase in cytosolic [Ca^{2+}] is then followed by a decrease in blood glucose. Although the pancreatic β-cell contains ~10,000 ISGs, only 100-200 ISG's are capable of quickly releasing their insulin content in response to increases in cytosolic [Ca^{2+}][138]. This means that there is a "reserve pool" of ISGs which can be induced to release insulin, resulting in the minute-to-minute regulation of insulin secretion in response to changes in blood glucose levels. The release of insulin is then slowed or stopped when the pancreatic β-cell detects a decrease in glucose flux through the hexokinase reaction.

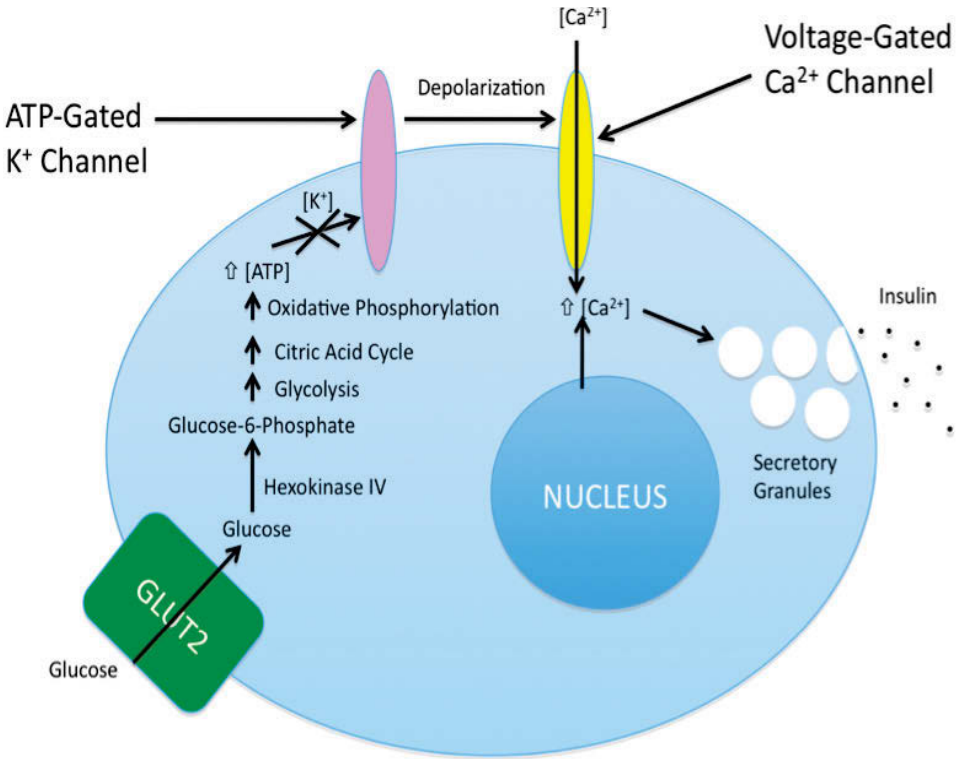

Figure 1.3: Mechanism of insulin secretion in pancreatic β-cells Insulin secretion within the pancreatic β cell is stimulated by glucose in blood plasma. Glucose is taken up by the cell via membrane receptors and detected in the hexokinase IV reaction that takes place within the cell. A series of following biochemical reactions ultimately results in exocytosis of insulin into the extracellular space.

One of the major hurdles for T1D therapy is the ability to reproduce the regulated mechanism of insulin secretion in pancreatic β-cells. Pancreatic β-cells use specialised structures (secretory granules) that many other cell types lack to perform this function. Consequently, the use of glucose-responsive promoters attached to the insulin gene has been investigated in an attempt to engineer the physiological production of insulin. The L-type pyruvate kinase (LPK), Spot 14 and glucose-6-phosphate promoters have been identified to regulate the expression of a variety of genes in the liver in response to extracellular glucose concentrations[131]. These promoters have been utilised in association with the insulin gene for gene transfer in attempts to reproduce the glucose-responsive production of insulin that occurs in normal β-cells. The glucose-responsive element (G1RE) found in the LPK promoter has been found to regulate transcription of proinsulin in response to glucose[139, 140]. In particular, a study by Thule *et al*, showed that by injecting diabetic rats with a construct containing three copies of the G1RE from the LPK promoter, an inhibitory element from the insulin-like growth factor binding protein-1 promoter and a modified proinsulin gene, normoglycaemia was nearly achieved[140, 141]. STZ-induced diabetic mice expressing a human proinsulin gene under the control of the LPK promoter expressed proinsulin mRNA in the liver, with the transcription of proinsulin mRNA regulated by diet. However, STZ-induced diabetic mice did not increase the expression of insulin mRNA due to inhibition of glucokinase by glucagon[142]. This was overcome by inducing basal levels of expression of transgenic insulin with a simian virus 40 enhancer that stimulated glucokinase expression, which in turn activated expression of transgenic insulin via the LPK promoter[139]. Promising work utilising a glucose-6-phosphate promoter showed that glucose-responsive production of insulin could be induced in rat hepatoma cells, however this was limited by low levels of insulin production as a consequence of the negative feedback by the insulin produced[143].

More recently, transcriptional analysis of BMSCs grown under varying concentrations of glucose identified a number of glucose-responsive promoters, and of particular interest, the early growth response-1 (EGR1) promoter which was capable of expressing insulin in transduced BMSCs in a glucose-responsive manner[144]. Upon implantation of the cells in STZ-diabetic induced NOD/*Scid* mice, the transduced cells were capable of restoring normoglycaemia, glucose tolerance and body weight in this model. Interestingly, the EGR1 promoter was not sensitive to transgenic expression of insulin, as it is known that the EGR1 promoter can be activated by both glucose and insulin[145]. However, as NOD/*Scid* mice are not a model of autoimmune diabetes, such work should ideally be performed in immune-competent models of autoimmune diabetes such as NOD mice that intrinsically develop insulitis around 3-4 weeks of age, and progress to fully-fledged diabetes between 12-30 weeks[146].

Investigating tissue-specific regulation of pancreatic hormones or proteins would hopefully reveal the underlying mechanisms governing the expression of those factors. As a result, the insulin promoter which is activated by glucose has been intensively studied to identify these glucose-responsive elements in the hopes of better recreating the physiological regulation of insulin production[147, 148]. A study by Sander *et al*, discovered a strong glucose-responsive element (Z element) in the distal region of the human insulin promoter[147], elucidating one of the mechanisms that provides glucose-sensitive regulation of insulin in primary cultured islet cells. More recently, pancreatic derived factor (PANDER), a newly discovered cytokine-like protein that is strictly expressed in the pancreatic islets was analysed for its glucose-responsive nature of expression[149]. It revealed that the 5`-untranslated region (UTR) of the PANDER promoter contained the glucose-responsive elements that drive PANDER expression that mimic that of insulin expression, and that the PANDER promoter could potentially be used to drive transgenic insulin expression in alternative cell targets.

One of the limitations of transcriptionally regulated insulin production in transplanted alternative cell targets is their delay in responding with immediate insulin secretion when challenged with glucose. As insulin secretion is linked to insulin transcription, the minute-to-minute glycaemic control which occurs in normal β-cells is not present in these engineered target cells. This is due to the absence of secretory granules which store and immediately secrete insulin in response to fluctuations in blood glucose concentrations. To overcome this limitation, engineering a promoter expressing high levels of insulin in response to fluctuating glucose concentrations, yet possessing insulin-sensitivity as a feedback mechanism could more closely mimic the normal physiology of insulin secretion. However, the successful adaptation of this technology *in vivo* would require the development of granules similar to ISGs to regulate glycaemia.

1.5.5 Gene transfer of insulin

Our laboratory has shown that the ability of liver cells to store and secrete insulin, and undergo pancreatic differentiation, is linked to the induced expression of certain β-cell transcription factors. We were the first to show a number of cutting-edge developments in this field and very importantly have never seen the development of exocrine differentiation and tissue destruction often seen in studies of liver-directed gene therapy where *Pdx-1* was utilised[78, 150]. This is, in part, due to the alternative choice of genes used for the viral delivery to hepatocytes. We have shown that a human liver cell line (Huh7), which endogenously expresses β-cell transcription factors, upon expression of the insulin gene (Huh7ins) developed insulin storage granules and exhibited regulated secretion of insulin in response to increasing concentrations of glucose. After transplantation of Huh7ins into NOD/*Scid* mice, diabetes was reversed[76].

In several animal models we have delivered *INS-FUR*, within the lentiviral vector HMD, to the liver by using a surgical technique that isolated the liver from the circulation, allowing the lentiviral vector to settle in the liver without the problem of excessive inactivation from the blood. We permanently reversed diabetes in STZ-diabetic rats[77] and spontaneously-diabetic NOD mice[133]. In both studies, we reported spontaneous expression of key β-cell transcription factors (*Pdx-1, Neurog3* and *NeuroD1*), which are important in the development of insulin storage and regulated insulin expression in pancreatic β-cells[151-154]. Some later stage transcription factors (*Pax4 and Nkx2.2*) were also expressed. Our lentiviral transduction procedure may have represented a cellular insult, making progenitor cells permissive to a pancreatic developmental shift. Consistent with this, expression of *Pdx-1*, but only at the mRNA level, was also observed after treatment with the empty vector alone. Expression of insulin was necessary for protein expression of transcription factors. There was also expression of pancreatic hormones, development of insulin secretory granules and normal intravenous glucose tolerance tests were observed in the STZ-diabetic rat and NOD mouse. Furthermore, insulin expression was restricted to the liver. In the NOD mouse study, there was no evidence of intrahepatic inflammation or autoimmune destruction of the insulin-secreting liver tissue. By contrast, in our NOD mouse study and a similar study by Elsner *et al*, a simple injection of insulin into the portal circulation resulted in unregulated constitutive release of insulin, no pancreatic transdifferentiation and an abnormal glucose response[116, 133]. Pancreatic transdifferentiation of the liver has been seen in other situations; following a dose of the hepatotoxin carbon tetrachloride[155] and when oval cells were cultured in high glucose[156, 157]. We are yet to define the mechanism that has resulted in pancreatic differentiation in our studies, which is being analysed at the molecular level in our laboratory.

We have also reversed diabetes in a diabetic pig model, which was characterised by normal glucose tolerance, together with expression of β-cell transcription factors[134]. However,

reproducible results were problematic in the large animal due to the complexity of the surgical approach. Subsequently, viral delivery of *INS-FUR* has become a popular choice for gene therapy, with a number of studies showing amelioration of hyperglycaemia in rodent models. However, abnormal glucose tolerance was observed due to a lack of pancreatic transdifferentiation and expression of β-cell transcription factors[136, 137, 158, 159].

Studies in our laboratory have also shown that these insulin-secreting liver cells are resistant to the detrimental effects of β-cell cytotoxins and pro-inflammatory cytokines that play a principle role in the pathogenesis of T1D[160, 161]. In other experiments, no infiltrates of immune cells were observed in NOD mice engineered to express insulin in their livers[133, 162]. These studies established that liver cells are appropriate candidates for the creation of artificial β-cells, and also highlighted that dual expression of insulin and β-cell transcription factors gave a better outcome than expression of either alone[163]. Xu *et al*, studied the retroviral transduction of BMSCs with an insulin gene under the control of the CMV promoter and their ability to restore normoglycaemia in STZ-diabetic mice[123]. It was found that these BMSCs successfully expressed insulin and were able to maintain normoglycaemia for at least 42 days. In addition, the transduced BMSCs were able to evade the autoimmune destruction that ordinarily targets pancreatic islets.

1.5.6 β-cell transcription factors and their role in pancreatic development and mature β-cell function

The pancreas as a whole organ is derived from the endoderm during embryonic development. Transcription factors play a significant role in pancreatic embryogenesis, particularly in determining islet cell differentiation (Figure 1.4). During adult life, transcription factors regulate the expression of islet cell hormones[164, 165].

Forkhead Box factor *FoxA1* and *FoxA2* expression is directly implicated in endodermal formation, with *FoxA2* deletions resulting in the disruption of endoderm formation in mouse models[166]. Homeobox factor *Pdx-1* is considered the "master regulator" as it plays a significant role in the early development of the pancreas, being expressed in both the endoderm and pancreatic buds[164, 167]. *Pdx-1* expression levels are regulated by the interaction between the transcription factors, hepatocyte nuclear factor (HNF)-3β, HNF-1α, and SP1/3, and *Pdx-1* itself[168]. Homozygous *Pdx-1 -/-* mice are apancreatic, and while they survive foetal development, they die a few days following birth[169, 170]. This confirms the necessity of embryonic *Pdx-1* expression for successful pancreatic development.

Following the fusion of the dorsal and ventral buds, the differentiation of exocrine and endocrine pancreatic compartments occurs rapidly, with the basic helix-loop-helix factors, *Hes-1* and *Neurog3*, in the pancreatic precursor directing the respective compartmental fates via notch signalling[171]. The notch signalling pathway plays a major role in the control of cell identity, proliferation, differentiation, and apoptosis[172]. Subsequent differentiation of the various islet cell-types (α, β, γ and pancreatic polypeptide (PP)) is directed by the hierarchical expression of various transcription factors[164]. Lineage analyses have shown that all hormone-producing cells express *Neurog3*[171]. In mice, *Neurog3* deletions result in the absence of endocrine cells[173], testament to its necessity in endocrine cell development. *Neurog3* activates the persistent expression of *NeuroD1* that maintains the endocrine cell differentiation program[174]. In fact, *NeuroD1*-/- mice show a reduction in the development of insulin-producing β-cells[175].

As soon as the endocrine cell fate has been programmed, the paired homeobox factors, *Pax4* and *Pax6*, direct the fates of individual hormone-producing cells[164]. Studies in mice show that homozygous *Pax4* deficiency results in a lack of β and γ cells[164, 167], and mice that are

homozygous *Pax6* deficient lack α cells[176]. Collectively these studies suggest that *Pax4* is required for determining β and γ-cell fate, while *Pax6* is required for determining α-cell fate.

Differentiation into β-cells is ultimately driven by the NK homeobox factors, *Nkx2.2* and *Nkx6.1*. Knocking out the *Nkx6.1* gene in mice results in the absence of β-cells[177], however all other cell types develop. Interestingly, *Nkx2.2* is expressed in other cell types including α and PP-cells, however when *Nkx2.2* is knocked out, insulin-producing cells (IPCs) are absent[178]. Consequently, *Nkx2.2* and *Nkx6.1* are imperative in β-cell differentiation. More recently, a leucine zipper transcription factor (*MafA*) has been discovered downstream of *Nkx6.1* in the lineage analysis and was found to be involved in the maintenance of β-cell function, specifically through interactions with *Pdx-1* and *NeuroD1* that modulated insulin transcription[179]. The modification of transcription and subcellular localisation of fundamental transcription factors, such as *FoxA2*, *MafA*, *NeuroD1* and *Pdx-1* will alter important cellular processes, such as β-cell differentiation, cell cycle arrest and function, and accordingly represents an interesting potential target for the development of an artificial β-cell[180].

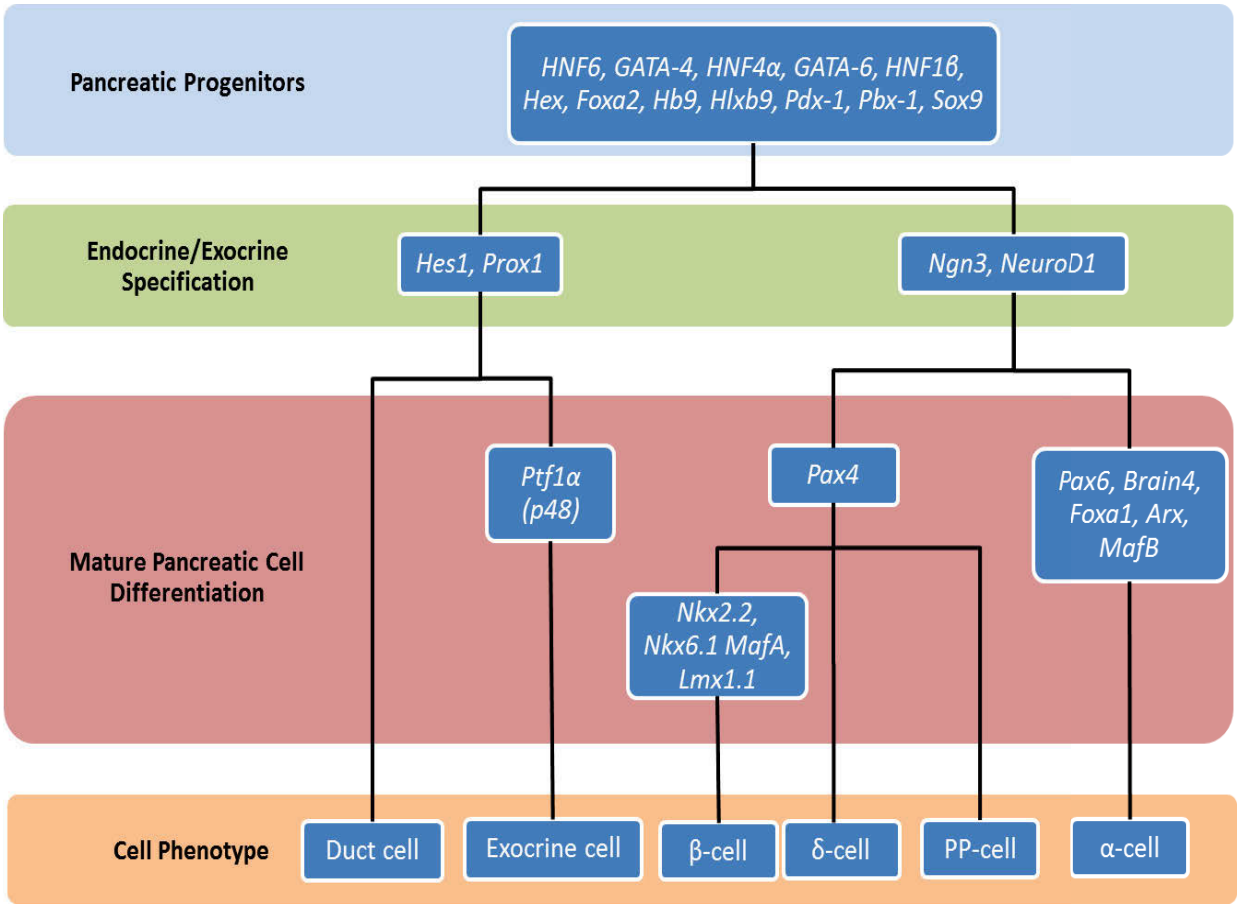

Figure 1.4: Schematic representation of the transcription factor hierarchy involved in pancreatic development and cellular differentiation The early endoderm of the gut receives signals from the mesenchyme and notochord to initiate formation of the pancreatic buds, with expression of *FoxA2* and *Hb9* detectable in the pancreatic precursors. *Pdx-1* then drives the subsequent differentiation of the pancreatic precursor cells by interacting with *Pbx-1*. *Neurog3* and *Hes1*, mediate endocrine and exocrine differentiation, respectively, with *NeuroD1* functioning to maintain the endocrine cell fate. *Pax6* and *Pax4* then mediate the differentiation of α-cells and β-cells, respectively, with the final differentiation process towards a β-cell phenotype being governed by *Nkx2.2* and *Nkx6.1* (Adapted from Gerace et al, 2015)

Many of the transcription factors that are involved in pancreatic development and differentiation are also involved in the functionality of mature β-cells. β-cells contain specific and unique genes encoding for insulin, GLUT2, islet amyloid polypeptide and glucokinase that are fundamental to their function[164]. It is the transcriptional regulation of these genes and many others that results in the morphological and phenotypical changes that occur during development. The method by which these factors regulate gene expression is via a networking system (Figure 1.5A). As a result, transcription of particular β-cell genes is not dependent upon a single factor. Due to the redundancy in the networking approach, single knockout of a transcription factor can diminish but not completely abolish transcription of a particular gene.

The co-operative function of various transcription factors and the complexes they form plays a significant role in the transcription of the insulin gene in β-cells (Figure 1.5B). *Pdx-1* plays a substantial role in transcriptional activation of insulin by binding to specific DNA elements (A boxes) on the insulin promoter and forming complexes with other co-activators such as p300 and E47[164]. The complex formed (*Pdx-1*/p300-*NeuroD1*/E47) binds the A1 site and maintains basal promoter activity, simultaneously enhancing insulin transcription by recruiting and activating basal transcription machinery[181]. The complex (E47/*NeuroD1*) that binds E boxes acts as a potent transcriptional activator of the insulin and glucagon genes. However, it has been found that overexpression of E47 results in inhibition of glucagon gene transcription and activation of insulin gene transcription. As a result, it can be deduced that the ratios of E47/*NeuroD1* in the pancreatic tissue direct the transcription of islet-cell specific genes[182]. It is important to note that some of these transcription factors are present in other cell types and that the specific combination of factors involved in the regulation of insulin transcription in β-cells can be similarly reproduced in other cell types. This provides the basis for targeting other tissues as potential sources of insulin production.

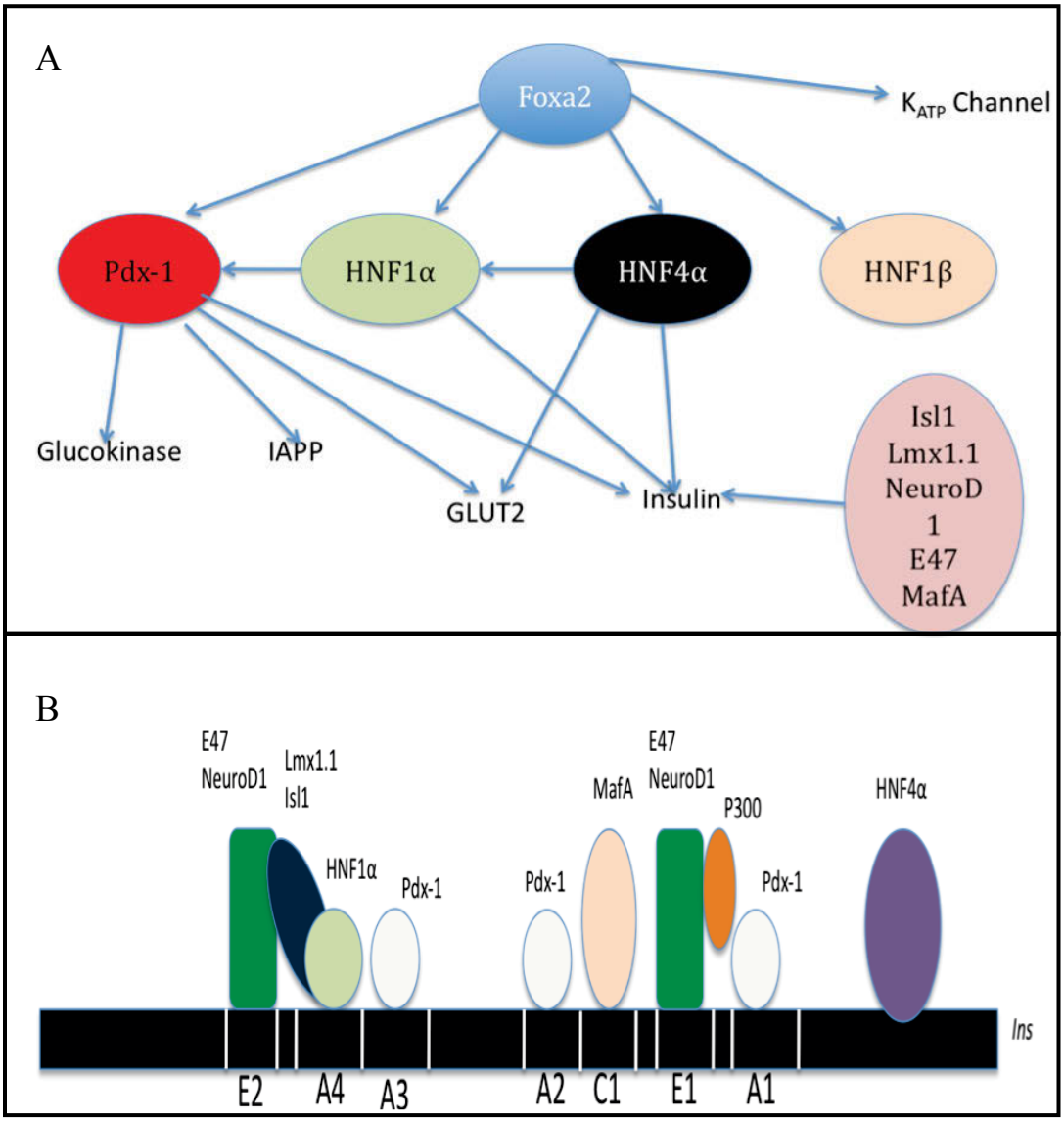

Figure 1.5: Transcriptional gene regulation in β-cells A) Model of the networking approach to transcriptional activation of a variety of genes in β-cells and B) Schematic representation of the insulin gene promoter, and the major transcription factors that function either individually or co-operatively in activating insulin gene expression.

1.5.7 Gene transfer of β-cell transcription factors

Genetically engineering other cells within the body to produce insulin is an attractive alternative to pancreas and islet transplantation, as these cells would not likely express the same auto-antigens that caused β-cell destruction in the first instance. Due to the common origin of the liver and pancreas[109], the ability to transdifferentiate tissue from liver to pancreas has been studied to a greater extent than other tissues types, particularly for the generation of IPCs through the transfer of pancreatic transcription factors.

1.5.7.1 Pdx1

Ferber *et al*, demonstrated the potential of transcription factors to be directly delivered to liver tissue, via a recombinant adenovirus-mediated transfer of *Pdx-1*[78]. Considering *Pdx-1* plays a significant role in early embryonic development of the pancreas, an attempt to demonstrate the ability of adenovirus-mediated delivery of *Pdx-1* to ameliorate hyperglycaemia by inducing expression of endogenous insulin was performed. Results showed that expression of *Pdx-1* in livers of diabetic mice induced insulin expression and secretion leading to restoration of normoglycaemia. However, normoglycaemia was transient and only maintained for 8 days. In addition, exocrine differentiation of liver to pancreatic tissue resulted in the development of hepatitis and an increased likelihood of autoimmune destruction[78, 183].

Similarly, Kojima *et al,* employed the use of a helper-dependent adenovirus (HDAD) to deliver *Pdx-1* to the livers of STZ-diabetic mice[183]. These mice developed hepatitis due to unexpected exocrine differentiation of the transduced cells. This was likely related to the use of a potent ubiquitously expressed elongation factor-1α promoter, which resulted in continuous unrestricted expression of *Pdx-1* at high levels. To date, several studies in which

Pdx-1 has been transferred to hepatocytes to induce the process of transdifferentiation have been performed[93, 184-187]. In addition, direct delivery of *Pdx-1* has been achieved in a variety of other differentiated cell types, including mouse pancreas via the bile duct[188], rat intestinal epithelium-derived cells[189] and primary duct cells[190]. One study showed how combinations of pancreatic transcription factors (*Pdx-1*, *Neurog3* and *MafA*) were successful in converting pancreatic exocrine cells *in vivo* to closely resemble β-cells[191], and thus provided evidence for the use of transcription factor combinations. The newly generated IPCs are indistinguishable from normal islets and display all the characteristic hallmarks of normal β-cells, however the limited number of successfully converted exocrine cells and the fact they did not organise themselves into islet structures limited their effectiveness.

Pdx-1 continues to be utilised as a mediator of IPC production due to its proven ability to induce pancreatic transdifferentiation. The move to stem cells as targets has come as no surprise considering their plasticity and regenerative capabilities. *Pdx-1* has been delivered to MSCs from a variety of sources, including BMSCs[94, 123, 192-195], umbilical cord MSCs (UC-MSCs)[196], and adipose-derived MSCs (AD-MSCs)[92, 197, 198] with varying success in the generation of glucose-responsive IPCs. Despite the obvious attraction of MSCs as targets for *Pdx-1* delivery, embryonic stem cells (ESCs) have also been pursued as a potential target. A study by Miyazaki *et al*, showed that a murine ESC line (EB3) could be induced to differentiate into IPCs following transfection with *Pdx-1*, however transdifferentiation was not substantial enough for therapeutic use due to a lack of expression of the insulin 1, glucagon, PP gene, or GLUT2 genes, which are all specific to the endocrine pancreas *in vivo*[199]. This was followed by a number of studies in other ESC lines[200-202] showing their capacity to differentiate into IPCs.

1.5.7.2 Neurog3

The role of *Neurog3* in defining endocrine cell fate would logically point towards its more frequent use in gene therapy; however this is not the case. Most studies have reported low levels of insulin production after delivery of *Neurog3*[190, 203-206]. Of the few reported attempts at utilising *Neurog3* for β-cell engineering, a study using adenoviral transfer of *Neurog3* and betacellulin to hepatic progenitor cells (oval cells) resulted in the production of insulin and transdifferentiation of the oval cell population[207]. However, as mentioned previously, the most successful use of *Neurog3* delivery was observed using a combinatorial approach[191].

1.5.7.3 NeuroD1

In order to prevent *Pdx-1*-induced exocrine differentiation, Kojima *et al*, expressed *NeuroD1* in conjunction with betacellulin within a HDAD vector to the livers of STZ-treated diabetic mice[183]. It was found that *NeuroD1*-betacellulin delivery restored and maintained normoglycaemia for greater than 120 days, with associated up-regulation of the upstream and downstream pancreatic transcription factors, including *Neurog3*, *Pax6*, *Pax4*, *Nkx2.2*, and *Nkx6.1*. However, whilst the use of betacellulin would not likely be acceptable for clinical application, the use of *NeuroD1* resulted in no significant hepatotoxicity or development of hepatitis, marking *NeuroD1* as a worthy alternative transcription factor for directing differentiation to a β-cell like phenotype. *NeuroD1* is also an ideal alternative as it has been shown to be the strongest inducer of insulin expression (as compared to *Pdx-1*, *Neurog3*, and *Pax4*) in primary duct cells[190]. Similar studies showing the ability of *NeuroD1* to strongly induce insulin expression have been performed using hepatocytes[208].

Promising results using viral delivery of *NeuroD1* to hepatocytes have also been reported by our laboratory. Specifically, a genetically modified rat liver cell line (H4IIE) which does not

express β-cell transcription factors was engineered to express both insulin and *NeuroD1*[163]. The engineered cell line developed storage granules and reversed diabetes in NOD/*Scid* mice following transplantation. It also stimulated the expression of the β-cell transcription factors, *Pdx-1*, *NeuroD1*, *Pax6*, *Nkx2.2*, and *Nkx6.1*, in addition to rat insulin 1 and 2, glucagon, somatostatin, pro-convertases 1 and 3, and pancreatic polypetpide. The engineered cells also regulated secretion of insulin in response to increasing concentrations of glucose. Interestingly, the stand-alone expression of *NeuroD1* in the H4IIE cells resulted in expression of β-cell transcription factors and some storage of insulin, but GSIS was absent. As a result, *NeuroD1* could potentially be used in future gene therapy protocols to induce safe differentiation of target tissues.

1.5.7.4 Pax4

As mentioned earlier, *Pax4* deficiencies in mice results in the lack of β and γ cells[164, 167], therefore it can be deduced that *Pax4* is required for determining β-cell fate and could be used for the generation of IPCs. Overexpression of *Pax4* in mouse embryonic stem cells selected for nestin expression has been shown to drive differentiation to a β-cell phenotype[209], with the resultant IPCs capable of maintaining normal blood glucose levels for 14 days. Similarly, Liew *et al*, reported that overexpression of *Pax4* in human ESCs enhances their propensity to form putative β-cells[210]. However, the capacity for teratoma formation of undifferentiated ESCs limits their potential for clinical application.

1.5.7.5 Nkx6.1

The β-cell specific expression of *Nkx6.1* theoretically makes it an ideal choice as a factor to drive β-cell differentiation. However a study by Gefen-Haleri *et al*, showed that ectopic expression of *Nkx6.1* alone, although capable of inducing the expression of immature

pancreatic markers, such as *Neurog3* and *Isl-1*, was not capable of inducing expression of pancreatic hormones[211]. In addition, *Nkx6.1* did not appear to be a strong inducer of expression of upper-hierarchy β-cell transcription factors, such as *Pdx-1* and *NeuroD1*. In fact, only upon co-expression with ectopic *Pdx-1* was there substantial insulin expression and glucose regulated processed hormone secretion. Consequently, the inability to induce expression of the full repertoire of β-cell transcription factors makes *Nkx6.1* an inferior choice for β-cell engineering.

1.5.8 Suicide gene therapy

Suicide gene therapy is grounded on the concept of delivering a bacterial or viral gene to cells, whose enzyme product is able to convert a non-toxic prodrug to its toxic form resulting in cell death[212]. Consequently, this controllable system of cell death has been assessed as an alternative therapy to traditional cancer treatments such as chemotherapy and radiation therapy. Suicide gene therapy has been assessed in the treatment of leukaemia[213], prostate cancer[214] and breast cancer[215] amongst many others.

A number of systems exist that function via enzymatic conversion of a prodrug to its lethal form. The most commonly assessed systems are the herpes simplex virus thymidine kinase gene[216, 217] with ganciclovir as the prodrug, and the *Escherichia coli* cytosine deaminase gene (CD)[218, 219] with 5-fluorocytosine (5-FC) as the prodrug. Following conversion of the toxic prodrug to its lethal form, apoptosis is induced in targeted cells via interference of the mitochondrial pathway[218]. The CD system has been further improved by fusion with the uracil phosphoribosyltransferase (UPRT) gene (CDUPRT) which facilitates the conversion of the toxic 5-fluorouracil (5-FU) to 5-FU monophosphate, further sensitising 5-FU-resistant tumour cells to low concentration of 5-FU[220].

Tumour cell destruction is exacerbated further by the "local bystander" effect, a phenomenon which does not require complete tumour transduction with suicide genes, yet results in significant tumour regression via diffuse uptake of the enzyme—converted toxic product of the administered prodrug[221]. To improve the targeted delivery of the suicide gene therapy system to tumours, a number of cellular vehicles with homing capabilities have been targeted to express suicide genes and deliver the system locally to tumours[222, 223]. MSCs have demonstrated tumour-homing capabilities where they participate in tumour stroma formation[222], and as such have been targeted for as vehicles for the delivery of CD or CDUPRT as a treatment for a number of cancers[219, 224, 225].

The use of suicide gene therapy also holds potential in improving the safety profile of cell therapies for alternative diseases. Demonstrating safety in any newly developed cell therapy is a key checkpoint in progressing through clinical trials, and as such, suicide gene therapy provides a mechanism through which administered cells could be destroyed in the event of adverse events. Within the context of T1D this can be achieved by primarily engineering the selected target cells for expression of a suicide gene, e.g. CDUPRT, and thereafter differentiating the cells towards the pancreatic lineage. As such, the differentiated cells would also possess the suicide therapy safety feature, whereby following transplantation, and in the event of any unexpected changes to the transplanted cells, they can be destroyed upon the administration of the non-toxic 5-FC.

In addition, determining the ability of transplanted cells to restore normoglycaemia in a selected model of diabetes is an essential requirement of assessing the efficacy of any cell therapy for T1D. This is most commonly performed via routine blood glucose monitoring, however in order to demonstrate that a cell transplant is directly responsible for the restoration of normoglycaemia, traditionally surgical removal of the graft is performed,

followed by an expected increase in blood glucose concentrations. With respect to improving experimental design, the incorporation of a suicide gene therapy feature in the transplanted cells allows for non-invasive removal of the graft, a significant advantage over surgical graft removal. As such, diabetic animals transplanted with cells possessing the suicide feature would require fewer invasive surgical procedures and are therefore at reduced risk of post-surgery associated complications.

1.6 Mesenchymal stem cells as a therapy for T1D

MSCs were originally identified by Friedenstein *et al*, in 1976 as a fibroblast-like cell population[226]. The definition of MSCs has evolved over time due to the changing understanding of MSC biology. Currently, the International Society for Cellular Therapies (ISCT) has defined MSCs as a heterogeneous stem cell population characterised by; (i) adherence to plastic under standard culture conditions; (ii) a fibroblast-like morphology; (iii) the capacity to differentiate into osteocytes, chondrocytes and adipocytes; (iv) lack of expression of haematopoietic markers CD11b, CD14, CD34, CD19 or CD79a, CD45, HLA-DR and the vascular marker CD31[227-231]; (v) expression of CD13, CD44, CD54, CD73, CD90, CD105, CD146, CD166, CD200, SCA-1 and STRO-1[227, 229-232]. However, differences in these characteristics are observed across strains and species, making the translation of preclinical animal to clinical human studies challenging. Consequently, there is a requirement for a universal classification of MSCs to standardise their utility in the clinical setting.

Although MSCs are predominantly isolated from the bone marrow[233, 234], they also reside in other tissues and organs such as the placenta[235], cord blood[236], umbilical cord Wharton's jelly[237], lung[238] and adipose tissue[233]. In addition to their capacity to undergo tri-lineage differentiation, they show high plasticity by their ability to differentiate into cells of ectodermal, endodermal and mesodermal lineage[239]. Due to their ease of isolation, *ex vivo* expanded MSCs have been assessed in the pre-clinical and clinical setting for their benefits in tissue repair and regeneration. It is now well established that the effects elicited by MSCs are mediated by; (i) the secretion of immunomodulatory and cytoprotective factors that provide a protective microenvironment and; (ii) the recruitment and modulation of immune cells in areas of tissue damage to provide an anti-inflammatory effect[240].

1.6.1 Immunomodulatory properties of MSCs

MSCs show immunomodulatory properties both *in vitro* and *in vivo*, which are facilitated by complex mechanisms that inhibit the function of different populations of immune cells (Figure 6). However, reports of varying MSC regulatory function *in vitro* in comparison to *in vivo* complicate standard characterisation of MSC regulatory function. The most significant demonstration of MSC immunomodulation *in vitro* is their inhibitory effect on T cell proliferation and DC differentiation, both of which are considered to be key factors in activating autoimmune diseases[227, 231, 241, 242]. MSCs also possess the ability to modulate B cell proliferation and differentiation, NK cell proliferation and cytotoxicity; and T regulatory (T_{reg}) cell maturation by altering the secretion of cytokines from DCs, Th1 and Th2 cells, and NK cells[243]. In addition, MSCs secrete biological factors (Table 1.6) such as growth factors, cytokines, chemokines and hormones that exert paracrine effects on immune cells, enhancing the MSC immunomodulatory repertoire[244].

1.6.1.1 T cells and T_{regs}

The immunomodulatory properties of MSCs were initially observed through their inhibition of T cell proliferation via mitogens, CD3/CD28 and alloantigens[245, 246]. However, recent *in vitro* data has suggested that MSCs arrest T cells at the G0/G1 phase of the cell cycle by down-regulation of cyclin D2 and inhibition of co-stimulatory molecule expression, which results in T cell anergy without induction of apoptosis[247, 248]. These processes are mediated by direct cell-to-cell contact between MSCs and T cells. In particular, binding of programmed death 1 (PD-1) to its ligands PD-L1 and PD-L2 has been implicated in inhibition of T-cell proliferation via direct contact of MSCs and target cells, thereby inducing a tolerogenic microenvironment[249]. In fact, MSCs express several receptors which facilitate these interactions, including MHC class I, the vascular cell adhesion molecule, intercellular

adhesion molecule-1, activated leucocyte cell adhesion molecule, lymphocyte functional antigen-3 and some integrins[250]. MSCs are also able to secrete soluble factors such as prostaglandin E2 (PGE2), indoleamime 2,3-dioxygenase (IDO) and transforming growth factor beta 1 (TGF-β1) that inhibit T cell proliferation and function[230]. Furthermore, the secretion of PGE2 and TGF-β1 leads to increases in IL-10 production by DCs, promoting the activation of T_{regs}[251, 252].

1.6.1.2 B cells

Similar to their ability to suppress T cell proliferation, MSCs block B cell proliferation through the induction of G0/G1 phase cell cycle arrest in a dose-dependent manner via the secretion of IDO, PGE2 and nitric oxide[253-255]. A study by Corcione *et al*, demonstrated that MSCs were capable of significantly down-regulating the expression of chemokine receptors CXCR4, CXCR5 and CXCR7 of B cells[254]. Despite these effects, no changes in B cell co-stimulatory molecule or cytokine expression were observed. Contrary to these results, exposure to activated B cells increased B cell survival and proliferation[256]. A possible explanation for these conflicting reports is the difference in isolation methods and the state (activated or naïve) of the B cells on which the analyses were performed. Interestingly, MSCs activated by IFN-γ decrease B cell antibody production[257].

1.6.1.3 Natural killer cells

NK cells are known to display cytolytic activity against cells with little-to-no expression of MHC class I molecules, and as a result it was believed that high levels of MHC class I expression on MSCs enabled MSCs to evade NK cell surveillance[258]. However, NK cells are proficient in lysing MSCs despite their high levels of MHC class I. NK cell-mediated MSC lysis is believed to occur via NK cell receptors which have their counterpart ligands expressed on MSCs.

More importantly, MSCs are able to inhibit IL-2 induced NK cell proliferation via cell-to-cell contact and the secretion of TGF-β, soluble human leukocyte antigen-G and PGE2[251, 259]. MSCs also inhibit the cytotoxic functions of NK cells via PGE2 and IDO-mediated down-regulation of NK cell receptors, resulting in decreased IFN-γ secretion from NK cells[260].

1.6.1.4 Dendritic cells

DCs have an important role in the presentation of antigens to naïve T cells immediately after their maturation. MSC-mediated inhibition of DC maturation from monocytes thereby indirectly inhibits T cell activation[261]. Zhang *et al*, reported that MSCs inhibited the up-regulation of CD1a, CD40, CD80 and CD86 on DCs and *in vitro* DC differentiation[262]. Furthermore, MSCs modulate the cytokine secretory profile of DCs by inhibiting the production of tumour necrosis factor-α, IFN-γ and IL-12; and conversely increasing DC production of IL-10[252, 261]. Consequently, inhibition of T cell proliferation is further enhanced by DC maturation under the influence of MSCs. The mechanism through which this occurs is poorly understood, however it is potentially mediated by PGE2 secretion.

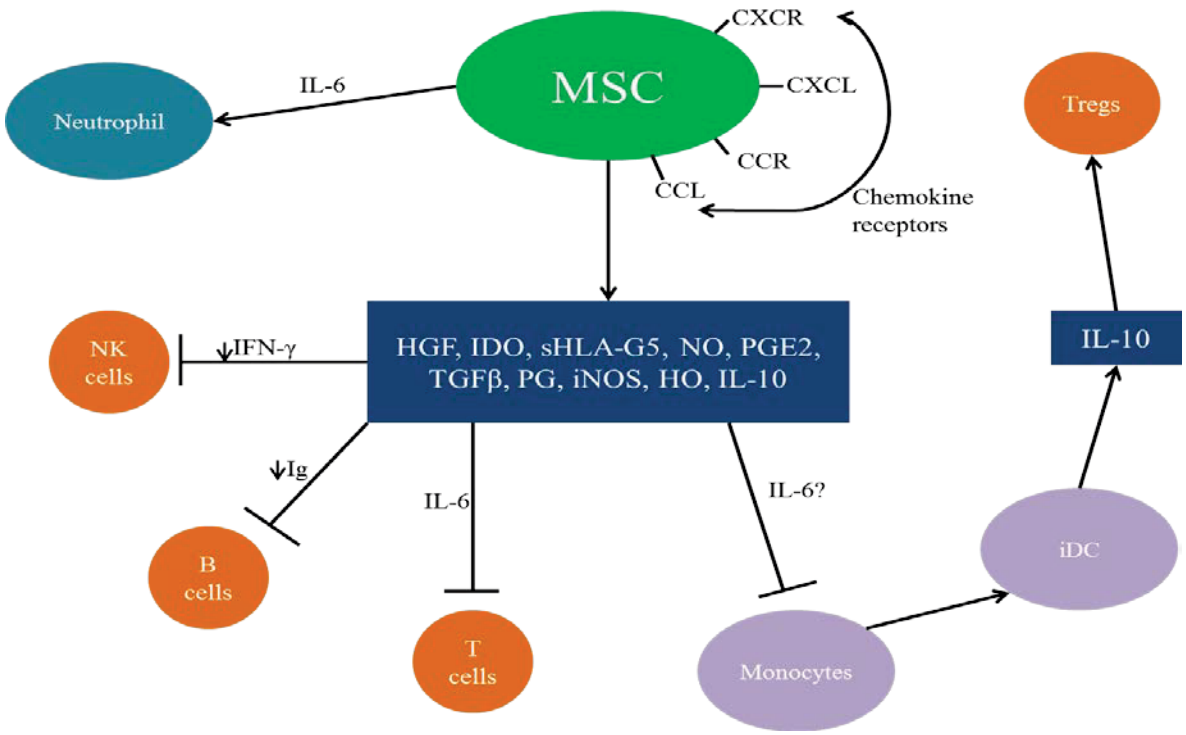

Figure 1.6: Schematic representation of the potential mechanism by which MSCs regulate the immune response MSCs express chemokine receptors and secrete soluble factors which regulate the functions of subpopulations of immune cells, thereby modulating the immune response. Abbreviations: HGF- hepatocyte growth factor, IDO- indoleamine 2,3- dioxygenase, sHLA-G5- soluble human leucocyte antigen-G5, NO- nitric oxide, PGE2- prostaglandin E2, TGFβ- tumour growth factor β, PG- prostaglandin, iNOS- inducible nitric oxide synthase, HO- heme oxygenase, IL-10- interleukin 10.

Table 1.6: List and function of the soluble factors secreted by MSCs

Name	Function
IDO	Inhibition of proliferation through reduction of tryptophan
NO	Inhibition of cell activation
HGF	Inhibition of proliferation, cytotoxicity
sHLA-G5, TGF-β	Inhibition of proliferation, cytotoxicity, promotion of T_{reg} generation
PGE2	Inhibition of proliferation: cytotoxicity, stimulation of cell activation and inhibition of DC and T_{reg} stimulation
IFN-γ, TNF-α, IL-1β	Promote chemokine production and immunosuppressive factors such as NO or IDO
IL-6	Regulates migration, stimulates mitosis and angiogenesis
IL-10	Inhibition of apoptosis
IL-15	Regulates T and NK cell activation and proliferation
VEGF	Inhibition of apoptosis, stimulates angiogenesis
LIF	Inhibition of apoptosis
SCF	Supports growth and differentiation
Jagged 1	Enhances differentiation
CCLs and CXCLs	Promote migration of leucocytes
M-CSF	Involved in the proliferation, differentiation, and survival of monocytes, macrophages, and bone marrow progenitor cells
FGF	Involved in angiogenesis
Ang1	Involved in vascular development and angiogenesis
GM-CSF	Stimulates stem cells to produce granulocytes and monocytes

Abbreviations: IDO- indoleamine 2,3-deoxygenase, NO- nitric oxide, HGF- hepatocyte growth factor, sHLA-G5- soluble human leukocyte antigen G5, TGF-β- transforming growth factor β, PGE2- prostaglandin E2, IFN-γ- interferon γ, TNF-α- tumour necrosis factor α, IL-1β- interleukin 1β, IL-6- interleukin 6, , IL-10- interleukin 10, IL-15- interleukin 15, VEGF- vascular endothelial growth factor, LIF- leukaemia inhibitory factor, SCF- stem cell factor, CCL- chemokine ligand, CXCL- CXC-chemokine ligand, M-CSF- macrophage colony stimulating factor, FGF- fibroblast growth factor, Ang1- angiopoietin 1, GM-CSF- granulocyte macrophage colony stimulating factors.

1.6.2 MSCs as an immunomodulatory therapy for T1D

MSC modulation of immune responses *in vivo* remains under intense investigation in autoimmune disease states such as Graft-vs-host disease and Crohn's disease following allogeneic bone marrow transplantation[263, 264]. Within the context of T1D, MSCs have been assessed for use as an immunomodulatory therapy in small animal models of diabetes such as NOD mice[265-268] and STZ-induced diabetic animals[269-273], where improvements in the glycaemic control of treated animals have been observed. Through these early studies, MSC interventions demonstrated improved T1D outcomes through two mechanisms; (i) MSC migration to areas of pancreatic injury and modification of the islet microenvironment to promote the survival and regeneration of surviving β-cells and; (ii) abrogating inherent autoimmunity against β-cells[274-276]. In addition, MSCs can be co-transplanted with pancreatic islets, thereby protecting the islets from allogeneic immune responses[277, 278]. The success of MSC immunotherapy in pre-clinical animal models of diabetes are summarised in Table 1.7.

1.6.2.1 Promotion of the survival and regeneration of existing β-cells

A number of studies have demonstrated that adult β-cells possess the capacity to self-duplicate and regenerate[279, 280]. Due to the fact that MSCs are capable of modifying the tissue microenvironment, MSC infusions can promote the survival and regeneration of existing β-cells, leading to increases in β-cell mass and restoration of normoglycaemia[281-284]. In fact, a number of studies have demonstrated this phenomenon following intravenous injection of MSCs to diabetic mice, resulting in increased insulin levels and reduced hyperglycaemia[269, 285, 286]. Similarly, a single treatment of UC-MSCs in humans provided lasting reversal of autoimmunity that allowed regeneration of islet β-cells and improvement glycaemic control[287-290]. However, the success of such interventions is closely related to the time of diagnosis. In many cases, people with long-standing T1D would possess very little to no

remaining β-cells, and consequently would unlikely be capable of regenerating sufficient quantities of *de novo* β-cells to ameliorate their hyperglycaemia.

1.6.2.2 Modulation of autoimmunity

As previously mentioned, MSCs possess wide-ranging modulatory effects on immune cells, and therefore their use in abrogating autoimmune diseases has been well documented. The autoimmune nature of T1D unsurprisingly ignited interest in the use of MSCs as a potential cell therapy. A number of pre-clinical diabetic animal studies showed that transplantation of MSCs results in glycaemic restoration as a consequence of suppressed T cell proliferation and increased T_{reg} cell presence within pancreatic islets[265-268, 271-273]. In a recently published clinical trial, MSCs injected through liver puncture successfully reduced the levels of islet-cell antibodies, glutamic acid decarboxylase, and insulin antibodies of two patients in 12 months, suggesting immune-modulated cell tolerance[291].

1.6.2.3 Pancreatic islet and MSC co-transplantation

Alternatively, MSCs recruit and increase the numbers of immunosuppressive host cells during co-transplantation of islets to promote graft survival. Specifically, following human islet transplantation in an advanced humanised mouse model, human bone marrow-derived MSCs increased quantities of T_{regs} and caused immune tolerance of the transplanted islets[292]. In fact, the co-transplantation of MSCs and pancreatic islets was able to achieve a state of normoglycaemia in diabetic rats likely via MSC trophic factor secretion which protected the transplanted islets[293]. In addition, MSCs in close contact with pancreatic islets began to express *Pdx-1* (a fundamental transcription factor in β-cell development) and to differentiate into IPCs[293]. The protective effects of MSCs on transplanted islets has also been observed in a diabetic model of non-human primates that resulted in significantly enhanced islet engraftment and function associated with increased numbers of T_{regs}[294].

The collective results of these pre-clinical studies[265-269, 271-273, 285, 286, 292-294] demonstrate the success of MSCs as an immunomodulatory cell therapy for the treatment of T1D. Nevertheless, solutions are required to overcome the challenges of the loss of immunosuppressive characteristics over time and the requirement for high cell doses. In addition, the fact that animal studies have shown that MSCs derived from diabetic sources were unable to suppress immune responses in people with diabetes raises concern over the utility of autologously sourced MSCs[295], potentially limiting the isolation of MSCs to allogeneic sources.

Table 1.7: Summary of the major MSC immunotherapy studies in pre-clinical animal models of T1D

Intervention	Outcomes	Fresh/Frozen	Reference
Mice received 100–150×10^6 UC-MNCs retro-orbitally into the venous plexus.	Treated animals displayed significantly lowered blood glucose levels, reduction in insulitis and increased lifespan compared to untreated mice.	Fresh	260
Mice received 1×10^6 AD-MSCs by i.p. injection.	Treated animals displayed reversal of hyperglycaemia characterised by increased serum insulin, amylin, and glucagon-like peptide 1 levels. This improved outcome was associated with down-regulation of the $CD4^+$ Th1-based immune response and expansion of regulatory T cells (Tregs) in the pancreatic lymph nodes.	Fresh	261
Mice received 1x10^5 MSCs either i.p. or i.v.	MSCs reduced the capacity of diabetogenic T cells to infiltrate pancreatic islets. This was not associated with the modification of diabetogenic T cell homing, but with preferential migration of MSCs to pancreatic lymph nodes.	Fresh	262
Mice received 1x10^6 GFP^+ bone marrow cells by tail-vein injection.	Treated animals displayed reduced blood glucose levels, with the majority of transplanted cells localised to ductal and islet structures. Their presence was accompanied by a proliferation of recipient pancreatic cells that resulted in insulin production.	Fresh	264
Mice received 2.5x10^6 hMSCs injected through the chest wall into the left ventricle.	Treated animals displayed lowered blood glucose levels and increases in mouse insulin as a result of increased numbers of islets.	Fresh	265
Mice received 0.5x10^6 MSCs administered systemically.	Treated mice exhibited significant reductions in blood glucose levels, reaching nearly normoglycaemic values 1-month post transplantation. An increase in morphologically normal pancreatic islets was observed.	Fresh	267
Rats received 2–4×10^6 MSCs via tail vein injection.	Treated animals exhibited enhanced insulin secretion and sustained normoglycaemia. Islets from treated rats expressed high levels of *Pdx-1* and these cells were also positive for insulin staining.	Fresh	268
Mice received a co-transplantation of primary hBMSCs and human islets at serial ratios under the kidney capsule.	Treated animals exhibited good blood glucose control and increased levels of serum insulin and C-peptide when islets were co-transplanted with hBMSCs. hBMSCs also increased the percentage of T_{regs} and prevented cytokine-induced loss-of-function of transplanted islets.	Fresh	287
Mice received 5×10^5 MSC injected i.v. once a week for 4 weeks.	Treated animals exhibited delayed onset of diabetes. BALB/c-MSC trafficked to the pancreatic lymph nodes of treated animals. Administration of BALB/c-MSC temporarily resulted in reversal of hyperglycaemia in 90% of treated animals.	Fresh	290

Abbreviations: UC-MNCs – umbilical cord mononuclear cells, NOD - non-obese diabetic, T1D - type 1 diabetes, AD-MSC - adipose derived mesenchymal stem cells, CB-MSC – cord blood mesenchymal stem cells, MSC - mesenchymal stem cells, T_{regs} – regulatory T cells, CD – cluster of differentiation, STZ – streptozotocin, GFP, green fluorescent protein, cGy – centigray, NOR – non-obese resistant, BMSC – bone marrow mesenchymal stem cells, NSG – NOD/*Scid* gamma, hBMSC – human bone marrow mesenchymal stem cells, PBMCs - peripheral blood mononuclear cells

1.6.3 MSCs as targets for the generation of surrogate β-cells

Ex vivo generation of IPCs is commonly performed via differentiation of precursor/stem cells using unique chemical regimens[296-300]. Alternatively, IPCs can be generated via viral-mediated gene transfer resulting in the transdifferentiation of lineage-committed cells such as hepatocytes[76-78, 133, 134], pituitary cells[75, 111] and endocrine K cells[131, 301]. Currently, encapsulation of IPCs is necessary to prevent recurrent autoimmune destruction or allorejection[302, 303]. Although micro-encapsulation technology for the most part protects IPCs from $CD4^+$ T cell-mediated destruction, these capsules are not impervious to cytokine-induced apoptosis and require improvements to maintain the survival and function of the encapsulated cells[304]. MSCs are an attractive target for generating IPCs due to their reported immune-modulatory properties. Potentially, IPCs generated from MSCs may retain some MSC-like qualities that could eliminate the need for encapsulation. Currently, there are two methods of generating IPCs from MSCs: chemically-induced and viral-mediated transdifferentiation.

1.6.3.1 Chemically-induced transdifferentiation

Deriving IPCs from stem cells has most commonly been performed by adapting *in vitro* transdifferentiation protocols to yield high numbers of fully functional IPCs[296, 297]. IPCs can be obtained from MSCs via the use of high glucose culture medium[298, 299] or nicotinamide-enriched medium to induce transdifferentiation[300]. The resulting differentiated cells express insulin at both the mRNA and protein level, and ameliorate hyperglycaemia in STZ-rats[300]. Similarly, it is possible to induce glucose-responsive IPC transdifferentiation from BMSCs *in vitro* using a three-step protocol resulting in high expression levels of *Pdx-1,* insulin and glucagon[305]. In addition, BMSCs isolated for expression of primitive stage-specific embryonic antigen-1 (SSEA-1) and a number of MSC markers such as CXC chemokine

receptors, octamer-binding transcription factor-4 and SCA-1 were induced to differentiate into IPCs in defined transdifferentiation medium[306]. These SSEA-1$^+$ cells were able to further differentiate into islet-like clusters that stained positive with dithizone staining and were capable of secreting insulin in a glucose-responsive manner. MSCs derived from adipose tissue[307-309] and umbilical cord blood/Wharton's jelly[310-312] have been subjected to similar chemically-defined transdifferentiation protocols that also resulted in the successful generation of IPCs.

1.6.3.2 Viral-mediated transdifferentiation

Gene therapy in the form of viral-mediated gene transfer has been investigated as a method to re-introduce normal copies of DNA into abnormal cells, or other cell types, as a means of treating genetic diseases for some time. Early concerns regarding the safety of viral vectors for gene therapy as a consequence of the results of the 1999 severe *Scid* trial[121] led to modern engineering of viral vectors that do not replicate and efficiently transduce genes into target cells[132]. Ideally, β-cell engineering would employ integrating viral vectors that provide sustained therapeutic gene expression over the life of the patient. To this end, viral-mediated transdifferentiation is an attractive method of obtaining surrogate β-cells as they would be less likely to express identical autoantigens against which the primary autoimmune response was developed.

The ability to induce pancreatic transdifferentiation has been studied mostly in hepatocytes due to the fact that the liver and pancreas are derived from the same endodermal origin[114]. Since transcription factors play a significant role in determining islet-cell fate during pancreatic embryogenesis, our laboratory and many others have investigated the direct transfer of β-cell transcription factors and insulin as mediators of pancreatic transdifferentiation[76-78, 93, 133, 134, 150, 204]. We have shown that the lentiviral delivery of *INS*-

FUR via intervallic infusion in full flow occlusion is as successful as the direct transfer of β-cell transcription factors in mediating transdifferentiation and reversing diabetes[77, 133, 134].

Due to the success of gene transfer in generating IPCs from a number of cell types, and the requirement for encapsulation to translate the basic research into the clinical setting, MSCs have become an attractive target for combinatorial gene and cell therapy. Consequently, a number of studies were performed investigating the *ex vivo* targeting of MSCs for viral-mediated transdifferentiation into IPCs. A study by Karnieli *et al*, utilised retrovirus for the transduction of BMSCs with the key pancreatic transcription factor *Pdx-1*, resulting in glucose-responsive production of insulin[94]. Furthermore, when these cells were transplanted under the renal capsule of STZ-diabetic *Scid* mice, they were able to reduce glucose levels after five weeks for a period of 6-8 weeks, after which abnormal glucose tolerance was observed. In fact, *Pdx-1* has been delivered to MSCs from a variety of tissue sources, including BMSC[123, 192-195], UC-MSC[196], and AD-MSC[92, 197, 198] with varying success in the generating glucose-responsive IPCs.

Insulin transfer to MSCs has been performed less often when compared to transcription factor transfer, most likely due to the fact that *ex vivo* transfer of insulin alone is insufficient to induce pancreatic transdifferentiation, and, most commonly results in constitutive insulin secretion. As mentioned previously, Xu *et al*,[123] showed that BMSCs expressing the human insulin were able to restore normoglycaemia in STZ-diabetic mice. The results showed that BMSCs successfully expressed insulin and were able to maintain normoglycaemia for at least 42 days. In addition, transduced BMSCs were able to evade autoimmune destruction that ordinarily targets pancreatic islet. Similarly, AAV and retroviral vectors have been utilised to transduce human BMSC with insulin under the control of the CMV promoter[313, 314], however this resulted in cells that constitutively secreted insulin. Since the engineered BMSC did not express the GLUT2 and islet glucokinase genes, it is unlikely that they would be glucose-

responsive. This feature would only develop following transdifferentiation rather than forced insulin expression. As a result, induction of pancreatic transdifferentiation for the production of IPCs should be mediated via transfer of specific pancreatic transcription factors, either alone or in combination, and in addition to the expression of insulin. The success of MSC-derived IPCs in pre-clinical animal models of diabetes is summarised in Table 1.8.

Table 1.8: Summary of the major MSC-derived IPCs in pre-clinical animal models of T1D

Intervention	Outcomes	Fresh/Frozen	Reference
Chemical-differentiation	Human BMSCs formed spheroid islet-like clusters containing IPCs that expressed multiple pancreatic genes. The clusters released insulin in a glucose-dependent manner and ameliorated diabetes in STZ-treated nude mice.	Fresh	291
Chemical-differentiation	BMSCs transdifferentiated into IPCs that upon transplantation acquired islet-like architecture. The aggregates developed an endocrine gene expression profile and demonstrated expression of proinsulin and/or secretion of active insulin upon glucose challenge. Sub-capsular renal transplantation of these aggregates lowered circulating blood glucose levels.	Fresh	293
Chemical-differentiation	Differentiated BMSCs expressed multiple pancreatic genes and exhibited glucose-stimulated insulin release. Upon transplanted into STZ-induced diabetic mice they imparted reversal of hyperglycaemia and improved metabolic profiles in response to IPGTT.	Fresh	294
Chemical-differentiation	Pancreatic genes were expressed in the differentiated cells. C-peptide release was increased after glucose challenge *in vitro*, and upon transplantation of differentiated cells into diabetic rats, blood sugar levels decreased.	Fresh	305
Viral-mediated	hMSCs were successfully differentiated into IPCs. The IPCs expressed multiple islet-cell genes and released insulin/C-peptide in a weak glucose-regulated manner. Following transplantation into STZ-induced diabetic mice, normoglycaemia was obtained within 2 weeks and maintained for at least 42 days.	Fresh	189
Viral-mediated	Differentiated cells expressed of all four islet hormones. However, the cells lacked expression of *NeuroD1*. Significant insulin content and glucose-stimulated insulin release was demonstrated *in vitro*. Cell transplantation into STZ-diabetic immune-deficient mice resulted in further differentiation, including induction of *NeuroD1* and reduction of hyperglycaemia.	Fresh	190
Viral-mediated	BMSCs self-assembled to form functional pancreatic islet-like structures. Differentiated BMSCs also expressed islet genes and exhibited glucose-induced insulin secretion. Grafted animals were able to maintain their body weight and survive for relatively longer periods of time than hyperglycaemic sham-grafted controls.	Fresh	191
Viral-mediated	Differentiated AD-MSC expressed some islet genes. Transduced cells secreted increasing amounts of insulin in response to increasing concentrations of glucose and upon transplantation in STZ-diabetic rats resulted in lowered blood glucose and higher glucose tolerance.	Fresh	193
Viral-mediated	STZ-treated mice transplanted with transduced ASCs showed significantly decreased blood glucose levels and increased survival, compared to control mice. Expression of *Pdx1* in ASCs did not induce the pancreatic phenotype *in vitro*. Upon transplantation the cells engrafted in the pancreas, wherein they expressed insulin and C-peptide.	Fresh	86
Viral-mediated	The body weight in diabetic mice that received GFP-mMSCs expressing the human insulin gene was increased by 6% within 6 weeks after treatment.	Fresh	117

Abbreviations: BMSC – bone marrow mesenchymal stem cells, IPCs – insulin producing cells, STZ – streptozotocin, IPGTT – intraperitoneal glucose tolerance test, hMSCs – human mesenchymal stem cells, *Pdx-1* – pancreatic and duodenal homeobox 1, *NeuroD1* – neuronal differentiation 1, AD-MSC – adipose derived mesenchymal stem cells, GFP – green fluorescent protein

1.6.4 Considerations for the use of MSCs in T1D clinical trials

Due to the success of MSC infusions and MSC-derived IPCs in pre-clinical animal models of diabetes, a number of human clinical trials have been undertaken and are currently in progress (Table 1.9). In translating pre-clinical studies to the human clinical setting, many of those conducting clinical trials have failed to consider the scientific basis of MSC function that makes their use in the pre-clinical setting so successful. Maintenance of MSC function for successful clinical trials is highly linked to choice of donor, preliminary *ex vivo* cell culture conditions, cryopreservation and post-storage culture conditions; four caveats that have been overlooked and are a hallmark of the current clinical failure of MSCs for the treatment of T1D and other diseases[315].

Many clinical trials utilising MSCs have been harvested from a single donor, culture expanded and cryopreserved prior to administration to a trial participant. Donor variability is a concern that requires careful assessment prior to harvesting MSCs for clinical trials, as phenotype, age and gender can affect MSC function and growth characteristics[313, 314, 316]. Consequently, the choice of a suitable donor is critical, as MSCs with a dampened immunomodulatory profile are less likely to perform as well *in vivo* as MSCs with a robust immunomodulatory profile. As such, profiling of multiple donors for MSC immunomodulatory function should be included as a necessary control step prior to the commencement of a clinical trial. Compounding single donor harvesting is the fact that MSCs constitute a small proportion of the cellular fraction of the tissue from which they are sourced (BMSC, 0.001-0.02% and AD-MSC, 1-10%)[317, 318]. As a result, culture expansion is required to generate clinically sufficient quantities of MSCs for transplantation, a process that results in phenotypic changes such as a decrease in proliferative capacity and self-renewal. In addition, the off-the-shelf "one harvest, multiple therapies" concept fails in the clinic, mainly

due to the extensive *ex vivo* culture required, referenced in the Prochymal® study (Table 1.9). The major contributing factor to the success vs failure in pre-clinical vs clinical trials of MSCs is that pre-clinical studies utilise freshly harvested MSCs from either single or multiple animal donors followed by immediate transplantation into the animals to be treated. Minor cell expansions are acceptable; however ongoing expansion for upscaling of cell quantities ultimately detrimentally affects MSCs in the clinical setting.

Naturally, storage of cell therapies is a crucial process in conducting clinical trials. With trial participants required to travel long distances to receive treatment, the need to preserve stocks of therapeutic cells in the interim is imperative. Cryopreservation is the most popular form of cell preservation and in the clinical setting is a practical form of bio-banking. However, a number of studies have shown that cryopreserved MSC have an impaired immunosuppressive profile in comparison to fresh MSCs, explaining the failure of many clinical trials utilising cryopreserved, culture expanded MSCs[319-321]. This feature is characterised by increases in expression of heat shock proteins, a lack of IFN-γ mediated IDO production and a reduced immunosuppressive effect on T-cell populations. Interestingly, post-cryopreservation culture for 24 hours reverses these effects[319]. As such, successful clinical use of MSC for the treatment of T1D (and many other diseases) requires careful trial organisation, focusing on the appropriate and responsible use of MSCs. In future, regulation of critical processes such as donor choice, minimal post-harvest expansion, and post-freeze MSC culture could result in more successful clinical trials that fulfil the promise of pre-clinical studies and that of the exciting prospect of MSCs as a cellular therapy for T1D.

Table 1.9: Summary of the major ongoing and completed clinical trials utilising MSCs as a treatment for T1D

Trial Number	Phase	Intervention	Outcomes	Fresh/Frozen	Status	Reference
NCT01068951	N/A	Intravenous, autologous transplantation of MSCs (approximately $2x10^6$ cells/kg body weight)	Patients in the control arm showed loss in both C-peptide peak values and C-peptide when calculated as area under the curve during the first year. In MSC-treated patient, these responses were preserved or even increased. No side effects of MSC treatment were observed	Fresh	Completed 2014	276
NCT01374854	1/2	1×10^6/kg UC-MSCs are infused through the pancreatic artery along with BM-MNCs by interventional therapy and another same dose of UC-MSCs administered one week post-intervention	C-peptide increased 105.7% in 20 of 21 responders versus 7.7% decrease in control subjects. HbA1C decreased 12.6% in treated versus 1.2% increase in control subjects. Daily insulin requirements decreased 29.2% in treated versus no change in control subjects.	Fresh	Completed 2012	277
NCT00703599	1/2	I.v. administration of autologous activated stromal vascular fraction derived from 100-120ml lipoaspirates following mini-liposuction of abdominal adipose tissue	Not reported	Frozen	Estimated completion of 2009	278
NCT01219465	1/2	Intravenous transfusion of UC-MSCs ($2x10^7$ cells/kg body weight)	No reported acute or chronic side effects in MSC-treated versus saline control. Both HbA1c and C-peptide in MSC-treated patients were significantly better than either pre-therapy values or saline control patients during the follow-up period	Fresh	Completed 2012	279
NCT01996228 NCT01350219	1/2	Human UC-MSCs within the Stem Cell Educator device	A single treatment provided lasting reversal of autoimmunity that allowed regeneration of islet β-cells and improvement of metabolic control in subjects with long-standing T1D	Fresh	Recruiting	282-285
NCT02057211	2	Transfusion of autologous MSC versus sham MSC transfusion vs placebo control	N/A	Fresh	Recruiting	N/A
NCT00646724	1/2	Co-transplantation of islet allograft and MSC autograft	Not reported	Frozen	Estimated completion of 2012	N/A
NCT01143168	1	Multiple transplantation of BM-MNC + UC-MSCs	Not reported	Frozen	Estimated completion of 2011	Cellonis Biotech Pty Ltd.
NCT01322789	1/2	Four consecutive intravenous infusions, one week apart followed by four consecutive infusions 1 month apart	Not reported	Frozen	Estimated completion of 2015	N/A

NCT01496339	1/2	1×10^6/kg MenSCs are infused through the pancreatic artery or intravenously once a week in four consecutive therapies	Not reported	Frozen	Estimated completion of 2014	S-Evans Biosciences Pty Ltd.
NCT02644759	1/2	Purification of autologous, leukapheresis-derived $CD34^+/CD133^+$ stem cells and transplantation into the pancreatic artery and capillaries via interventional radiology techniques. Halting immune attack on pancreatic β-cells through immunomodulation by incubation of patient's leukapheresis UC-MSCs for 3-6 hours, and return of the patient's own white blood cells back via intravenous injection	N/A	Fresh	Ongoing, not recruiting	Stem Cells Arabia
NCT00690066	2	Intravenous infusion of *ex vivo* cultured adult human MSCs vs placebo intravenous infusion of excipients of PROCHYMAL®	Not reported	Frozen	Completed 2014	Osiris/ Mesoblast International Sarl
NCT01157403	2/3	Intravenous autologous transplantation of BMSC (approximately $2.5x10^6$ cells/kg body weight)	Not reported	Frozen	Estimated completion of 2014	N/A

Clinical trial data was acquired from www.clinicaltrails.gov using the search terms “Mesenchymal stem cells” and “Type 1 diabetes”. Abbreviations: MSC, mesenchymal stem cells; T1D, Type 1 diabetes; UC-MSC, umbilical cord mesenchymal stem cells; BM-MNC, bone marrow mononuclear cells; BMSC, bone marrow derived mesenchymal stem cells; MenSCs, menstrual blood mesenchymal stem cells, AD-MSC, adipose tissue derived mesenchymal stem cells; CD, cluster of differentiation

1.7 Thesis research project

There are two hurdles associated with the clinical development of the current gene therapy approach developed in our laboratory: (i) the use of cell lines that are tumour-derived and (ii) the direct delivery of the insulin gene to the liver, which involves invasive surgery. To overcome these shortcomings, I used primary bone marrow-derived mesenchymal stem cells as targets for *ex vivo* gene modification that were subsequently returned to a syngeneic host at the less invasive subcutaneous site.

Stromal cells were first isolated from the bone marrow of NOD mice, and BMSCs were enriched for using antibody-based fluorescence-assisted cytometric sorting (FACS). Enriched BMSCs were subsequently nucleofected to express the bioluminescent luciferase (*Luc2*) and *CDUPRT* genes to assess the persistence of a subcutaneous transplant of BMSCs in immune-competent (NOD) and immune-deficient (NOD/*Scid*) animal models of diabetes. *CDUPRT* is a pro-drug converting enzyme, otherwise known as a suicide gene that is routinely used in the Martiniello-Wilks laboratory[219, 322]. In this study CDUPRT was utilised as a cell therapy experimental 'off' switch. *CDUPRT* converts the largely non-toxic pro-drug 5-fluorocytosine (5-FC) into the toxic metabolite 5-fluorouracil (5-FU) that causes BMSC death.

Bioluminescent BMSCs were later targeted for gene transfer with the lentiviral vectors encoding the *INS-FUR*, and murine *NeuroD1* and *Pdx1* genes for differentiation into IPCs. Based on the previous success of this approach in H4IIE cells, it was expected that BMSCs forced to express *INS-FUR* and *NeuroD1* would transdifferentiate into surrogate β-cells that are characterised by the expression of β-cell transcription factors and GSIS. Upon transplantation into the STZ-NOD/*Scid* diabetic mouse model, it was expected that the cells would reverse diabetes. Suicide gene therapy in the form of the *CDUPRT* gene was installed

as a clinical fail-safe switch that enabled the non-invasive removal of the transplanted cells to correlate restoration of normoglycaemia to the cell transplantation, and also destroy the graft in the event of unexpected changes in the engrafted cells.

The aims of this project were:

1. To isolate a primitive population of mesenchymal stem cells from NOD mouse bone marrow.
2. Monitor the persistence of a syngeneic transplant of luciferase (*Luc2*)-expressing BMSCs in an immune-competent and immune-deficient model of diabetes.
3. Investigate the capacity for *INS-FUR*, *NeuroD1* and *Pdx1* to induce transdifferentiation in mouse BMSCs.
4. Determine the efficacy and safety of *INS-FUR* gene modified BMSCs to reverse diabetes in STZ-diabetic NOD/*Scid* mice.

Chapter 2

General Methods

2.1 Culture and maintenance of parental and gene-modified BMSCs

For all parental BMSC culture purposes, the culture medium (complete medium) was composed of α-MEM (Lifetechnologies™), 1% 100x Penicillin-Streptomycin-Glutamine (P/S/G) (Lifetechnologies™), 10ng/ml basic fibroblast growth factor (bFGF) and 20% Foetal Calf Serum (FCS) (Lifetechnologies™). Prior to cryopreservation, cells were sub-passaged in 6-well plates (BD Biosciences Falcon®) in a 4-fold serial dilution. Sub-passaging of cells was carried out when one well of a 6-well plate had reached 85-90% confluency. The cells were then expanded to 10x 175cm^2 flasks at early, mid and late passage for cryopreservation in 10% dimethyl sulfoxide (DMSO)/FCS.

For BMSCs nucleofected to express the *Luc2* and *CDUPRT* genes, 200µg/ml of Hygromycin B (Lifetechnologies™, USA) was added to the complete media for cell selection and maintenance. Nucleofected BMSCs gene-modified with lentiviral vectors that were sorted for green fluorescent protein (GFP) or mCherry expression were also maintained in complete media + 200µg/ml of Hygromycin B. The cells were subsequently expanded to 10 x 175cm^2 flasks for cryopreservation.

2.2 Cell proliferation assays

Cells were initially expanded in T75 flasks, and subsequently 2.5x10^3 cells/well in triplicate (technical) were seeded in 24-well plates (BD Biosciences Falcon®) and grown in complete media for a total of 15 days. On days 0, 3, 7, 11 and 15, cells were detached with 1x TrypLE™ Express Enzyme (Lifetechnologies™, USA) and assessed for viability by trypan

blue exclusion using 0.4% Trypan Blue Solution (Lifetechnologies™, USA). Total cell and viable cell counts were recorded, and the data represented on growth curves as mean ± standard deviation (SD).

2.3 Clonogenicity assays

Cells were resurrected in T75cm^2 flasks and cultured for a period of 1 week. Following detachment, the cells were resuspended in culture medium to a concentration of 5x10^2 cells/ml and 1ml of cells was added to 10cm^2 tissue-culture treated plates (BD Biosciences Falcon®) containing 9ml of culture medium in triplicate (technical and biological) (n=3). The plates were then incubated at 37ºC/5% CO_2 for 10 days, after which the media was removed and the cells washed with 1x Phosphate Buffered Saline (PBS). The cells were then stained with 0.4% methylene blue/60% methanol for 1 hour, and de-stained in a series of three washes with tap water and left to dry overnight. The total number of colonies per plate was counted by eye, with a colony described as having a minimum diameter of ~1-2 mm and consisting of at least 50 cells. Images of clonogenicity assays were obtained using the Epson® Perfection 4870 Photo scanner and Epson® Scan software.

2.4 Differentiation assays

2.4.1 Adipogenic differentiation

Cells were harvested at ~85-90% confluency and resuspended in cold culture medium to a concentration of 2.5x10^4 cells/ml. Adipogenesis assays were setup in 24-well plates (BD Biosciences Falcon®) as described in Figure 2.1. Briefly, 2.5x10^4 cells/ml of each cell population were seeded into a 24-well plate in triplicate (technical and biological) (n=3) and

grown to 80-90% confluency. At this point, the media was removed and replenished with either control medium (α-MEM, 1% P/S/G and 2% FCS) or adipogenic differentiation medium (α-MEM, 1% P/S/G, 2% FCS, 1µM Dexamethasone, 0.5µM 3-Isobutyl-1-methyl-xanthine, 100µM Indomethacin and 10µg/ml Insulin). The cells were incubated at 37ºC/5% CO_2 for 10 days, during which the media was changed every 3 days.

On day 10 of the assay, the media was removed from the plates and the cells washed with 1x PBS. The PBS was removed and the cells fixed in 500µl of 10% neutral buffered formalin (Sigma-Aldrich, Australia) for 30 min. The fixative agent was removed and the cells washed with 1x PBS. After carefully removing the PBS, the cells were stained with 1ml of 0.2% (w/v) Oil Red O (Fronine®) for 15 min. Following staining, the Oil Red O was removed and the cells washed twice with 1x PBS. The cells were then stored in 1x PBS + 0.2% sodium azide (Sigma-Aldrich™, Australia) at 4ºC.

2.4.2 Osteogenic differentiation

Cells were harvested at ~85-90% confluency and resuspended in cold culture medium to a concentration of $1.25x10^4$ cells/ml. Osteogenesis assays were setup in 24-well plates as described in Figure 2.1. Briefly, $1.25x10^4$ cells/ml of each cell population were seeded into a 24-well plate in triplicate (technical and biological) (n=3) and grown to 90-100% confluency. At this point, the media was removed and replenished with either control medium (DMEM (GIBCO®, Lifetechnologies™), 1% P/S/G and 1% FCS) or osteogenic differentiation medium (D-MEM, 1% P/S/G, 10% FCS, 0.1µM Dexamethasone, 0.2mM ascorbic acid (asc) and 10mM β-glycerophosphate). The cells were incubated at 37ºC/5% CO_2 for 35 days, during which the media was changed every 3 days.

On day 35 of the assay, the media was removed from the plates and the cells washed with 1x PBS. The PBS was removed and the cells fixed in 500µl of 10% neutral buffered formalin (Sigma Aldrich, Australia) for 30min. The fixative agent was removed and the cells washed with 1x PBS. After carefully removing the PBS, the cells were stained with 1ml of 2% (w/v) (pH 4.1) Alizarin Red S (Fronine®) for 45 min. Following staining, the Alizarin Red S was removed and the cells washed twice with 1x PBS. The cells were then stored in 1x PBS + 0.2% sodium azide (Sigma-Aldrich™, Australia) at 4ºC.

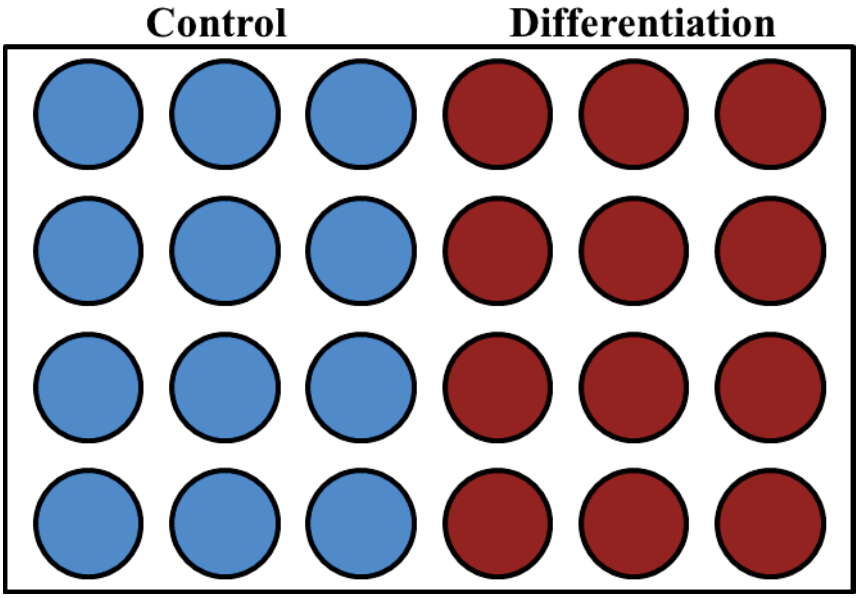

Figure 2.1: Schematic representation of adipogenesis and osteogenesis differentiation assay Stromal cells, BMSC and double positive cells were compared for their capacity to undergo adipogenic and osteogenic differentiation. The schematic illustrates the setup of individual plates that were biologically repeated three times (n=3). Control assays are denoted in blue and differentiation assays are denoted in red.

2.4.3 Chondrogenic differentiation

Stromal cells and BMSC (2 x 10^5) were centrifuged at 450g for 10 min in triplicate U-bottom wells of a 96 well plate. Chondrogenic medium contained high glucose, serum-free DMEM (Lifetechnologies™, USA), 500ng/mL bone morphogenic protein-2 (R&D Systems), 10ng/mL transforming growth factor β3 (R&D Systems), 10µM dexamethasone (Sigma), 50µg/mL ascorbate-2-phosphate (Sigma), 40µg/mL proline (Sigma), 100µg/mL pyruvate (Sigma) and 50mg/mL ITS + Pre-mix (BD Biosciences). High-glucose, serum-free DMEM was used as control medium. Media were replaced every 3 to 4 days for 25 days. Cells and micro-mass were embedded in agar, fixed in 10% formalin for 2 hours prior to paraffin embedding. Sections (5µm) were stained with 1% Toluidine blue (pH 2.0-2.5) to show cartilage formation (purple staining).

2.4.4 Analysis of differentiation assays

Qualitative scoring of positively stained cells was performed according to the method described by Wang *et al*[237]. For adipogenic differentiation, the number of positively stained cells in ten high power fields (40x magnification) per well of a 24-well plate were counted and scored according to the number and intensity of stained vesicles within individual cells. For osteogenic differentiation, the number of positively stained cells in ten high power fields (40x magnification) per well of a 24-well plate were counted and scored according to staining intensity correlating to immature (brown) or mature (red) osteogenesis. The data was analysed using GraphPad Prism 7®. Values expressed as count per cm^2 represented as mean ± SD. A two-way ANOVA with Bonferroni's post-hoc tests was performed ($p< 0.05$).

2.5 Bacterial preparation of plasmids

2.5.1 Bacterial transformation

2.5.1.1 Mammalian expression plasmids

Purified plasmid DNA or ligation material (10-100ng) was added to 25ul of One Shot® TOP10 Chemically competent *E. coli* (Lifetechnologies™) and incubated on ice for 30 min. The *E. coli* were heat-shocked at 42ºC for 45 sec, and immediately transferred to ice for 2 min. S.O.C medium (Lifetechnologies™, USA) (250µl) was added to the transformation reactions, the bacterial suspensions transferred to 15ml falcon tubes and incubated at 37ºC with shaking at 225rpm for 1 hour. Two volumes (50µl and 100µl) of the bacterial cultures were then spread on selective Luria Broth (LB) agar plates (10g/L Tryptone, 5g/L Yeast extract, 5g/L NaCl) containing Hygromycin B (100µg/ml) and incubated overnight at 37ºC.

2.5.1.2 Lentiviral expression plasmids

Purified plasmid DNA or ligation material (10-100ng) was added to 25ul of One Shot® Stbl3 TOP10 Chemically competent *E. coli* (Lifetechnologies™) and incubated on ice for 30 min. The *E. coli* were heat-shocked at 42ºC for 30 sec, and immediately transferred to ice for 2 min. S.O.C medium (Lifetechnologies™, USA) (250µl) was added to the transformation reactions, the bacterial suspensions transferred to 15ml falcon tubes and incubated at 37ºC with shaking at 225rpm for 1 hour. Two volumes (50µl and 100µl) of the bacterial cultures were then spread on selective LB agar plates (10g/L Tryptone, 5g/L Yeast extract, 5g/L NaCl) containing Ampicillin (100µg/ml) and incubated overnight at 37ºC.

2.5.2 Generation of plasmid clones

Five to ten single colonies were selected from selective LB agar plates containing and restreaked onto new selective LB agar plates and incubated overnight at 37ºC to confirm true antibiotic resistance due to successful transformation. A single colony from each restreaked, clonal plate was inoculated in a 15ml falcon tube containing 3-5ml S.O.C medium (Lifetechnologies™, USA) supplemented with the appropriate antibiotic and incubated for 16 hours at 37ºC/225rpm.

2.5.3 Plasmid glycerol stocks

One 15ml falcon tube of each transformant culture was centrifuged at 12,000g for 5 min, and the pellet resuspended in 1ml of 1:1 1x M9 minimal salts (Lifetechnologies™)/50% Glycerol. The resuspended cells were then transferred to new cryovials and stored at -80ºC.

2.5.4 Plasmid preparation (Miniprep)

Plasmid DNA was isolated from the bacterial pellets using the PureLink® Quick Plasmid Miniprep Kit (Lifetechnologies™) according to the manufacturer's instructions. Briefly, cultures of plasmid transformants were centrifuged at 12,000g for 5 min and resuspended in 250µl of Resuspension Buffer (R3) containing RNase A (20mg/ml). An equal volume of Lysis Buffer (L7) was added, and the mixture inverted gently and incubated for 5 min at room temperature. Precipitation Buffer (N4) (350µl) was added and the tube mixed immediately until the mixture became clear. The lysate was centrifuged at 12,000g for 10 min and the supernatant loaded onto a spin column in a 2ml wash tube. The supernatant was centrifuged through the column at 12,000g for 1 min, and the flow-through discarded. Wash Buffer (W10) (500µl) with ethanol was added to the column, incubated for 1 min at room

temperature and centrifuged at 12,000g for 1 min. The flow-through was discarded, 700µl of Wash Buffer (W9) with ethanol was added to the column and the column centrifuged twice at 12,000g for 1 min. Following the final centrifugation, the column was transferred to a 1.5ml collection tube and 20µl of Nuclease-free water (Lifetechnologies™) was added directly to the column and incubated for 1min at room temperature. The column was then centrifuged at 12,000g for 2 min, and the recovered purified plasmid DNA was stored at -20ºC for long-term storage, or used immediately in subsequent experiments.

All plasmid DNA preparations were assessed for purity on a 1% (w/v) agarose gel, run at 90V in 1x Tris/Borate/EDTA (TBE) buffer for 90 min. Plasmid quality and concentration was assessed using the NanoDrop™ 2000 spectrophotometer (Thermofisher Scientific™). Following the confirmatory diagnostic digest of the generated plasmids, plasmids identified as positive for the incorporation of the genes of interest were prepared for either nucleofection or transduction using the PureLink® Quick Plasmid Midiprep/Megaprep Kit (Invitrogen, Lifetechnologies™) according to the manufacturer's instructions.

2.6 Gene expression profiling

2.6.1 RNA extraction

RNA extraction was performed from 1 x T175 flask of the respective cell populations with TRIzol® Reagent (Life Technologies™) according to the manufacturer's instructions with slight modifications. Briefly, the cells were detached with 1x TrypLE™ Express Enzyme and centrifuged at 1,000g for 5 min to obtain a pellet. TRIzol® Reagent (1ml) was added to the cell pellet and homogenised by pipetting, followed by incubation at room temperature for 5 min. Chloroform (Sigma-Aldrich, Australia) (0.2ml) per 1ml of TRIzol® Reagent was added to the homogenate, then mixed by rapid shaking for 15 sec and incubated at room temperature for 3 min. The TRIzol® Reagent:Chloroform homogenate was subsequently centrifuged at 12,000g for 15 min at 4ºC to separate the aqueous, inner and organic phases. Following phase separation, the aqueous phase was removed and transferred to a new microcentrifuge tube to which one volume of 100% Isopropanol (Sigma-Aldrich, Australia) was added. The aqueous phase:isopropanol mixture was inverted and incubated for 10 min at room temperature to precipitate the RNA, followed by centrifugation at 12,000g for 10 min at 4ºC to obtain an RNA pellet. The RNA pellet was washed twice with 70% Ethanol (Sigma-Aldrich™, Australia) by centrifugation at 7,500g for 5 min at 4ºC, and resuspended in 20µl of Nuclease-free water for storage at -80ºC or for immediate use in DNaseI treatment in preparation for cDNA synthesis.

The purified RNA was assessed for quality on a 1% (w/v) agarose gel, run at 90V in 1x TBE buffer for 90 min. RNA purity and concentration was assessed using the NanoDrop™ 2000 spectrophotometer.

2.6.2 DNase I treatment of RNA

To remove potential genomic DNA contamination carried over through RNA extraction, DNase I treatment of RNA samples was performed using DNaseI, Amplification Grade (Invitrogen™, Thermofisher Scientific) according to the manufacturer's instructions. Briefly, RNA was DNase I treated as detailed in Table 2.1.

Table 2.1: Components of DNase I treated RNA reactions

Component	Volume (µl)
RNA (1µg)	x µl
DNase I Reaction Buffer (10x)	1µl
DNase I, Amp Grade (1U/µl)	1µl
dH_2O	x µl to 10µl

The reactions were incubated for 15 min at room temperature. To stop the reaction and inactivate the DNase I, 1µl of 25mM, pH 8.0 ethylenediaminetetraacetic acid (EDTA) was added and the reactions incubated for 10 min at 65ºC. The DNase I treated RNA was subsequently stored at -80ºC or used immediately in cDNA synthesis.

2.6.3 cDNA synthesis

Prior to gene expression profiling of target genes via reverse transcriptase polymerase chain reaction (RT-PCR), reverse transcription of the total RNA population was performed using SuperScript® III First-Strand Synthesis SuperMix (Invitrogen™, Thermofisher Scientific) according to the manufacturer's instructions. Briefly, DNase I treated RNA was utilised as

template for cDNA synthesis in simultaneous enzyme (RT-positive) vs no-enzyme (RT-negative) reactions. cDNA synthesis reactions were setup as detailed in Table 2.2.

Table 2.2: Components of cDNA synthesis reactions

Component	RT-positive	RT-negative
DNase I treated RNA (500ng)	x µl	x µl
Random hexamers (50ng/µl)	1µl	1µl
Annealing buffer	1µl	1µl
dH_2O	x µl to 8µl	x µl to 8µl
Incubate for 5 min at 65ºC		
2x First-Strand Reaction Mix	10µl	10µl
SuperScript™ III/RNaseOUT™ Enzyme Mix	2µl	-
dH_2O	-	2µl

The reactions were incubated as follows using a Mastercycler® (Eppendorf™, Germany):

1. 25ºC for 10 min
2. 50ºC for 50 min
3. 85ºC for 5 min

The generated cDNA was stored at -20ºC or used immediately in PCR.

2.6.4 PCR amplification of target genes

The detection of gene targets from the cDNA of various cell samples was performed using PCR Mastermix (Promega®) according to the manufacturer's instructions. Briefly, individual PCR reactions were setup as detailed in Table 2.3.

Table 2.3: Components of PCR mastermix

Component	Final Concentration	Volume (µl)
2x PCR Mastermix (Promega®)	1x	12.5
Forward Primer (10µM)	0.4µM	1
Reverse Primer (10µM)	0.4µM	1
cDNA (25ng/µl)	-	1
RNase-Free Water	-	9.5

The reactions were run on a Mastercycler® with the following conditions:

1. Initial denaturation: 94ºC for 2 min
2. Denaturation: 94ºC for 30 sec
3. Annealing: temp specific to primer set for 30 sec
4. Extension: 74ºC for 1 min

Cycle number (30-40 depending on gene target)

5. Final extension: 74ºC for 5 min

In addition to the RT-positive, a PCR negative (dH_2O only) and RT-negative PCR were set up as controls.

2.6.5 Assessment of PCR products

Prior to running the PCR products on an agarose gel, all electrophoresis apparatus was cleaned with RNeazy® (Invitrogen™, Thermofisher Scientific) to remove any contaminating RNases. PCR products (10µl) were prepared for gel electrophoresis by addition of 2µl of Gel loading dye, Blue (6x) (NEB®, USA) and run on a 1% (w/v) agarose gel stained with 0.5% (v/v) GelRed™ (Biotium®) in 1x TBE buffer at 90V for 90 min. Quick-load® 100bbp DNA ladder and Quick-load® 1kb DNA ladder (NEB®, USA) were used as the standards. Gel images were obtained on the InGenius3 (Syngene®) UV transilluminator and analysed using the GeneSys image acquisition software (Syngene®).

2.7 Bioluminescence imaging

BLI was performed using an IVIS Lumina II Imaging System (Perkin Elmer/Thermofisher Scientific). The system consists of a highly sensitive charge-coupled device (CCD) cooled camera (-90ºC) mounted inside a light-tight imaging chamber (Figure 2.2). The CCD chip is 2.7cm^2 consisting of 2,048 x 2,048 pixels at 13.5µm each. The camera is capable of detecting a minimum radiance of 100 photons/second/cm^2/steridian (p/s/cm^2/sr) and can achieve a minimal image pixel resolution of 50µm. The Lumina II allows a two-dimensional image for analysis. The grey scale photographic images and bioluminescence colour images were superimposed using the Living Image version 3.1 software overlay (Thermofisher Scientific). For quantification, a region of interest (ROI) was manually selected and kept constant between cell culture or mouse images. The area of ROI was kept constant and the BLI intensity was presented as the mean Average Radiance ± SEM (p/s/cm^2/sr) as recommended in the Living Image version 3.1 software manual.

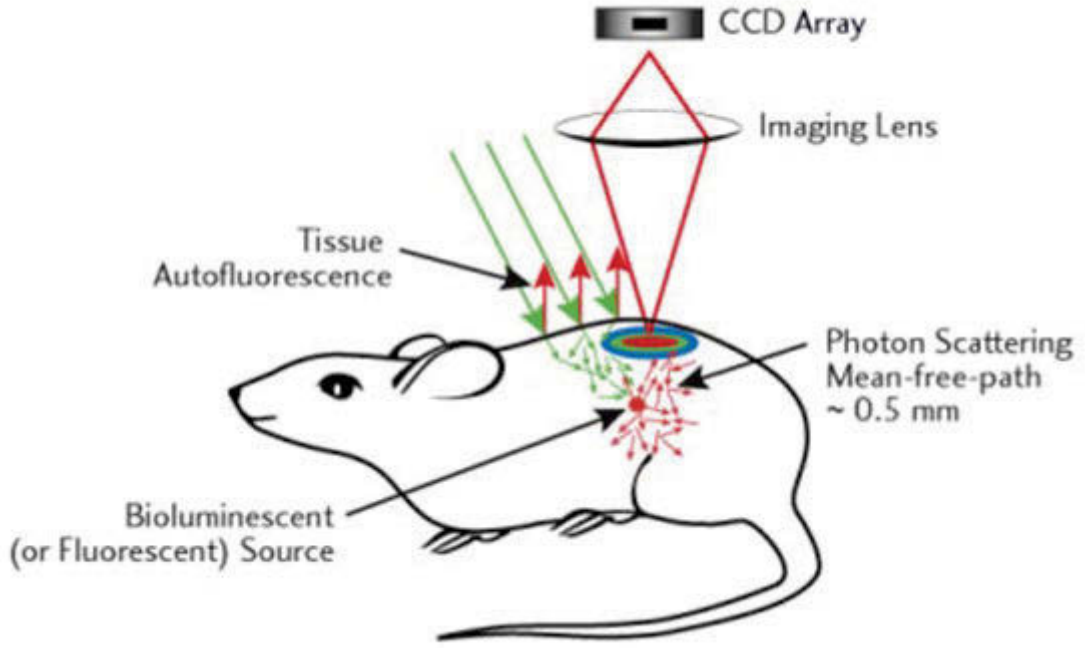

Figure 2.2: Bioluminescence signal detection (Adapted from Living Imaging Software, User's Manual, Version 4.2, Caliper Life Sciences).

2.8 Analytical assessment of insulin concentration

The concentration of human insulin in harvested cell supernatants was analysed using the ARCHITECT™ i4000SR Immunoassay Analyser (Abbott Diagnostics©). Briefly, samples were thawed at room temperature, vortexed and 200µl of each sample transferred to an assay tube. The samples were subsequently loaded on the ARCHITECT™ i4000SR Immunoassay Analyser pre-calibrated with the ARCHITECT™ Insulin Reagent Kit (8K41). Once loaded, samples, anti-insulin coated paramagnetic microparticles, and anti-insulin acridinium-labelled conjugate were combined. Insulin present in the sample bound to anti-insulin coated microparticles and anti-insulin acridinium-labelled conjugate. The sample was subsequently washed, incubated with pre-trigger and trigger solutions, and the resulting chemiluminescent reaction was measured as relative light units (RLUs). A direct relationship exists between the

amount of insulin in the samples and the RLUs detected by the ARCHITECT™ Optical system, with resulting concentrations expressed as μU/ml converted to pmol/L. The analytical sensitivity of the assay is <1.0μU/ml.

2.9 Statistical Analyses

All statistical analysis was performed using GraphPad Prism 7®. Values are represented as mean ± SD or SEM. One-way or two-way ANOVA with Tukey's and Bonferroni's post-hoc tests respectively were performed ($p < 0.05$).

Chapter 3

Isolation and characterisation of murine bone marrow derived mesenchymal stem cells from NOD mice

Introduction

MSCs reside within a number of adult tissues and organs including the placenta[235], cord blood[236], umbilical cord Wharton's jelly[237], lung[238] and adipose tissue[233], however they are predominantly isolated from the bone marrow[233, 234]. A number of techniques commonly used to isolate and enrich for MSCs include antibody-based cell sorting[323], low and high-density culture[324], positive and negative selection[325], frequent media changes[326] and enzymatic digestion[327]. For the purposes of this research, antibody-based positive and negative selection cell sorting was used to enrich for a primitive population of MSCs from the stromal fraction of NOD bone marrow. Two cell surface markers CD45 (also known as leukocyte common antigen or protein tyrosine phosphatase, receptor type C) and Ly6 (also known as stem cell antigen 1) were used to identify MSCs as $CD45^{-}/Ly6^{+}$ with respect to cell surface marker expression.

As mentioned in Section 1.6, the current definition of MSCs by the International Society for Cellular Therapies characterises MSCs as (i) plastic adherent under standard culture conditions; (ii) fibroblast-like in morphology; (iii) possess multi-lineage differentiation potential; (iv) lack expression of haematopoietic markers CD11b, CD14, CD34, CD19 or CD79a, CD45, HLA-DR and the vascular marker CD31[227-231]; and (v) express CD13, CD44, CD54, CD73, CD90, CD105, CD146, CD166, CD200, Sca-1 and Stro-1[227, 229-232]. To confirm the identity of the sorted BMSC population, functional assays such as clonogenicity and multi-lineage differentiation assays were performed. In addition, native BMSCs should not intrinsically express pancreatic genes, therefore gene expression profiling of BMSCs was performed to characterise native BMCSs with respect to pancreatic gene expression.

Specific Aims

- Identify and enrich a unique population of BMSCs from NOD mice via FACS analysis and sorting.
- Confirm the identity of NOD BMSCs through via clonogenicity and multi-lineage differentiation functional assays.
- Characterise the pancreatic gene expression profile of native NOD BMSCs via RT-PCR.

3.2 Specific methods

3.1.1 Sourcing of animals

Twenty female NOD mice at six weeks of age (19-23g) were sourced from the Animal Resources Centre (WA, Australia). They were housed within the Ernst Facility at UTS in a polycarbonate green line individually ventilated cage (IVC) system, with corncob bedding, irradiated rat and mouse feed (Gordon's Specialty Stock Feeds) and unlimited reverse osmosis (RO) water. All bedding and housing equipment was autoclaved prior to use. The temperature and humidity of the animal rooms was maintained within 22-24^{o}C and 40-60% respectively. A maximum of four animals were housed per cage and monitored daily by the Ernst Facility technicians until they were required for experimental work, after which animals were monitored daily by the researcher and Ernst Facility technicians.

All animal work was approved by the UTS Animal Care and Ethics Committee (ACEC 2011-447A; ACEC 2009-244A) and complied with the Australian code for the care and use of animals for scientific purposes[328].

3.1.2 Surgical isolation of mesenchymal stromal cells

This methodology was developed by Dr Martiniello-Wilks. Twenty female NOD mice were checked daily for eight weeks prior to euthanasia at fourteen weeks of age. Mice were euthanised within a CO_2 chamber, followed by a cervical dislocation to confirm death and ensure no post-death sensation. The mice were subsequently submerged in 80% ethanol to ensure sterility and transferred to a biosafety hood for further manipulation.

A circumferential incision was made in the skin below the ankles of the hind legs using a surgical scalpel, and a subsequent perpendicular cut ~1cm in length was made proximal to the initial incision on the lateral side of the tibia using surgical scissors. The skin was then pulled back the length of the entire limb to the hip and removed, revealing the muscle belly beneath. The hind limbs were washed with 80% ethanol to remove any fur, and subsequently removed from the animals. Muscle tissue was excised from the femurs, and the femurs detached from the entirety of the limb. Epiphyses were cut from the proximal and distal joints of the femurs and retained in 1x PBS for downstream culture of mesenchymal stromal cells.

Using a 23 Gauge PrecisionGlide™ needle (BD Medical®) and 1x PBS, bone marrow was flushed from the femurs into a 50ml falcon tube and centrifuged at 1200g for 5 min. The cell pellet was then resuspended in 10ml of culture media (α-MEM, 1% P/S/G and 20%) transferred to a 75cm^2 culture flask (BD Biosciences Falcon®) containing epiphyses and incubated at 37^{o}C/5% CO_2 for an initial period of six weeks. Plastic adherent stromal cells were then subcultured and expanded for two passages (with epiphyses) prior to flow-assisted cytometric sorting (FACS) of unique stem cell populations.

3.1.3 FACS sorting a unique population of MSCs

This methodology was developed by Dr Martiniello-Wilks. Plastic adherent stromal cells (passage 2) were washed with Hank's Balanced Salt Solution (HBSS) (Lifetechnologies™, USA) and incubated with 1x TrypLE™ at 37^{o}C/5% CO_2 for 10 min to detach the cells from the flasks. One volume of culture medium was added to the detached cells to inactivate the TrypLE™, and the cells subsequently centrifuged at 1200g for 5 min. The cell pellet was washed by resuspension in HBSS and centrifugation at 1200g for 5 min.

The stromal cells were resuspended in 1x PBS + 5% FCS to a concentration of $5x10^6$ cells/ml, and 100µl of resuspended cells ($5x10^5$ cells/tube) aliquoted into four new 5mL Round Bottom Polystyrene Test Tubes with Cell Strainer Snap Caps (Corning™) on ice. Staining of stromal cells with rat anti-mouse CD45 monoclonal antibody (mAb) conjugated to allophycocyanin (APC) (0.2mg/ml) (BD Pharmingen™) and rat anti-mouse Ly6 (Sca-1) mAb conjugated to phyoerythrin (PE) (0.2mg/ml) (BD Pharmingen™) was setup as per Table 3.1. Briefly, cells were stained with each antibody individually for 30 min and washed with cold 1x PBS + 5% FCS. Following antibody staining, cells were resuspended in 100µl of 1x PBS + 5% FCS and sorted at the Advanced Cytometry Facility (Centenary Institute, Sydney, Australia) on a BD FACSAria™ II using the voltage settings in Table 3.2. Flow cytometry data was analysed using BD FACSDiva™ software (Version 6.1.3). The stromal cells were sorted into two distinct populations based on the expression pattern of the selected markers: $CD45^-/Ly6^+$ (BMSC) and $CD45^+/Ly6^+$ (Double positive). Sorted cells were centrifuged at 1200g for 5 min, resuspended in 5mls of culture medium (α-MEM + 20% FCS + 1% P/S/G) and transferred to a T25cm^2 flask (BD Biosciences Falcon®) and incubated at 37ºC/5% CO_2.

Table 3.1: Stromal cell antibody staining setup for FACS

Antibody Staining	Volume of cells (µl)	Volume of CD45-APC conjugated antibody (µl)	Volume of Ly6-PE conjugated antibody (µl)	[Final Antibody]
Unstained control	100	0	0	-
CD45-APC conjugated	100	2	0	4µg/ml
Ly6-PE conjugated	100	0	2	4µg/ml
CD45-APC/Ly6-PE conjugated	100	2	2	4µg/ml

Table 3.2: Flow cytometry voltage settings for isolating BMSCs

Detector	Voltage (V)
FSC	109
SSC	365
B576_D (PE)	335
R660_C (APC)	578

3.1.4 Culture and maintenance of sorted mesenchymal stromal cell populations

Sorted cells were centrifuged at 1200g for 5 min, resuspended in 5ml of culture medium (α-MEM + 20% FCS + 1% P/S/G) and transferred to a T25cm^2 flask and incubated at 37^{o}C/5% CO_2. Following cell attached, bFGF was added to the culture medium and subsequent cell culture was performed in the presence of bFGF as outlined in Section 2.1. The sorted BMSCs and double positive cells were sub-passaged for 60 passages. Sorted cells were expanded and cryopreserved at early, mid and late passage. Mesenchymal stromal cells were treated similarly. For the purposes of this study, early, mid and late passages were defined as P3-15, P15-30 and P30-60 respectively.

3.1.5 Cell proliferation assays

Early, mid and late passage cryopreserved single positive BMSCs, double positive cells and mesenchymal stromal cells were resurrected in T75cm^2 flasks and cultured for a period of 1 week. Cell proliferation assays were subsequently performed as outlined in Section 2.2.

3.1.6 Clonogenicity assays

Early, mid and late passage cryopreserved single positive BMSCs, double positive cells and mesenchymal stromal cells were resurrected in a T75cm^2 flask and cultured for 1 week, after which clonogenicity assays were subsequently performed as outlined in Section 2.3.

3.1.7 Differentiation assays

3.1.7.1 Adipogenic differentiation

Early, mid and late passage cryopreserved single positive BMSCs, double positive cells and mesenchymal stromal cells were resurrected in a T75cm^2 flask and expanded to 3x T175cm^2 flasks within 2 weeks. Adipogenesis assays were subsequently performed as outlined in Section 2.4.1.

3.1.7.2 Osteogenic differentiation

Early, mid and late passage cryopreserved single positive BMSC, double positive cells and mesenchymal stromal cells were resurrected in a T75cm^2 flask and expanded to 3x T175cm^2 flasks within 2 weeks. Osteogenesis assays were subsequently performed as outlined in Section 2.4.2.

3.1.7.3 Chondrogenic differentiation

Mid passage cryopreserved single positive BMSC and mesenchymal stromal cells were resurrected in a T75cm^2 flask and expanded to 3x T175cm^2 flasks within 2 weeks. Chondrogenesis assays were subsequently performed as outlined in Section 2.4.3.

3.1.8 Gene expression profiling of native BMSCs

Characterisation of the gene expression profile of native single positive BMSCs in comparison to mesenchymal stromal cells and double positive cells at early passage (P3-20) was performed as described in Section 2.6. A number of pancreatic genes and hormones were analysed including *FoxA2*, *Pdx-1*, *NeuroD1*, mouse insulin 1 (*Ins1*), mouse insulin 2 (*Ins2*), glucagon (*Gcg*), somatostatin (*Sst*), pancreatic polypeptide (*Ppy*), synaptophysin (*Syp*),

Nkx6.1, pro-convertase 1/3 (*Pcsk1*), pro-convertase 2 (*Pcsk2*), glucose transporter 2 (*Slc2a2*), glucokinase (*Gck*) and β-actin (*Actb*). The optimal PCR conditions for each primer set including forward and reverse primer sequences are outlined in Table 3.3. Mouse pancreas and mouse liver were utilised as positive and negative controls respectively.

Table 3.3: List of murine primers used for gene expression profiling

Gene target	Forward primer	Reverse primer	Annealing Temp (^{o}C)	Cycle number	Product size (bp)	Existing/Designed
Foxa2	GAGCAGCGGCCAGCGAGTTA	CCCAGGCCGGCGTTCATGTT	61	40	131	Existing
Pdx1	CCTTCGGGCCTTAGCGTGTC	CGCCTGCTGGTCCGTATTG	61	40	392	Existing
Neurod1	GCTCCAGGGTTATGAGATCG	CTCTGCATTCATGGCTTCAA	53.7	40	204	Existing
Ins1	GACCAGCTATAATCAGAGACC	AGTTGCAGTAGTTCTCCAGCTG	56.8	30	368	Designed
Ins2	GAGTCCCACCCCACCCAG	TCCACTTCACGGCGGGACA	62	30	124	Existing
Gcg	ATGAAGACCATTTACTTTGTGGCTG	CGGCCTTTCACCAGCCACGC	60	35	380	Designed
Sst	ATGCTGTCCTGCCGTCTCCA	CTAACAGGATGTGAATGTCTTCCA	60	35	351	Designed
Ppy	TACTGCTGCCTCTCCCTGTT	CCAGGAAGTCCACCTGTGTT	61.2	35	268	Designed
Syp	ACCTCGGTGGTGTTTGGCTTCC	CCTGGAGGTGCGCGCATGAA	56.2	40	106	Existing
Nkx6.1	ATCTTCTGGCCCGGAGTGATG	GGCTGCGTGCTTCTTTCTCCA	62	40	284	Existing
Pcsk1	GATGGCTACACAGACAGCAT	GGATCAGCCAAATCCACCAG	52.9	40	406	Existing
Pcsk2	TCGCCAAGTTGCAGCCAGAAC	CTTCGGCCACGTTCAAGTCTA	52.9	40	313	Existing
Slc2a2	GGATAAATTCGCCTGGATGA	TTCCTTTGGTTTCTGGAACT	55	40	298	Existing
Gck	TATGAAGACCGCCAATGTGA	TTTCCGCCAATGATCTTTTC	55	40	244	Existing
Actb	CCATCATGAAGTGTGACGTTG	TACTCCTGCTTGCTGATCCA	61	30	243	Existing

3.2 Results

3.2.1 FACS sorting and analysis

Stromal cells isolated from the femurs of NOD mice were cultured for two passages and subsequently stained with CD45-APC and Ly6-PE conjugated mAbs alone and in combination. FACS analysis histograms of unstained, single mAb and double mAb stained stromal cells were generated to illustrate the identification of unique stromal cell sub-populations as characterised by their surface marker expression profiles. BMSCs identified by flow cytometry correspond to the $CD45^{-}/Ly6^{+}$ cell population (Figure 3.1D) (orange). Double positive cells are an uncharacterised hematopoietic stem cell population corresponding to the $CD45^{+}/Ly6^{+}$ cell population (Figure 3.1D) (red), and were sorted as a control population to highlight the enhanced properties of BMSCs by comparison. The raw cell acquisition data for the identification of BMSC and double positive cells is represented in Table 3.4. As can be seen in Table 3.4, the respective percentages of BMSC and double positive cells enriched via FACS were 33.2% and 17.3%.

Immediately post-sorting, an aliquot of BMSC and double positive cells were tested for purity according to their surface marker expression profiles via FACS analysis (Figure 3.2). Raw data analysis of the purity check indicated that the sorted BMSCs and double positive cell sub-populations showed 72.5% and 40.5% purity respectively (Table 3.5). In addition, whilst sorted BMSC did not contain any contaminating double positive cells, purity analysis of the double positive cells showed a minor contamination (0.01%) with BMSCs.

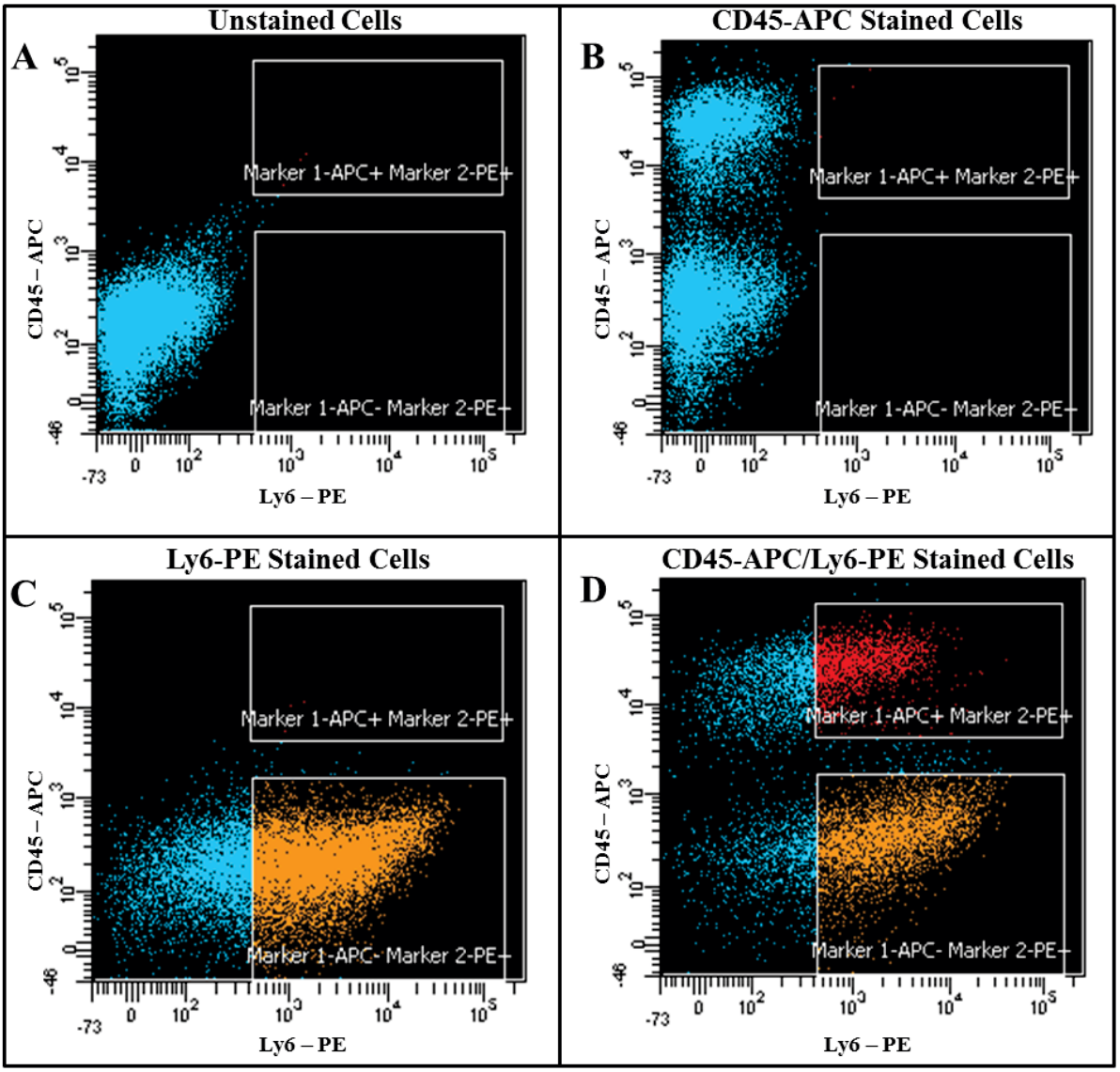

Figure 3.1: Identification of NOD mouse bone marrow stromal cell subpopulations using immunofluorescence staining and flow cytometry Following culture for 2 passages, NOD mouse bone marrow stromal cells were stained with: nil antibody (Unstained; A), CD45 mAb conjugated to fluorochrome APC (CD45-APC; B), Ly6 MAb conjugated to fluorochrome PE (Ly6-PE; C), or both mAbs (CD45-APC/Ly6-PE; D). Fluorescence dot plots of CD45-APC (y-axis) and Ly6-PE (x-axis) were used to identify the BMSC ($CD45^-/Ly6^+$; orange) and double positive ($CD45^+/Ly6^+$; red) cell subpopulations ready for cell sorting using the BD FACSAria™ II instrument.

Table 3.4: Stained cell acquisition and analysis of NOD BMSCs and double positive cells

Cell staining sample	All events (%)	Viable cells (%)	Singlets (%)	APC events (%)	PE events (%)	$CD45^+/Ly6^+$ events (%)	$CD45^-/Ly6^+$ events (%)
Unstained	20,000	19,956	14,132	-	-	-	-
	100	99.8	70.7				
CD45-APC	20,000	17,434	14,915	14,845	-	4	-
	100	87.2	74.6	74.2		0.0	
Ly6-PE	20,000	17,460	14,338	-	14,248	3	10,108
	100	87.3	71.7		71.2	0.0	50.5
CD45-APC/Ly6-PE	10,000	9,092	7,753	-	-	1,732	3,321
	100	91.0	77.5			17.3	33.2

Stromal cells were divided into four groups for FACS analysis: Unstained, CD45-APC stained, Ly6-PE stained and CD45-APC/Ly6-PE stained. Two sub-populations of cells were sorted from stromal cells stained with both CD45-APC and Ly6-PE: BMSC (orange) and double positive cells (red). The final percentages of each sorted cell population were determined as a fraction of the total cell count.

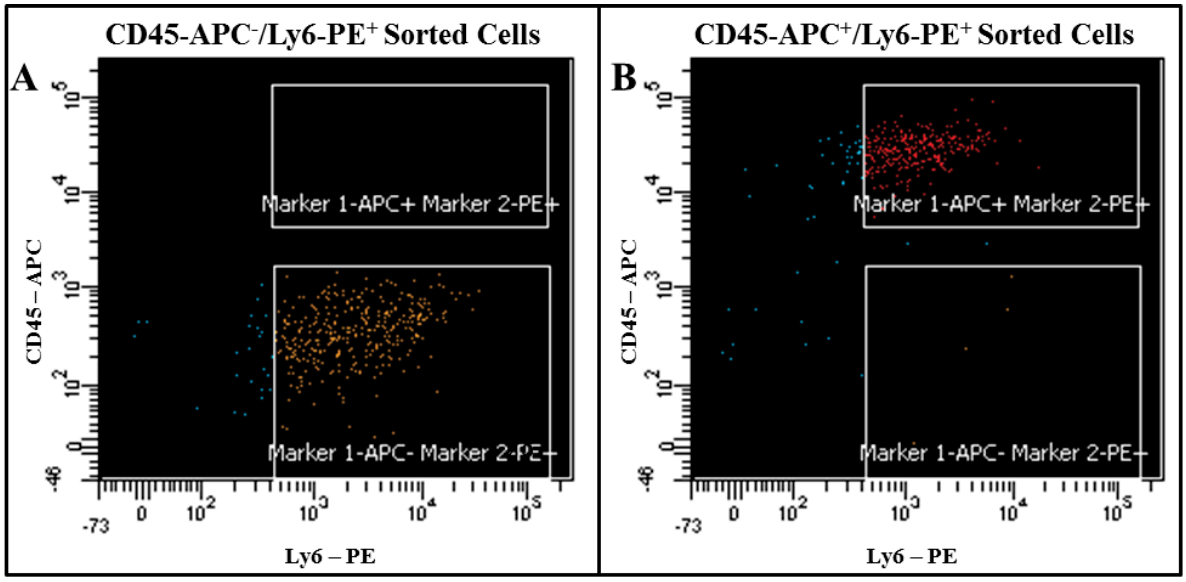

Figure 3.2: Purity check of sorted NOD mouse bone marrow cell subpopulations Following cell sorting, BMSCs (CD45-APC$^-$/Ly6-PE$^+$) (A) and double positive (CD45-APC$^+$/Ly6-PE$^+$) cell (B) subpopulations were assessed for cell purity prior to their expansion in cell culture for BMSC functional assays. Fluorescence dot plots of CD45-APC (y-axis) and Ly6-PE (x-axis) were used to identify the BMSCs (CD45$^-$/Ly6$^+$; orange) and double positive (CD45$^+$/Ly6$^+$; red) cell subpopulations using the BD FACS Aria™ II instrument.

Table 3.5: Purity analysis of sorted BMSCs and double positive cells

Sorted sample	All events (%)	Viable cells (%)	Singlets (%)	CD45$^+$/Ly6$^+$ events (%)	CD45$^-$/Ly6$^+$ events (%)
Double positive (CD45-APC$^+$/Ly6-PE$^+$)	679	336	326	275	4
	100	49.5	48.0	40.5	0.01
BMSC (CD45-APC$^-$/Ly6-PE$^+$)	476	392	375	-	345
	100	82.4	78.8		72.5

FACS sorted BMSCs (orange) and double positive cells (red) were further analysed for their purity with respect to CD45-APC and Ly6-PE marker expression. The final percentages for purity of each sorted cell population were determined as a fraction of the total cell count.

3.2.2 Cell morphology

Freshly flushed bone marrow cells were transferred to tissue-culture treated flasks in the presence of complete medium containing epiphyses (Section 3.1.4) and selected for plastic adherence over two passages *in vitro*. Bone marrow stromal cells are a heterogeneous population of cells including hematopoietic stem cells and precursors, endothelial cells, neuronal-like cells, fibroblasts and monocytes. The absence of basic fibroblast growth factor in the complete medium negatively selected for non-fibroblast like cells, whilst plastic adherence (a defining characteristic of MSCs) was utilised to enrich for plastic-adherent cells. Non-adherent cells were discarded with successive media changes and sub-passaging prior to the FACS enrichment of BMSC and double positive cell populations.

To enrich for BMSCs, FACS sorting was performed on P2 adherent stromal cells to positively select for Ly6 and negatively select for CD45 expressing mesenchymal stem cells, also denoted as $CD45^{-}/Ly6^{+}$ BMSC. BMSCs displayed the characteristic fibroblast-like phenotype of mesenchymal stem cells (Figure 3.3), and maintained their fibroblast-like phenotype through successive sub-passaging. During early passage BMSC diameter varied (~50-150μm) and decreased with increasing passage (~20-70μm). In addition, during passage 5-8, BMSCs entered a phase of senescence leading to a decrease in cell growth and ultimately increased cell death (data not shown). However, upon the addition of bFGF to the culture medium a proportion of BMSCs (~15-20%) that resisted senescence continued to proliferate up to 60 passages (maximum culture period). Senescent-resistant BMSCs maintained their fibroblast-like phenotype through early, mid and late passage. By comparison, double positive cells at early passage display a similar fibroblast-like morphology to BMSCs however possessed an increased cytoplasmic volume and diameter (~100-200μm). With

increased passage the cells' cytoplasmic volume remained constant and the length of peripheral extensions increased.

Stromal cells, which did not undergo flow sorting, were maintained in culture under identical conditions as BMSCs and double positive cells. At early passage, the stromal cell population consisted of a heterogeneous population of cells with varying morphologies. Cells within the stromal cell population were observed to possess a greater cytoplasmic volume and diameter (~100-300μm) in comparison to their sorted counterparts. With increased sub-passaging, plastic adherent cells were enriched, in particular fibroblast-like cells. Eventually with further sub-passaging, two populations of cells were observed within the stromal cell fraction morphologically similar to BMSCs and double positive cells.

The designated cell passage classifications were due to the fact that a pure population of BMSCs was obtained following an initial stromal cell culture period of 2 passages, after which the stromal cells were sorted into their respective populations. Upon return to culture, all sorted populations were P3. To obtain sufficient numbers of BMSCs for subsequent functional assays, BMSCs were required to be cultured through a period of senescence, which occurred between P5-8 and resulted in high rates of cell death. The passage classifications were subsequently reflective of challenges encountered during early cell culture.

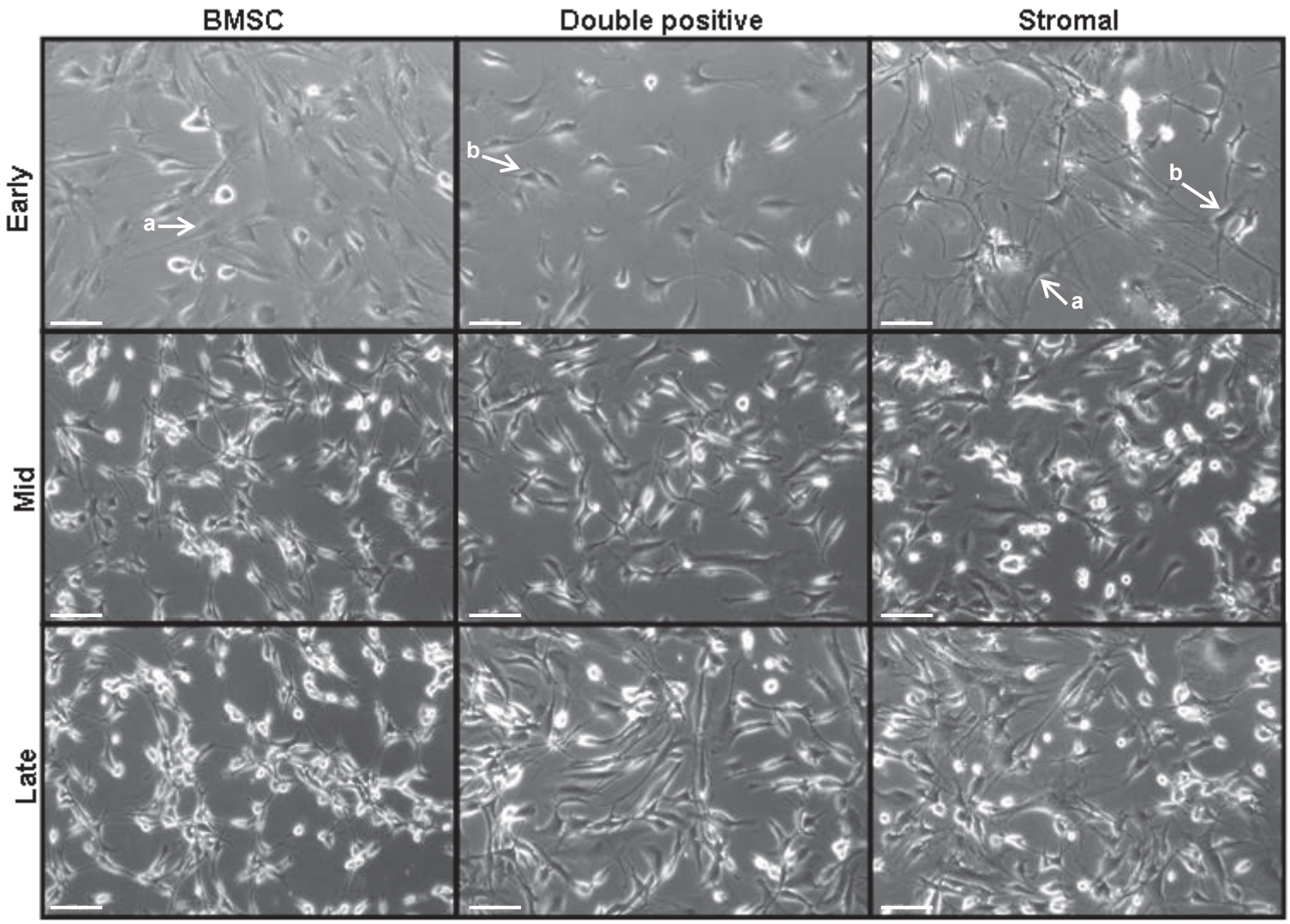

Figure 3.3: Effect of passage on the morphological characteristics of BMSCs, double positive and stromal cells Unsorted stromal cells, and sorted BMSCs and double positive cells were cultured *in vitro* for up to 60 passages. Cells were imaged at early, mid and late passage (as defined in Section 2.1) on a Leica DM Microscope. Fibroblast-like BMSCs (a) and double positive cells (b) are indicated by arrowheads. Images were obtained at 10x magnification, 100µm scale.

3.2.3 Cell proliferation

Cell proliferation assays were performed with early (P3-15), mid (P15-30) and late (P30-60) passage BMSCs, double positive, and stromal cells. Across all the cell populations an increase in the rate of proliferation was observed with increasing passage number. The growth curves for BMSCs, double positive and stromal cells displayed the characteristic features of sigmoidal mammalian cell growth with lag, log, stationary and death phases corresponding to Days 0-1, Day 1-7, Days 7-11 and Days 11-15 respectively. An inter-population analysis of cell proliferation shows that at early, mid and late passage, BMSCs demonstrate a significant increase in cell proliferation in comparison to double positive ($p<0.001$) and stromal cells ($p<0.005$) (Figure 3.4). In addition, there was a shift to the left in terms of log cell growth across all populations with increasing passage. An intra-population analysis of cell proliferation showed that there was a significant increase in BMSC proliferation at late and mid passage in comparison to early passage ($p<0.005$), a trend which was also observed in double positive ($p<0.01$) and stromal cells ($p<0.005$) (Figure 3.5).

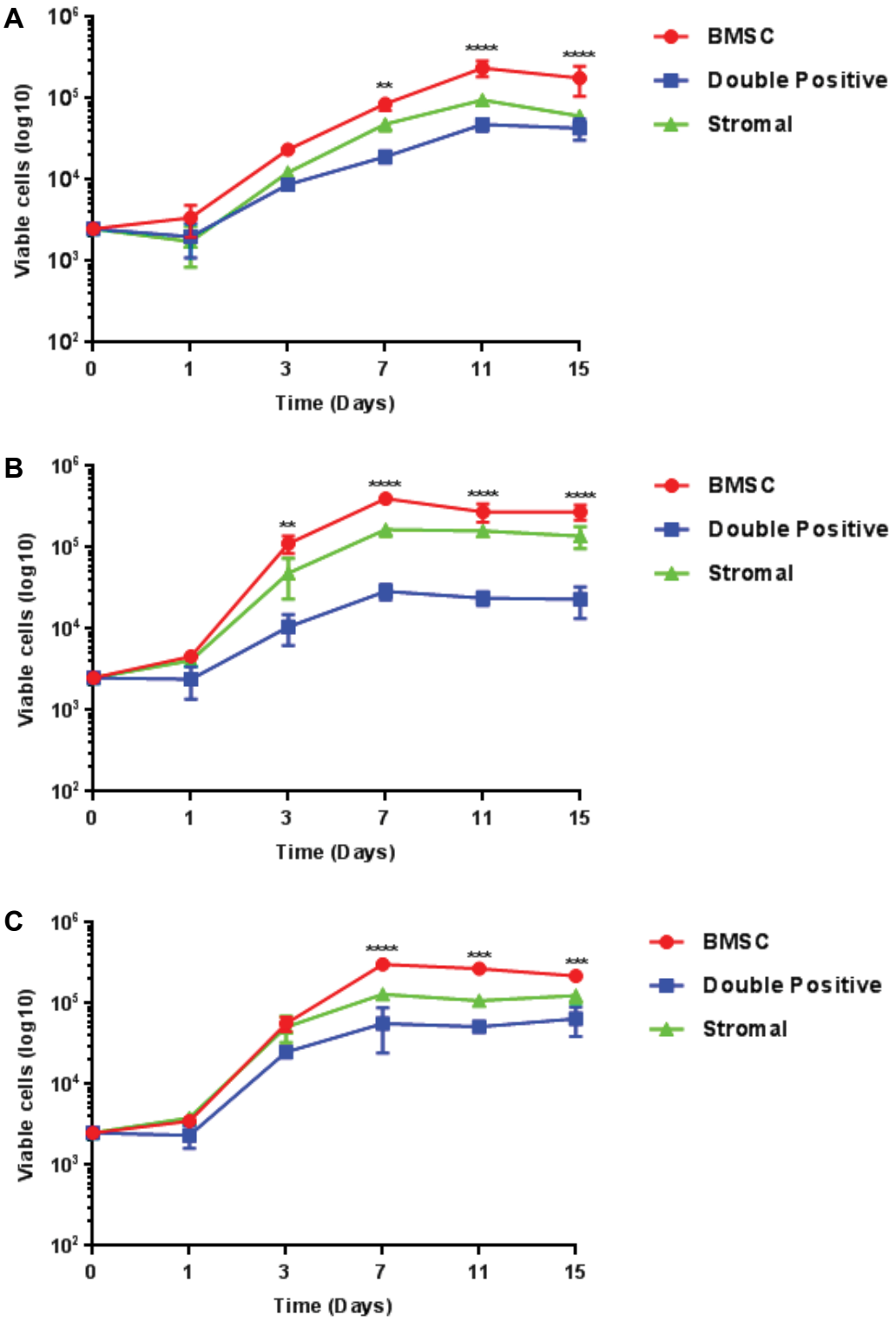

Figure 3.4: Inter-population analysis of passage on cell proliferation Comparison of early (A), mid (B) and late (C) passage BMSCs, double positive and stromal cell proliferation. Cells were maintained in complete α-MEM for a period of 15 days, during which cell viability was assessed via Trypan Blue 0.4% exclusion on Days 0, 1, 3, 7, 11 and 15. Data is expressed as mean viable cells ± SD (n=3). A two-way ANOVA with Tukey's post hoc was performed, *p<0.05.

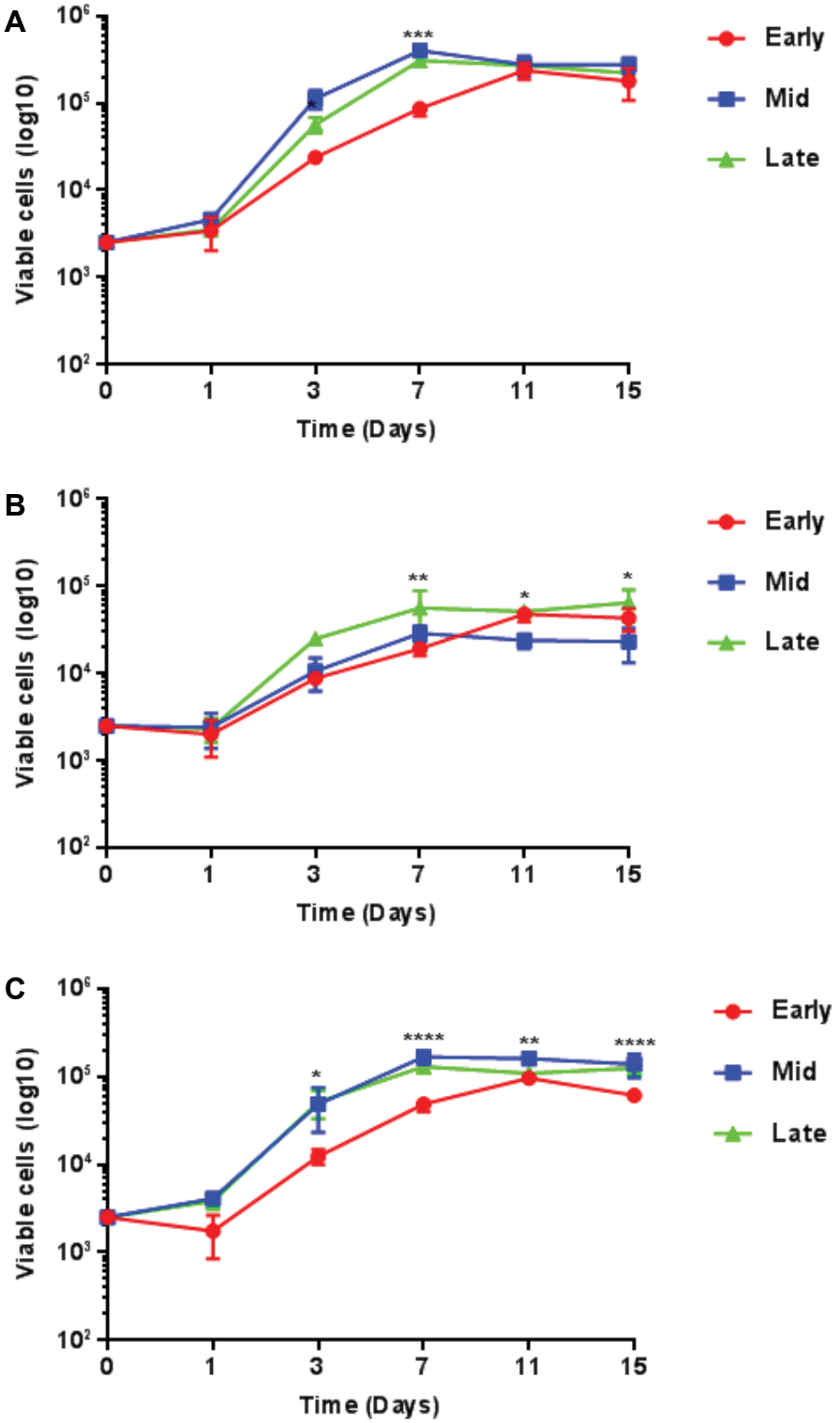

Figure 3.5: Intra-population analysis of passage on cell proliferation Comparison of BMSCs (A), double positive (B) and stromal cells (C) cell proliferation at early, mid and late passage. Cells were maintained in complete α-MEM for a period of 15 days, during which cell viability was assessed via Trypan Blue 0.4% exclusion on Days 0, 1, 3, 7, 11 and 15. Data is expressed as mean viable cells ± SD (n=3). A two-way ANOVA with Tukey's post hoc was performed, *p<0.05.

3.2.4 Clonogenicity assays

Clonogenicity assays were performed with early (P3-15), mid (P15-30) and late (P30-60) passage BMSCs, double positive and stromal cells as described in Section 2.3. Scanned images were obtained following methylene blue staining (Figure 3.6), and individual colonies were counted for a quantitative analysis of clonogenicity across all cell populations. With respect to methylene blue staining intensity, a qualitative visual comparison of BMSC (dark) and double positive (light) colonies illustrated a difference in staining intensity. At late passage, double positive stained colonies appeared to increase in staining intensity. This was likely a reflection of the minor contamination of the double positive cell population with BMSCs (0.01%) during the sorting process (Table 3.5). With ongoing culture BMSCs were enriched for, resulting in the increased frequency of dark staining colonies within the double positive population. In addition, stromal cells at early passage possessed a mix of BMSC (dark) and double positive (light) staining colonies. The number of intensely staining BMSC colonies increased with increasing passage, highlighting the enrichment of BMSCs simply through ongoing culture in defined media.

Inter-population quantitative analysis of clonogenicity at early, mid and late passage showed that BMSCs possessed enhanced clonogenicity in comparison to double positive and stromal cells (Figure 3.7). BMSCs showed an enhanced propensity to form colonies in comparison to double positive cells at early passage ($p<0.01$), mid passage ($p<0.005$) and late passage ($p<0.005$). By comparison, stromal cells showed improved clonogenicity from early passage ($p<0.001$) to late passage ($p<0.05$), likely a reflection of the predominating BMSCs that are enriched for with ongoing culture. No significant difference was observed in clonogenicity between double positive and stromal cells at late passage, further emphasising the improvement in stromal cell clonogenicity with passage.

An intra-population quantitative analysis of clonogenicity showed a significantly enhanced propensity of BMSCs to form colonies at mid and late passage in comparison to early passage ($p<0.01$) (Figure 3.8). A similar observation was observed with stromal cells with increasing passage ($p<0.001$). However, no change was observed in the propensity of double positive cells to form colonies with increasing passage.

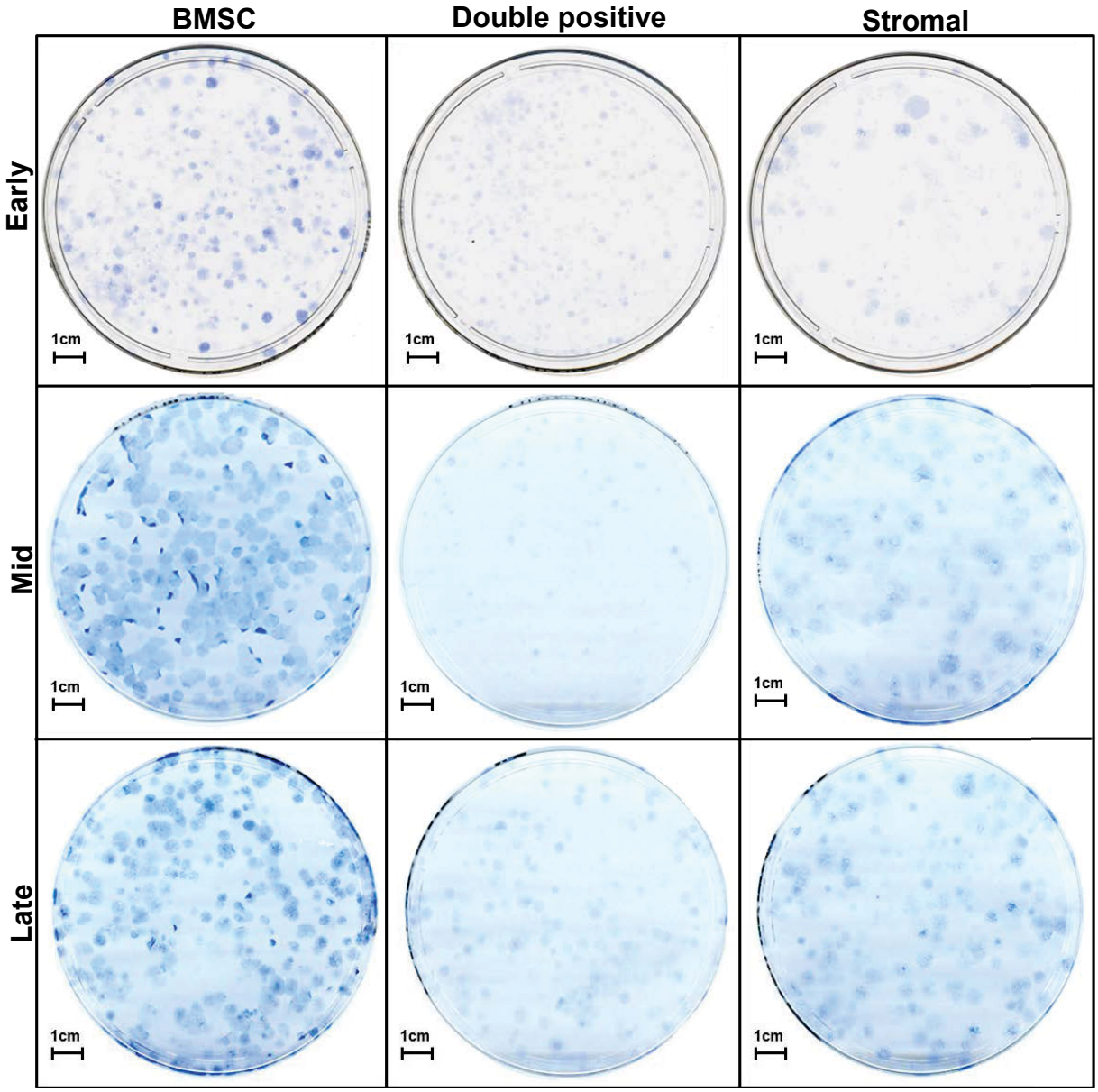

Figure 3.6: Comparative analysis of colony staining across cell populations 500 cells were seeded in 10cm^2 tissue-culture treated plates and incubated for 10 days, after which colonies were stained with 40% methylene blue/60% methanol. Images were obtained using the Epson® Perfection 4870 Photo Scanner.

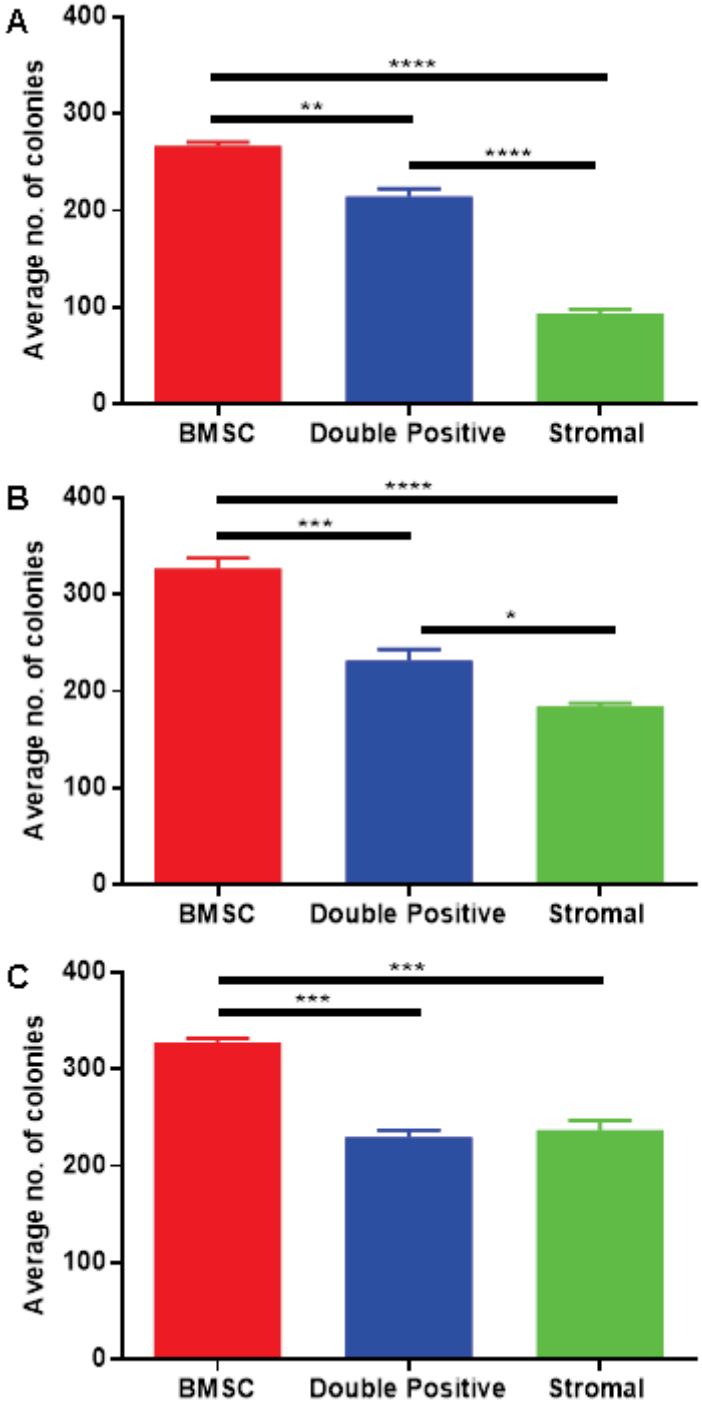

Figure 3.7: Inter-population quantitative analysis of clonogenicity 500 cells of BMSCs, double positive and stromal cells were seeded in 10cm^2 tissue-culture treated plates at early (A), mid (B) and late (C) passage, and incubated for 10 days, after which colonies were stained with 40% methylene blue/60% methanol. Data is represented as mean ± SEM (n=3). A one-way ANOVA and Tukey's post-hoc were performed, * $p<0.05$.

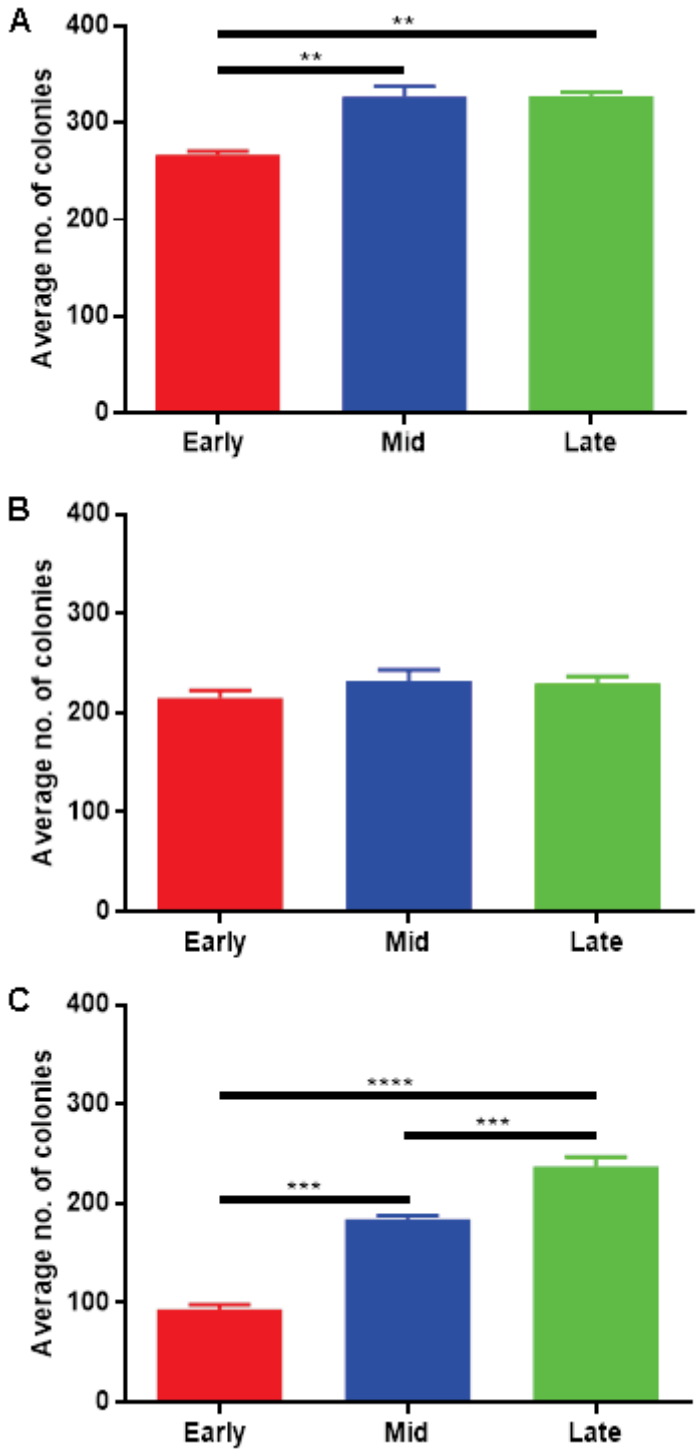

Figure 3.8: Intra-population quantitative analysis of clonogenicity 500 cells of BMSCs (A), double positive (B) and stromal cells (C) at early, mid and late passage were seeded in 10cm^2 tissue-culture treated plates and incubated for 10 days, after which colonies were stained with 40% methylene blue/60% methanol. Data is represented as mean ± SEM (n=3). A one-way ANOVA and Tukey's post-hoc were performed, * $p<0.05$.

3.2.5 Differentiation assays

3.2.5.1 Adipogenic differentiation

Adipogenic differentiation assays were performed with early (P3-15), mid (P15-30) and late (P30-60) passage BMSCs, double positive and stromal cells as detailed in Section 2.4.1. Images of each cell population under control and differentiation conditions were subsequently obtained at early (Figure 3.9), mid (Figure 3.10) and late passage (Figure 3.11) on a Leica DM microscope at 20x magnification. Qualitative assessment of adipogenic differentiation shows that at all passages, BMSCs were capable of differentiating into adipocytes as indicated by the extensive Oil Red O staining that correlates with lipid production. In addition, variations in Oil Red O staining intensity can also be observed within BMSCs that have differentiated, highlighting both immature and mature adipocyte differentiation. By comparison double positive cells did not undergo adipogenic differentiation, and stromal cells showed a diminished propensity to undergo adipogenic differentiation. Stromal cell adipogenesis was mainly comprised of immature adipocyte differentiation.

Quantitative analysis of adipogenic differentiation was assessed by scoring the degree of adipogenic differentiation with respect to the broad range of adipocytes (immature and mature) observed within a population. An inter-population comparison (Figure 3.12) showed that BMSCs display an enhanced propensity to undergo adipogenic differentiation in comparison to double positive and stromal cells across all passage ranges ($p<0.001$). In addition, stromal cells display a similar propensity to undergo adipogenic differentiation in comparison to double positive cells across all passage ranges ($p<0.001$). An intra-population comparison (Figure 3.13) showed that BMSCs display a diminished adipogenic

differentiation potential with increasing passage ($p<0.001$). A similar trend was observed with stromal cells with increasing passage ($p<0.001$), albeit at a much lower mean cell count.

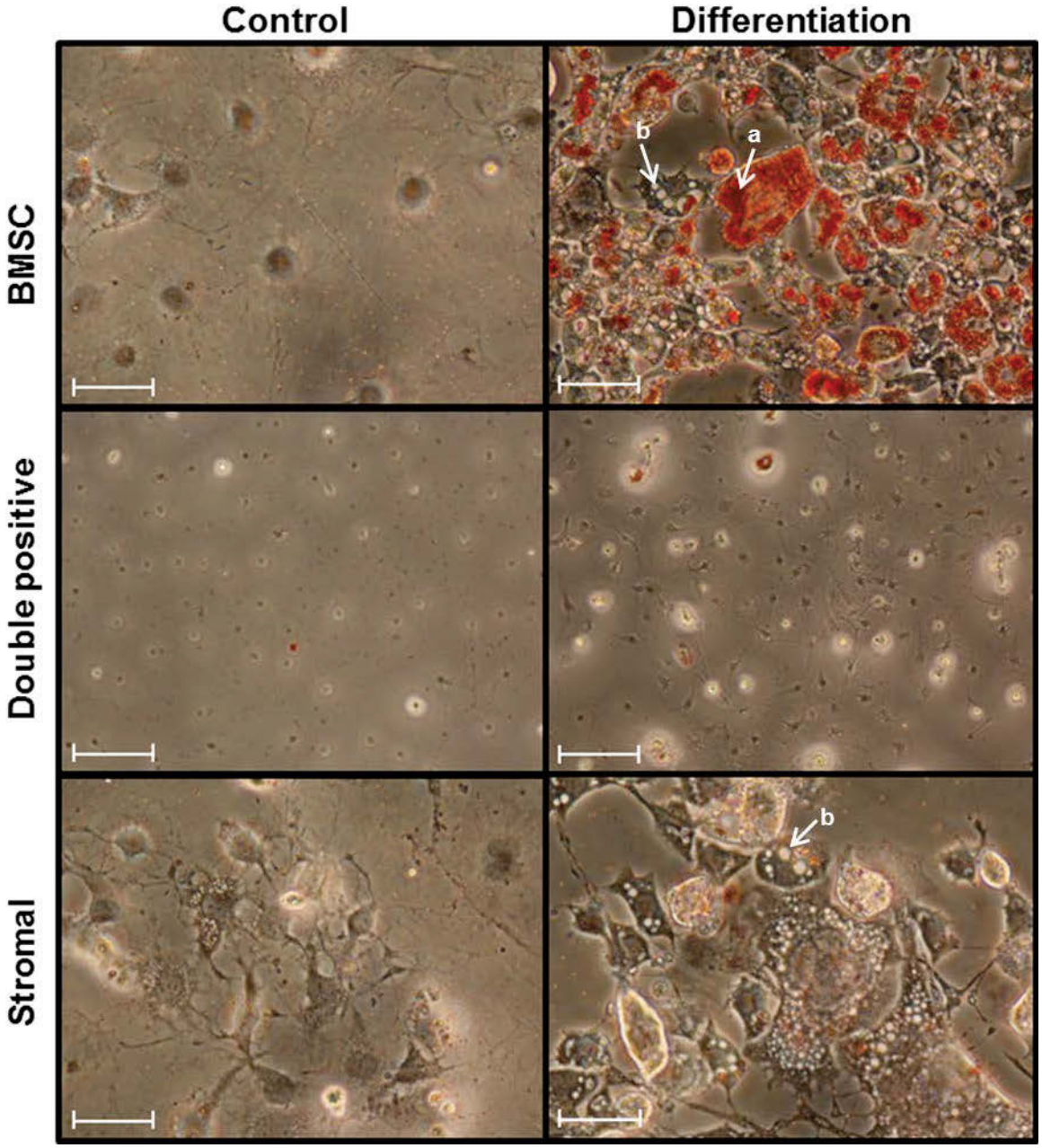

Figure 3.9: Inter-population schematic of adipogenesis at early passage $2.5x10^4$ cells/ml of each cell population were seeded into a 24-well plate in triplicate and incubated in either adipogenic Control or Differentiation medium for 10 days. The cells were subsequently fixed with 10% formalin and stained with 0.2% (w/v) Oil Red O. Mature (a) and immature (b) adipocytes are indicated by arrowheads. Images were acquired on a Leica DM Microscope at 20x magnification, 100µm scale.

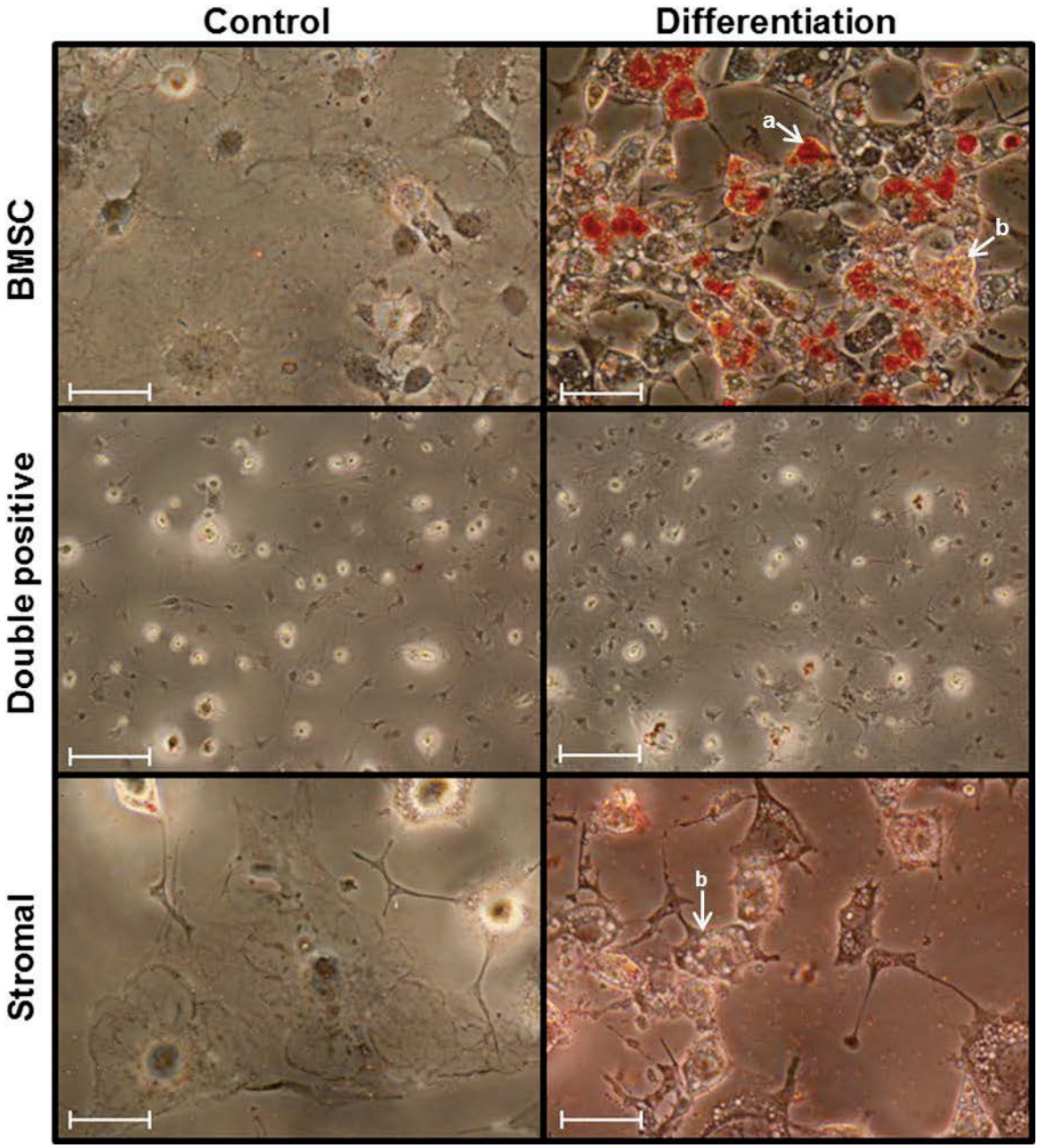

Figure 3.10: Inter-population schematic of adipogenesis at mid passage $2.5x10^4$ cells/ml of each cell population were seeded into a 24-well plate in triplicate and incubated in either adipogenic Control or Differentiation medium for 10 days. The cells were subsequently fixed with 10% formalin and stained with 0.2% (w/v) Oil Red O. Mature (a) and immature (b) adipocytes are indicated by arrowheads. Images were acquired on a Leica DM Microscope at 20x magnification, 100µm scale.

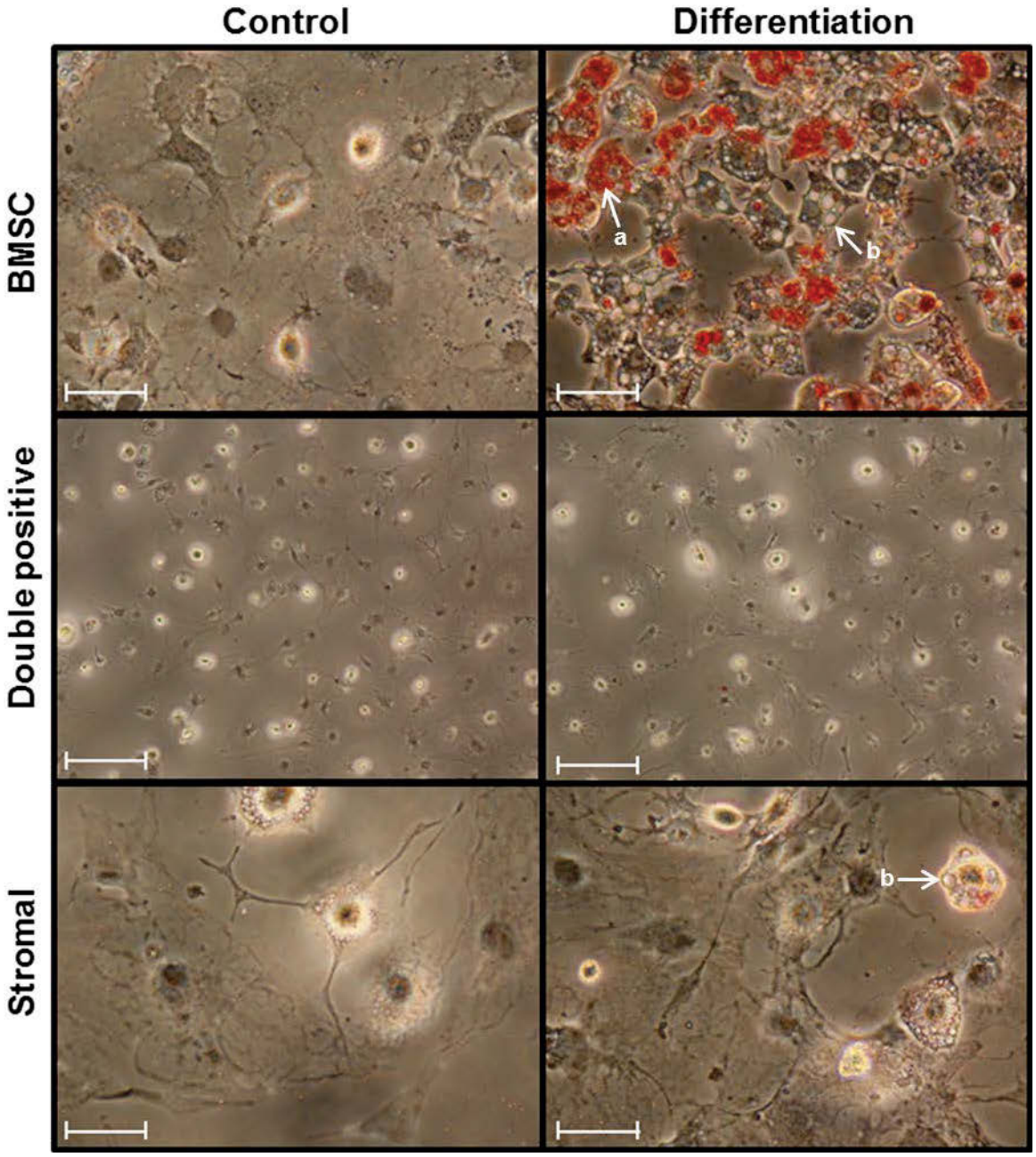

Figure 3.11: Inter-population schematic of adipogenesis at late passage 2.5x10^4 cells/ml of each cell population were seeded into a 24-well plate in triplicate and incubated in either adipogenic Control or Differentiation medium for 10 days. The cells were subsequently fixed with 10% formalin and stained with 0.2% (w/v) Oil Red O. Mature (a) and immature (b) adipocytes are indicated by arrowheads. Images were acquired on a Leica DM Microscope at 20x magnification, 100µm scale.

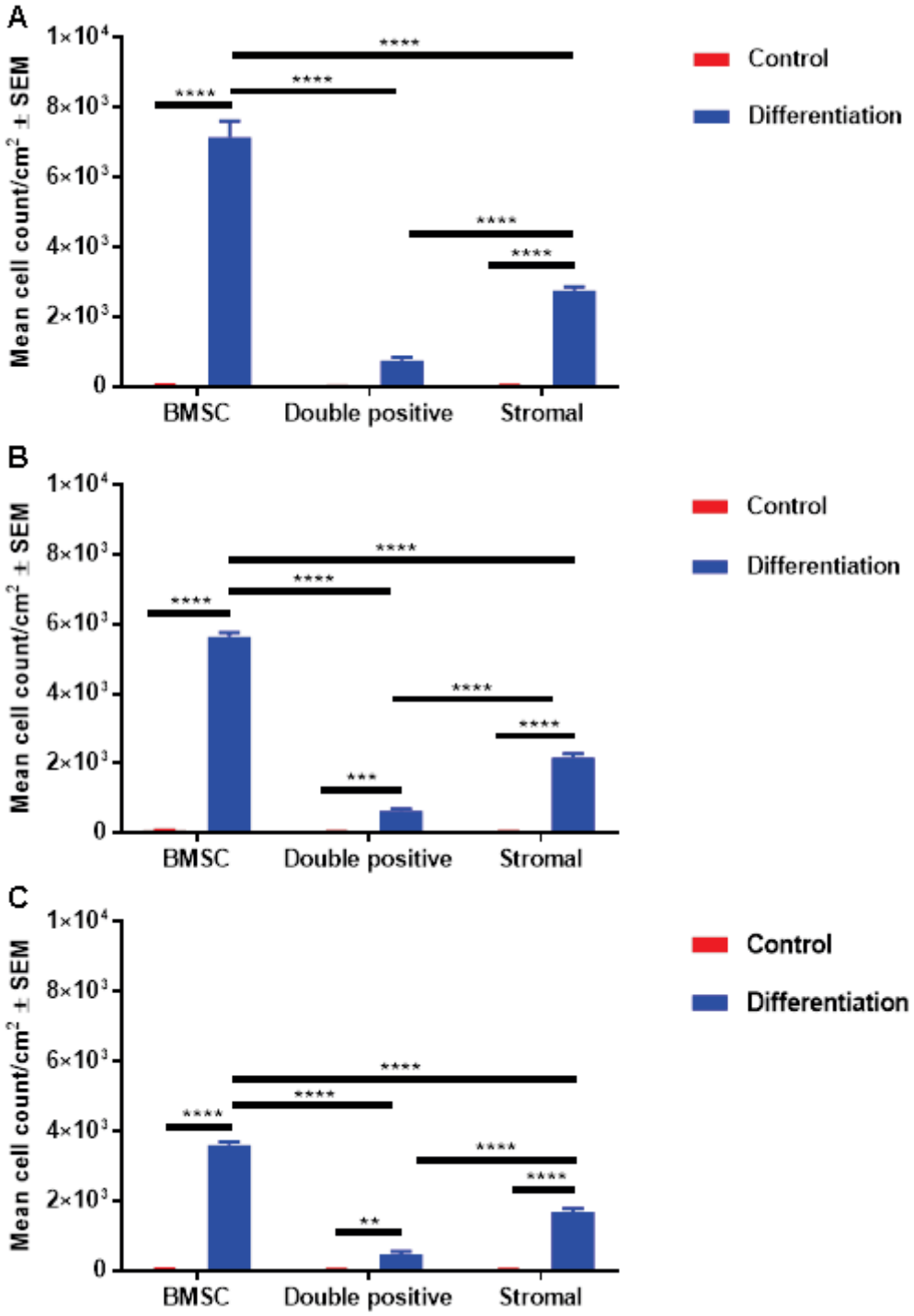

Figure 3.12: Inter-population quantitative analysis of adipogenesis Quantitative data was obtained from BMSCs, double positive and stromal cells at early (A), mid (B) and late passage (C) under control and differentiation adipogenesis conditions. The data is represented as mean ± SEM (n=3). A two-way ANOVA and Tukey's post-hoc were performed, * $p<0.05$.

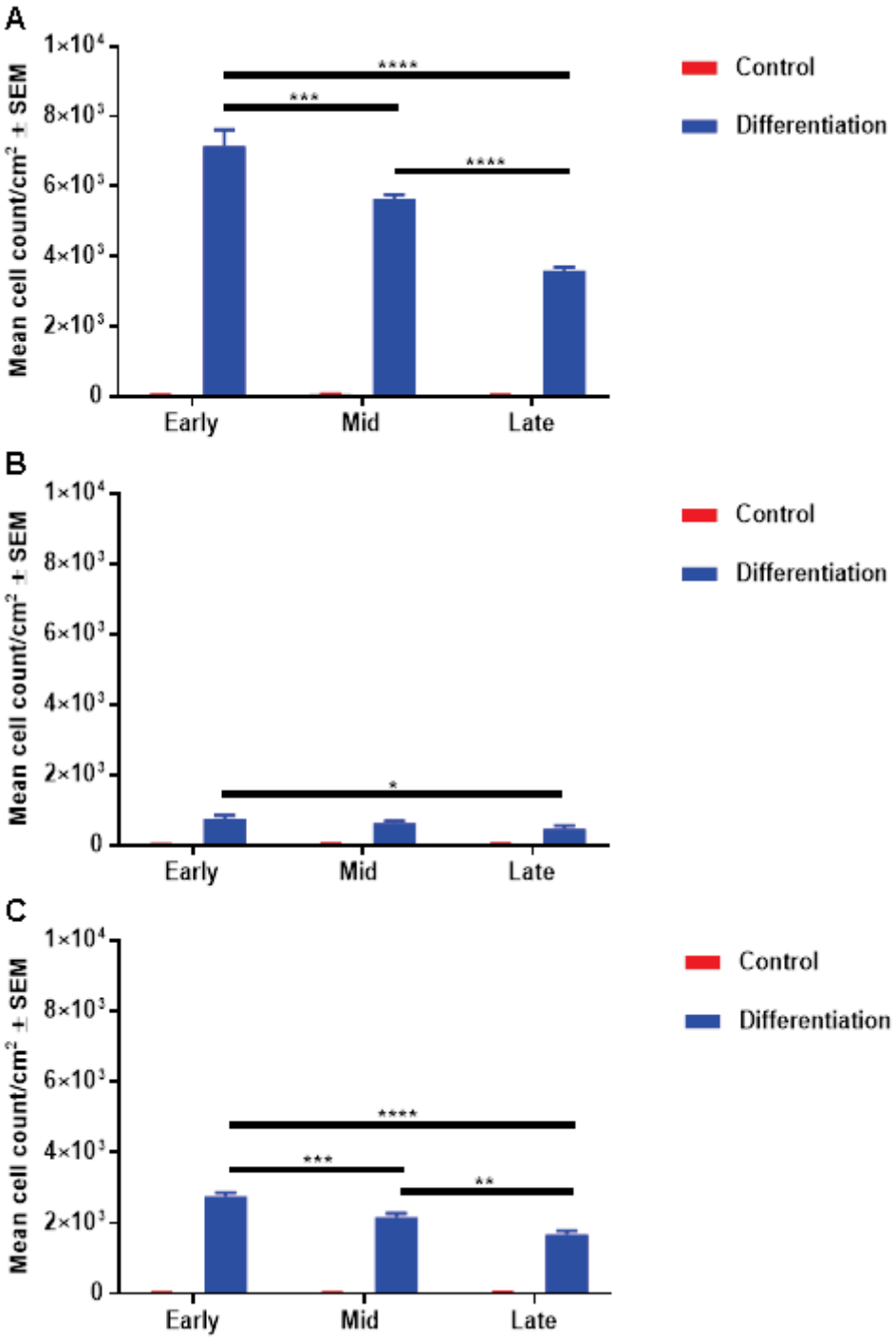

Figure 3.13: Intra-population quantitative analysis of adipogenesis Quantitative data was obtained from BMSC (A), double positive (B) and stromal cells (C) at early, mid and late passage under control and differentiation adipogenesis conditions. The data is represented as mean ± SEM (n=3). A two-way ANOVA and Tukey's post-hoc were performed, * $p<0.05$.

3.2.5.2 Osteogenic differentiation

Osteogenic differentiation assays were performed with early (P3-15), mid (P15-30) and late (P30-60) passage BMSCs, double positive and stromal cells as detailed in Section 2.4.2. Images of each cell population under control and differentiation conditions were subsequently obtained at early (Figure 3.14), mid (Figure 3.15) and late passage (Figure 3.16) on a Leica DM microscope at 20x magnification. Qualitative assessment of osteogenic differentiation shows that at all passages, BMSCs were capable of differentiating into osteocytes as indicated by the extensive Alizarin Red S staining. By comparison double positive cells did not undergo osteogenic differentiation, and stromal cells show a diminished propensity to undergo osteogenic differentiation. This correlates with the trends observed with the adipogenic differentiation of each cell sub-population.

Quantitative analysis of osteogenic differentiation was assessed by scoring the degree of osteogenic differentiation, which correlates with early matrix mineralisation (red) and calcification (brown) of the osteogenic lineage. An inter-population comparison (Figure 3.17) showed that BMSCs displayed an enhanced propensity to undergo osteogenic differentiation in comparison to double positive cell across all passage ranges ($p<0.001$). In comparison to stromal cells, BMSCs showed an enhanced propensity to undergo osteogenic differentiation at early and mid-passage ($p<0.001$), which decreased at late passage ($p<0.05$). In addition, stromal cells displayed a similar propensity to undergo osteogenic differentiation in comparison to double positive cells across all passage ranges ($p<0.001$). An intra-population comparison (Figure 3.18) showed that BMSCs displayed a diminished osteogenic differentiation potential with increasing passage ($p<0.001$). This trend was also observed with stromal cells with increasing passage ($p<0.001$). Despite the negligible levels of osteogenic

differentiation of double positive cells, a significant reduction in their potential for osteogenic differentiation was also observed with increasing passage ($p<0.001$).

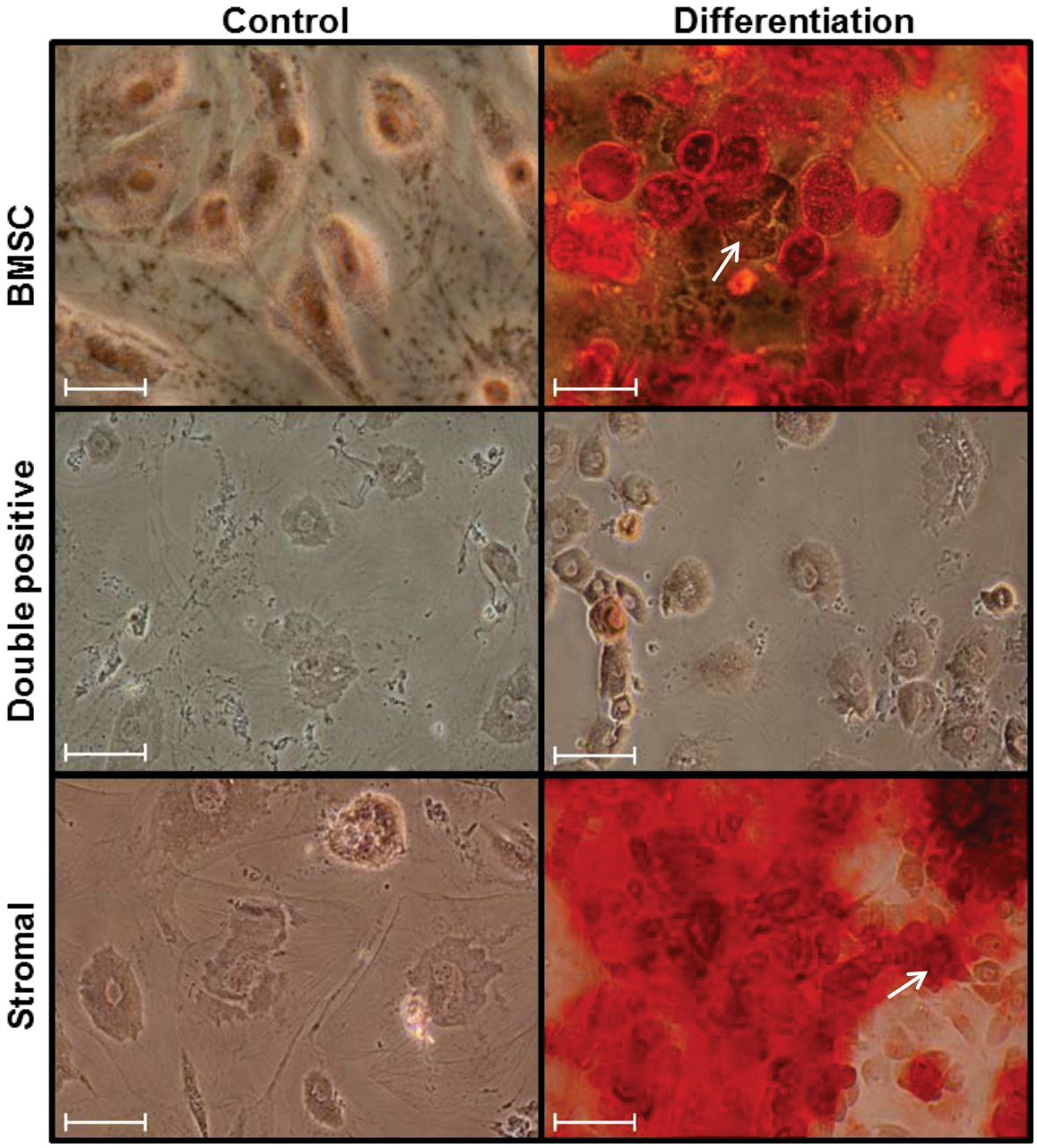

Figure 3.14: Inter-population schematic of osteogenesis at early passage $1.25x10^4$ cells/ml of each cell population were seeded into a 24-well plate in triplicate and incubated in either osteogenic Control or Differentiation medium for 35 days. The cells were subsequently fixed with 10% formalin and stained with 2% (w/v) Alizarin Red S. Osteocytes are indicated by arrowheads. Images were acquired on a Leica DM Microscope at 20x magnification, 100µm scale.

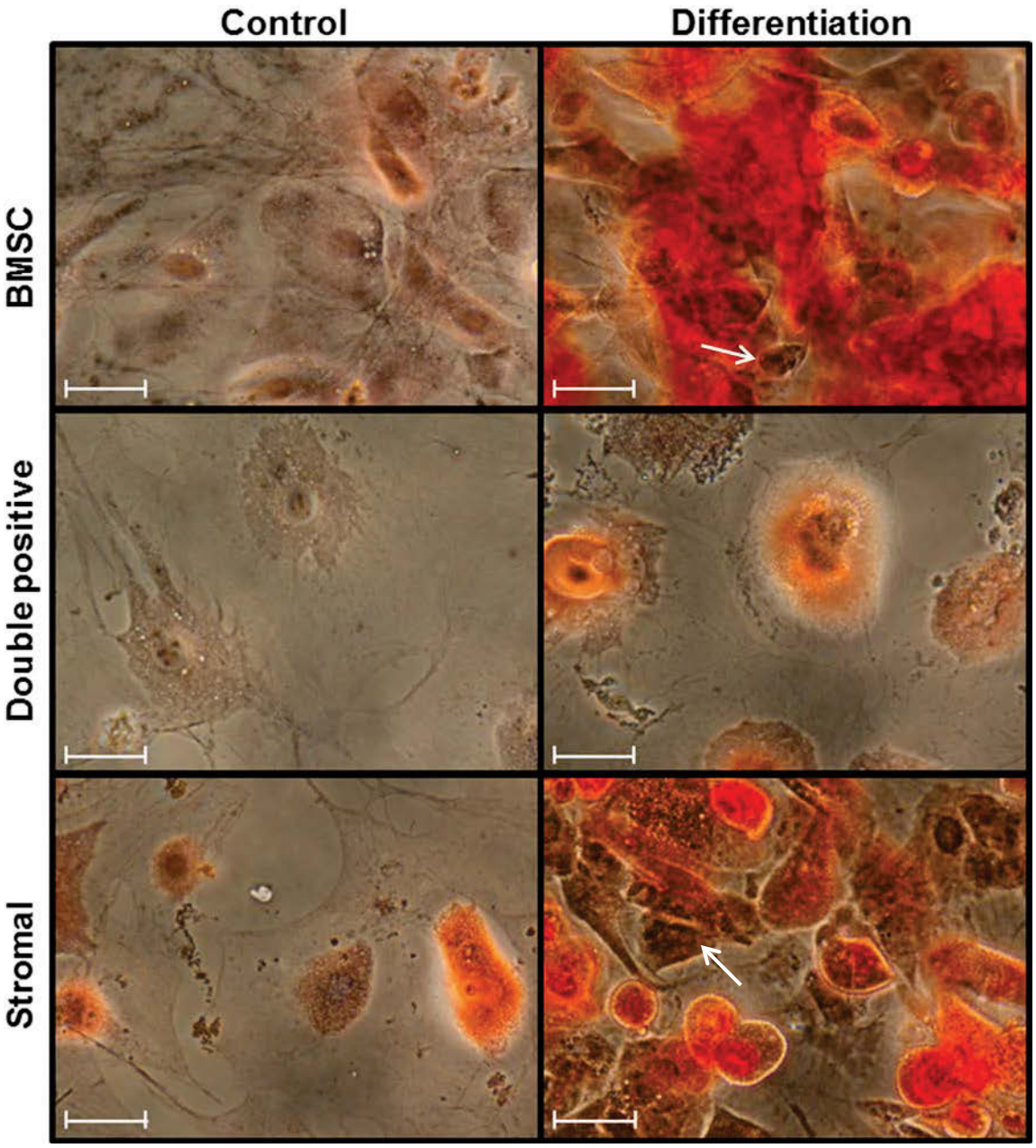

Figure 3.15: Inter-population schematic of osteogenesis at mid passage $1.25x10^4$ cells/ml of each cell population were seeded into a 24-well plate in triplicate and incubated in either osteogenic Control or Differentiation medium for 35 days. The cells were subsequently fixed with 10% formalin and stained with 2% (w/v) Alizarin Red S. Osteocytes are indicated by arrowheads. Images were acquired on a Leica DM Microscope at 20x magnification, 100µm scale.

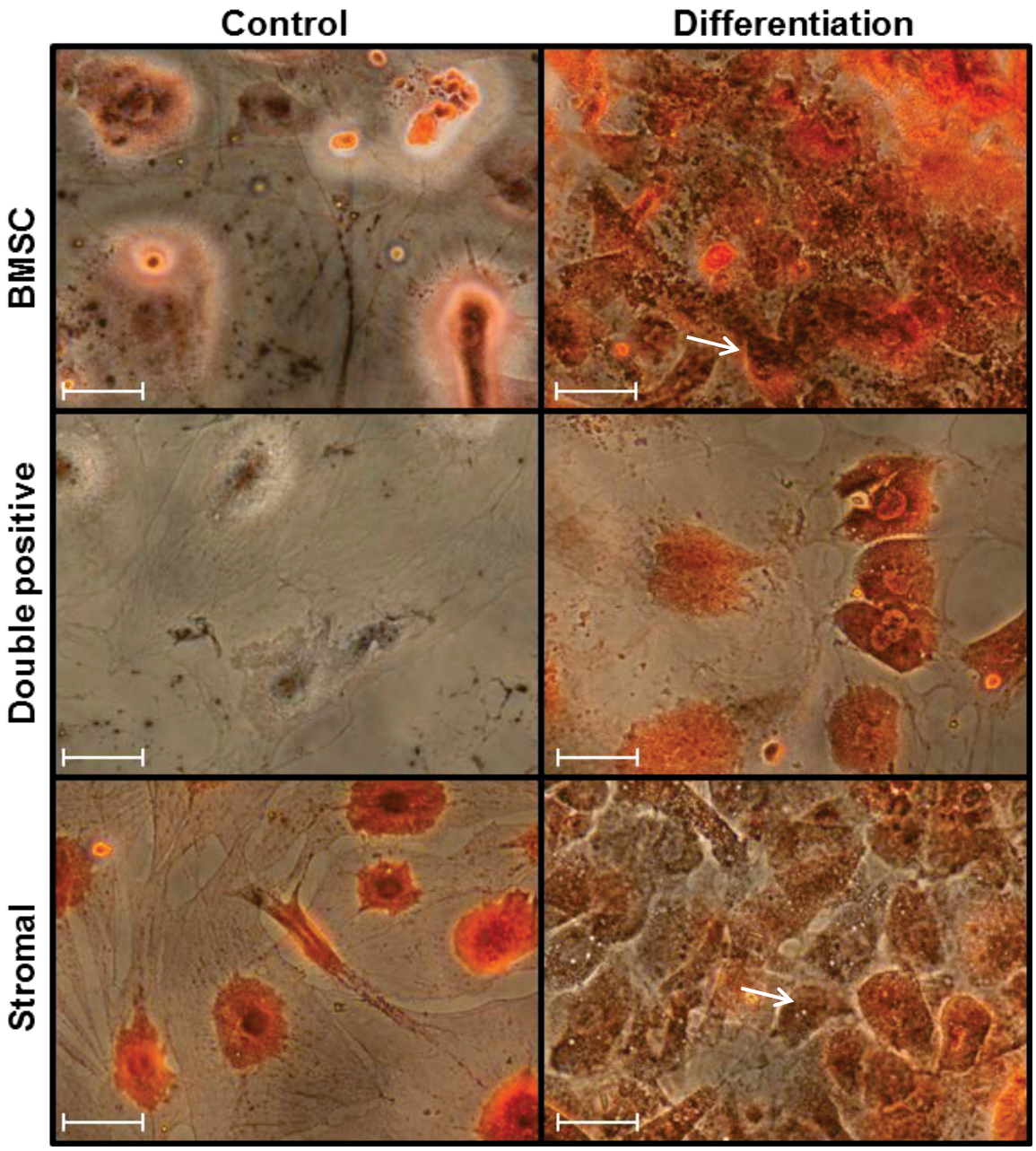

Figure 3.16: Inter-population schematic of osteogenesis at late passage $1.25x10^4$ cells/ml of each cell population were seeded into a 24-well plate in triplicate and incubated in either osteogenic Control or Differentiation medium for 35 days. The cells were subsequently fixed with 10% formalin and stained with 2% (w/v) Alizarin Red S. Osteocytes are indicated by arrowheads. Images were acquired on a Leica DM Microscope at 20x magnification, 100µm scale.

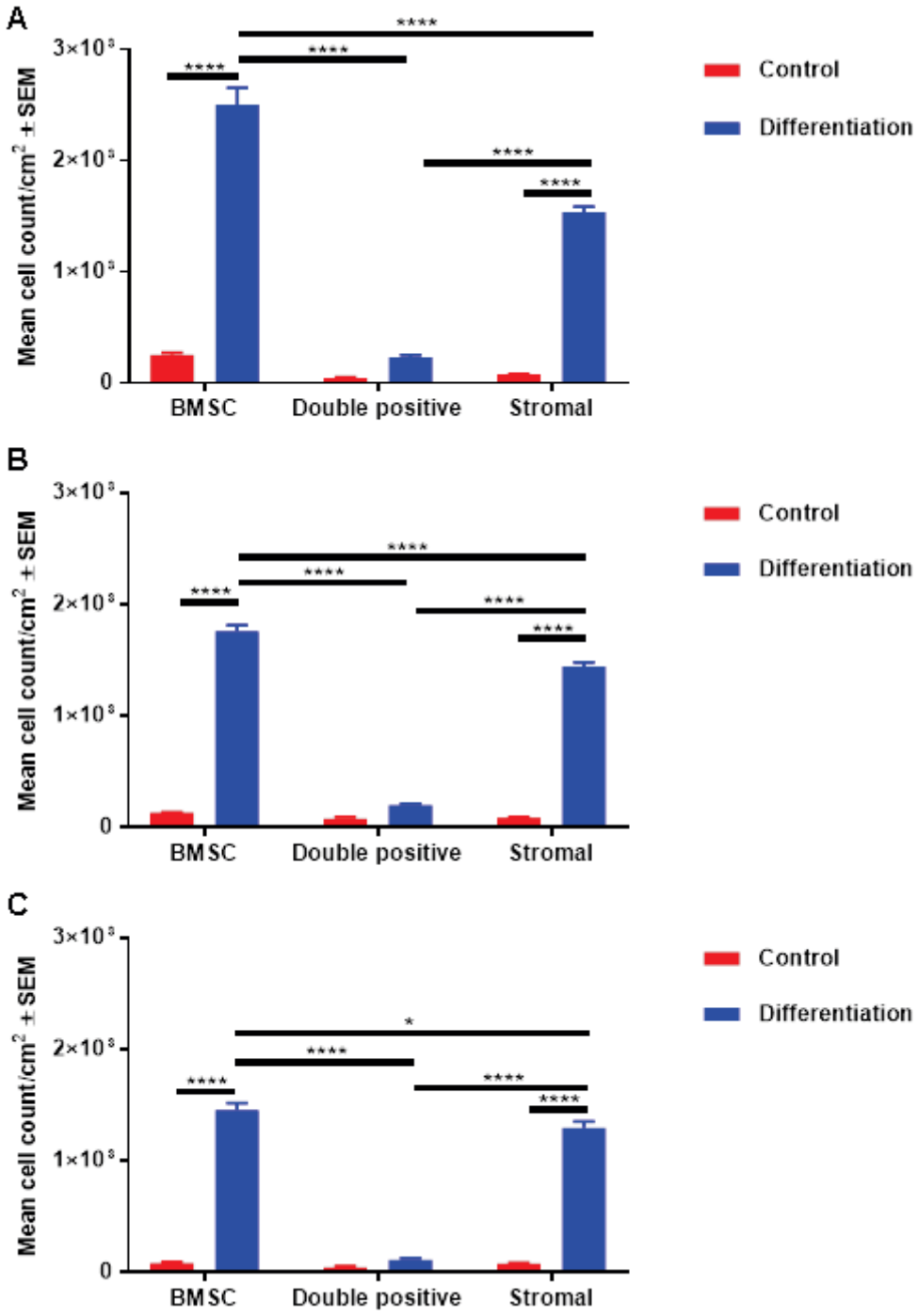

Figure 3.17: Inter-population quantitative analysis of osteogenesis Quantitative data was obtained from BMSC, double positive and stromal cells at early (A), mid (B) and late (C) passage under control and differentiation osteogenesis conditions. The data is represented as mean ± SEM (n=3). A two-way ANOVA and Tukey's post-hoc were performed, * $p<0.05$.

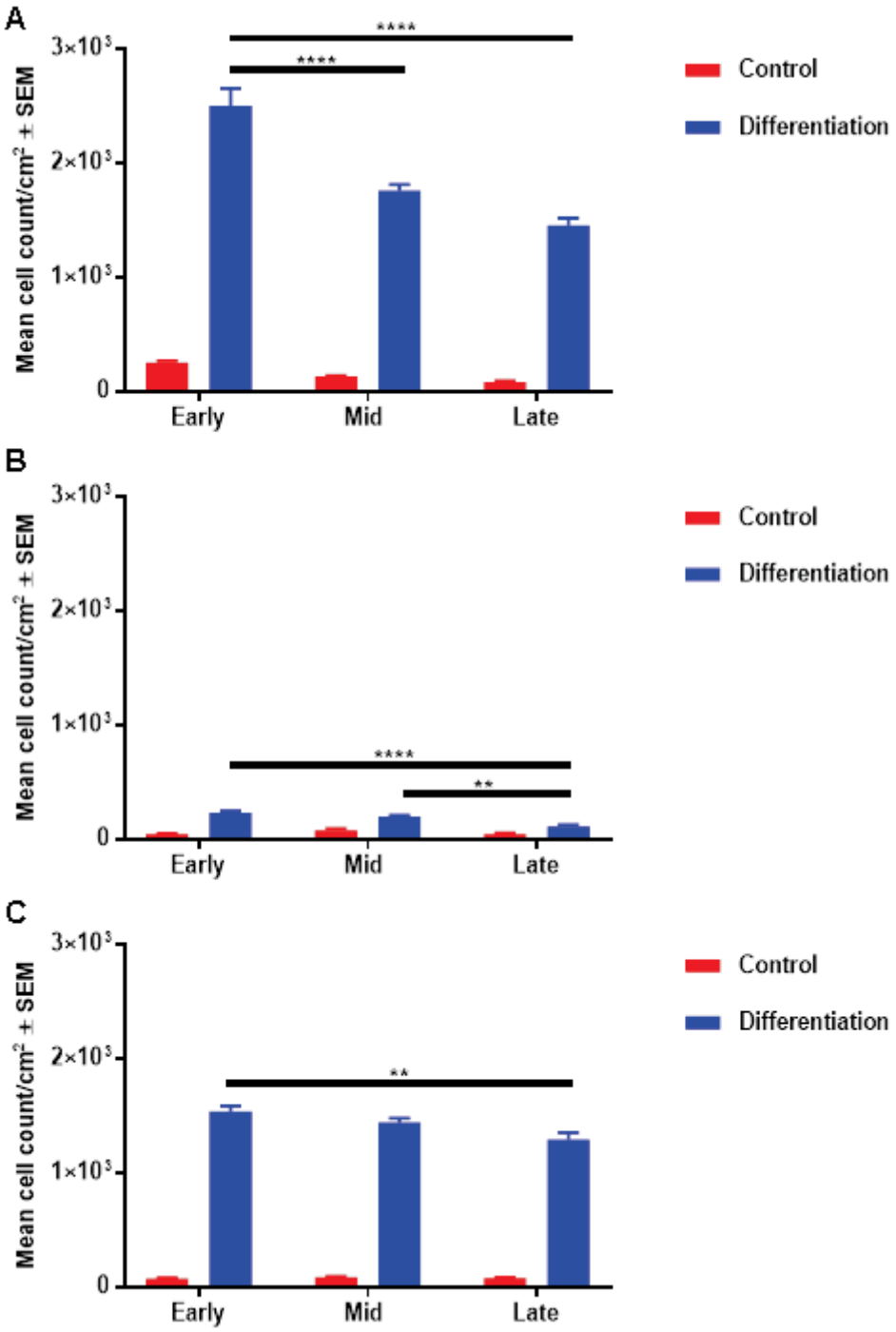

Figure 3.18: Intra-population quantitative analysis of osteogenesis Quantitative data was obtained from BMSC (A), double positive (B) and stromal cells (C) at early, mid and late passage under control and differentiation osteogenesis conditions. The data is represented as mean ± SEM (n=3). A two-way ANOVA and Tukey's post-hoc were performed, * $p<0.05$.

3.2.5.3 Chondrogenic differentiation

Chondrogenesis was assessed by exposing mid (P15-30) passage BMSC and stromal cells to chondrogenesis differentiation or control medium for 25 days as detailed in Section 2.4.3. Following formalin fixation, paraffin embedding and slide mounting, cells were stained with Toluidine blue and assessed for cartilage formation (Figure 3.19). Mature mammalian cartilage showing purple staining, was included as a positive control for Toluidine blue (C). Stromal cells failed to form micro-masses and showed characteristics similar to BMSC exposed to control medium (data not shown). BMSC exposed to control medium failed to form micro-masses and did not differentiate into mature cartilage (Ai and Bi). In contrast, BMSC exposed to chondrogenesis medium developed into well-formed micro-masses of 3-4 mm in diameter (Aii) and underwent chondrogenesis shown with Toluidine blue staining (Bii).

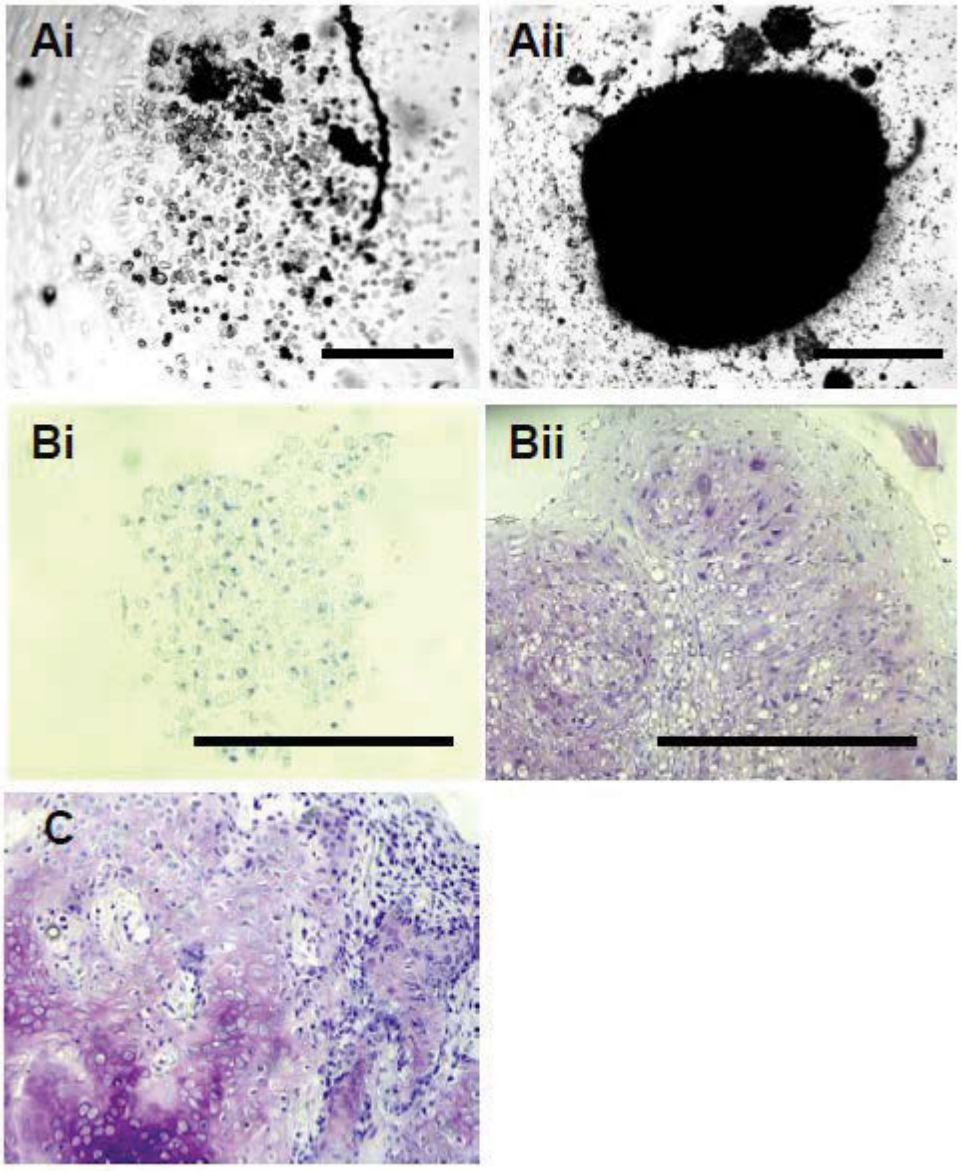

Figure 3.19: BMSC micro-mass chondrogenesis Mid-passage BMSC were centrifuged at 450g for 10 min in U-bottom 96 well plates and exposed to control (i) or chondrogenesis differentiation (ii) medium for 25 days. BMSC were photographed using a digital dissecting microscope (A; Nikon, scale 1 mm) prior to fixation. Following paraffin embedding, sectioning (5uM) and staining with Toluidine blue, cartilage formation (purple staining) was assessed using inverted low power light microscopy (B; Nikon, scale 1 mm). Sections of mature mammalian cartilage were also stained with Toluidine blue and used as a positive control (C). These assays were performed by Dr Martiniello-Wilks.

3.2.6 Gene expression profiling

A number of pancreatic transcription factors, hormones and proteins were assessed via RT-PCR for their intrinsic expression in BMSCs, double positive and stromal cell sub-populations (Figure 3.20). There was a lack of expression of all assessed transcription factors, hormones and proteins in all cell-subpopulations (Lanes 2-4), albeit very low detection of *Pcsk1* in double positive cells (Lane 3). By comparison, all genes that were assessed were detected in the mouse pancreas positive control (Lane 1). The genes that were detected in the negative control mouse liver (Lane 5) were *FoxA2*, *Scl2a2* and *Gck* which was as expected.

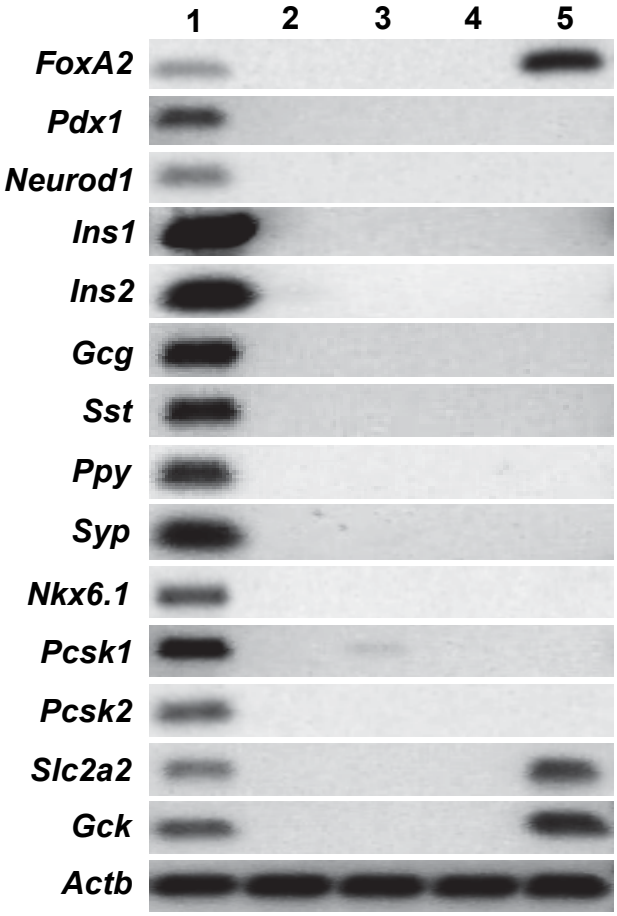

Figure 3.20: RT-PCR gene expression profiling of native BMSCs, double positive and stromal cells

Pancreatic transcription factors, hormones and proteins were assessed via RT-PCR for their expression in the positive control mouse pancreas (Lane 1), BMSC (Lane 2), Double positive cells (Lane 3), Stromal cells (Lane 4) and the negative control mouse liver (Lane 5). RT-PCR products were run on a 1% (w/v) agarose gel at 90V for 90 min and visualised on the InGenius3 UV transilluminator.

3.3 Discussion

The International Society for Cellular Therapy released a Position Statement in 2006 describing the minimal criteria for defining human multi-potent mesenchymal stromal cells, otherwise known as MSCs[229]. In brief, three criteria were assigned to these cells showing a fibroblast-like morphology (a) plastic adherence; (b) expression of CD105 in the human or CD106 in the mouse, CD90, and CD73 and the lack expression of haematopoietic stem cell marker CD34, and leukocyte CD45, CD14, CD11b, CD79, CD19 and HLA-DR cell surface markers; (c) ability to differentiate into adipocytes (fat), osteoblasts (bone) and chondrocytes (cartilage) *in vitro*[229].

In this study we isolated a sub-population of murine MSCs from the bone marrow of non-obese diabetic (NOD) mice using a FACS sorting technique developed by Martiniello-Wilks. Martiniello-Wilks used FACS sorting to identify a subset of murine BMSC isolated from C57BL/6 and albino C57BL/6 mice that displayed potent proliferation, clonogenicity and tri-lineage differentiation, when compared to the plastic adherent bone marrow stromal cell starting population (manuscript in preparation). Furthermore, these cells displayed a typical MSC phenotype of $CD45^{-}$ $CD34^{-}$, $CD31^{-}$, SCA-1 $(Ly6)^{+}$, $CD44^{+}$, $CD90^{+}$, $CD73^{+}$ and $CD106^{+}$ (manuscript in preparation). Similarly NOD BMSC isolated in this study displayed potent proliferation, clonogenicity and tri-lineage differentiation, hallmark characteristics of mesenchymal stem cells, when compared to the plastic adherent bone marrow stromal cell starting population. These BMSC also maintained their clonogenicity and tri-lineage differentiation potential beyond 30 passages *in vitro* providing evidence of their ability to self-renew without a fundamental change in their native functional characteristics. This is an important consideration given the potential of adult stem cells to undergo transformation and

the downstream devastating effects if this occurred during the development of a cell replacement therapy.

MSC isolation from a variety of tissue sources has been attempted using a number of methodologies including antibody-based cell sorting[323], low and high-density culture[324], positive and negative selection[325], frequent media changes[326] and enzymatic digestion[327]. Yet the success of each methodology in isolating true MSCs is limited by differences in isolated MSC function, molecular surface marker expression and genetic characterisation. To this day, and despite the growing interest in the utilisation of MSCs for regenerative medicine and the treatment of genetic/metabolic disorders; a single, effective, standardised method of isolating and enriching MSCs for clinical use has not been developed or agreed upon by the scientific community. As such, discrepancies in the reported characteristics and functions of MSCs are unsurprising.

3.3.1 Isolation and enrichment of BMSCs via FACS

This is the first study reporting BMSC isolation from the bone marrow of NOD mice, and enrichment using $CD45^{-}/Ly6^{+}$ FACS sorting for subsequent *ex vivo* expansion and gene modification. A variety of surface markers have previously been identified and utilised for the positive and negative selection of MSCs from murine bone marrow[326, 329] (Table 3.6). By comparison to other similar studies[326, 330], and using the surface markers previously mentioned, we report a reliable method of MSC enrichment with respect to percentage cell retrieval, cell morphology, cell proliferation, clonogenicity and tri-lineage differentiation into bone, fat and cartilage.

Table 3.6: Surface markers used for the identification of murine MSCs

Negative	Moderate/Heterogeneous	High
CD45, CD11b, Ter-119, CD31	CD73, CD51, CD61, CD71, CD80, CD95, CD120b, CD140a, MHC Class I	CD24, CD29, CD44, CD49e, CD81, CD106, Sca-1, CD105, PDGFRα

Initially, flushed bone marrow (containing a heterogeneous population of bone marrow cells) was cultured for two passages during which the plastic adherent stromal cells were retained and the largely non-adherent, hematopoietic stem cells discarded. Plastic adherent cells were retained as plastic adherence is a defining characteristic of BMSCs. Plastic adherent stromal cells were subsequently utilised for FACS sorting of the $CD45^-/Ly6^+$ cell population corresponding to BMSCs, which constituted 33.2% of the initial adherent stromal cell population. FACS analysis identified that 71.2% of the stromal cell population were $Ly6^+$ at passage two. By comparison, in a similar study where Ly6 was used as a positive selection marker for the enrichment of MSCs, increases in the frequency of Ly6 positive cells were observed with increasing passage, where >90% of the original stromal cell population were $Ly6^+$ by passage 3[330]. $Ly6^+$ cells were gated against $CD45^-/Ter\text{-}119^-$ surface expression profiles, which are common markers used for the negative selection of murine MSCs. The differences in percentage retrieval of $Ly6^+$ cells were likely a consequence of the difference in passage number, as it appears that surface marker expression evolves/changes rapidly with increasing passage. This suggests that at the time of sorting, post cell isolation is critical in obtaining MSCs of a particular surface expression profile, and that variations with regards to the timing of MSC enrichment are likely to ultimately lead to differences in enriched cell function. In addition, species-associated differences in MSC surface marker and gene expression profiles may also contribute to MSC fate and function[331-333].

3.3.2 Characterisation of BMSC morphology and function

A qualitative assessment of changes in MSCs post enrichment can be observed through changes in morphology observed in cell culture. It is widely accepted that MSCs possess a fibroblast-like morphology upon *ex vivo* culture in tissue culture treated dishes. The BMSCs enriched for in this study demonstrated a fibroblast-like morphology during all passages (early, mid and late). In fact, by comparison to stromal cells and double positive ($CD45^+/Ly6^+$) cells, BMSCs demonstrated a more stable morphology with increasing passage, with a reduction in cytoplasmic volume being the only discernible difference over time. Transient differences in BMSC morphology were observed with relation to high seeding densities and cell-to-cell contact, however these transient changes in morphology were reversible upon re-seeding at a lower density and by not allowing the cells to reach >90% confluency (data not shown). More importantly, the maintenance of the BMSCs' fibroblast-like morphology throughout early, mid and late passage suggests that morphology did not contribute to changes in BMSC proliferation, clonogenicity and differentiation potential observed in mid and late-passage. This is in contrast to evidence in the literature, which suggests that MSCs undergo age-related morphological changes[334-336]. However, the maintenance of the fibroblast-like morphology of BMSCs in this study is likely due to the addition of bFGF to the culture media post FACS sorting, a unique feature not utilised by all who conduct MSC research. This highlights the impact of differences in *ex vivo* culture methods on variations in MSC characteristics that are commonly reported in the literature[337, 338].

A common understanding of *ex vivo* cultured MSCs is their decreasing proliferative capacity with increasing passage and eventual senescence[339, 340]. In this study, BMSCs reached a state of senescence and showed increased numbers of apoptotic cells between passages 5-8 (data

not shown). However, the addition of bFGF to the culture media resulted in a number of cells resisting senescence and maintaining a fibroblast-like morphology with increasing passage. In addition, BMSCs that resisted senescence demonstrated increased proliferation rates with increasing passage. These results are supported by a study which showed that bFGF inhibits apoptosis and promotes proliferation of MSCs through a reduction in cellular oxidative stress[341]. The increase in bFGF-induced cell proliferation may also explain the increase in BMSC clonogenicity with increasing passage. However, improved cell proliferation and clonogenicity effects of bFGF were also observed with stromal and double positive cells suggesting that bFGF may be used to promote these characteristics in many fibroblast-like cell populations.

Of particular interest was the differentiation potential of culture expanded BMSCs. Despite demonstrating improved cell proliferation and clonogenicity (which is in contrast with the majority of the reported literature) the ability of BMSCs to undergo adipogenic and osteogenic differentiation decreased gradually with increasing passage. Although late stage BMSC (P30-60) in this study show less adipogenesis and osteogenesis than early passage cells, the fact that differentiation still occurs at these late passage numbers is remarkable. The majority of MSC literature reports an age-related loss of differentiation potential that occurs largely during early to mid-passage [342-344]. Although the addition of bFGF among other factors have been assessed in overcoming senescence-associated loss of MSCs[345-347] their use requires further investigation with respect to their impact on MSC differentiation [347]. This ultimately raises concerns over the identity of MSCs with extended culture and necessitates ongoing surveillance of stem-like properties amongst other defining characteristics. Standardised monitoring of MSC identity and function with extended culture is therefore paramount for the development of cell replacement therapies for the clinical setting.

Considering that enriched BMSCs were to be utilised as targets for the subsequent differentiation into IPCs in this study, it was important to determine the native gene expression profile of the enriched BMSCs with respect to pancreatic gene expression. Due to the difference in tissue source and primordial cell origin of MSCs and β-cells, it was expected that MSCs would not intrinsically express pancreatic genes which was confirmed by this study. However, it has been demonstrated that MSCs derived from pancreatic exocrine cell explants do express some pancreatic genes in a passage-dependent manner[348, 349].

3.3.3 Requirement for a tissue-specific classification of MSCs

To date, the identification and characterisation of MSCs *in vivo* is yet to be determined, which consequently limits our ability to directly relate our understanding of *ex vivo* identified MSCs with *in vivo* MSCs. Yet, it has been shown that tissue-specific enriched MSCs have a propensity to perform specific and various functions *in vivo*[350]. Unsurprisingly, a consensus on broadly defining MSCs has not been accepted in the MSC research community due to these tissue-specific differences. Currently, the criteria proposed by the ISCT for the isolation and enrichment of MSCs is being applied in a broad sense, whereas the evidence suggests that phenotypically MSCs may vary depending on their tissue source and method of isolation amongst other factors. Experimental variability and poor clinical outcomes is therefore most likely related to the application of specific tissue-derived MSCs as treatment for diseases beyond their *in vivo* function. It appears reasonable to suggest that specific sub-categories of criteria should be utilised to characterise MSCs isolated from bone-marrow, adipose tissue, dental pulp, or any other adult tissue source.

Considering the encouraging assessment of NOD BMSCs at various passages in this study, and the fact that deriving sufficient quantities of primary cells for differentiation into IPCs is

an ongoing challenge, culture expanded BMSCs were identified as suitable targets for differentiation into IPCs. The subsequent chapters assess the success of culture expanded BMSCs as targets for T1D gene therapy with respect to their ability to persist in immune-competent and immune-deficient models of diabetes (Chapter 4) and their capacity to differentiate into functional IPCs that reverse diabetes upon transplantation (Chapter 5).

Chapter 4

Monitoring the persistence of bioluminescent BMSC in immune-competent and immune-deficient mice

Introduction

One of the challenges of T1D cell replacement therapy that has yet to be overcome is the requirement for encapsulation of the surrogate IPCs as a means of protecting against allogeneic or recurrent autoimmune responses. A viable, long-term cure for T1D requires ongoing graft function throughout the life-time of the patient. Despite encapsulation proving successful in interfering with the immunological aspect of cell transplantation; it has become clear that encapsulated islets or surrogate IPCs lose function over time. However, the proven *in vitro* immunomodulatory/immune-evasive capacity of MSCs presents the possibility of the development of a treatment for T1D without the need for encapsulation.

Despite some success in pre-clinical models of T1D, the fate of intravenously administered native MSCs raises doubts over the potential for sustained effect. It has become apparent that the majority of intravenously administered MSCs become entrapped in the lungs[351, 352], of which some escape and migrate to other organs such as the liver and spleen, or localise to areas of tissue damage. A study has shown however that 24 hours post-administration that MSCs are no longer viable[351], which raises questions concerning the therapeutic window of MSCs; whether improved clinical outcomes are a consequence of MSCs that have escaped entrapment or if direct injection into the site of interest would further improve those outcomes.

As a consequence of the conjecture, and considering the common alternative subcutaneous route of administration of surrogate IPCs in other animal models of diabetes, it was of particular interest to determine the survival of a subcutaneous graft of native BMSCs in both immune-competent and immune-deficient animal models of diabetes. To permit the visualisation of cell survival following transplantation, BMSCs were gene-modified to

express the bioluminescent reporter *Firefly luciferase* (*Luc2*), and cell grafts monitored over time via *in vivo* bioluminescence imaging (BLI). The use of a bioluminescent reporter over traditional fluorescent reporters was due to the improved sensitivity, dynamic capability and the broad application of luciferase by comparison. Non-invasive BLI technology is an established and sensitive tool for assessing cell replacement therapy efficacy and treatment outcome in living preclinical small animal models. Furthermore, preclinical BLI results often serve as the decision point of a cell replacement therapy's suitability (efficacy and safety) for clinical trial testing in humans. This study utilised an IVIS Lumina II imaging system (Perkin Elmer/Thermofisher Scientific).

In addition, the *in vivo* transplantation of surrogate IPCs that successfully reverses hyperglycaemia is commonly confirmed via graft removal and as a consequence recurring hyperglycaemia. To eliminate the need for invasive graft removal, BMSCs were also gene-modified to express the suicide gene *CDUPRT*, which allowed for the non-invasive destruction of the suicide gene-expressing BMSCs following administration of the non-toxic prodrug 5-FC. As a result, BMSC-*Luc2/CDUPRT* cells that were used as targets for differentiation into surrogate IPCs could be eliminated in a safer and more efficient manner.

Specific Aims

- Generate mammalian expression vectors encoding the *Luc2* and *CDUPRT* genes.
- Gene-modify BMSCs to express *Luc2* and *CDUPRT* via nucleofection.
- To monitor the survival of a syngeneic transplant of BMSC-*Luc2/CDUPRT* in NOD and NOD/*Scid* mice via BLI.

4.1 Specific methods

4.1.1 Bacterial preparation of plasmids

The manipulation of genetic material and generation of genetically modified organisms was approved by the UTS Biosafety Committee (2001-19-R-GC; 2009-02-R-GC). The mammalian dual expression plasmid pVITRO2-hygro®-mcs (InvivoGen®, USA) (Figure 4.1), a vector encoding the luciferase reporter gene *Luc2* (*Photinus pyralis*) pGL4.20 (*Luc2*/Puro) (Promega®) (Figure 4.2) and a vector encoding CDUPRT pORF5-Fcy::Fur (InvivoGen®) (Figure 4.3) were transformed in One Shot® TOP10 Chemically competent *E. coli* (Lifetechnologies™) according to the manufacturer's instructions and described in Chapter 2, Section 2.5.1. Of the four plasmid cultures for each plasmid transformant, one culture was used for glycerol stocks and three cultures were used for plasmid mini-prepping as described in Section 2.5.2 and Section 2.5.3 respectively.

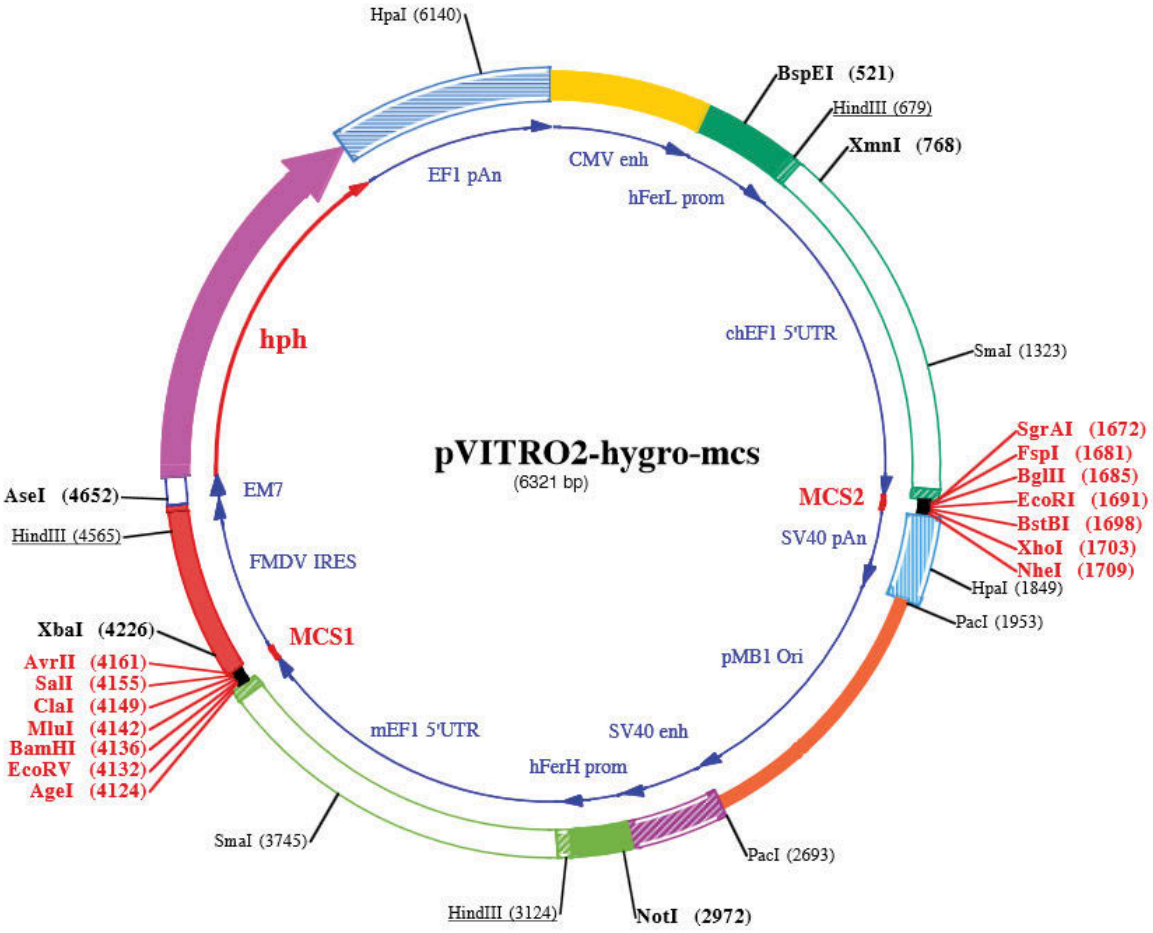

Figure 4.1: Diagrammatic representation of the pVITRO2-hygro-mcs mammalian expression plasmid

pVITRO2-hygro-mcs allows the ubiquitous and constitutive co-expression of two genes of interest. The plasmids carry two human ferritin composite promoters, FerH (heavy chain) and FerL (light chain). To eliminate the iron regulation, their 5'UTRs have been replaced by the 5'UTR of the mouse and chimpanzee EF-1α genes. pVITRO2-hygro-mcs possesses the Hygromycin B antibiotic resistance selectable marker that is active both in *E. coli* and mammalian cells. The plasmid contains two multiple cloning sites (MCS) for the convenient cloning of the cDNAs of interest.

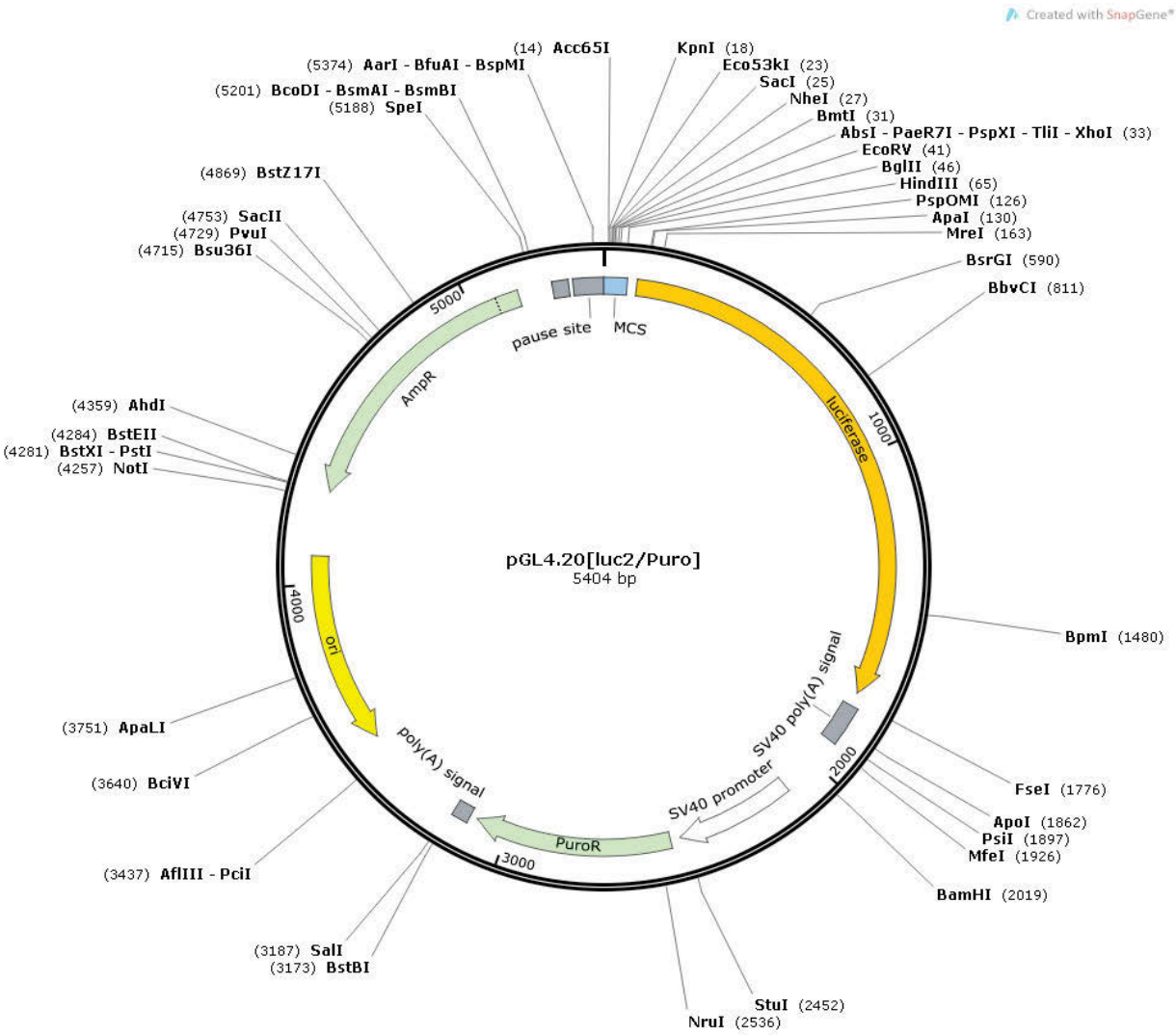

Figure 4.2: Diagrammatic representation of the pGL4.20 mammalian expression plasmid pGL4.20[*luc2*/Puro] encodes the luciferase reporter gene *luc2* (*Photinus pyralis*) and is designed for high expression and reduced anomalous transcription. This vector also contains a mammalian selectable marker for Puromycin resistance in which the number of transcription factor binding sites has been reduced and mammalian codon-optimised. The pGL4.20[*luc2*/Puro] plasmid is a basic vector with no promoter. It contains an MCS to allow for the cloning of a promoter of choice.

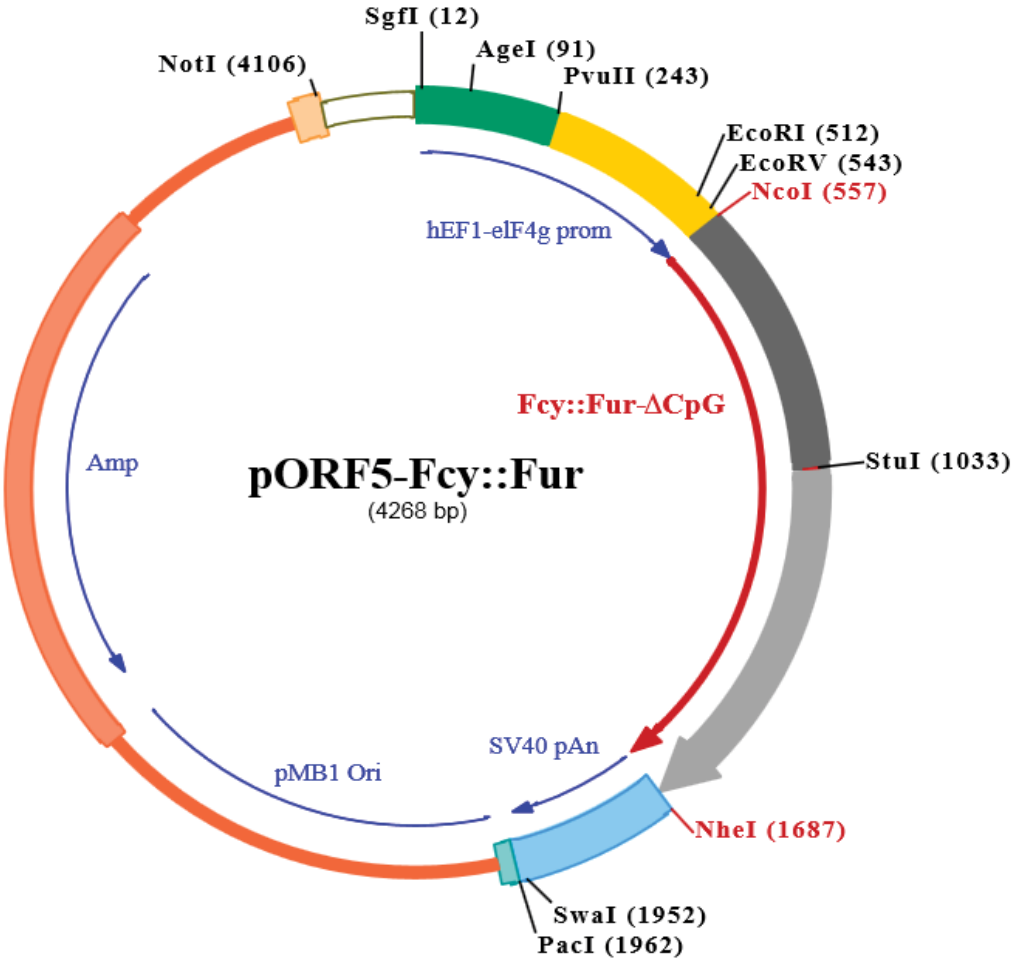

Figure 4.3: Diagrammatic representation of the pORF5-Fcy::Fur mammalian expression plasmid pORF5-Fcy::Fur allows the constitutive expression of the fusion of yeast fcy1and fur1genes encoding cytosine deaminase and uracil phosphoribosyl-transferase (*CDUPRT*) respectively. Restriction sites flanking the *CDUPRT* gene allow for sub-cloning into many compatible destination vectors.

4.1.2 Bioluminescent tracking and suicide plasmid cloning

4.1.2.1 Restriction digestion of pVITRO2-mcs and pGL4.20

In preparation for the ligation of the pVITRO2-mcs plasmid and *Luc2* gene, both pVITRO2-mcs and pGL4.20 were digested with the restriction enzymes EcoRV-HF (New England Biolabs®) and BamHI-HF (New England Biolabs®) according to Table 4.1. All reactions were incubated at 37ºC for 2 hours.

Table 4.1: EcoRV-HF/BamHI-HF digest of pVITRO2-mcs and pGL4.20

Components	pVITRO2-mcs (µl)	pGL4.20 (µl)
Plasmid DNA (~200ng/µl)	15	30
Cutsmart Buffer (10x)	5	5
EcoRV-HF (20U/µl)	1	1
BamHI-HF (20U/µl)	1	1
dH_2O	28	13
Total volume	50	50

4.1.2.2 Gel extraction of digested pVITRO2-mcs and Luc2

The restriction digest reactions were run on 1% (w/v) agarose gels at 90V in 1x TBE buffer for 90 min. The bands corresponding to digested pVITRO2-mcs, *Luc2* and *CDUPRT* were excised from the gel and transferred to 2ml microfuge tubes. DNA was then extracted from the gel pieces using the PureLink® Quick Gel Extraction Kit (Lifetechnologies™) according to the manufacturer's instructions. Briefly, gel pieces were solubilised in three volumes of Gel Solubilisation Buffer (L3) at 50ºC for 10 min. To improve DNA yields, one volume of 100% isopropanol was added to the dissolved gel pieces. The dissolved gel pieces were then transferred to Quick Gel Extraction Columns inside wash tubes and centrifuged at 12,000g for 1 min. The bound DNA was washed twice with 500µl of Wash Buffer (W1) containing ethanol, and eluted from the column in 20µl of Nuclease-free water. The gel purified DNA was stored at -20ºC for long-term storage, or used immediately in subsequent experiments.

To confirm purity of the DNA fragments, a sample of the gel purified DNA was run on a 1% (w/v) agarose gel at 90V in 1x TBE buffer for 90 min. DNA quality and concentration was assessed using a NanoDrop™ 2000 spectrophotometer (Thermofisher™).

4.1.2.3 Ligation of pVITRO2-mcs and Luc2

Digested pVITRO2-mcs (EcoRV-HF/BamHI-HF) was dephosphorylated using recombinant Shrimp Alkaline Phosphatase (rSAP) (New England Biolabs®) according to the manufacturer's instructions. Briefly, 2µg of digested plasmid DNA was incubated with 10x rSAP Buffer (New England Biolabs®) and 1U/ml rSAP at 37ºC for 30 min, followed by rSAP inactivation at 65ºC for 5 min. In addition, purified *Luc2* was diluted to 50ng/µl with dH_2O in preparation for use in the ligation reactions. Ligation of dephosphorylated pVITRO2-mcs (EcoRV-HF/BamHI-HF) and *Luc2* was performed at three insert:vector backbone ratios as

outlined in Table 4.2, and incubated at 16°C for 16 hours (overnight). A negative control of dephosphorylated pVITRO2-mcs (EcoRV-HF/BamHI-HF) was setup to account for potential vector backbone re-ligation.

Table 4.2: Ligation of pVITRO2-mcs and the *Luc2* gene

Component	3:1 (µl)	6:1 (µl)	10:1 (µl)	-ve control (µl)
***Luc2* (50ng/µl)**	1	2	3	-
Dephosphorylated pVITRO2-mcs (50ng/µl)	1	1	1	1
Ligase buffer (10x)	1	1	1	1
T4 DNA Ligase (400U/µl)	1	1	1	1
dH_2O	6	5	4	7
Total	10	10	10	10

4.1.2.4 Restriction digestion of pVITRO2-Luc2 and pORF5-Fcy::Fur

Following the ligation of pVITRO2-mcs and *Luc2* to generate pVITRO2-*Luc2*, and in preparation for the ligation of pVITRO2-*Luc2* and the *CDUPRT* gene, both pVITRO2-*Luc2* and pORF5-Fcy::Fur were digested with the restriction enzymes EcoRI-HF (New England Biolabs®) and NheI-HF (New England Biolabs®) according to Table 4.3. All reactions were incubated at 37°C for 2 hours.

Table 4.3: EcoRI-HF/NheI-HF digest of pVITRO2-*Luc2* and pORF5-Fcy::Fur

Components	pVITRO2-*Luc2* (µl)	pORF5-Fcy::Fur (µl)
Plasmid DNA (~500ng/µl)	10	20
Cutsmart Buffer (10x)	5	5
EcoRI-HF (20U/µl)	1	1
NheI-HF (20U/µl)	1	1
dH_2O	33	23
Total volume	50	50

4.1.2.5 Gel extraction of digested pVITRO2-Luc2 and CDUPRT

The restriction digest reactions were run on a 1% (w/v) agarose gel at 90V in 1x TBE buffer for 90 min. The bands corresponding to digested pVITRO2-*Luc2* and *CDUPRT* were excised from the gel and transferred to 2ml microfuge tubes. DNA was then extracted from the gel pieces using the PureLink® Quick Gel Extraction Kit (Lifetechnologies™) according to the manufacturer's instructions and as described in Section 4.1.2.2.

4.1.2.6 Ligation of pVITRO2-Luc2 and CDUPRT

Digested pVITRO2-*Luc2* (EcoRI-HF/NheI-HF) was dephosphorylated using recombinant Shrimp Alkaline Phosphatase (rSAP) (New England Biolabs®) according to the manufacturer's instructions. Briefly, 2µg of digested plasmid DNA was incubated with 10x rSAP Buffer (New England Biolabs®) and 1U/ml rSAP at 37°C for 30 min, followed by rSAP

inactivation at 65ºC for 5 min. In addition, purified *CDUPRT* was diluted to 50ng/µl with dH_2O in preparation for use in ligation reactions.

Ligation of dephosphorylated pVITRO2-*Luc2* (EcoRI-HF/NheI-HF) and *CDUPRT* were performed at three insert:vector backbone ratios as outlined in Table 4.4, and incubated at 16ºC for 16 hours (overnight). A negative control of dephosphorylated pVITRO2-*Luc2* (EcoRI-HF/NheI-HF) was setup to account for potential vector backbone re-ligation.

Table 4.4: Ligation of pVITRO2-*Luc2* and the *CDUPRT* gene

Component	3:1 (µl)	6:1 (µl)	10:1 (µl)	-ve control (µl)
***CDUPRT* (50ng/µl)**	1	2	3	-
Dephosphorylated pVITRO2-*Luc2* (50ng/µl)	1	1	1	1
Ligase buffer (10x)	1	1	1	1
T4 DNA Ligase (400U/µl)	1	1	1	1
dH_2O	6	5	4	7
Total	10	10	10	10

4.1.2.7 Transformation of ligation reactions in TOP10 E.coli

Transformation of ligation reactions was performed as outlined in Section 2.5.1.1. Selection of *E.coli* expressing pVITRO2 plasmids was performed using Hygromycin B (100µg/ml) as outlined in Section 2.5.2. Successfully generated plasmids were subsequently mini-prepped as described in Section 2.5.4 following confirmation of transgene function.

4.1.2.8 In vitro bioluminescence imaging of putative pVITRO2-Luc2 clones

To confirm successful ligation of the *Luc2* gene into the pVITRO2-mcs backbone, an alternative technique to confirmatory restriction enzyme digestion that assesses *Luc2* function

was employed. *In vitro* BLI of the putative pVITRO2-*Luc2 E. coli* clones was performed. BLI imaging allows for the detection of the bioluminescent signal produced following the addition of the *Luc2* substrate D-luciferin (Gold Biotechnology®, USA). Briefly, 100µl of the putative pVITRO2-*Luc2 E. coli* clone cultures was aliquoted in triplicate into a 96-well plate (PerkinElmer®, USA). Negative controls of 1x D-PBS and pVITRO2-mcs *E. coli* culture (100µl of each in triplicate) were included in the assay. BMSC-*LacZ/Luc2* ($1x10^5$ cells/well) that co-expresses *Luc2* and the β-galactosidase gene *LacZ* were used as a positive control. The BMSC-*LacZ/Luc2* cell line was previously generated in Dr Rosetta Martiniello-Wilks' laboratory via nucleofection of a pVITRO2-mcs plasmid possessing the *Luc2* and *LacZ* genes in a similar fashion to the nucleofection procedure described in Section 4.1.3. Imaging of the 96-well plate was performed on the IVIS Lumina II (Caliper Life Sciences, USA) both prior to and following addition of the D-luciferin (30mg/ml) substrate. D-luciferin (300µg/ml) was added to the wells of the plate (1:1) that contained controls and experimental samples, and the plate imaged according to the *in vitro* BLI acquisition settings (Table 4.5).

Table 4.5: *In vitro* BLI acquisition settings

Incubation time (min)	Exposure time (sec)	F stop (F/s)	Field of View (FoV)	Binning
2	10	1	D	Small

4.1.2.9 Confirmation of CDUPRT ligation into pVITRO2-Luc2

To confirm the successful ligation of the *CDUPRT* gene into the pVITRO2-*Luc2* backbone, confirmatory restriction enzyme digestion was performed using EcoRI-HF (New England Biolabs®) and NheI-HF (New England Biolabs®) on miniprepped plasmid DNA of the putative pVITRO2-*Luc2/CDUPRT* clones. Confirmatory restriction enzyme digestion

reactions were setup as outlined in Table 4.6 and incubated at 37ºC for 2 hours. The products from the restriction digest were subsequently run on a 1% (w/v) agarose gel at 90V in 1x TBE buffer for 90 min. To re-confirm the function of the *Luc2* gene in the newly generated pVITRO2-*Luc2/CDUPRT* construct, BLI was performed as outlined in Section 4.1.2.8.

Table 4.6: Diagnostic digest of pVITRO2-*Luc2/CDUPRT*

Component	Volume (µl)
Plasmid DNA (500ng/ul)	1
Cutsmart Buffer (10X)	1
EcoRI-HF (20U/µl)	1
NheI-HF (20U/µl)	1
dH_2O	6
Total	10

4.1.3 Generation of tracking and suicide BMSC via nucleofection

4.1.3.1 Antibiotic sensitivity assay

To determine the optimal concentration of Hygromycin B (Lifetechnologies™) with which to select stable tracking BMSC-*Luc2* and suicide BMSC-*Luc2/CDUPRT* clones, a preliminary antibiotic sensitivity assay utilising parental BMSCs that do not possess Hygromycin B antibiotic resistance were cultured in the presence of increasing concentrations of Hygromycin B, ranging from 0-500µg/ml. Initially, $5x10^5$ parental BMSCs were seeded in triplicate in complete media in 6-well plates per concentration of Hygromycin B (0µg/ml, 62.5µg/ml, 125µg/ml, 250µg/ml and 500µg/ml). Following cell adherence, the media was removed and replenished with complete media containing Hygromycin B at the

aforementioned concentrations. The assays were subsequently incubated at 37ºC/5% CO_2 for 14 days. Cell viability was assessed at Day 0, 1, 3, 5, 7, 10 and 14 via Trypan Blue exclusion with 0.4% Trypan Blue solution (Lifetechnologies™). The optimal concentration was determined as the concentration at which >90% cell death was observed within 5-7 days.

4.1.3.2 Nucleofection of BMSCs

Early passage single positive BMSCs were cultured in complete medium as outlined in Section 2.1, and thereafter expanded to 85% confluency in 5 x 175cm^2 flasks. On the day of nucleofection, the cells were detached with 1x TrypLE™, washed twice with 1x HBSS, and assessed for viability by Trypan Blue exclusion with 0.4% Trypan Blue Solution. The cells were subsequently reconstituted in 1x HBSS to a concentration of 1x10^6 viable cells/ml, and 1ml (1x10^6 cells) transferred to an Amaxa® certified cuvette (Lonza™).

In preparation for the setup of the nucleofection reactions, 0.5ml of Nucleofection Supplement® (Lonza™) was added to 2.25ml of Nucleofector Solution® (Lonza™) to generate a working Nucleofector solution® which is stable for 3 months at 4ºC. To setup a nucleofection reaction, 100µl of working Nucleofector Solution® and 5µg of either pVITRO2-*Luc2* or pVITRO2-*Luc2/CDUPRT* was added to the cuvette containing 1x10^6 cells. An additional positive control nucleofection reaction was setup with 2µg pmax-GFP® (Lonza™).

The appropriate program for nucleofection of BMSCs was selected on the Nucleofector® (Lonza™) prior to running the program. The cuvette was subsequently transferred to the cuvette holder of the Nucleofector® and the nucleofection program started. Once the program was complete, the cuvette was removed from the Nucleofector® and 500µl of pre-warmed complete media was added to the cells with an Amaxa certified pipette (Lonza™). The cells

were subsequently transferred to a well of a 6-well plate containing 2ml of complete media and incubated at 37ºC/5% CO_2. GFP expression from BMSCs nucleofected with pmax-GFP® can be detected within 3-8 hours post-nucleofection via fluorescence microscopy. For BMSC nucleofected with pVITRO2-*Luc2* or pVITRO2-*Luc2/CDUPRT* that did not possess a fluorescent reporter, nucleofection efficiency was unable to be assessed post-nucleofection.

4.1.3.3 Antibiotic selection of stable BMSC-Luc2 and BMSC-Luc2/CDUPRT clones

The nucleofected cells were cultured for one week with a single media change prior to the selection of stable clones. To select for stable clones, nucleofected BMSCs were detached with 1x TrypLE™ Express Enzyme and resuspended in 12ml of complete media containing 200µg/ml Hygromycin B. The resuspended BMSCs were subsequently transferred to 12 wells of a 24-well plate, with each well receiving 1ml of cells. Antibiotic selection of stable BMSC-*Luc2* and BMSC-*Luc2/CDUPRT* clones was performed for a period of 2 weeks; after which individual clones were expanded and assessed for functional expression of *Luc2* and *CDUPRT*.

4.1.4 *In vitro* functional determination of *Luc2* expression in BMSCs

To determine the *in vitro* luciferase activity of BMSC-*Luc2*, BMSC-*Luc2* and BMSC-*LacZ/Luc2* (positive control) were transferred to a tissue culture treated 96-well ViewPlate microplate (PerkinElmer®) in a linear concentration in triplicate as outlined in Figure 4.4. The cells were allowed to attach overnight, washed twice with 1x HBSS and 100µl of PBS added to all wells prior to the addition of the bioluminescent substrate D-luciferin (300µg/ml) 1:1 (final concentration 150µg/ml). BLI was performed at multiple time-points (t=0, 15, 30, 60, 90, 120 and 180 min) to determine the stability of luciferase activity over a 3-hour period. To

determine the *in vitro* luciferase activity of BMSC-*Luc2/CDUPRT*, BLI was performed as outlined in Figure 4.4; however, BMSC-*Luc2* were substituted as the positive control.

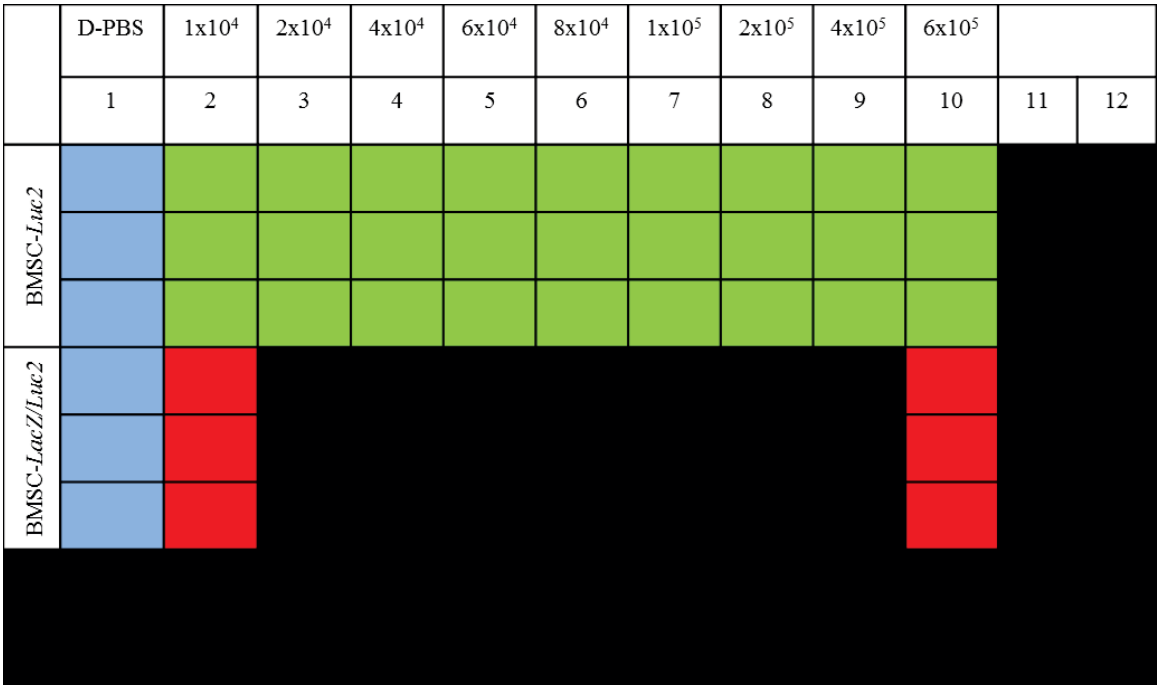

Figure 4.4: Schematic representation of 96-well microplate for determination of *Luc2* function

BMSC-*Luc2* or BMSC-*Luc2/CDUPRT* (green) were seeded in a linear concentration alongside BMSC-*LacZ/Luc2* (red) which were seeded at the highest and lowest concentration of the linear range. D-PBS was used as the solvent for D-luciferin (30mg/ml) and was subsequently used as an auto-bioluminescent control (blue). Empty wells (black). The cells were incubated with 1:1 D-luciferin (300µg/ml)/HBSS and imaged on the IVIS Lumina II according to the *in vitro* BLI acquisition settings (Table 4.5).

4.1.5 *In vitro* functional determination of *CDUPRT* expression in BMSCs

Mid-passage BMSC-*Luc2* (negative control) and BMSC-*Luc2/CDUPRT* were cultured to 80-90% confluency in a T175 flask, detached with 1x TrypLE™ Express Enzyme and resuspended to $5x10^3$ cells/ml in complete media containing 200µg/ml Hygromycin B. BMSC-*Luc2* and BMSC-*Luc2/CDUPRT* ($5x10^2$ cells/well) were transferred to half of a 96-well ViewPlate microplate in preparation for 5-FC (Invivogen®) and 5-FU (Invivogen®) drug

sensitivity assays as outlined in Figure 4.5A and Figure 4.5B respectively. Three biological replicates were setup per assay.

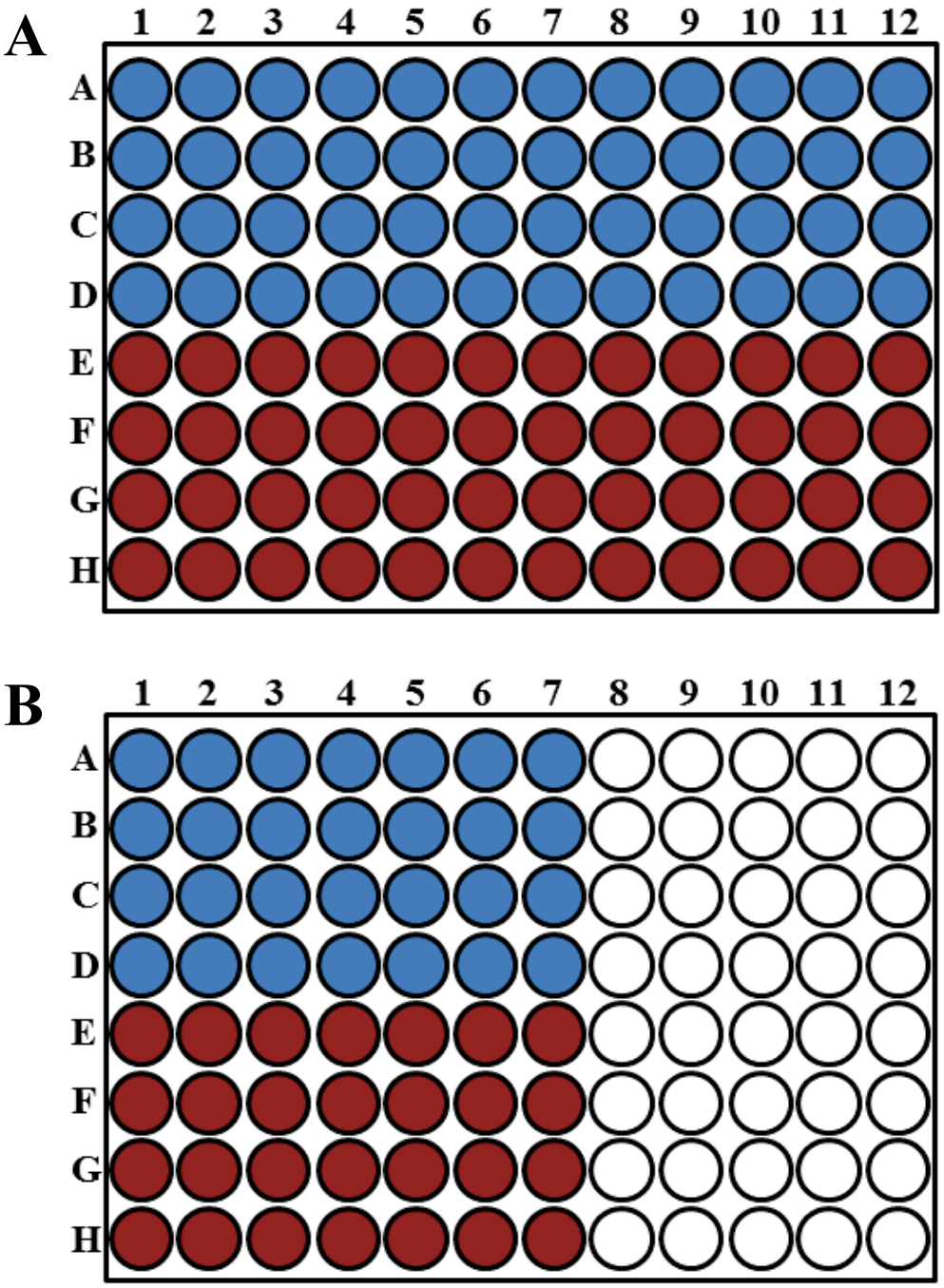

Figure 4.5: Schematic representation of 96-well microplate for 5-FC and 5-FU drug sensitivity assays BMSC-*Luc2* (blue) were seeded alongside BMSC-*Luc2/CDUPRT* (red) at $5x10^2$ cells/well. A serial dilution of 5-FC (A) (n=3) and 5-FU (B) (n=3) was added to the appropriate wells, the plates incubated for 5 days and BLI performed on the IVIS Lumina II following the addition of 1:1 D-luciferin (300µg/ml) and 1x HBSS. Image acquisition settings were as described for *in vitro* BLI studies.

Following cell attachment, a 2-fold serial dilution of 5-FC and a 10-fold serial dilution of 5-FU was setup in complete media containing 200µg/ml Hygromycin B and added to the respective wells of the 96-well ViewPlate microplate as outlined in Table 4.7.

Table 4.7: Serial dilution of 5-FC and 5-FU drug sensitivity assays

Well	5-FC stock: 20mg/mL	5-FU stock: 10mg/ml
	Final conc. of 5-FC (µg/mL)	Final conc. of 5-FU (µg/ml)
1	0	0
2	2	0.01
3	4	0.1
4	7.8	1
5	15.6	10
6	31.3	100
7	62.5	-
8	125	-
9	250	-
10	500	-
11	1000	-
12	2000	-

The plates were subsequently incubated at 37ºC/5% CO_2 for 5 days, after which the plates were imaged for *Luc2* expression on the IVIS Lumina II for viable cells following the addition of 1:1 D-luciferin (300µg/ml) according to the *in vitro* BLI acquisition settings.

4.1.6 Monitoring the persistence of BMSC-*Luc2/CDUPRT* in NOD and NOD/*Scid* mice

4.1.6.1 Sourcing of animals

Six female NOD and NOD/*Scid* mice at six weeks of age (19-23g) were sourced from the Animal Resources Centre (WA, Australia). They were housed within the Ernst Facility at UTS in a polycarbonate green line IVC system, with corncob bedding, irradiated rat and mouse feed (Gordon's Specialty Stock Feeds) and unlimited RO water. All bedding and housing equipment was autoclaved prior to use. The temperature and humidity of the animal rooms was maintained within 22-24ºC and 40-60% respectively. A maximum of four animals were housed per cage and monitored daily by the Ernst Facility technicians until they were required for experimental work, after which animals were monitored daily by the researcher and Ernst Facility technicians.

All animal work was approved by the UTS Animal Care and Ethics Committee (ACEC 2011-447A; ACEC 2009-244A) and complied with the Australian code for the care and use of animals for scientific purposes[328].

4.1.6.2 Subcutaneous transplantation of BMSC-Luc2/CDUPRT in NOD and NOD/Scid mice

Mid-passage BMSC-*Luc2* were cultured to 80-90% confluency in ten T175cm^2 flasks, washed three times with 1x HBSS to remove all traces of media and FCS, detached with 1x TrypLE™ Express Enzyme and resuspended in 1x HBSS for transplantation into NOD and NOD/*Scid* mice. Following assessment of cell viability via 0.4% Trypan Blue exclusion, the cells were resuspended in 1x HBSS to a working concentration of 1x10^7 cells/ml, and

subsequently diluted 10-fold to additional working concentrations of $1x10^6$ and $1x10^5$ cells/ml. NOD (n=4) and NOD/*Scid* (n=4) mice of 6-10 weeks of age received $1x10^4$, $1x10^5$ and $1x10^6$ cells in duplicate per animal as illustrated in Figure 4.6. Age matched NOD (n=2) and NOD/*Scid* (n=2) mice receiving no cells were utilised as negative controls. Two control mice were used due to the imaging setup that was implemented. Three animals comprising of two experimental and one control were imaged simultaneously, which allowed for the visualisation of the difference in bioluminescence between experimental and control animals in the same image acquisition.

Mice receiving cell injections were initially anaesthetised with Isoflurane and O_2 on the Stinger™ Research Anaesthesia System (Advanced Anaesthesia Specialists®), transferred to a Class II Biosafety Cabinet under sterile and aseptic conditions, and maintained under stable anaesthesia with a mobile breathing circuit. Delivery of Isoflurane (VCA®) and O_2 throughout the procedure was maintained at 2.5 L/min Isoflurane and 1.5 L/min O_2. Whilst animals were maintained under anaesthesia on the breathing circuit, using a 1ml Ultra-Fine Insulin Syringe (BD Medical®) and 26 Gauge PrecisionGlide™ needle, $1x10^4$, $1x10^5$ and $1x10^6$ BMSC-*Luc2* were injected in duplicate subcutaneously under the abdomen. Following cell injection, the animals were transferred to fresh IVC with an unlimited supply of RO water and feed for recovery and post-procedure care.

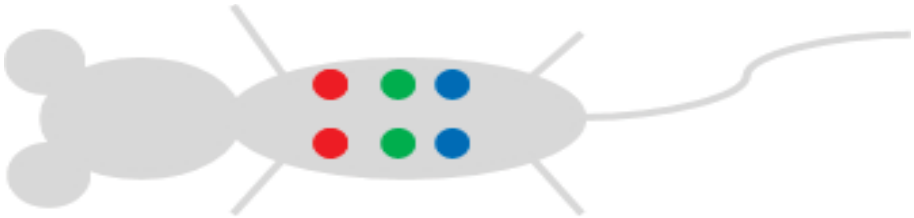

Figure 4.6: Illustration of BMSC-*Luc2/CDUPRT* injections in NOD and NOD/*Scid* mice NOD and NOD/*Scid mice* (n=4) received 1x10^4 (red), 1x10^5 (green) and 1x10^6 (blue) BMSC-*Luc* injections subcutaneously in duplicate. Age matched negative control NOD and NOD/*Scid* (n=2) received no cells. Following cell injection, animals were imaged for a period of 12 weeks on the IVIS Lumina II for *Luc2* expression following the administration of D-luciferin (15mg/ml) at 150mg/kg or 10µl/g. Image acquisition settings were as described for *in vivo* BLI studies.

4.1.6.3 In vivo BLI of transplanted BMSC-Luc2/CDUPRT in NOD and NOD/Scid mice

BMSC-*Luc2/CDUPRT* were imaged with D-luciferin (Perkin Elmer/Thermofisher Scientific) *in vitro* and *in vivo* using pre-optimised substrate concentrations, optimal imaging time and Lumina II settings. In viable cells displaying the presence of oxygen and ATP, firefly luciferase converts the substrate D-luciferin to oxyluciferin producing light, CO_2, AMP and inorganic phosphate as by-products.

The mice receiving BMSC-*Luc2/CDUPRT* injections were subsequently imaged on the IVIS Lumina II for a period of 12 weeks at 3-4 day intervals, beginning on Day 0 and concluding on Day 84 (Week 12). Prior to imaging, the mice were anaesthetised on the Stinger™ Research Anaesthesia System at 2.5 L/min Isoflurane and 1.5 L/min O_2. Mice were imaged in two groups of three consisting of two experimental and one control that were subsequently transferred to the IVIS Lumina II stage and maintained under anaesthesia via the multi-animal breathing manifold. BLI images were subsequently acquired following the

intraperitoneal administration of D-luciferin (15mg/ml) at 150mg/kg or 10µl/g according to the *in vivo* BLI image acquisition settings (Table 4.8).

Table 4.8: *In vivo* BLI acquisition settings

Incubation time (min)	Exposure time (sec)	F stop (F/s)	Field of View (FoV)	Binning
5	30	1	D	Medium

4.1.6.4 Analysis of BLI data

Qualitative and quantitative analysis of BLI data was performed via the processing of images acquired on the IVIS Lumina II. Qualitative analysis of individual animal BLI data involved observing *Luc2* expression over a period of 12 weeks, specifically identifying variations in bioluminescence with respect to time post cell injection. Quantitative analysis of BLI data required the generation of regions of interest in areas where bioluminescent signal is observed which simultaneously correlates to the site of cell injection. Quantitative BLI data is represented as surface radiance units (photons/sec/cm^2/sr) and was analysed on GraphPad Prism 7®.

4.2 Results

4.2.1 Generation of the bioluminescent tracking and suicide plasmids

The generation of the bioluminescent tracking plasmid (pVITRO2-*Luc2*) and the bioluminescent suicide plasmid (pVITRO2-*Luc2*/*CDUPRT*) was performed according to the cloning strategy outlined in Figure 4.7.

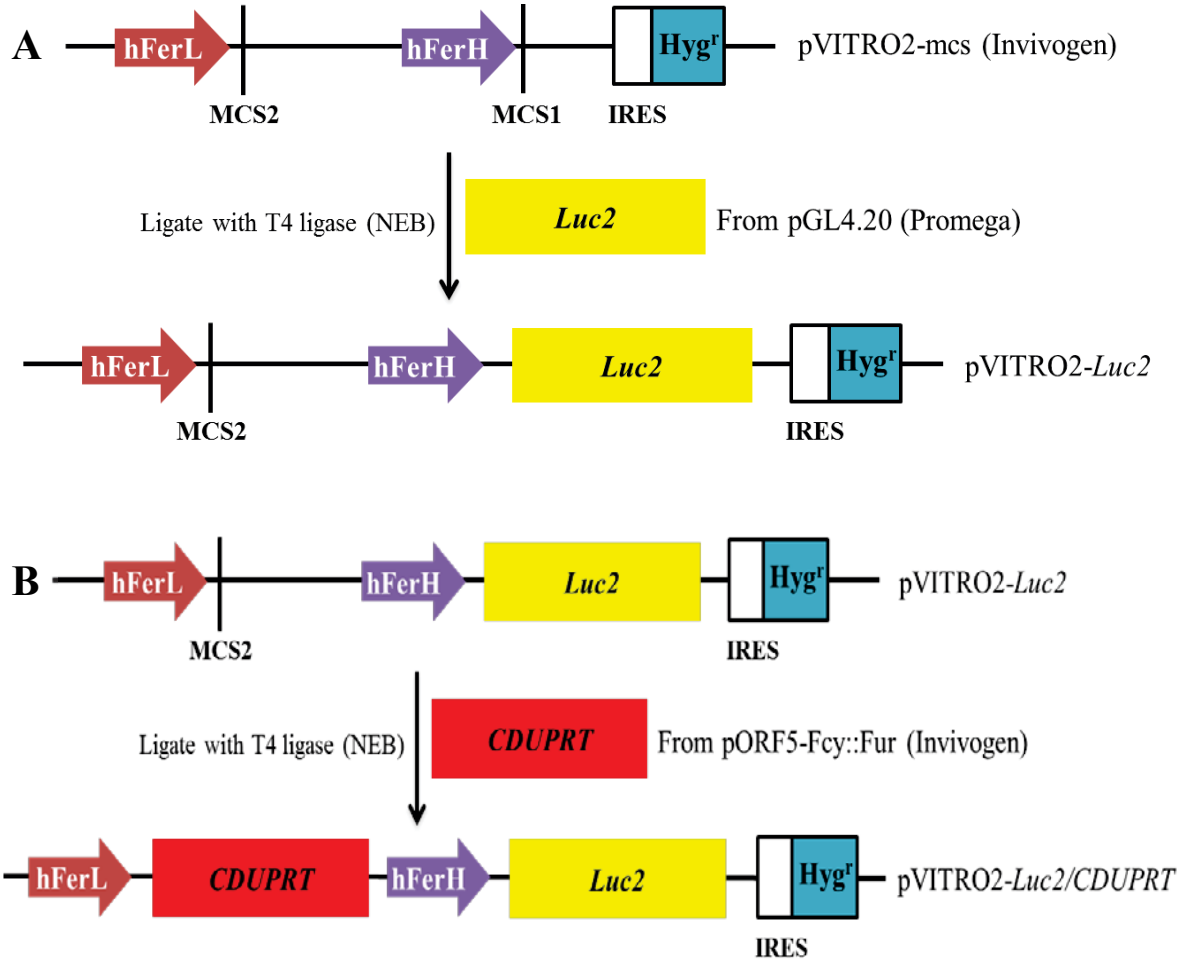

Figure 4.7: Cloning strategy for the generation of bioluminescent tracking and suicide plasmids A) The luciferase gene was excised from the pGL4.20 plasmid and sub-cloned into MCS1 of pVITRO2-hygro-mcs to generate the tracking plasmid pVITRO2-*Luc2*. B) CDUPRT was excised from the pORF5-Fcy::Fur plasmid and sub-cloned into MCS2 of the pVITRO2-*Luc2* plasmid to generate the suicide plasmid pVITRO2-*Luc2*/*CDUPRT*.

4.2.1.1 Cloning of the bioluminescent plasmid pVITRO2-Luc2

In order to clone the *Luc2* gene into the pVITRO2-mcs plasmid as outlined in Figure 4.7A, both the pGL4.20 and pVITRO2-mcs plasmids were digested with EcoRV-HF and BamHI-HF restriction enzymes, the products of which were run on a 1% (w/v) agarose gel (Figure 4.8). As can be seen in Lane 2, digest of the pVITRO2-mcs plasmid with EcoRV-HF and BamHI-HF generated two products of 6317bp and 4bp, the smaller of which could not be detected. Digest of the pGL4.20 plasmid generated two products of 3426bp and 1978bp, the larger of which corresponded to the pGL4.20 digested plasmid backbone and the smaller of which corresponded to the *Luc2* gene. Following gel purification of the pVITRO2-mcs backbone and the *Luc2* gene, the purified products were run on a 1% (w/v) agarose gel to confirm the purity of the fragment extraction (Figure 4.9). Both the purified pVITRO2-mcs backbone and the *Luc2* gene were ~200ng/µl as quantified by NanoDrop™ 2000 spectrophotometry.

The purified and dephosphorylated pVITRO2-mcs backbone (EcoRV-HF/BamHI-HF cut) and *Luc2* gene were subsequently ligated as described in Section 4.1.2.3 and Figure 4.7A. The ligation products were diluted 1 in 2 with dH_2O, transformed into TOP10 *E. coli* and selected for antibiotic resistance on Hygromycin B containing LB agar plates. Of the three insert:backbone molar ratios assessed during ligation, the molar ratio of 10:1 ligation transformation resulted in the generation of five bacterial colonies. Both the 3:1 and 6:1 ligation transformations did not produce colonies. The dephosphorylated pVITRO2-mcs backbone (EcoRV-HF/BamHI-HF cut) assessed as a negative ligation control did not result in any bacterial colonies, whereas transformation of uncut pVITRO2-mcs resulted in >100 colonies.

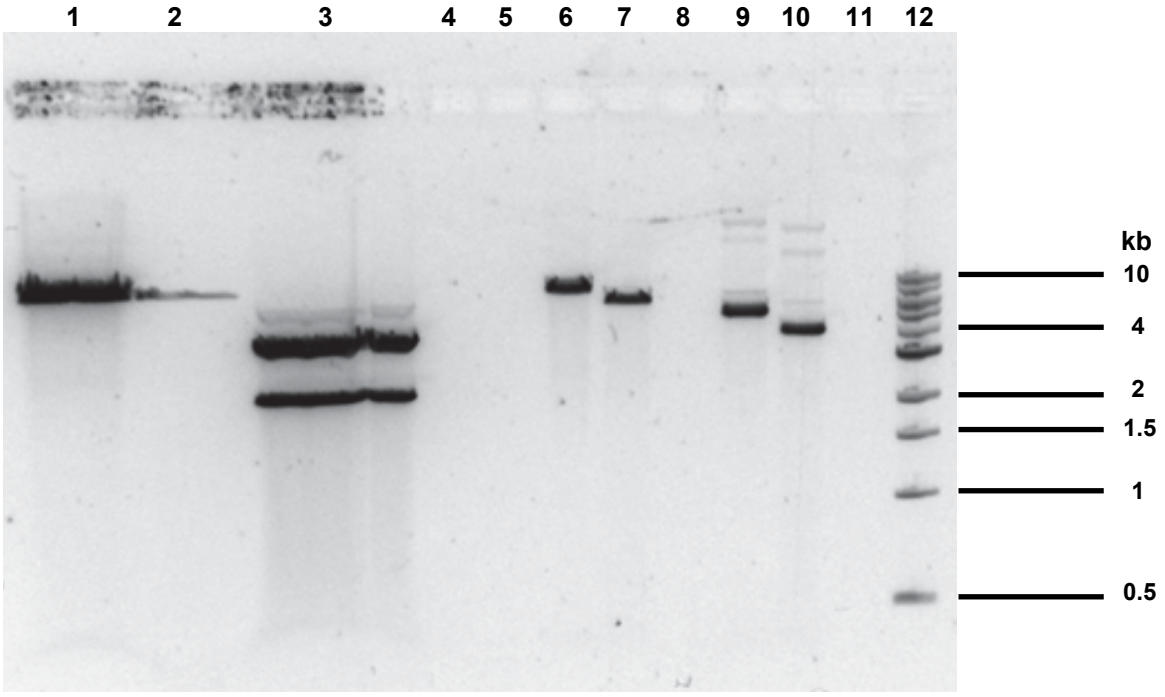

Figure 4.8: EcoRV-HF/BamHI-HF digest of pVITRO2-mcs and pGL4.20 The pVITRO2-mcs and pGL4.20 plasmids were digested with EcoRV-HF and BamHI-HF restriction enzymes, and the products run on a 1% (w/v) agarose gel containing 0.5% (v/v) GelRed™ at 90V for 90 min. The gel image was captured using an InGenius3® UV transilluminator. Lane 1: pVITRO2-mcs (EcoRV-HF/BamHI-HF), Lane 2: empty, Lane 3: pGL4.20 (EcoRV-HF/BamHI-HF), Lane 4-5: empty, Lane 6: pVITRO2-mcs (EcoRV-HF), Lane 7: pGL4.20 (BamHI-HF), Lane 8: empty, Lane 9: pVITRO2-mcs (uncut), Lane 10: pGL4.20 (uncut), Lane 11: empty, Lane 12: 1kb DNA ladder (NEB®).

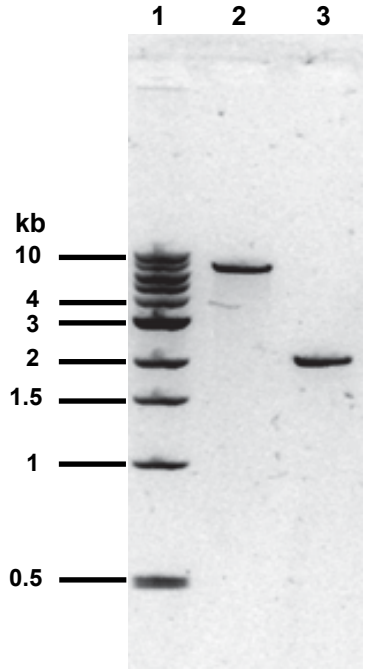

Figure 4.9: Gel extraction of EcoRV-HF/BamHI-HF digested fragments The fragments corresponding to the pVITRO2-mcs backbone (EcoRV-HF/BamHI-HF cut) and the *Luc2* gene were gel purified and re-run on a 1% (w/v) agarose gel containing 0.05% GelRed™ at 90V for 90 min. The gel image was captured using an InGenius3® UV transilluminator. Lane 1: 1kb DNA ladder (NEB®), Lane 2: pVITRO2-mcs backbone (EcoRV-HF/BamHI-HF cut), Lane 3: *Luc2* gene.

To assess the success of *Luc2* ligation into the pVITRO2-mcs plasmid, the five bacterial colonies that resulted from selective LB-agar growth were re-streaked onto new selective LB-agar plates to confirm true antibiotic resistance, of which all successfully developed clonal bacterial spread plates. A single colony from each clonal spread plate was grown overnight in selective LB media, and each clonal bacterial culture subsequently utilised in BLI as described in Section 4.1.2.8 to determine *Luc2* function and consequently successful ligation into the pVITRO2-mcs plasmid (Figure 4.10). As can be seen in Figure 4.10, the five putative pVITRO2-*Luc2 E. coli* clones all expressed moderate luciferase activity in comparison to the positive control (Lane 8), of which Clone 1 was subsequently midi-prepped and utilised in downstream cloning and nucleofection of BMSCs. The successfully generated pVITRO2-*Luc2* bioluminescent tracking plasmid schematic is represented in Figure 4.11.

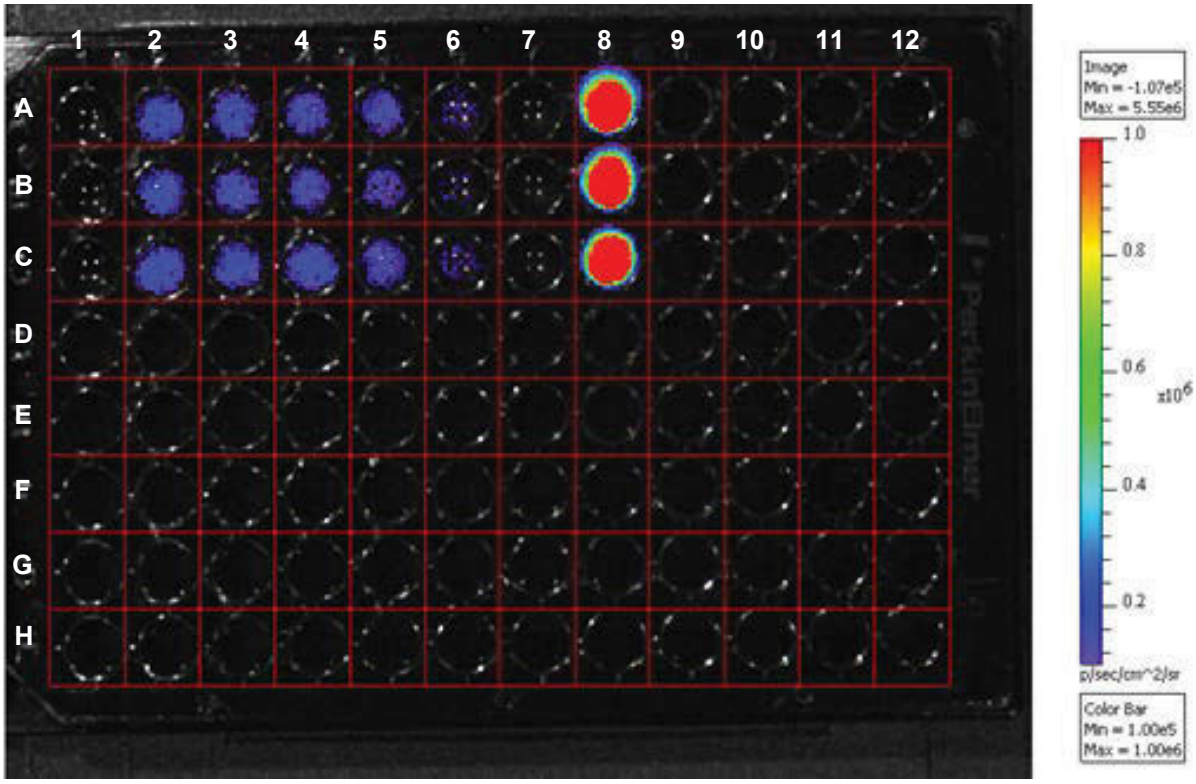

Figure 4.10: *In vitro* BLI of putative pVITRO2-*Luc2 E. coli* clones Overnight cultures of putative clones of *E. coli* (100µl) transformed with pVITRO2-*Luc2* were assessed via BLI for luciferase activity. The cells were incubated with 1:1 D-luciferin (300µg/ml) and imaged on the IVIS Lumina II according to the *in vitro* BLI acquisition settings. Lane 1: D-PBS, Lane 2-6: pVITRO2-*Luc2 E. coli* clones 1-5, Lane 7: pVITRO2-mcs *E. coli*, Lane 8: BMSC-*LacZ/Luc2*.

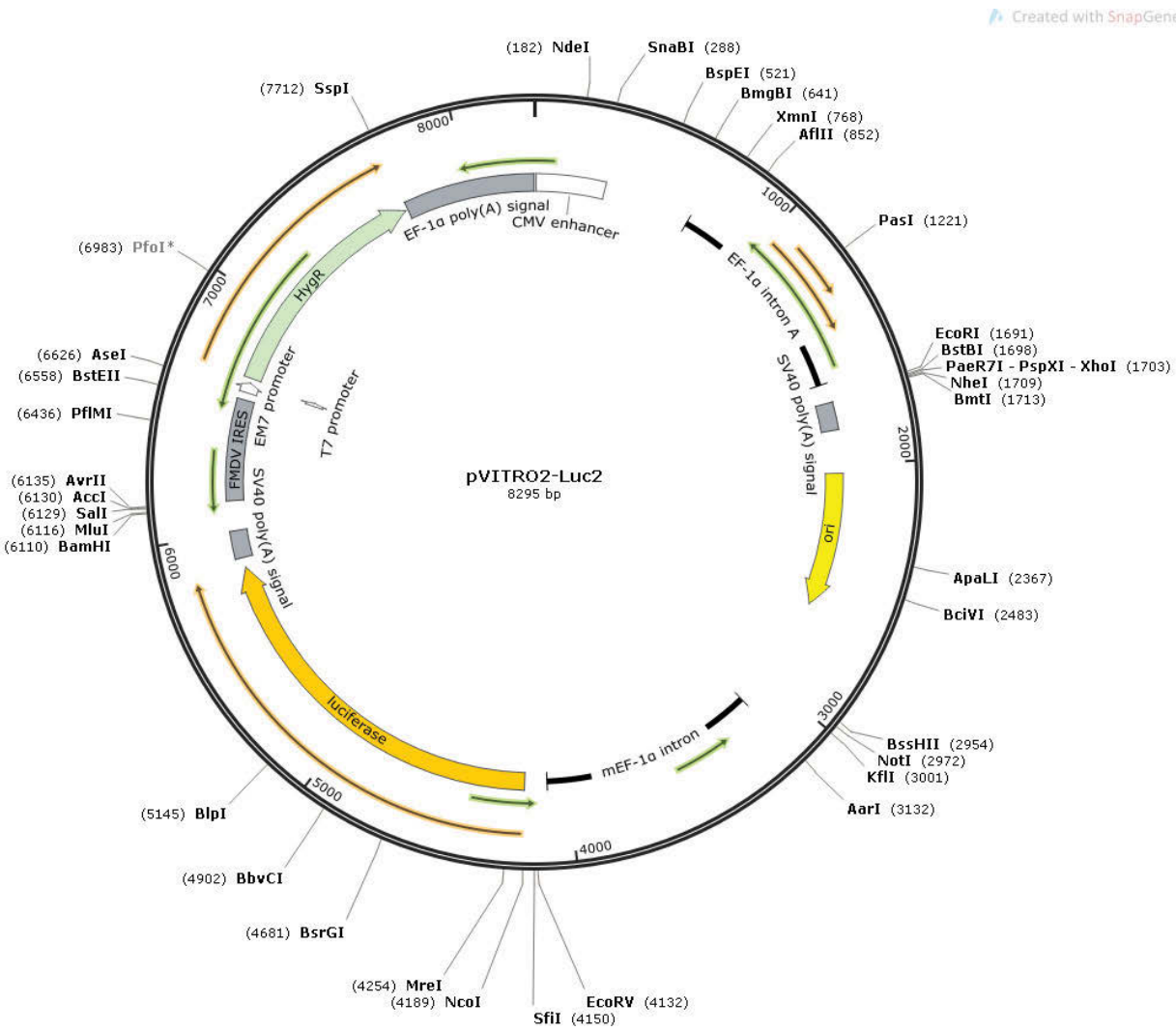

Figure 4.11: Schematic representation of the pVITRO2-*Luc2* bioluminescent tracking plasmid The bioluminescent tracking plasmid generated following cloning of the *Luc2* gene (orange) from the pGL4.20 plasmid into multiple cloning site 1 of the pVITRO2-mcs plasmid. Hygromycin antibiotic resistance allows for both bacterial and mammalian cell selection of the plasmid, whilst *Luc2* gene expression is driven by the composite ferritin/mouse EF-1α 5' UTR promoter.

4.2.1.2 Cloning of the suicide plasmid pVITRO2-Luc2/CDUPRT

In order to clone the *CDUPRT* gene into the pVITRO2-*Luc2* plasmid as outlined in Figure 4.7B, both the pORF5-Fcy::Fur and pVITRO2-*Luc2* plasmids were digested with EcoRI-HF and NheI-HF restriction enzymes, the products of which were run on a 1% (w/v) agarose gel (Figure 4.12). As can be seen in Lane 3, the digest of the pVITRO2-*Luc2* plasmid with EcoRI-HF and NheI-HF generated two products of 8277bp and 18bp, the smaller of which could not be detected. Digest of the pORF5-Fcy::Fur plasmid generated two products of 3093bp and 1175bp, the larger of which corresponded to the pORF5-Fcy::Fur digested plasmid backbone and the smaller of which corresponded to the *CDUPRT* gene. Following gel purification of the pVITRO2-*Luc2* backbone and the *CDUPRT* gene, the purified products were run on a 1% (w/v) agarose gel to confirm the purity of the fragment extraction (Figure 4.13). The concentration of the purified pVITRO2-*Luc2* backbone and the *CDUPRT* gene were ~100ng/µl as quantified by NanoDrop™ 2000 spectrophotometry.

The purified and dephosphorylated pVITRO2-*Luc2* backbone (EcoRI-HF/NheI-HF cut) and the *CDUPRT* gene were subsequently ligated as described in Section 4.1.2.6 and Figure 4.7B. The ligation products were diluted 1 in 2 with dH_2O, transformed into TOP10 *E. coli* and selected for antibiotic resistance on Hygromycin B containing LB agar plates. Of the three insert:backbone molar ratios assessed during ligation, the molar ratios of 6:1 and 10:1 ligation transformations resulted in the generation of one and nine bacterial colonies respectively. The 3:1 ligation transformations did not produce colonies. The dephosphorylated pVITRO2-*Luc2* backbone (EcoRI-HF/NheI-HF cut) assessed as a negative ligation control did not result in any bacterial colonies, whereas transformation of uncut pVITRO2-*Luc2* resulted in >100 colonies.

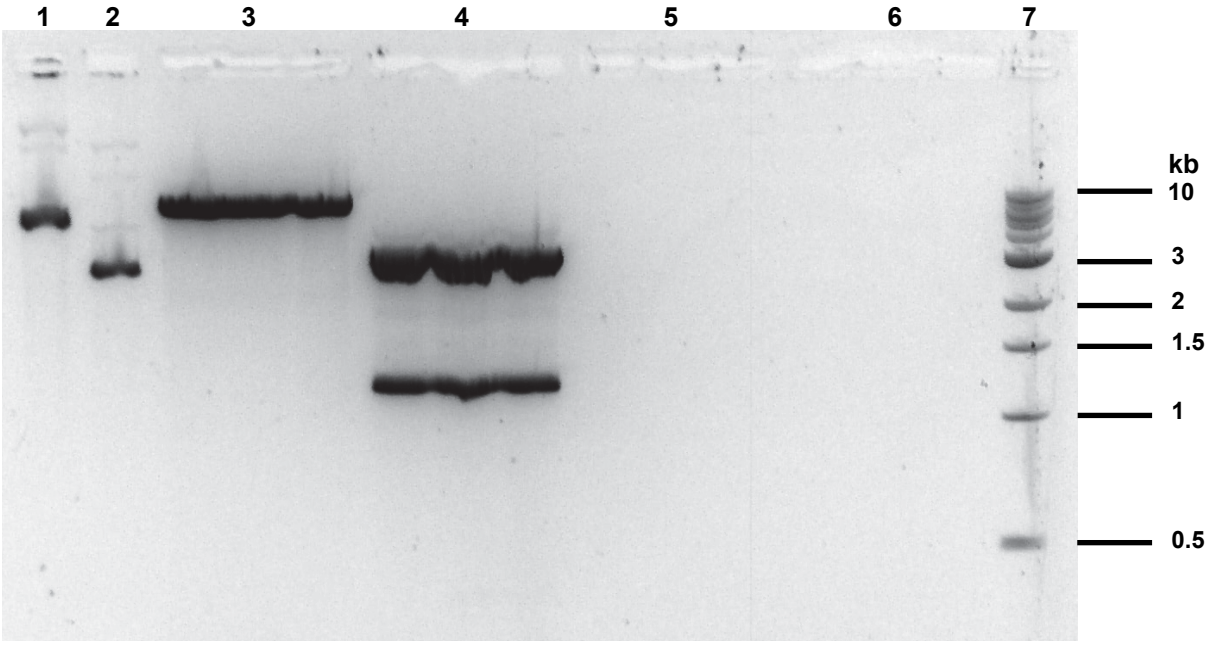

Figure 4.12: EcoRI-HF/NheI-HF digest of pVITRO2-Luc2 and pORF5-Fcy::Fur The pVITRO2-*Luc2* and pORF5-Fcy::Fur plasmids were digested with EcoRI-HF and NheI-HF restriction enzymes, and the products run on a 1% (w/v) agarose gel containing 0.5% (v/v) GelRed™ at 90V for 90 min. The gel image was captured using an InGenius3® UV transilluminator. Lane 1: pVITRO2-*Luc2* (uncut), Lane 2: pORF5-Fcy::Fur (uncut), Lane 3: pVITRO2-*Luc2* (EcoRI-HF/NheI-HF), Lane 4: pORF5-Fcy::Fur (EcoRI-HF/NheI-HF), Lane 5-6: empty, Lane 7: 1kb DNA ladder (NEB®).

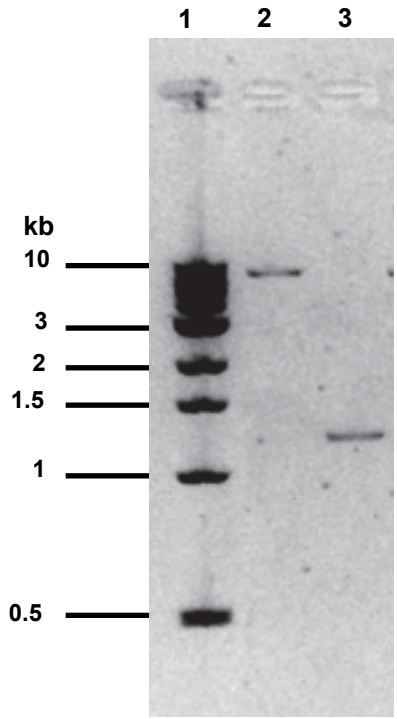

Figure 4.13: Gel extraction of EcoRI-HF/NheI-HF digested fragments The fragments corresponding to the pVITRO2-*Luc2* backbone (EcoRI-HF/NheI-HF cut) and the *CDUPRT* gene were gel purified and re-run on a 1% (w/v) agarose gel containing 0.05% GelRed™ at 90V for 90 min. The gel image was captured using an InGenius3® UV transilluminator. Lane 1: 1kb DNA ladder (NEB®), Lane 2: pVITRO2-*Luc2* backbone (EcoRI-HF/NheI-HF cut), Lane 3: *CDUPRT* gene.

To assess the success of *CDUPRT* ligation into the pVITRO2-*Luc2* plasmid, the ten bacterial colonies that resulted from selective LB-agar growth were re-streaked onto new selective LB-agar plates to confirm true antibiotic resistance, of which all successfully developed clonal bacterial spread plates. A single colony from each clonal spread plate was grown overnight in selective LB media, and a 2ml aliquot of overnight bacterial culture utilised for plasmid isolation. A diagnostic restriction digest with EcoRI-HF and NheI-HF was conducted on the ten putative pVITRO2-*Luc2/CDUPRT* plasmids, the products of which were run on a 1% (w/v) agarose gel (Figure 4.14). As can be seen, nine of the ten plasmids possessed the *CDUPRT* gene, which was released following restriction digestion.

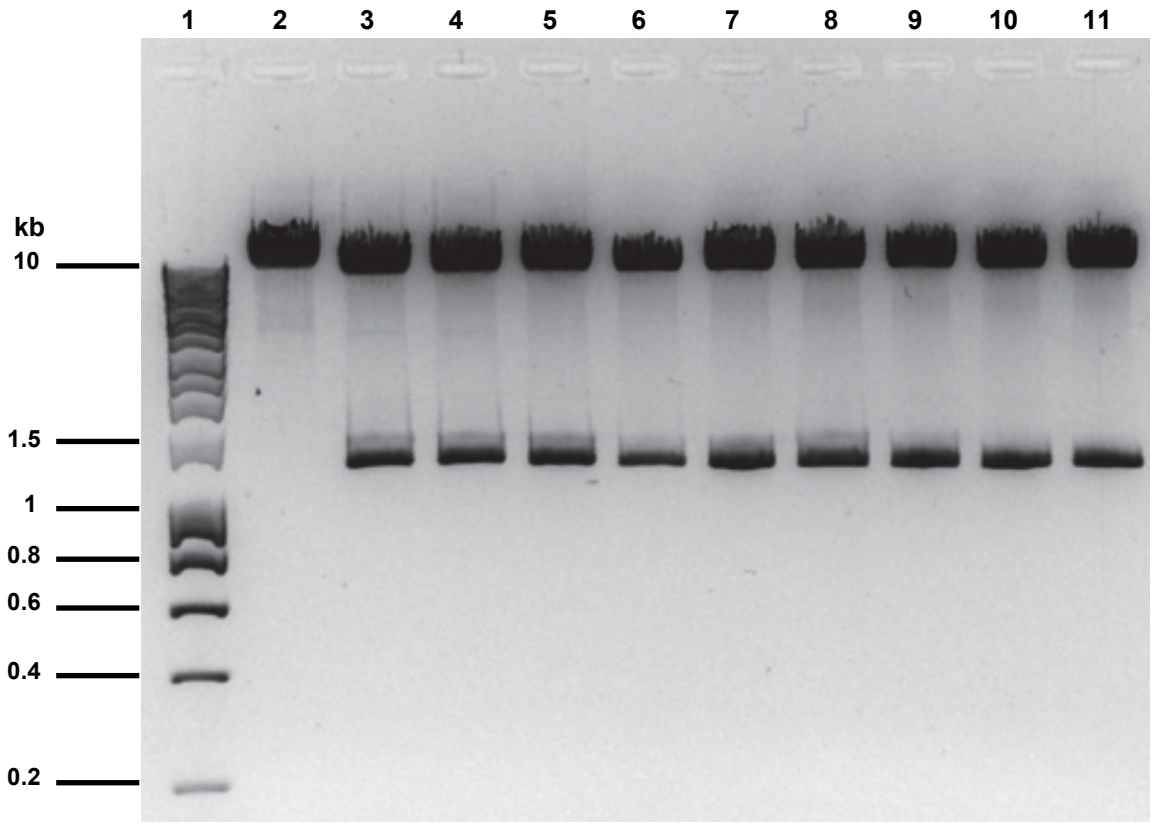

Figure 4.14: Diagnostic digest of putative pVITRO2-*Luc2/CDUPRT* plasmids Ten putative pVITRO2-*Luc2/CDUPRT* plasmids were isolated from their respective overnight bacterial cultures and subsequently digested with EcoRI-HF and NheI-HF, and the products run on a 1% (w/v) agarose gel containing 0.5% (v/v) GelRed™ at 90V for 90 min. The gel image was captured using an InGenius3® UV transilluminator. Lane 1: 1kb DNA hyperladder (Bioline®), Lanes 2-11: Putative pVITRO2-*Luc2/CDUPRT* #1-10 (EcoRI-HF/NheI-HF cut).

With the remaining bacterial culture of the ten putative pVITRO2-*Luc2/CDUPRT* clones, BLI was performed as described in Section 4.1.2.8 to re-confirm *Luc2* function (Figure 4.15). As can be seen in Figure 4.15, seven of the ten putative pVITRO2-*Luc2/CDUPRT E. coli* clones demonstrated moderate luciferase activity and three clones demonstrated weak luciferase activity in comparison to the positive control (Lane 12). Clone 3, which demonstrated the strongest luciferase activity was subsequently midi-prepped and utilised in downstream nucleofection of BMSCs. The successfully generated pVITRO2-*Luc2/CDUPRT* suicide plasmid schematic is represented in Figure 4.16.

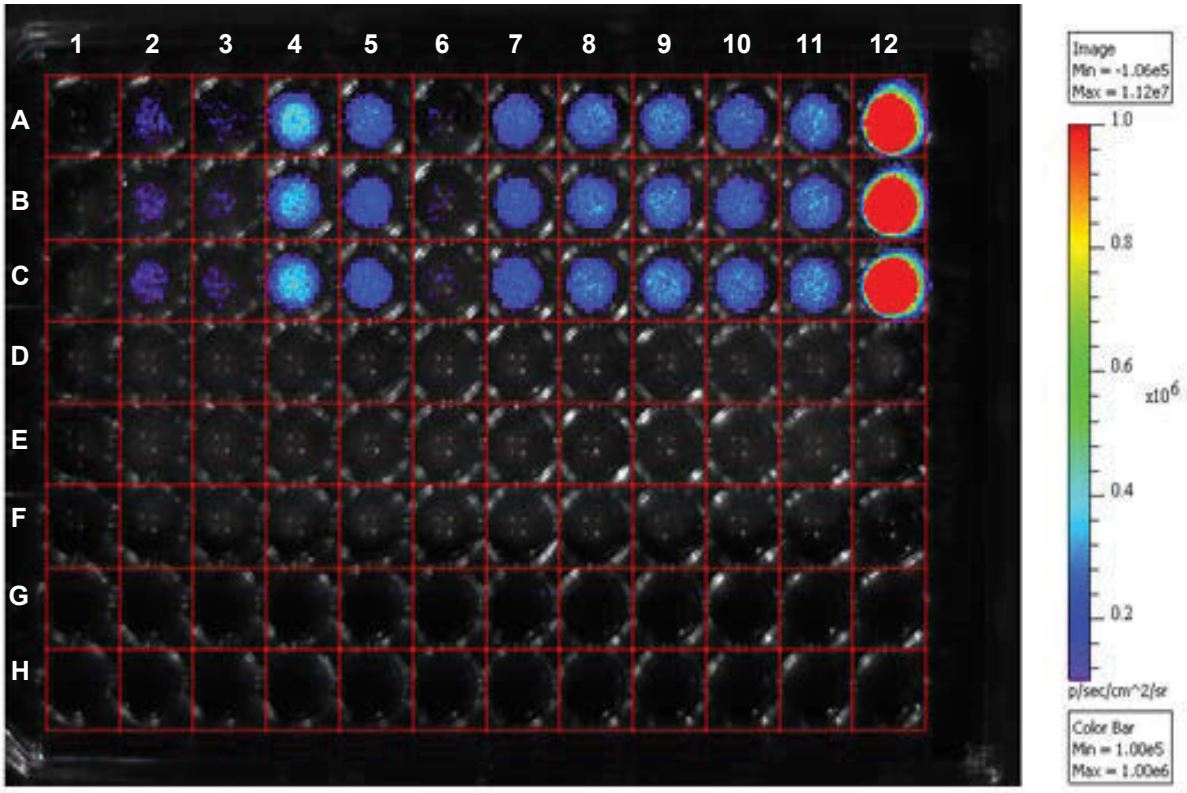

Figure 4.15: *In vitro* BLI of putative pVITRO2-*Luc2/CDUPRT E. coli* clones Overnight cultures of putative clones of *E. coli* (100µl) transformed with pVITRO2-*Luc2/CDUPRT* were assessed via BLI for luciferase activity. The cells were incubated with 1:1 D-luciferin (300µg/ml) and imaged on the IVIS Lumina II according to the *in vitro* BLI acquisition settings. Lane 1: D-PBS, Lane 2-11: pVITRO2-*Luc2/CDUPRT E. coli* clones 1-10, Lane 12: BMSC-*LacZ/Luc2*.

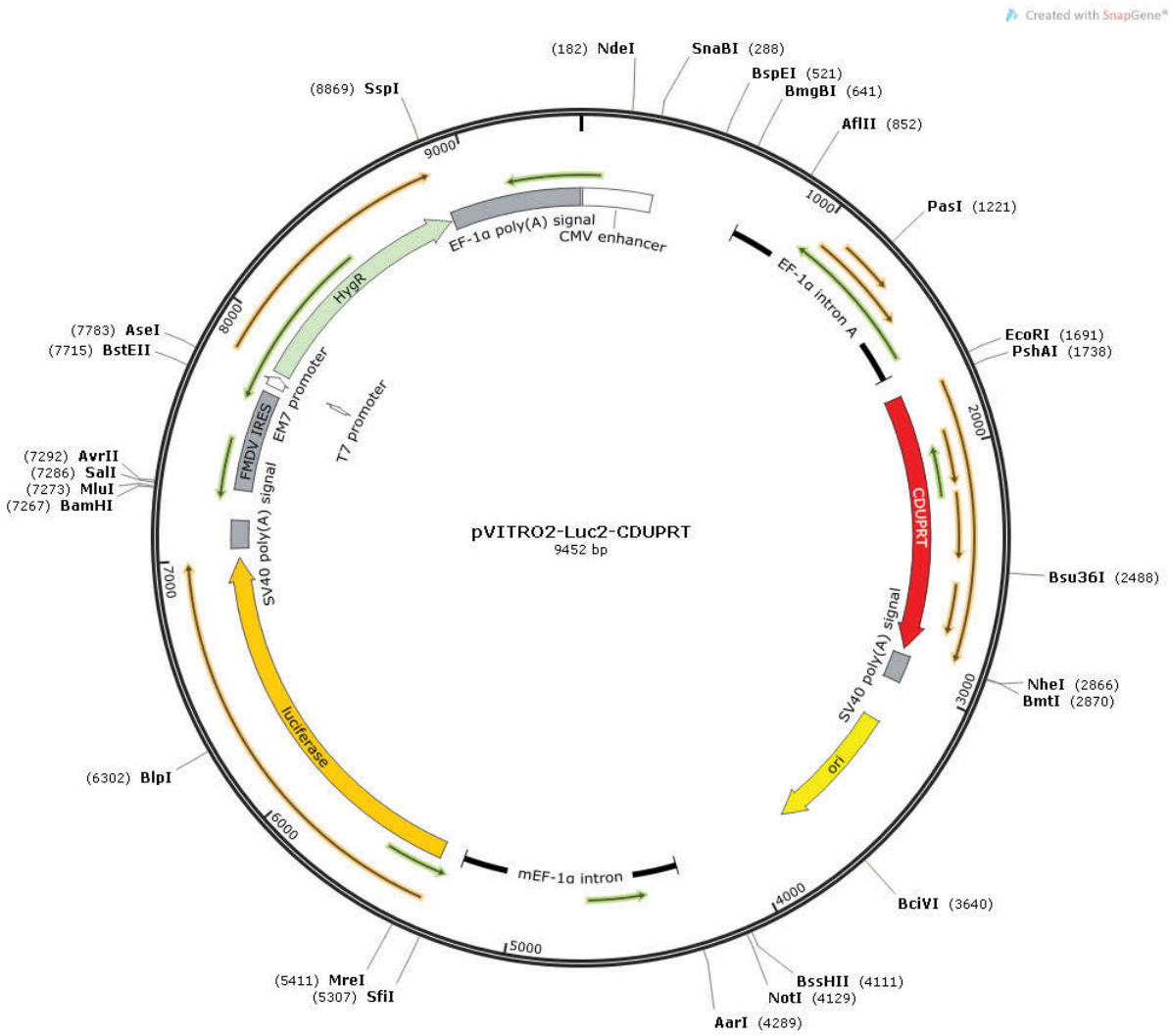

Figure 4.16: Schematic representation of the pVITRO2-*Luc2/CDUPRT* suicide plasmid The bioluminescent tracking plasmid generated following cloning of the *CDUPRT* gene (red) from the pORF5-Fcy::Fur plasmid into multiple cloning site 2 of the pVITRO2-*Luc2* plasmid. Hygromycin antibiotic resistance allows for both bacterial and mammalian cell selection of the plasmid. Both *Luc2* (orange) and *CDUPRT* gene expression are driven by composite ferritin/mouse EF-1α 5' UTR promoters.

4.2.2 Generation of tracking and suicide BMSCs via nucleofection

4.2.2.1 Determination of Hygromycin B sensitivity of native BMSCs

To select for stable BMSCs expressing the tracking and suicide genes, an antibiotic sensitivity assay was performed on native BMSCs to determine the optimal concentration of Hygromycin B to utilise in the culture medium post-nucleofection (Figure 4.17). The optimal antibiotic concentration was designated as the concentration at which >90% cell death was observed, corresponding to between 125-250µg/ml. As a result, 200µg/ml of Hygromycin B was thereafter used in the selection of BMSC nucleofected with the tracking and suicide plasmids, and in the ongoing culture of BMSC-*Luc2* and BMSC-*Luc2/CDUPRT*.

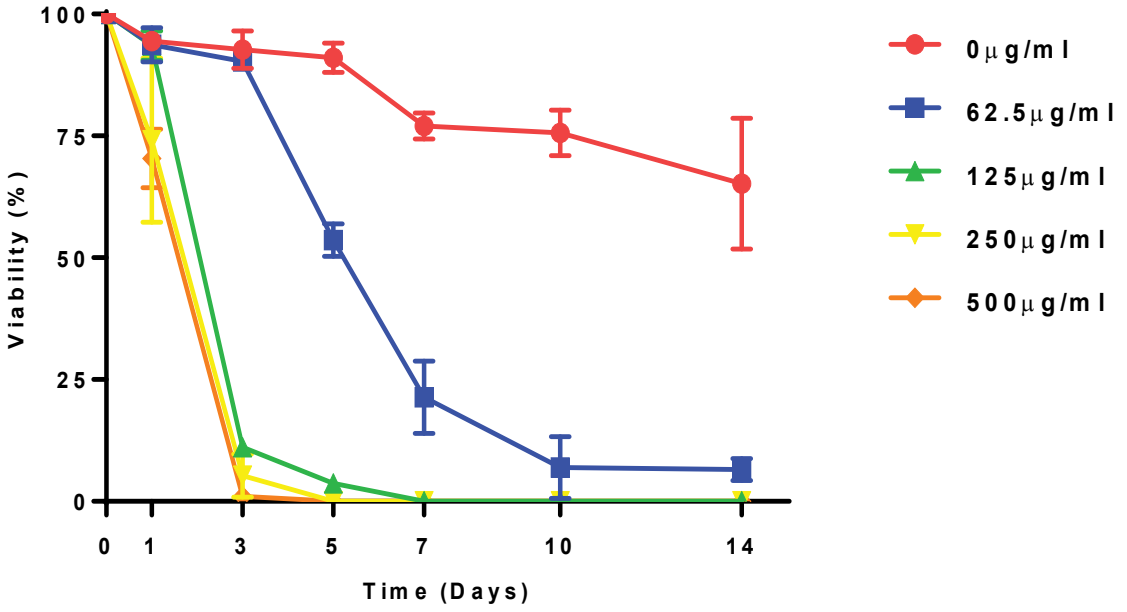

Figure 4.17: BMSC antibiotic sensitivity assay BMSC were seeded at a concentration of $5x10^5$ cells/well in triplicate of a 6-well plate, and cultured for 14 days in the presence of varying concentrations of Hygromycin B. Cell viability was assessed at Day 0, 1, 3, 5, 7, 10 and 14 via Trypan Blue exclusion. Data is represented as mean ± SD (n=3).

4.2.2.2 Nucleofection and selection of BMSC-Luc2 and BMSC-Luc2/CDUPRT

The nucleofection efficiency of BMSC nucleofected with the pVITRO2-*Luc2* and pVITRO2-*Luc2/CDUPRT* plasmids was not determined due to a lack of a fluorescent reporter for downstream analysis. However, BMSCs that were nucleofected with pmax-GFP® (positive control) and analysed by Trypan blue exclusion and fluorescence microscopy showed that ~50% of viable BMSCs were GFP^+ at 6 hours post-nucleofection, which increased to ~70-75% GFP^+ at 24 hours post-nucleofection (Figure 4.18). Variations in GFP fluorescence intensity were also observed amongst GFP^+ BMSCs.

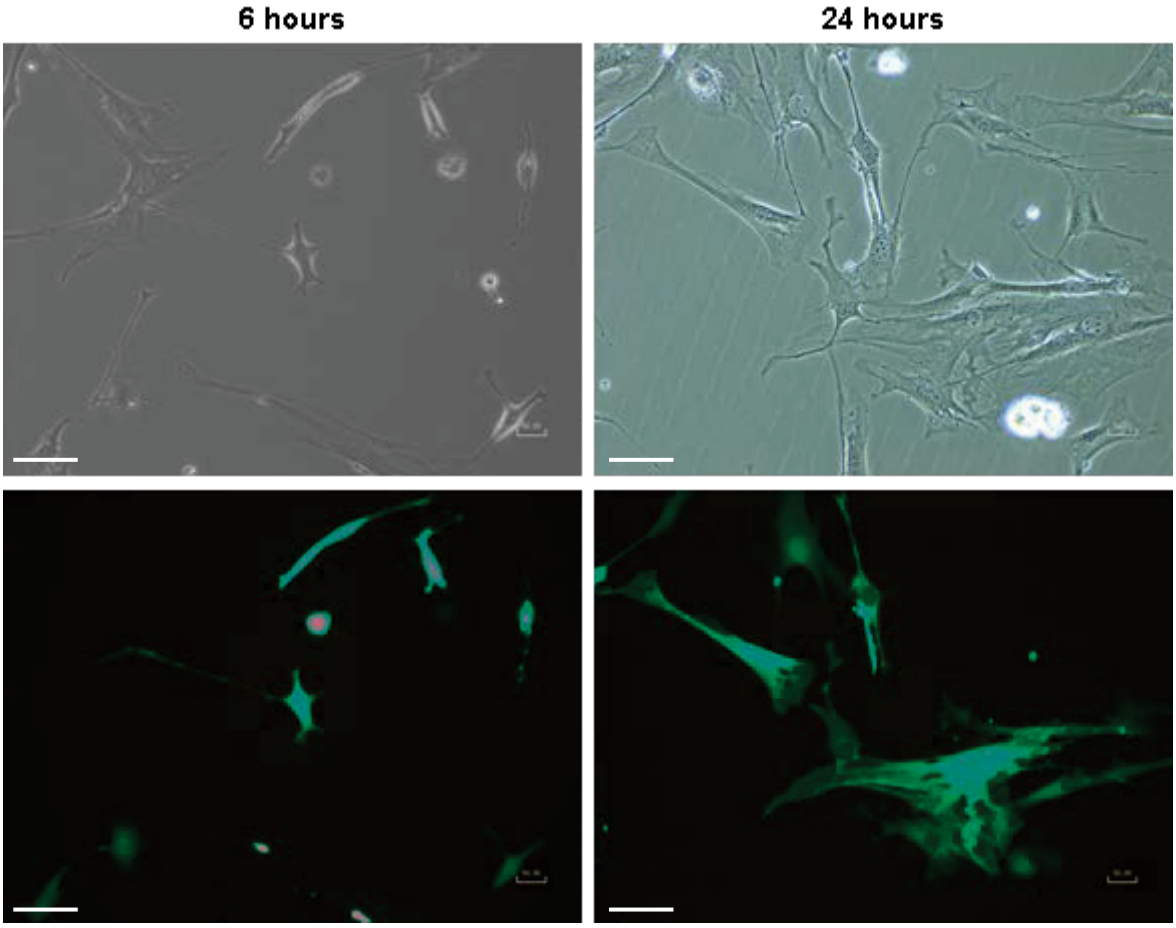

Figure 4.18: Nucleofection of BMSCs with pmax-GFP® BMSCs nucleofected with pmax-GFP® were transferred to a T75 flask containing complete α-MEM and imaged at 8 and 24 hours post nucleofection. Phase and fluorescent images were obtained using a Nikon Eclipse TS100 microscope at 20x magnification, 100µm scale.

Nucleofection of early-passage BMSCs with pVITRO2-*Luc2* and pVITRO2-*Luc2/CDUPRT* yielded one and two stable clones respectively following Hygromycin B selection (Figure 4.19). By comparison to parental BMSCs (~50-150µm), and despite retaining a fibroblast-like morphology, nucleofected BMSC demonstrated a reduced cytoplasmic volume and diameter (~30-100µm). Each clone of nucleofected BMSC was culture expanded in complete α-MEM containing 200µg/ml Hygromycin B, cryopreserved and utilised in subsequent functional transgene analysis.

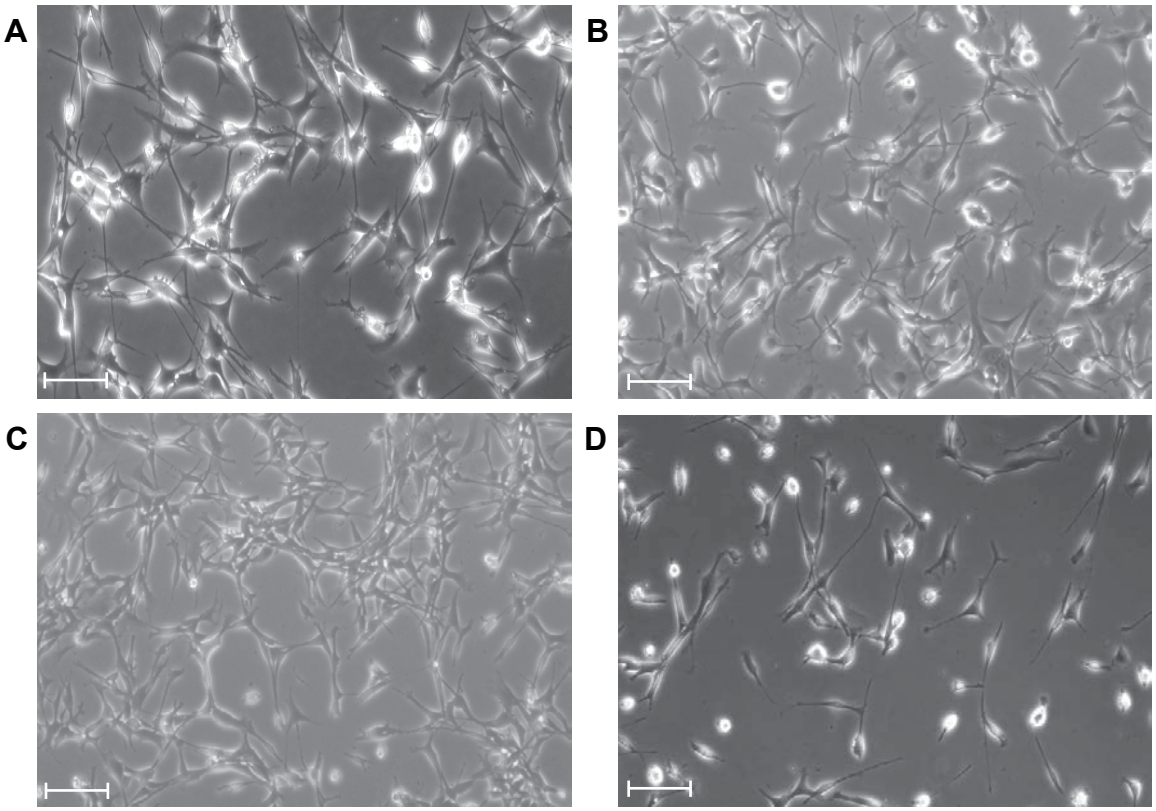

Figure 4.19: Nucleofection of BMSCs with tracking and suicide plasmids BMSCs nucleofected with the tracking and suicide plasmids were selected for with Hygromycin B and culture expanded in complete α-MEM containing 200µg/ml Hygromycin B. Images are of parental BMSC (A), BMSC-*Luc2* (B), BMSC-*Luc2/CDUPRT* clone 1 (C) and BMSC-*Luc2/CDUPRT* clone 2 at equivalent passage (P15). Images were acquired on a Leica DM Microscope at 10x magnification, 100µm scale.

4.2.2.3 In vitro characterisation of functional Luc2 activity in tracking and suicide BMSCs

Functional luciferase activity was assessed in BMSC-*Luc2* (Figure 4.20A), and BMSC-*Luc2/CDUPRT* clone 1 and clone 2 (Figure 4.21A and Figure 4.22A) via BLI at multiple time-points following incubation with D-luciferin. A linear regression analysis of luminescent signal represented as average radiance (photons/sec/cm^2/sr) was performed, demonstrating a linear correlation between cell concentration and units of luminescence in each of the *Luc2*-expressing BMSC cell lines (Figure 4.21B, Figure 4.22B and Figure 4.23B). All *Luc2*-expressing BMSC clones demonstrated R^2 values of >0.98 at each time point between t=0 and t=3 hours. The linear correlation between cell concentration and luminescence confirmed the selection of clonal populations of *Luc2*-expressing BMSCs. In addition, the overlapping linear regression at multiple time-points demonstrated stability in luminescent signal up to 3 hours post incubation with D-luciferin. As can be seen from the BLI image in Figure 4.20, the luminescent signal from BMSC-*Luc2* was significantly stronger ($p<0.001$) than in the previously generated BMSC-*Luc2/LacZ* (1D7) cell line. By comparison, no significant difference was observed in luminescent signal between BMSC-*Luc2* and the two BMSC-*Luc2/CDUPRT* clones. At 24 hours post addition of D-luciferin, bioluminescent signal in BMSC-*Luc2* and BMSC-*Luc2/CDUPRT* clone 1 fell below the baseline (background) luminescence. Due to the improved stability of luminescence determined by tightly overlapping linear regression analysis of BMSC-*Luc2/CDUPRT* clone 1 (Figure 4.21) in comparison to clone 2, clone 1 was utilised as the target for downstream lentiviral gene modification.

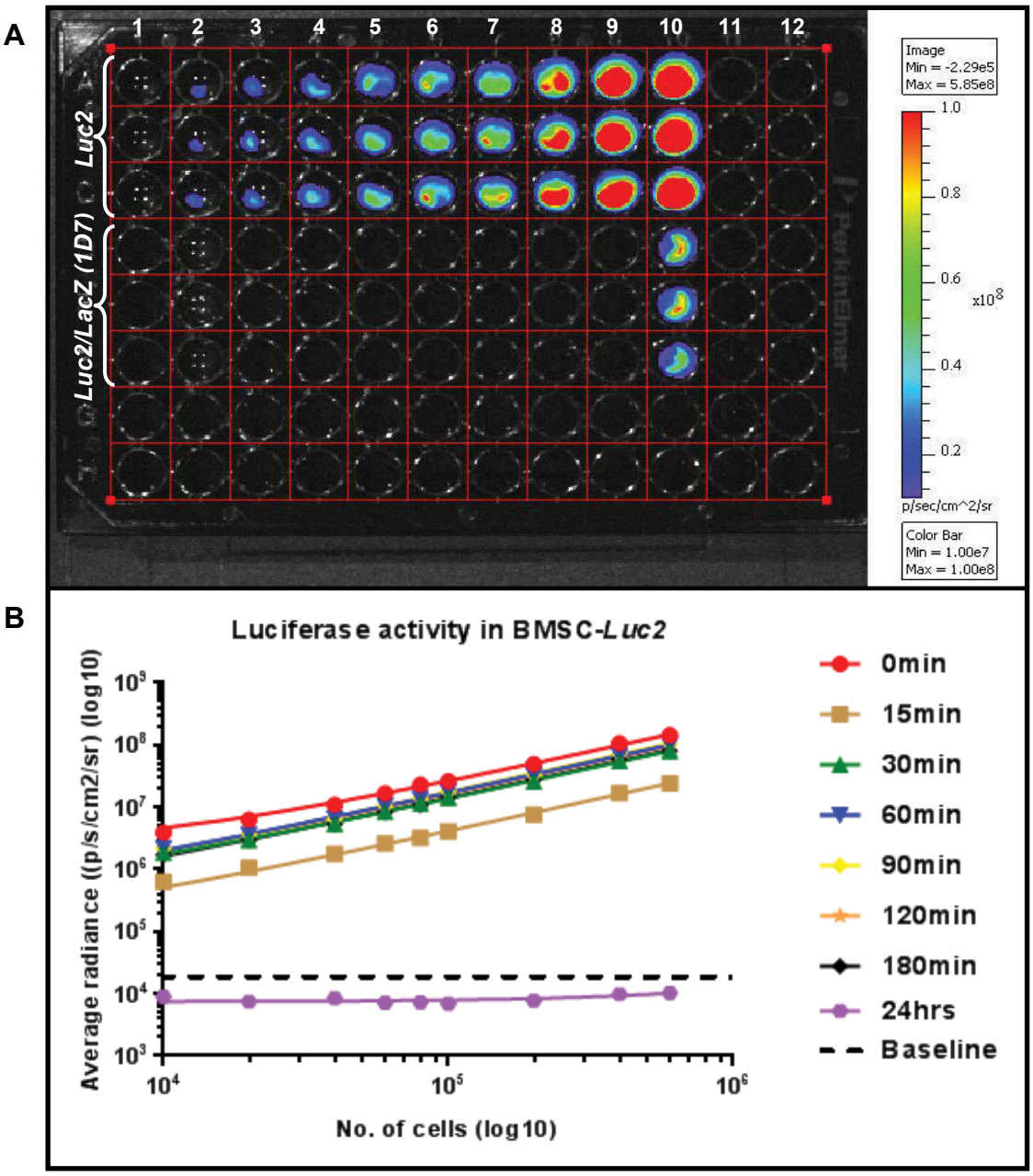

Figure 4.20: *In vitro* functional characterisation of luciferase activity in BMSC-*Luc2* (A) BLI was utilised to assess luciferase activity in BMSC-*Luc2* over a linear cell concentration range in comparison to an existing *Luc2*-expressing BMSC cell line (BMSC-*Luc2/LacZ* (1D7)). The cells were incubated with 1:1 D-luciferin (300µg/ml) and imaged on the IVIS Lumina II according to the *in vitro* BLI acquisition settings. The image represented is at t=30. Lane 1: D-PBS, Lane 2-10: BMSC-*Luc2* and BMSC-*Luc2/LacZ* (control). (B) Linear regression analysis of luminescent signal at multiple time-points post incubation with D-luciferin was performed using GraphPad Prism 7®. Data is represented as mean ± SD of triplicates.

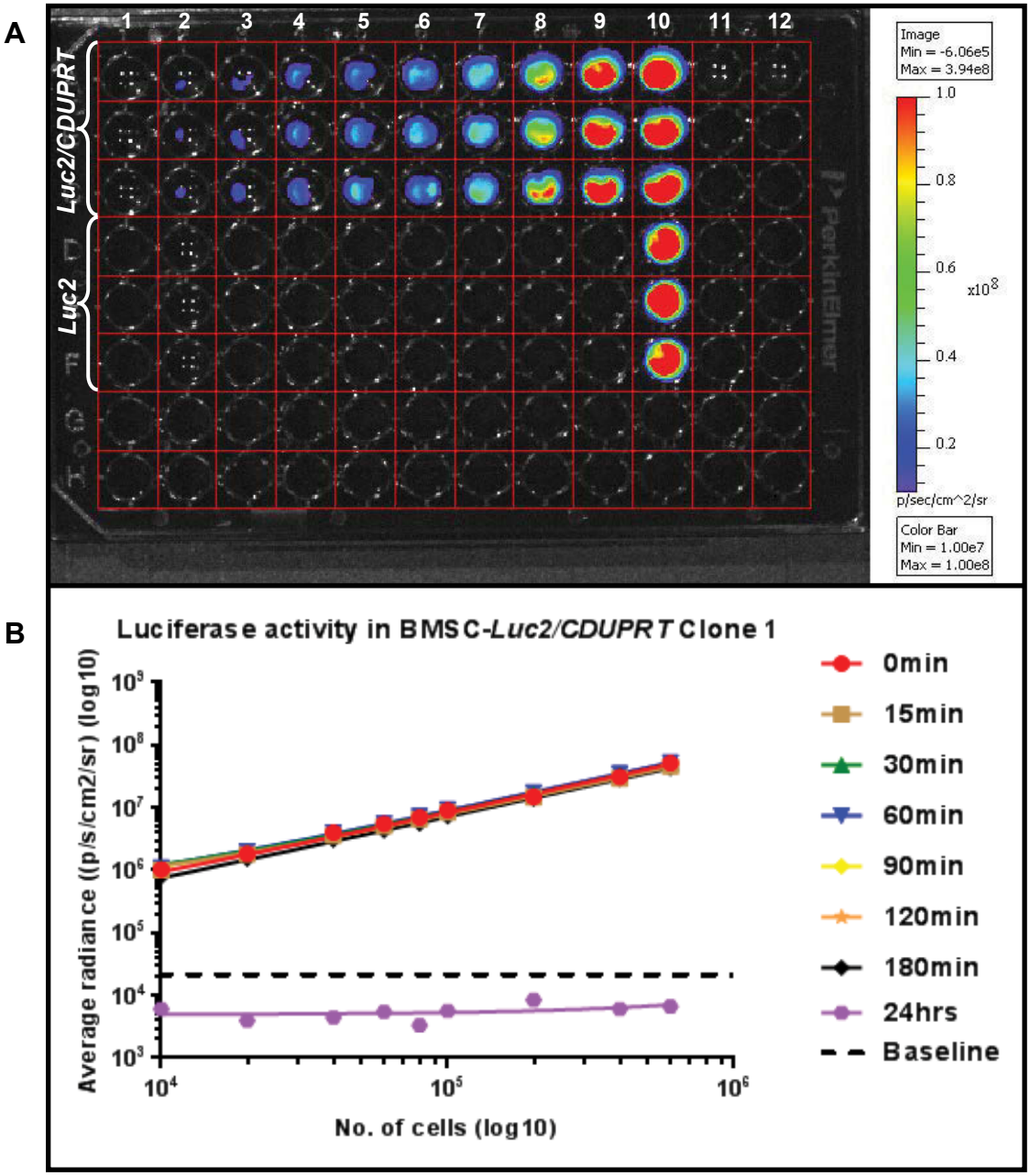

Figure 4.21: *In vitro* functional characterisation of luciferase activity in BMSC-*Luc2/CDUPRT* clone 1 (A) BLI was utilised to assess luciferase activity in BMSC-*Luc2/CDUPRT* clone 1 over a linear cell concentration range in comparison to BMSC-*Luc2*. The cells were incubated with 1:1 D-luciferin (300µg/ml) and imaged on the IVIS Lumina II according to the *in vitro* BLI acquisition settings. The image represented is at t=30. Lane 1: D-PBS, Lane 2-10: BMSC-*Luc2/CDUPRT* clone 1 and BMSC-*Luc2* (control). (B) Linear regression analysis of luminescent signal at multiple time-points post incubation with D-luciferin was performed using GraphPad Prism 7®. Data is represented as mean ± SD of triplicates.

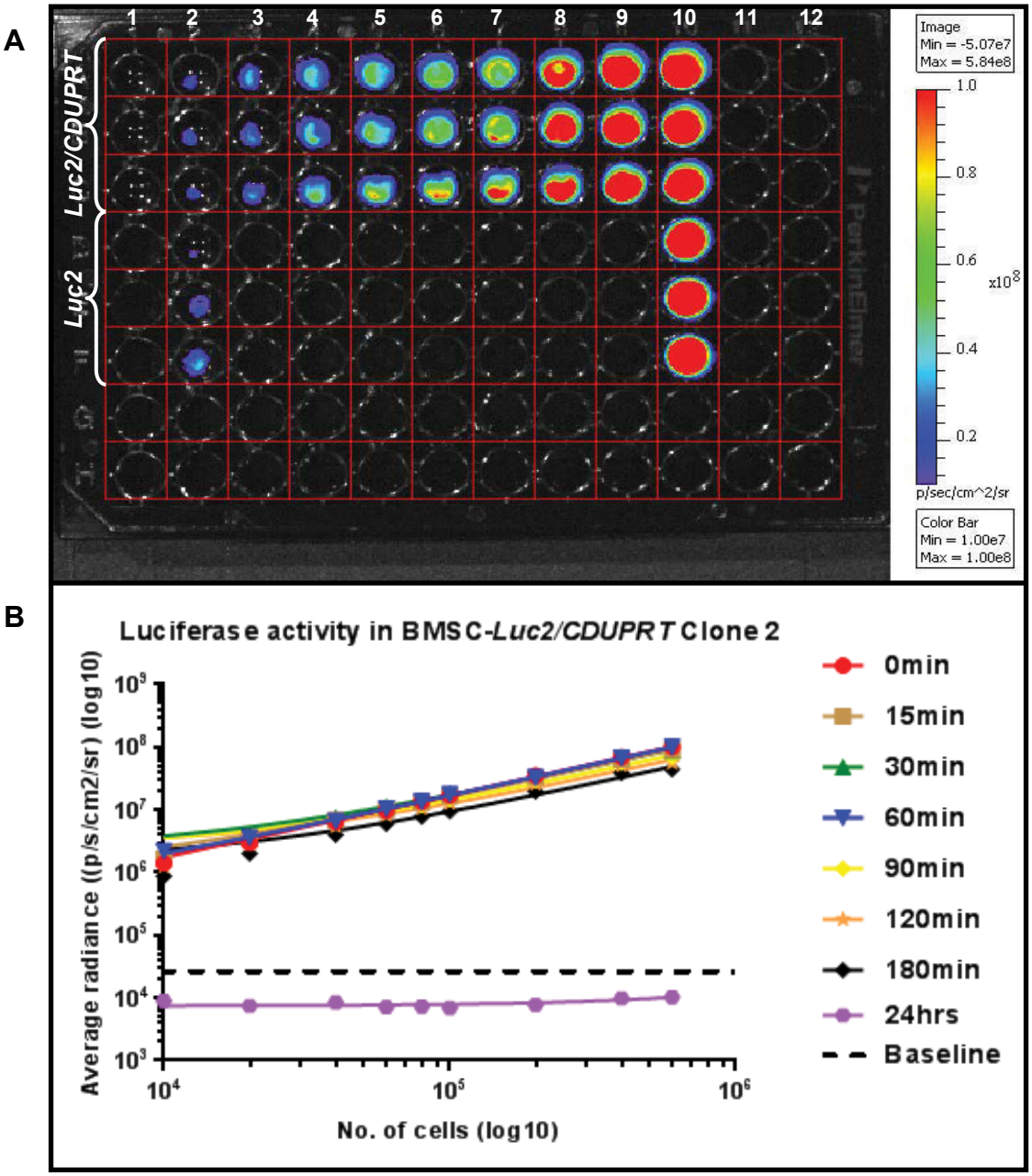

Figure 4.22: *In vitro* functional characterisation of luciferase activity in BMSC-*Luc2/CDUPRT* clone 2 (A) BLI was utilised to assess luciferase activity in BMSC-*Luc2/CDUPRT* clone 2 over a linear cell concentration range in comparison to BMSC-*Luc2*. The cells were incubated with 1:1 D-luciferin (300µg/ml) and imaged on the IVIS Lumina II according to the *in vitro* BLI acquisition settings. The image represented is at t=30. Lane 1: D-PBS, Lane 2-10: BMSC-*Luc2/CDUPRT* clone 2 and BMSC-*Luc2* (control). (B) Linear regression analysis of luminescent signal at multiple time-points post incubation with D-luciferin was performed using GraphPad Prism 7®. Data is represented as mean ± SD of triplicates.

4.2.2.4 In vitro characterisation of functional CDUPRT activity in suicide BMSCs

Functional *CDUPRT* activity was assessed in BMSC-*Luc2/CDUPRT* clone 1 following the addition of 5-FC (Figure 4.23A) and 5-FU (Figure 4.23B) via BLI. Bioluminescence correlates to cell viability[353], and therefore decreases in bioluminescence correlated with a decrease in cell viability. There was a significant decrease in bioluminescence in BMSC-*Luc2/CDUPRT* clone 1 in comparison to parental BMSC-*Luc2* following the addition of 5-FC ranging from 31.3-2000µg/ml ($p<0.005$), confirming functional *CDUPRT* activity in BMSC-*Luc2/CDUPRT* clone 1. The concentrations at which there is a >90% reduction in bioluminescent signal following addition of 5-FC for BMSC-*Luc2* and BMSC-*Luc2/CDUPRT* clone 1 in comparison to their untreated controls were 500µg/ml and 31.25µg/ml respectively. A similar trend is observed following the addition of 5-FU, where there was a significant decrease in bioluminescence in BMSC-*Luc2/CDUPRT* clone 1 in comparison to parental BMSC-*Luc2* following the addition of 5-FU ranging from 1-1000µg/ml ($p<0.005$), and re-confirming functional *CDUPRT* activity in BMSC-*Luc2/CDUPRT* clone 1. The concentrations at which there was a >90% reduction in bioluminescent signal following the addition of 5-FU for BMSC-*Luc2* and BMSC-*Luc2/CDUPRT* clone 1 in comparison to their untreated controls were 1000µg/ml and 1µg/ml respectively. BMSC-*Luc2/CDUPRT* clone 1 will be referred to as BMSC-*Luc2/CDUPRT* hereafter.

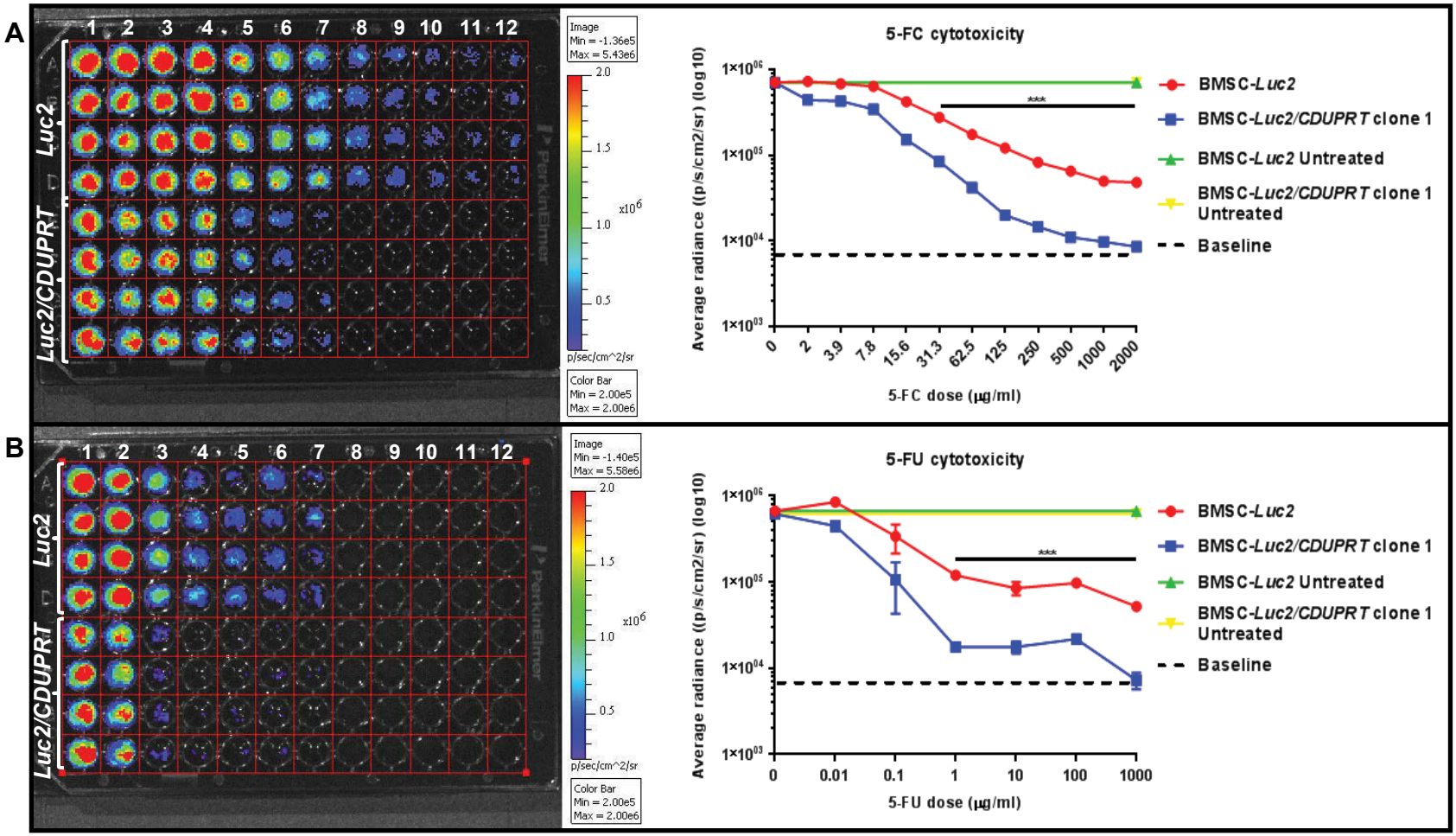

Figure 4.23: *In vitro* functional characterisation of *CDUPRT* activity BMSC-*Luc2* and BMSC-*Luc2/CDUPRT* clone 1 ($5x10^2$ cells/well) were plated in 96-well ViewPlates, and the functional activity of *CDUPRT* assessed following the addition of 5-FC (A) and 5-FU (B) via BLI. For 5-FC BLI data: Lanes 1-12 contains 2-fold serial dilutions of 5-FC from 0-2000µg/ml. For 5-FU BLI data: Lanes 1-7 contains 10-fold serial dilutions of 5-FU from 0-1000µg/ml. Graphical data is represented as mean radiance ± SEM (n=3). A two-way ANOVA and Sidak's post-hoc were performed, * $p<0.05$.

4.2.3 Persistence of BMSC-*Luc2/CDUPRT* in NOD and NOD/*Scid* mice

The persistence of BMSC-*Luc2/CDUPRT* was assessed in immune-competent (NOD) and immune-deficient (NOD/*Scid*) models of diabetes via BLI (Figure 4.24). Cells were transplanted at $1x10^4$, $1x10^5$ and $1x10^6$ cells/injection to determine the lowest cell concentration and the length of time for which bioluminescent signal can be detected. As can be seen in Figure 4.24, bioluminescent signal can be detected in immune-deficient NOD/*Scid* mice for 12 weeks. By comparison, the bioluminescent signal persisted for a period of 3 weeks in immune-competent NOD mice. Quantitative analysis of BLI data shows that in both NOD/*Scid* (Figure 4.25) and NOD mice (Figure 4.26), there was an increase in bioluminescent signal with increase in cell dose as expected. Bioluminescence detected at the highest cell dose ($1x10^6$ cells) was significantly stronger ($p<0.001$) than that detected at the lowest cell dose ($1x10^4$ cells) and in the negative control. As a consequence, bioluminescence was detected for a longer period of time at the highest cell dose. In addition, bioluminescent signal at the lowest cell dose ($1x10^4$ cells) was not detected using the optimal *in vivo* BLI settings outline in Table 4.8. This was due to the intensity of bioluminescence at the lowest cell dose being only slightly higher than background bioluminescence. In order to detect bioluminescence from the lowest cell dose, the minimum and maximum were required to be reduced; however, this resulted in the detection of background bioluminescence, which was not desirable.

However, a significant decrease in bioluminescence was observed at the highest cell dose when comparing t=0 to the experimental endpoint of control animals (NOD, $p<0.001$; NOD/*Scid*, $p<0.001$). In NOD/*Scid* animals specifically (Table 4.9), bioluminescence from low and mid cell doses ($1x10^4$ and $1x10^5$ cells respectively) significantly decreased within a period of 2 weeks ($p<0.005$), yet in comparison to control animals a significant difference in

bioluminescence was observed until week 9, after which there was no significant difference in bioluminescence in comparison to control animals. In addition, the higher than expected Day 0 control data point can be attributed to bioluminescence spill-over as a consequence of imaging control and treated animals in the same image capture.

In NOD animals specifically (Table 4.10), bioluminescence from low and mid cell doses significantly decreased at one and two weeks post transplantation respectively ($1x10^4$; p=ns, $1x10^5$; $p<0.01$), after which there was no significant difference in bioluminescence between low and mid cell doses with that of control animals. Bioluminescent signal was significantly higher than control animals at the highest cell dose two weeks post transplantation; however there was no significant difference observed by week 3.

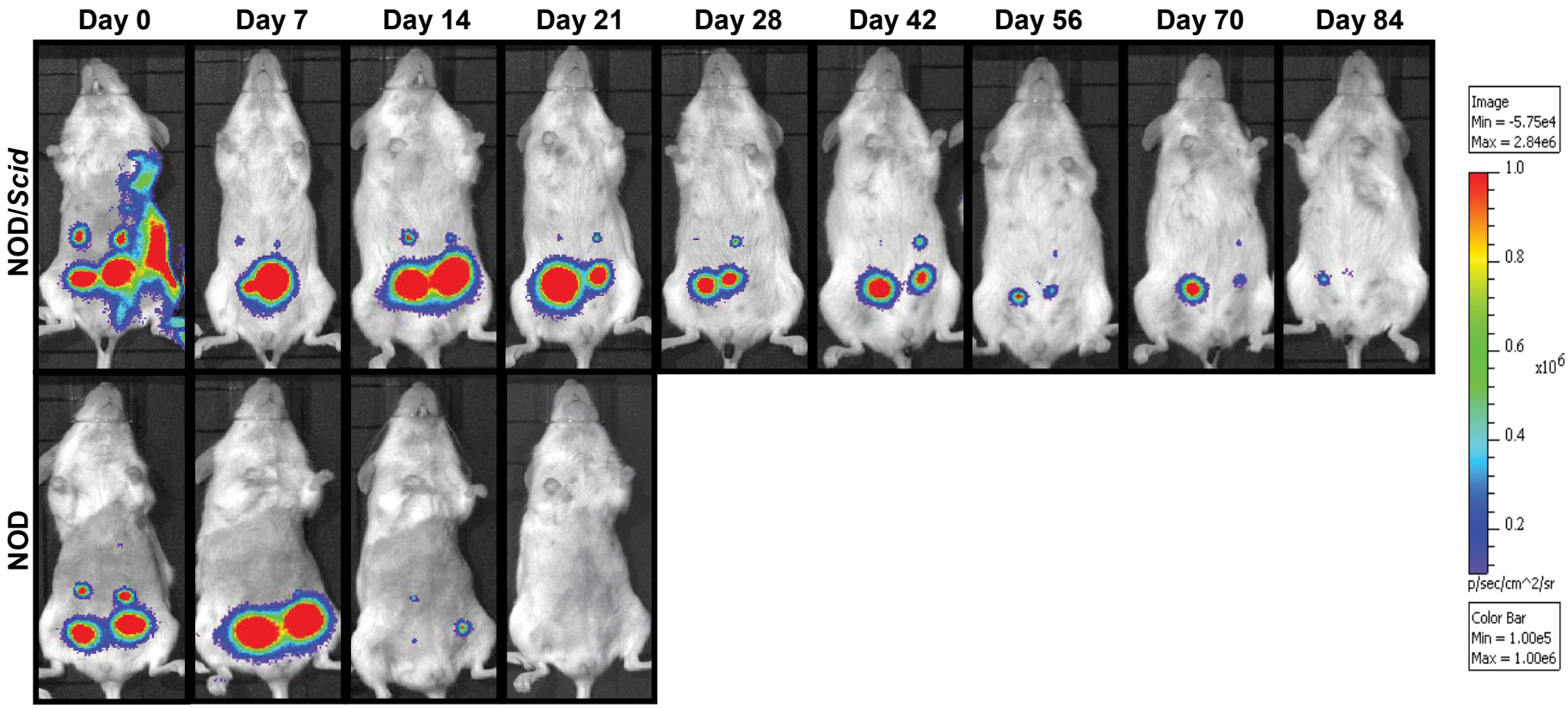

Figure 4.24: *In vivo* BLI of BMSC-*Luc2/CDUPRT* in NOD and NOD/*Scid* mice BMSC-*Luc2/CDUPRT* were transplanted subcutaneously at three cell concentrations ($1x10^4$, $1x10^5$ and $1x10^6$ cells/inj) in duplicate into NOD and NOD/*Scid* mice (n=4) (each mouse received six injections in total as described in Section 4.1.6.2 and illustrated in Figure 4.6). Animals receiving no cells (data not shown) were run alongside as a negative control (n=2). BLI images were subsequently acquired following the intraperitoneal administration of D-luciferin (15mg/ml) at 150mg/kg or 10µl/g according to the *in vivo* BLI image acquisition settings. Regions of interest were setup using the Living Image 3.1 (PerkinElmer™) corresponding to the location of the cell injections for BLI data to be acquired. All images are representative of a single experimental NOD/*Scid* and NOD animal.

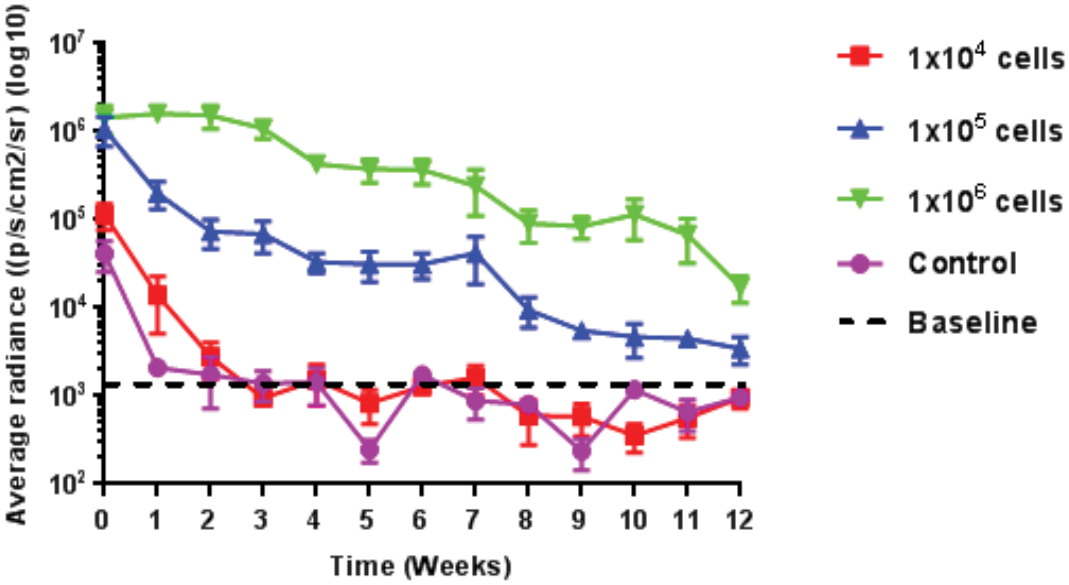

Figure 4.25: Analysis of *in vivo* BLI data in NOD/*Scid* mice BMSC-*Luc2/CDUPRT* were transplanted subcutaneously at three cell concentrations ($1x10^4$, $1x10^5$ and $1x10^6$ cells/inj) in duplicate in NOD/*Scid* mice (n=4). Animals receiving no cells were run alongside as a negative control (n=2). Following the capture of bioluminescent images, regions of interest were drawn surrounding the areas corresponding to the sites of cell transplantation. Quantitative data was subsequently analysed using GraphPad Prism 7®. Data is represented as average radiance ± SEM. A two-way ANOVA and Tukey's post hoc test were performed, * $p<0.05$.

Table 4.9: Significance in the change in bioluminescent signal in NOD/*Scid* mice

	Week												
	0	1	2	3	4	5	6	7	8	9	10	11	12
$1x10^4$ cells	****	***	ns	ns	ns	ns	ns	ns	ns	ns	ns	ns	ns
$1x10^5$ cells	****	****	****	***	***	***	***	***	***	**	ns	*	ns
$1x10^6$ cells	****	****	****	****	****	***	****	***	***	***	**	**	*

A two-way ANOVA with Sidak's post-hoc was performed comparing BLI of animals transplanted with tracking BMSCs in comparison to normal animals for the duration of the experiment. Data is represented as significance, * $p<0.05$.

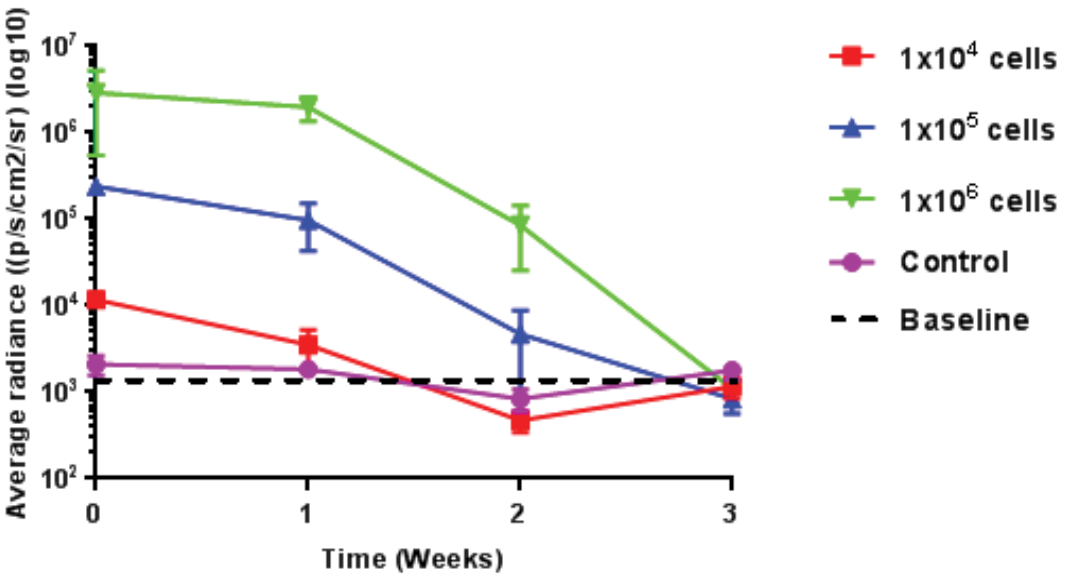

Figure 4.26: Analysis of *in vivo* BLI data in NOD mice BMSC-*Luc2/CDUPRT* were transplanted subcutaneously at three cell concentrations ($1x10^4$, $1x10^5$ and $1x10^6$ cells/inj) in duplicate in NOD mice (n=4). Animals receiving no cells were run alongside as a negative control (n=2). Following the capture of bioluminescent images, regions of interest were drawn surrounding the areas corresponding to the sites of cell transplantation. Quantitative data was subsequently analysed using GraphPad Prism 7®. Data is represented as average radiance ± SEM. A two-way ANOVA and Tukey's post hoc test were performed, * $p<0.05$.

Table 4.10: Significance in the change in bioluminescent signal in NOD mice

	Week			
	0	1	2	3
$1x10^4$ cells	****	ns	ns	ns
$1x10^5$ cells	****	*	ns	ns
$1x10^6$ cells	****	****	*	ns

A two-way ANOVA with Sidak's post-hoc was performed comparing BLI of animals transplanted with tracking BMSCs in comparison to normal animals for the duration of the experiment. Data is represented as significance, * $p<0.05$.

4.3 Discussion

4.3.1 Gene-modification of BMSCs via nucleofection

The dual promoter mammalian expression vector pVITRO2-mcs was successfully cloned to contain the *Luc2* and *CDUPRT* genes for nucleofection into NOD BMSCs. Nucleofection was utilised as a non-viral method of BMSC gene modification due to its reported success in modifying MSCs without affecting proliferation, phenotype or differentiation potential[354, 355]. Nucleofection of BMSCs with the pmaxGFP plasmid showed a transfection efficiency of ~70% at 24 hours post-nucleofection which is similar to that reported in the literature[354, 355]. In fact, nucleofection outperforms other transfection methods such as calcium phosphate precipitation, cationic polymer and standard electroporation with respect to gene-modification of MSCs[354, 356]. For the purpose of short-term/transient ectopic gene expression in difficult to transfect cells such as adult stem cells, nucleofection is a suitable alternative to tradition physical, non-viral methods of gene-modification. However, despite this success, variations in the transduction efficiency of MSCs have been observed across species[357]. In addition, stable transfection as a consequence of successful genomic integration is limited by the poor rate of integration (600 per million cells (0.06%)) with a ~5kb plasmid. With increasing plasmid size, integration events decrease further. As a result, due to higher transduction efficiency and genomic integration events, viral-mediated transduction remains the mainstay in generating gene-modified cells that stably express transgenes of interest[358-360].

4.3.2 Effect of 5-FC on native and *CDUPRT*-expressing BMSCs

The preliminary *in vitro* characterisation of luciferase expression from stably selected BMSC-*Luc2* and BMCS-*Luc2/CDUPRT* was equivalent (Figure 4.21 and 4.22). As a result, luciferase expression was utilised as a reporter for cell survival during the *in vitro* characterisation of *CDUPRT* function. The ability of CDUPRT to convert a non-toxic concentration of 5-FC to the toxic metabolite 5-FU was assessed by exposing parental BMSC-*Luc2* and BMCS-*Luc2/CDUPRT* to various concentrations of 5-FC *in vitro.* BMSCs expressing *CDUPRT* (BMCS-*Luc2/CDUPRT*) demonstrated a significant decrease in cell survival when compared with parental BMCSs (BMSC-*Luc2*) following the addition of >31.3ug/mL 5-FC, confirming the *in vitro* functional activity of *CDUPRT* (Figure 4.23). Owing to the toxicity of 5-FC >125ug/mL to parental BMSC-Luc2 cells, 5-FC was routinely used at <100ug/mL *in vitro*. In fact, at equivalent doses, 5-FU demonstrated significantly higher toxicity than 5-FC in cells expressing *CDUPRT*. This is due to the combined inhibition of DNA and RNA synthesis in BMSC-*Luc2/CDUPRT* as opposed to DNA inhibition alone in BMSC-*Luc2* following addition of 5-FU. Research conducted in rat prostate adenocarcinoma cells that were transduced to express the *CDUPRT* gene showed similar results[361]. In addition, the known metabolic pathway involved in the conversion of 5-FC to 5-FU and its toxic metabolites supports the results of this study (Figure 4.27A)[362, 363]. Due to the intracellular requirement of *CD* to convert 5-FC to 5-FU prior to the generation of 5-FU toxic metabolites, additional steps (both mechanical and enzymatic) are required for 5-FC killing of *CDUPRT* expressing cells in comparison to 5-FU. As a result, 5-FC toxicity is likely affected by its rate of cellular uptake, *CD* conversion and degradation, resulting in the observed differences in toxicity of 5-FC and 5-FU in *CDUPRT*-expressing cells.

However, of particular interest was the effect of 5-FC on parental BMSCs (BMSC-*Luc2*) that do not express the *CD* or *CDUPRT* genes, which are necessary for 5-FC conversion to 5-FU[364], and as such would not be susceptible to 5-FC mediated toxicity. Most data on the effect of 5-FC on mammalian cells that are engineered to express *CD* or *CDUPRT* are expressed as a function of cytotoxicity, which as expected increases in comparison to cells that do not express *CD* or *CDUPRT*[361, 362]. Following the addition of 5-FC to BMSC-*Luc2* that do not express *CDUPRT*, the observed decrease in bioluminescence in comparison to untreated BMSC-*Luc2* suggested that 5-FC may be involved in the inhibition of mammalian cell proliferation, or demonstrates cytotoxic effects at high doses (Figure 4.27B). In a similar study by Harrell *et al*[365] using primary vascular smooth muscle cells (VSMCs), treatment of parental VSMCs with 5-FC at a single concentration of 1mmol/L (equivalent to129µg.ml) did not result in a significant difference in cell numbers in comparison to untreated parental VSMCs, suggesting the absence of a cytotoxic effect of 5-FC on VSMCs. However, the lack of a dose-response curve failed to determine whether a cytotoxic effect would be observed at higher concentrations of 5-FC. Thus, the unique results reported in this study may be explained by cell-type dependent sensitivity to 5-FC. The significance of this finding highlights the potential for unintended effects of the co-delivery of 5-FC with *CD* or *CDUPRT*-engineered MSCs for the treatment of cancer for which it is currently assessed.

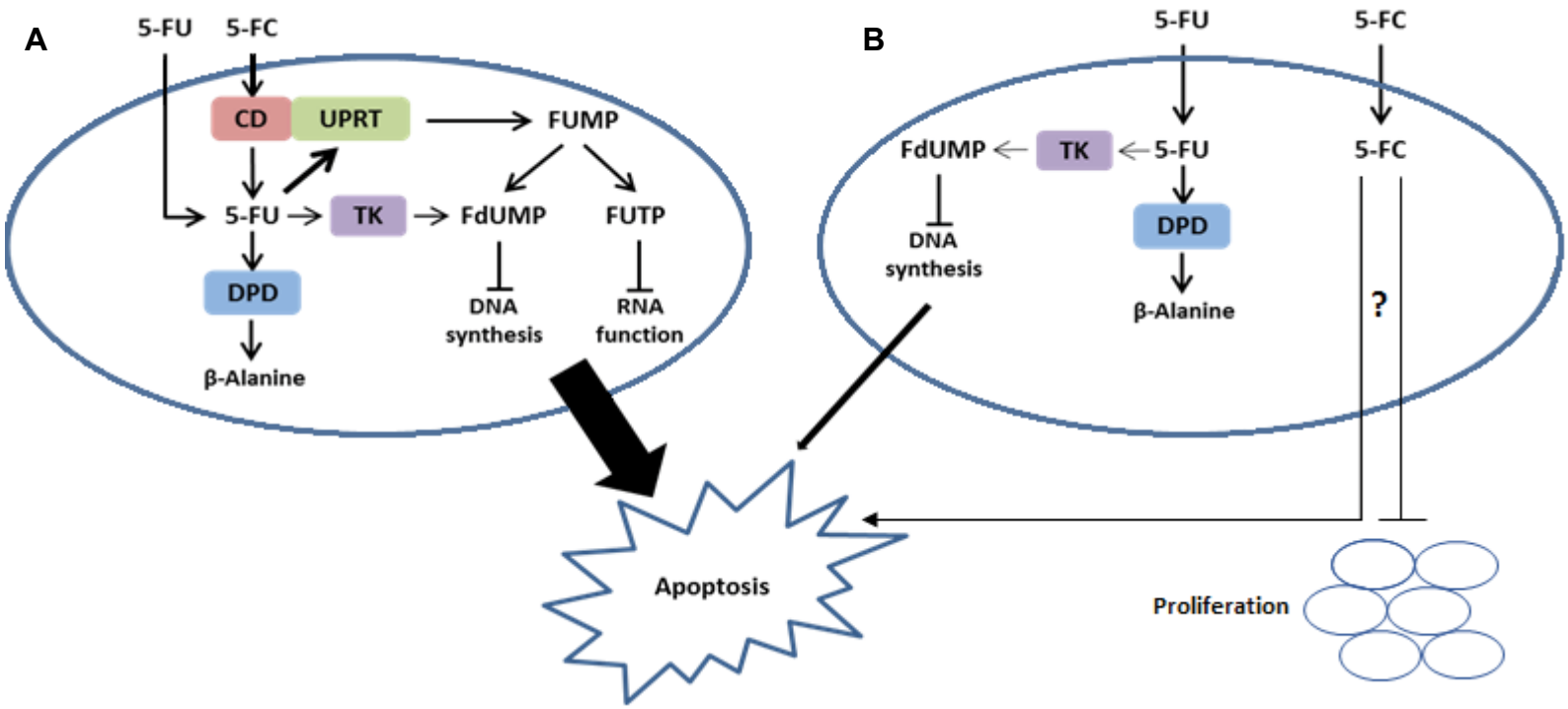

Figure 4.27: Mechanism of action of 5-FC and 5-FU in BMSCs In cells expressing *CDUPRT* (A), 5-FC is transported into the cell where it is converted into 5-FU by the *CD* component of *CDUPRT*. *UPRT* subsequently converts 5-FU into FUMP which is further processes into FdUMP and FUTP which inhibit DNA synthesis and RNA function respectively, leading to apoptosis. Endogenous DPD degrades 5-FU into non-toxic β-Alanine, which ultimately becomes the rate-limiting step in the conversion of 5-FU to its toxic metabolites. In cells that do not express *CDUPRT* (B), 5-FU toxicity is mediated by direct conversion to FdUMP via TK, leading to inhibition of DNA synthesis and apoptosis. In the absence of *CDUPRT*, 5-FC cannot be converted to 5-FU, and may result in the inhibition of cell proliferation or cytotoxicity through an unknown mechanism. Thickness of arrows is reflective of the predominating pathway or effect. Abbreviation: CDUPRT; cytosine deaminase::uracil phosphoribosyltransferase, CD; cytosine deaminase, FUMP; 5-fluorouridine monophosphate, FdUMP; 5-fluorodeoxyuridine monophosphate, FUTP; 5-fluorouridine triphosphate, DPD; dihydropyrimidine dehydrogenase.

4.3.3 Persistence of BMSCs in NOD and NOD/*Scid* mice

In vivo bioluminescence imaging as a means of tracking MSC survival and/or migration has been performed in a number of animal models of disease[366-368]. In this study, luciferase-expressing BMSCs were assessed for their ability to persist in immune-competent (NOD) and immune-deficient (NOD/*Scid*) models of diabetes. In immune-competent NOD mice, bioluminescence was detected from an autologous, subcutaneous transplant of BMSC-*Luc2/CDUPRT* up to 14 days post-transplantation, after which bioluminescence was no longer detected. Similarly, MSCs that were transduced to co-express luciferase and GFP, and subsequently transplanted via the kidney artery in Balb/c mice, were detected via BLI up to 14 days post transplantation[368]. This demonstrates that the site of cell administration in immune-competent models does not affect cell survival. In addition, the data from this study suggests that autologous BMSCs are not immune-privileged[369]. This may be due to a number of reasons including the over-expression of the non-mammalian *Luc2* and *CDUPRT* transgenes and contaminating foetal calf serum. Previous studies have demonstrated that sustained levels of high luciferase expression induce luciferase-specific immune responses in immune-competent animal models, limiting the utility of luciferase as an *in vivo* reporter[370, 371]. In addition, experiments in rats showed that rat MSCs grown in 20% FCS induce a substantial humoral response after repeated administrations, whereas cells grown under low FCS conditions reduce the immunogenicity in terms of IgG response over 1000-fold to barely detectable levels[372].

In immune-deficient NOD/*Scid* mice, bioluminescence was detected from a syngeneic, subcutaneous transplant of BMSC-*Luc2/CDUPRT* up to 12 weeks post-transplantation, after which bioluminescence was no longer detected. During the 12-week period post-transplantation, bioluminescence gradually decreased over time. Due to the nature of the

immune-deficient NOD/*Scid* model, loss of bioluminescence (and therefore BMSCs) was not immune-mediated as was likely the case in the immune-competent NOD model. These results are supported by similar studies, which show loss of MSCs in immune-deficient animal models[373-375]. However, these results should be carefully considered with respect to the common conditions of *ex vivo* MSC culture that does not recapitulate the MSC niche environment *in vivo*. MSCs are commonly cultured under normoxic (21% oxygen) conditions, which differs significantly from the hypoxic (<1% oxygen) *in vivo* conditions in which they reside. As a result, *ex vivo* cultured MSCs pre-conditioned under hypoxic (1-3% oxygen) conditions improves their migration and tissue regeneration potential[373].

However, it is well established within the field that the protective effects of MSCs are well observed following site-specific transplantation[376, 377] in comparison to intravenous (i.v.) transplantation[378] due to the entrapment of MSCs within the lung capillaries. Following i.v. administration of MSCs, the primary location of MSC migration is the lungs, where they become entrapped due to their large size and expression of adhesion molecules which determines the rate at which they are cleared[352, 379]. This ultimately diminishes the therapeutic effect of MSCs as the cells do not accumulate at the site of injury/disease in sufficient numbers. As a result, modulation of the expression of particular adhesion molecules represents a potential target for improving the therapeutic effectiveness of MSCs administered intravenously. The data presented highlights the limited timeframe within which the evaluation of the therapeutic effects of MSCs should occur in immune-competent and immune deficient animal models of diabetes. Evaluation of MSCs in short-term studies has demonstrated the protective benefits of MSCs[380], whereas long-term studies have shown little or no protection[381], which is reflective of their persistence in immune-competent models.

In summary, a mammalian dual expression vector possessing the *Luc2* and *CDUPRT* genes was successfully generated. Nucleofection of BMCSs with the pVITRO2-*Luc2* and pVITRO2-*Luc2/CDUPRT* plasmids was successful, however the low number of stable cell clones generated highlighted the limitations of nucleofection with regards to generating stable transgene-expressing cell lines. *In vitro* characterisation of the *Luc2* and *CDUPRT* genes demonstrated that both genes were functional in the selected BMSC clones. In addition, BMSC-*Luc2/CDUPRT* cells showed functional *CDUPRT* in the presence of 5-FC *in vitro*. Following transplantation, BMSCs persisted in immune-competent NOD mice for 2 weeks and in immune-deficient NOD/*Scid* mice for ~12 weeks (albeit with decreasing survival over time). This suggested an immune-mediated destruction of transplanted BMSCs in NOD mice, confirming that BMSCs are not immune-evasive when modified with non-mammalian genes. In fact, upon transplantation of a second injection of BMSCs, bioluminescence detected from transplanted cells disappeared within 5 days (data not shown). This was indicative of a strong secondary immune response and pointed strongly to an immune-mediated destruction of transplanted BMSCs as the likely cause of transplanted cell death.

In NOD/*Scid* mice, although BMSCs could be detected for a longer period of time, BMSC survival decreased during the observation period. This suggested that the site of transplantation contributed to the poor survival of BMSCs *in vivo*. The immune-deficient STZ-NOD/*Scid* model was therefore selected as the model of choice for evaluating the ability of lentiviral gene-modified BMSCs to reverse diabetes (Chapter 5), as the transplanted cells would survive for a sufficient period of time to observe a reduction in blood glucose levels. The intended purpose of the *in vivo* use of 5-FC in Chapter 5 was to demonstrate the success of the reversal of diabetes as a direct consequence of the transplanted BMSCs without requiring invasive graft removal. However, due to the observed death of BMSCs in the

chosen animal model of diabetes (NOD/*Scid*) in this study, 5-FC was not assessed for use *in vivo* as it was no longer required to destroy the cell graft to confirm diabetes reversal.

Chapter 5

Gene-modification of BMSC-*Luc2/CDUPRT* via the lentiviral transfer of human furin-cleavable insulin (*INS-FUR*), murine *NeuroD1* and *Pdx-1*

Introduction

The limitations of current target cell types for T1D gene therapy have resulted in the evaluation of alternative cell types for the generation of IPCs. MSCs represent an interesting alternative target for the treatment of T1D due to their ease of isolation, ability to be expanded *ex vivo*, high plasticity, immunomodulatory properties and capacity to function as biofactories[239, 240]. Previous research has shown that gene therapy can be utilised to direct the differentiation of MSCs towards the pancreatic lineage (specifically β-cells) which upon transplantation corrected hyperglycaemia for a short periods[94, 123, 192-195, 92, 197, 198]. However, despite the short-term success of MSC-derived surrogate IPCs upon transplantation, a number of practical challenges are yet to be overcome such as the generation of sufficient starting quantities of MSCs and the lack of cell proliferation following differentiation into IPCs, all of which prohibit the large-scale manufacture of a potential T1D cell therapy.

The advantage of tumour-derived liver cell lines such as Huh7 and the H4IIE previously investigated within our lab as targets for surrogate IPC generation is their capacity to generate large quantities of cells for gene-modification, and the ability of transdifferentiated cells to proliferate and function as surrogate β-cells. However, the use of tumour-derived cell lines in the clinical setting is hampered by their safety concerns. Considering that BMSCs are primary stem cells, their eventual differentiation into surrogate β-cells would result in the loss of early proliferative function. As a consequence, significant quantities are required prior to differentiation, as *ex vivo* expansion post-differentiation into IPCs is not possible. To overcome this, in this chapter I have evaluated the potential of *ex vivo* culture expanded BMSCs as targets for the generation of surrogate IPCs.

Ex vivo expanded BMSCs were initially gene-modified to express the pancreatic transcription factor *NeuroD1* and a modified form of human insulin known as furin-cleavable insulin (*INS-FUR*). *NeuroD1* is a pancreatic transcription factor involved in defining and maintaining endocrine cell fate during embryonic development of the pancreas, and has been shown to induce pancreatic transdifferentiation of liver tissue *in vivo*[150] and to rat hepatocytes *in vitro*[163], however has yet to be assessed in MSCs. Despite the success of exogenous pancreatic transcription factor transfer in inducing transdifferentiation in a variety of cell types, most cells fail to produce insulin in quantities similar to those observed in islets. Therefore, over-expression of *INS-FUR* that contains furin cleavage sites allows for the production of biologically active insulin in non-pancreatic tissues/cells that do not endogenously possess the proinsulin processing pro-convertase enzymes, as the furin cleavage sites allows the processing of proinsulin into insulin and c-peptide via the furin enzyme which is present in most cell types, including BMSCs. Following the assessment of *NeuroD1/INS-FUR* combinatorial gene therapy in inducing pancreatic differentiation of BMSCs, the transcription factor (*Pdx1*) known to successfully induce pancreatic differentiation of BMSCs in the literature[94, 123, 192-195, 92, 197, 198], was assessed in combination with *INS-FUR* as an alternative combinatorial therapy in an attempt to successfully generate surrogate IPCs from culture expanded BMSCs.

Specific Aims

- Generate novel lentiviral vectors expressing murine *NeuroD1*, *INS-FUR* and *Pdx1*.
- Characterise the gene expression profile of culture expanded BMSCs following lentiviral transduction with *NeuroD1* and *INS-FUR* via RT-PCR.

- Determine the ability of BMSCs expressing *NeuroD1* and *INS-FUR* to secrete insulin in a chronic and regulated manner.
- Characterise the gene expression profile of culture expanded BMSCs following lentiviral transduction with *Pdx1*.
- Determine the ability of BMSCs expressing *Pdx1* and *INS-FUR* to secrete insulin in a chronic and regulated manner.
- Determine whether BMSCs are capable of forming islet-like spheroids.
- Assess the ability of BMSCs expressing *INS-FUR* to reverse diabetes in STZ-diabetic NOD/*Scid* mice.

5.1 Specific methods

5.1.1 Generation of lentiviral plasmids containing *INS-FUR* and *NeuroD1*

The manipulation of genetic material and generation of genetically modified organisms was approved by the UTS Biosafety Committee (2001-19-R-GC; 2009-02-R-GC). The existing HMD (empty vector control) and HMD-*INS-FUR* lentiviral plasmids (Figures 5.1 and 5.2 respectively) used previously in our laboratory[77, 133, 134] were subsequently modified to express either *NeuroD1* alone (HMD-*NeuroD1*) or *INS-FUR* and *NeuroD1* in combination (HMD-*INS-FUR/NeuroD1*) prior to packaging. As illustrated in Figures 5.1 and 5.2, the existing lentiviral plasmids possess the enhanced green fluorescent protein (eGFP) reporter which allowed for the visualisation of transduction success, determination of transduction efficiency and FACS of positively transduced cells.

5.1.1.1 Synthesis and plasmid preparation of the NeuroD1-T2A-eGFP construct

Prior to cloning the HMD-*NeuroD1* and HMD-*INS-FUR*/*NeuroD1* lentiviral plasmids, the mouse (*Mus musculus*) *NeuroD1* cDNA was custom synthesised lacking a TAG stop codon, and contained a T2A peptide and eGFP at the 3` end using the GeneArt Gene Synthesis™ service (Thermofisher®) (Figure 5.3). Incorporation of a T2A peptide in the construct resulted in ribosomal skipping and the translation of two separate proteins (*NeuroD1* and eGFP) from a single mRNA template. The *NeuroD1* gene coding sequence was obtained from the National Centre for Biotechnology Information (NCBI) nucleotide database and was derived from the sequence with accession number NM_010894. The length of the custom *NeuroD1*-T2A-eGFP sequence is 1854bp. The custom synthesised pND1-T2A-eGFP plasmid was subsequently prepared for further manipulation as described in Section 2.5.

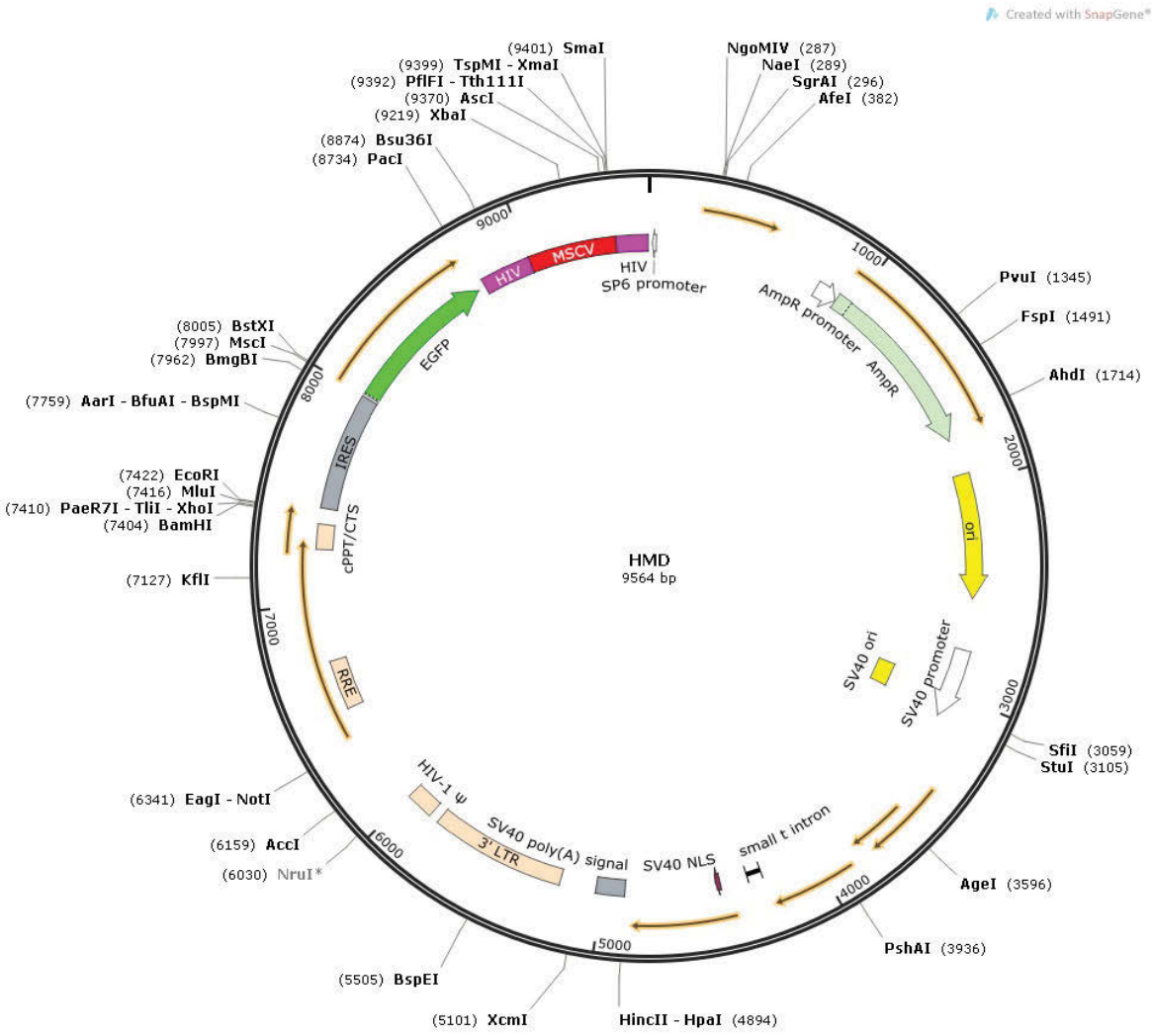

Figure 5.1: Diagrammatic representation of the existing HMD lentiviral plasmid The HMD lentiviral plasmid possesses features such as a hybrid murine stem cell virus (MSCV) promoter, an IRES allowing for dual expression of two upstream and downstream genes of interest (of which the GFP fluorescent reporter is one) and bacterial ampicillin resistance. The HMD lentiviral plasmid is utilised as the backbone for sub-cloning of genes of interest upstream and downstream of the IRES and as the empty vector when packaged for lentiviral transduction.

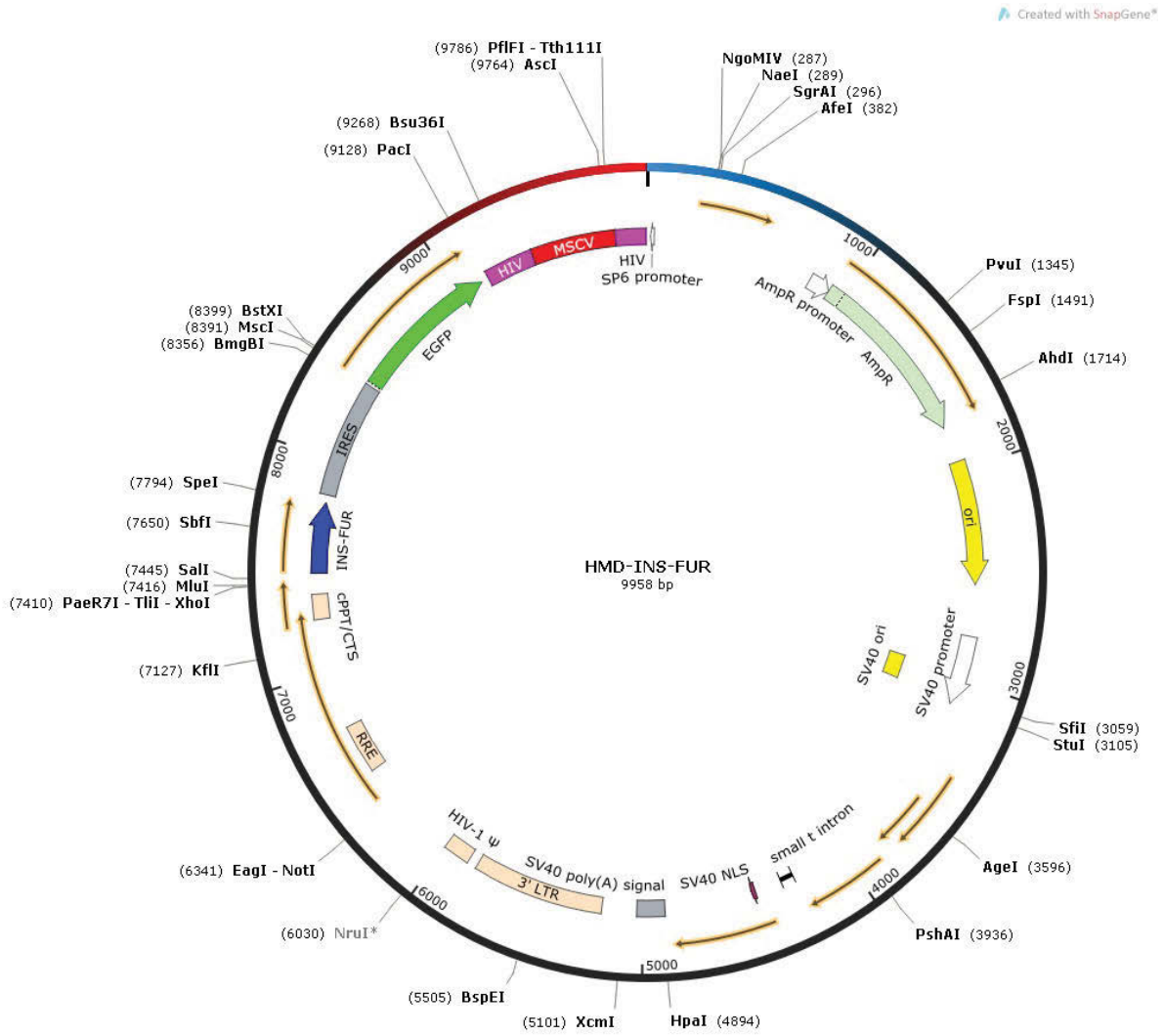

Figure 5.2: Diagrammatic representation of the existing HMD-*INS-FUR* lentiviral plasmid

The HMD-*INS-FUR* plasmid was developed by sub-cloning the human furin-cleavable insulin (*INS-FUR*) gene into the EcoRI site upstream of the IRES of the HMD plasmid. The GFP fluorescent reporter is co-expressed allowing for fluorescent detection of positively transduced cells expressing *INS-FUR*.

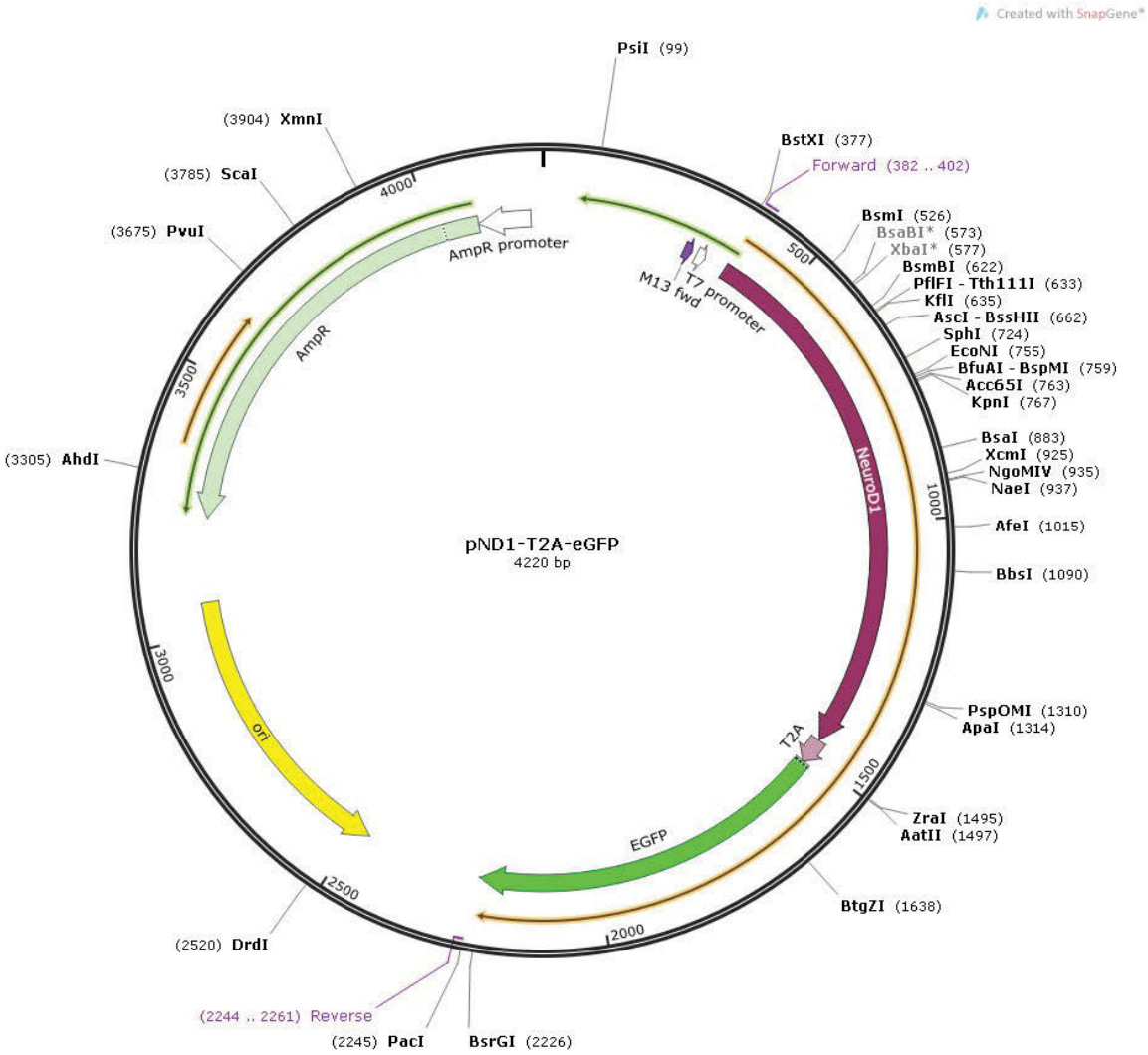

Figure 5.3: Diagrammatic representation of the pND1-T2A-eGFP sub-cloning plasmid

The pND1-T2A-eGFP sub-cloning plasmid was designed using the GeneArt Gene Synthesis™ service. A synthetic sequence encoding the murine *NeuroD1* cDNA linked to the eGFP gene via a T2A peptide was synthesised in a basic sub-cloning plasmid possessing bacterial ampicillin resistance. The *NeuroD1-T2A-eGFP* sequence was subsequently PCR amplified from pND1-T2A-eGFP for sub-cloning into the HMD lentiviral vectors.

5.1.1.2 PCR amplification of NeuroD1-T2A-eGFP

The forward primer was designed to contain a 5` MscI restriction site (yellow), and to overlap the ATG start codon (green) of the *NeuroD1* sequence. The addition of a spacer nucleotide (blue) between the MscI restriction site and the ATG start codon allowed for the inframe sub-cloning of *NeuroD1-T2A-eGFP* into the HMD vector. The reverse primer was designed to bind downstream of the 3` end of the eGFP sequence, with subsequent PCR amplification incorporating the existing PacI restriction site into the amplified *NeuroD1*-T2A-eGFP PCR product. The primer sequences were as follows:

- Forward: 5` GATACTTGGCCATATGACCAAATCATACAGCGA 3`
- Reverse: 5` CCATGAGGCCCAGTTAAT 3`

Briefly, *NeuroD1-T2A-eGFP* was amplified from the pND1-T2A-eGFP plasmid using Phusion® High-Fidelity PCR Mastermix with HF Buffer (New England Biolabs®) and the primers mentioned above according to the manufacturer's instructions (Table 5.1) in an Eppendorf™ Thermalcycler for 30 cycles with an optimal primer annealing temperature of 60ºC. The amplified *NeuroD1-T2A-eGFP* product (1854bp) was subsequently run on a 0.7% (w/v) agarose gel in 1x TBE buffer at 90V for 90 min and gel purified using the Wizard® SV Gel and PCR Clean-up System (Promega®) according to the manufacturer's instructions. Briefly, the excised gel slice containing *NeuroD1-T2A-eGFP* was solubilised in 1:1 (w/v) Membrane Binding Solution at 60ºC for 10 min. The gel mixture was subsequently transferred to a SV Minicolumn assembly and centrifuged at 16,000g for 1 min. Bound product was washed with 700µl Membrane Washing Solution (16,000g, 1min) and repeated with 500µl (16,000g, 5 min). To elute the bound product 30µl of dH_2O was added to the column, incubated at room temperature for 1 min and centrifuged at 16,000g for 1 min. The

eluted DNA quality and concentration was assessed using a NanoDrop® 2000 spectrophotometer (Thermofisher®) and stored at -20ºC prior to use in cloning.

Table 5.1: Phusion® HF PCR amplification of *NeuroD1-T2A-eGFP*

Component	Final Concentration	Volume (µl)
Phusion® High-Fidelity PCR Mastermix with HF Buffer	1x	12.5
Forward Primer (10µM)	0.5µM	1.25
Reverse Primer (10µM)	0.5µM	1.25
pND1-T2A-eGFP plasmid (10ng/µl)	-	1
RNase-Free Water	-	9

5.1.1.3 Restriction digestion of NeuroD1-T2A-eGFP and HMD-INS-FUR

In preparation for the ligation of *NeuroD1-T2A-eGFP* into the HMD-*INS-FUR* vector, both HMD-*INS-FUR* and *NeuroD1-T2A-eGFP* were digested with MscI (New England Biolabs®) and PacI (New England Biolabs®) according to Table 5.2. All reactions were incubated at 37ºC for 2 hours. Both digested HMD-*INS-FUR* and *NeuroD1-T2A-eGFP* were subsequently run on a 0.7% (w/v) agarose gel and gel purified using the Wizard® SV Gel and PCR Clean-up System (Promega®) as described in Section 5.1.1.2.

Table 5.2: MscI/PacI digest of HMD-*INS-FUR* and *NeuroD1*-T2A-eGFP

Components	HMD-*INS-FUR* (µl)	*NeuroD1-T2A-eGFP* (µl)
HMD-*INS-FUR* (~200ng/µl)	15	-
***NeuroD1-T2A-eGFP* (200ng/µl)**	-	30
Cutsmart Buffer (10x)	5	5
MscI (5U/µl)	1	1
PacI (10U/µl)	1	1
dH_2O	28	13
Total volume	50	50

5.1.1.4 Ligation of NeuroD1-T2A-eGFP and HMD-INS-FUR

The HMD-*INS-FUR* backbone was digested with MscI and PacI, and dephosphorylated using recombinant rSAP (New England Biolabs®) according to the manufacturer's instructions. In addition, purified *NeuroD1-T2A-eGFP* was diluted to 50ng/µl with dH_2O in preparation for use in the ligation reactions. Ligation of dephosphorylated HMD-*INS-FUR* (MscI/PacI) and *NeuroD1-T2A-eGFP* was performed at three insert:vector backbone ratios (3:1, 6:1 and 10:1) using T4 DNA ligase (400U/µl) as outlined in Table 5.3, and incubated at 16ºC for 16 hours (overnight). A negative control of dephosphorylated HMD-*INS-FUR* (MscI/PacI) was setup to account for potential vector backbone re-ligation.

Table 5.3: Ligation of HMD-*INS-FUR* and *NeuroD1-T2A-eGFP*

Component	3:1 (µl)	6:1 (µl)	10:1 (µl)	-ve control (µl)
***NeuroD1-T2A-eGFP* (50ng/µl)**	1	2	3	-
Dephosphorylated HMD-*INS-FUR* (50ng/µl)	1	1	1	1
Ligase buffer (10x)	1	1	1	1
T4 DNA Ligase (400U/µl)	1	1	1	1
dH_2O	6	5	4	7
Total	10	10	10	10

5.1.1.5 Restriction digestion and Quick Ligation™ of HMD-INS-FUR-NeuroD1

The resulting HMD-*INS-FUR/NeuroD1* vector was subsequently digested with EcoRI-HF (New England Biolabs®) to excise the *INS-FUR* gene according to Table 5.4, run on a 0.7% (w/v) agarose gel and gel purified using the Wizard® SV Gel and PCR Clean-up System (Promega®) as described in Section 5.1.1.2. Digested HMD-*INS-FUR/NeuroD1* (EcoRI-HF) was subsequently re-ligated using the Quick Ligation Kit™ (New England Biolabs®) according to the manufacturer's instructions to generate HMD-*NeuroD1*. Briefly, digested HMD-*INS-FUR/NeuroD1* (EcoRI-HF) was diluted to 50ng/µl and incubated in the presence of 1x Quick Ligase Reaction Buffer (2x) (New England Biolabs®), 2000U/µl Quick Ligase (New England Biolabs®) at 25°C for 5 min. The reaction was subsequently transferred to ice and used immediately in plasmid transformation reactions.

Table 5.4: EcoRI-HF digest of HMD-*INS-FUR/NeuroD1*

Components	HMD-*INS-FUR/NeuroD1*
HMD-*INS-FUR/NeuroD1* (~200ng/µl)	1
Cutsmart Buffer (10x)	1
EcoRI-HF (20U/µl)	1
dH_2O	7
Total volume	10

5.1.1.6 Transformation of Stbl3 E.coli with HMD-INS-FUR-NueroD1 and HMD-NeuroD1 plasmids

Transformation of ligation reactions was performed as outlined in Section 2.5.1.2. Selection of *E.coli* expressing lentiviral plasmids was performed using Ampicillin (100µg/ml) as outlined in Section 2.5.2. Bacterial colonies arising following transformation were subsequently mini-prepped as described in Section 2.5.4 for downstream diagnostic digest.

5.1.1.7 Diagnostic digest of putative HMD-INS-FUR-NueroD1 and HMD-NeuroD1 plasmids

To confirm successful ligation of *NeuroD1*-T2A-eGFP in putative *E.coli* clones expressing HMD-*INS-FUR-NeuroD1*, plasmid DNA isolated from each clone was digested with MscI and PacI according to Table 5.5. To confirm successful excision of *INS-FUR* in putative *E.coli* clones expressing HMD-*NeuroD1*, plasmid DNA isolated from each clone was digested with EcoRI-HF according to Table 5.6.

Table 5.5: Diagnostic digest of HMD-*INS-FUR/NeuroD1*

Components	HMD-*INS-FUR/NeuroD1*
HMD-*INS-FUR/NeuroD1* (~200ng/µl)	1
Cutsmart Buffer (10x)	1
MscI (5U/µl)	1
PacI (10U/µl)	1
dH_2O	6
Total volume	10

Table 5.6: Diagnostic digest of HMD-*NeuroD1*

Components	HMD-*NeuroD1*
HMD-*NeuroD1* (~200ng/µl)	1
Cutsmart Buffer (10x)	1
EcoRI-HF (10U/µl)	1
dH_2O	7
Total volume	10

5.1.2 Generation of the lentiviral plasmid containing *Pdx1*

The existing HMD lentiviral plasmid was subsequently modified to contain the codon-optimised murine *Pdx1* cDNA via sub-cloning from the AAV-*Pdx1* plasmid (Figure 5.4) kindly donated by Dr Grant Logan (Children's Medical Research Institute, Westmead Children's Hospital, Sydney, Australia) to generate HMD-*Pdx1*. The codon-optimised *Pdx1* cDNA was derived from the NCBI nucleotide database murine *Pdx1* sequence with accession number NM_008814.3.

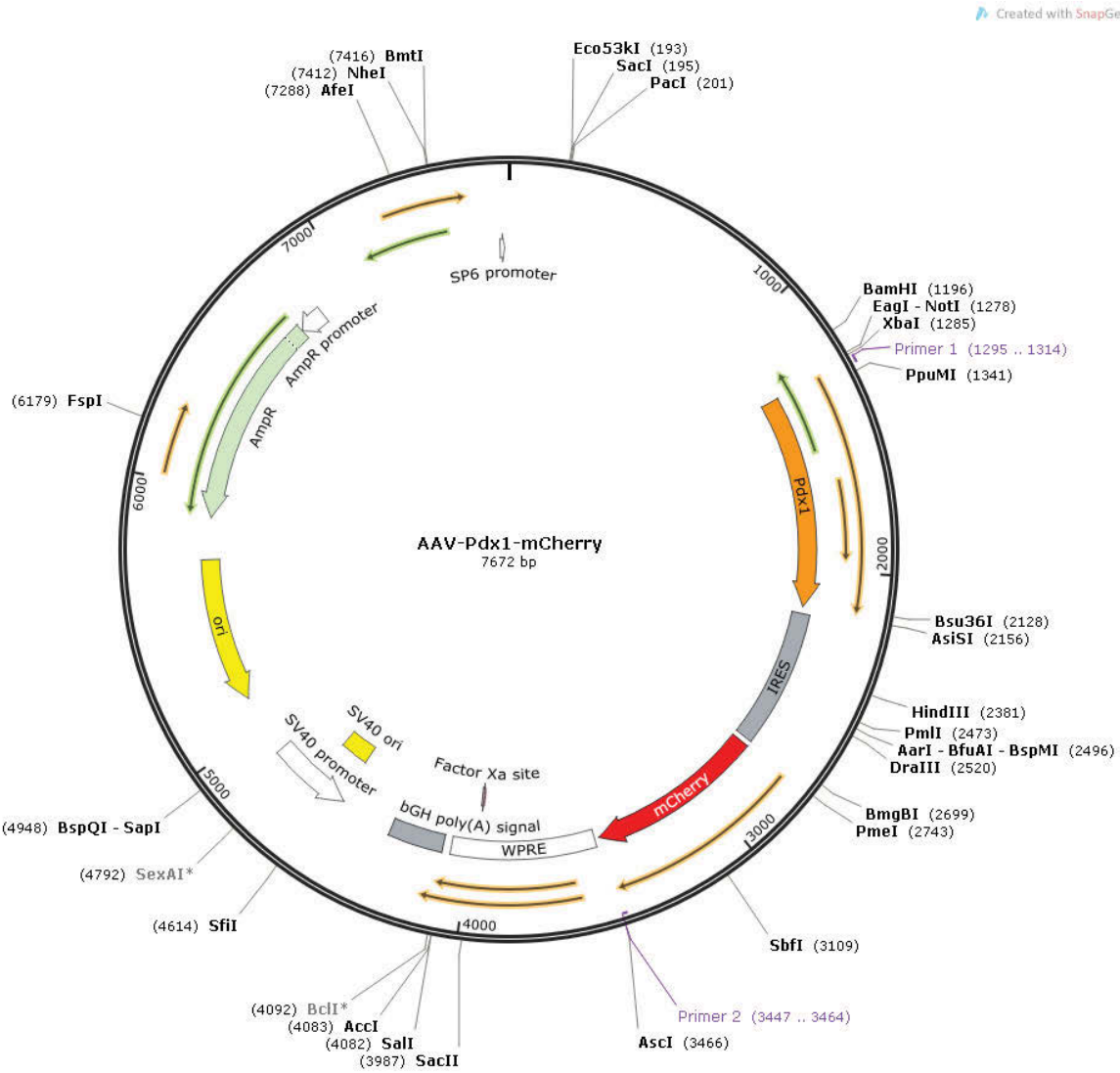

Figure 5.4: Diagrammatic representation of the AAV-*Pdx1* plasmid The AAV-*Pdx1* plasmid possesses the codon-optimised murine *Pdx1* cDNA upstream of the IRES element, and is co-expressed with the mCherry fluorescent reporter. The bacterial ampicillin resistance gene allows for bacterial selection of the plasmid.

5.1.2.1 PCR amplification of Pdx1-IRES-mCherry

The forward primer was designed to contain a 5` BamHI restriction site (yellow), and to overlap with the ATG start codon (green) of the codon-optimised *Pdx1* sequence for the inframe sub-cloning of *Pdx1-IRES-mCherry* into the HMD vector. The reverse primer was designed to contain a 3` PacI restriction site (blue), and to overlap with the TAA stop codon (red) of the *mCherry* sequence. The primer sequences were as follows:

- Forward: 5` GATACTGGATCCATGAACAGCGAGGAACAG 3`
- Reverse: 5` GCGCCGTTAATTAATTACTTGTACAGCTCGTC 3`

Briefly, *Pdx1-IRES-mCherry* was amplified from the AAV-*Pdx1* plasmid using Phusion® High-Fidelity PCR Mastermix with HF Buffer (New England Biolabs®) and the primers mentioned above according to the manufacturer's instructions (Table 5.7) in an Eppendorf™ Thermalcycler for 30 cycles with an optimal primer annealing temperature of 60ºC. The amplified *Pdx1-IRES-mCherry* product (2194bp) was subsequently run on a 0.7% (w/v) agarose gel in 1x TBE buffer at 90V for 90 min and gel purified using the Wizard® SV Gel and PCR Clean-up System (Promega®) according to the manufacturer's instructions and as described in Section 5.1.1.2.

Table 5.7: Phusion® HF PCR amplification of *Pdx1-IRES-mCherry*

Component	Final Concentration	Volume (µl)
Phusion® High-Fidelity PCR Mastermix with HF Buffer	1x	12.5
Forward Primer (10µM)	0.5µM	1.25
Reverse Primer (10µM)	0.5µM	1.25
AAV-*Pdx1* plasmid (10ng/µl)	-	1
RNase-Free Water	-	9

5.1.2.2 Restriction digestion of Pdx1-IRES-mCherry and HMD

In preparation for the ligation of *Pdx1-IRES-mCherry* into the HMD vector, both the HMD plasmid and the *Pdx1-IRES-mCherry* product were digested with BamHI-HF (New England Biolabs®) and PacI (New England Biolabs®) according to Table 5.8. All reactions were incubated at 37ºC for 2 hours. Both digested HMD and *Pdx1-IRES-mCherry* were subsequently run on a 0.7% (w/v) agarose gel and gel purified using the Wizard® SV Gel and PCR Clean-up System (Promega®) as described in Section 5.1.1.2.

Table 5.8: BamHI-HF/PacI digest of HMD and *Pdx1-IRES-mCherry*

Components	HMD (µl)	*Pdx1-IRES-mCherry* (µl)
HMD (~200ng/µl)	15	-
***Pdx1-IRES-mCherry* (200ng/µl)**	-	30
Cutsmart Buffer (10x)	5	5
BamHI-HF (20U/µl)	1	1
PacI (10U/µl)	1	1
dH_2O	28	13
Total volume	50	50

5.1.2.3 Ligation of Pdx1-IRES-mCherry and HMD

HMD backbone was digested with BamHI-HF and PacI, and dephosphorylated using recombinant rSAP (New England Biolabs®) according to the manufacturer's instructions. In addition, purified *Pdx1-IRES-mCherry* was diluted to 50ng/µl with dH_2O in preparation for use in the ligation reactions. Ligation of dephosphorylated HMD (BamHI-HF/PacI) and

Pdx1-IRES-mCherry was performed at three insert:vector backbone ratios (3:1, 6:1 and 10:1) using T4 DNA ligase (400U/µl) as outlined in Table 5.9, and incubated at 16ºC for 16 hours (overnight). A negative control of dephosphorylated HMD (BamHI-HF/PacI) was setup to account for potential vector backbone re-ligation.

Table 5.9: Ligation of HMD and *Pdx1-IRES-mCherry*

Component	3:1 (µl)	6:1 (µl)	10:1 (µl)	-ve control (µl)
***Pdx1-IRES-mCherry* (50ng/µl)**	1	2	3	-
Dephosphorylated HMD (50ng/µl)	1	1	1	1
Ligase buffer (10x)	1	1	1	1
T4 DNA Ligase (400U/µl)	1	1	1	1
dH_2O	6	5	4	7
Total	10	10	10	10

5.1.2.4 Transformation of Stbl3 E.coli with HMD-Pdx1 plasmid

Transformation of ligation reactions was performed as outlined in Section 2.5.1.2. Selection of *E.coli* expressing lentiviral plasmids was performed using Ampicillin (100µg/ml) as outlined in Section 2.5.2. Bacterial colonies arising following transformation were assessed for mCherry expression via fluorescence microscopy, and $mCherry^+$ colonies were subsequently mini-prepped as described in Section 2.5.4 for downstream diagnostic digest.

5.1.2.5 Diagnostic digest of putative HMD-Pdx1 plasmid

To confirm the successful ligation of *Pdx1-IRES-mCherry* in the putative *E.coli* clones expressing HMD-*Pdx1*, Plasmid DNA isolated from each clone was digested with BamHI-HF and AsiSI (New England Biolabs®) according to Table 5.10.

Table 5.10: Diagnostic digest of HMD-*Pdx1*

Components	HMD-*Pdx1*
HMD-*Pdx1* (~200ng/µl)	1
Cutsmart Buffer (10x)	1
BamHI-HF (20U/µl)	1
AsiSI (10U/µl)	1
dH_2O	6
Total volume	10

5.1.3 Packaging of lentiviral plasmids

Prior to packaging of the HMD-*NeuroD1*, HMD-*INS-FUR/NeuroD1* and HMD-*Pdx1* lentiviral plasmids, all plasmids were midi-prepped using the PureLink® Quick Plasmid Midiprep/Megaprep Kit (Invitrogen, Lifetechnologies™) according to the manufacturer's instructions. The concentration and purity of purified lentiviral plasmids was assessed using a NanoDrop® 2000 spectrophotometer (Thermofisher®).

5.1.3.1 Lentiviral plasmid transfection via calcium phosphate precipitation

The lentiviral plasmids were transfected using calcium phosphate precipitation in HEK293T cells (passages 5-10). On Day 1, HEK293T cells (passages 5-10) were split to obtain 80-90% confluency on Day 2. HEK293T cells were seeded in one T175 flask in complete high glucose DMEM (high glucose DMEM (Lifetechnologies™) containing 10% FCS and 1% 100x PenStrep (P/S) (Lifetechnologies™)). The following day (Day 2), the media was removed from the flask and replenished with 20ml of fresh complete high glucose DMEM. In

addition, two tubes containing the transfection reagents were prepared as outlined in Table 5.11 and 5.12 respectively.

Table 5.11: Transfection Tube 1

Plasmid/Reagents	Concentration/Volume
Lentiviral plasmid	105µg
VSV-G plasmid	70µg
ΔR8.2 plasmid	140µg
2M $CaCl_2$	210µl
dH_2O	Xµl
Total	1400µl

Table 5.12: Transfection Tube 2

Reagents	Volume (µl)
1M HEPES	70
2M NaCl	175
150mM Na_2HPO_4	16.1
dH_2O	1138.9
Total	1400

Using a transfer pipette, the contents of Tube 1 was transferred to Tube 2 and mixed by releasing bubbles. The mixture was incubated at room temperature for 30 min for complete precipitation, and subsequently transferred to one T175 flask containing 80-90% confluent HEK293T cells. The flasks were incubated for 3-4 hours at 37ºC/5% CO_2, after which the medium was removed; the cells were washed twice with 1x PBS and fresh complete high glucose DMEM added to the flasks. The cells were subsequently incubated for a further 2-3

days at 37ºC/5% CO_2, during which time the supernatant was initially harvested at 36 hours post transfection, and replenished/harvested every 12 hours thereafter. The harvested medium containing lentiviral particles was stored at 4ºC prior to filtration and concentration.

5.1.3.2 Lentivirus filtration and concentration

The harvested lentiviral particles stored at 4ºC were filtered through a Millex-HV 0.45µM polyvinylidene fluoride syringe filter (EMD Millipore©) to remove viral and cellular debris prior to centrifugation. Filtered lentivirus was subsequently concentrated using Amicon Ultra 100 kDa filters (EMD Millipore©) via centrifugation at 3000g for 30 min. The concentrated lentivirus was subsequently aliquoted in 1ml volumes into 1.5ml microcentrifuge tubes and stored at -80ºC prior to viral titration.

5.1.4 Titration of lentiviral plasmids

5.1.4.1 Transduction of NIH3T3 cells

Twenty-four hours prior to titration, $5x10^4$ NIH3T3 cells/well (P5-10) were seeded in each well of a 24-well plate to obtain 30-50% confluency on the day of transduction. On the day of transduction, cells in three wells were detached, counted and the average number used in viral titration calculations. In addition, 2-fold dilutions ranging from 1/2-1/128 of each lentiviral preparation (HMD-*NeuroD1*, HMD-*INS-FUR/NeuroD1* and HMD-*Pdx1*) were setup in complete high glucose DMEM + 8µg/ml Polybrene (Sigma-Aldrich©). The medium was removed from each well of the 24-well plate and 200µl of each viral dilution added to a well in triplicate. The 24-well plate was incubated for 4 hours at 37ºC/5% CO_2, after which the virus was removed from the wells, and the cells were washed twice with 1 x PBS and 500µl of complete high glucose DMEM added to each well. The 24-well plate was subsequently

incubated for 72 hours at 37ºC/5% CO_2, after which the cells were detached and fixed in 100µl of 4% paraformaldehyde for FACS analysis to analyse fluorescence expression. For HMD-*NeuroD1* and HMD-*INS-FUR/NeuroD1* transduced cells GFP expression was analysed, and for HMD-*Pdx1* transduced cells mCherry expression was analysed.

5.1.4.2 FACS analysis of transduced NIH3T3 cells

Fixed NIH3T3 cells transduced with HMD-*NeuroD1*, HMD-*INS-FUR/NeuroD1* and HMD-*Pdx1* were transferred to new individual 5mL Round Bottom Polystyrene Test Tubes with Cell Strainer Snap Caps (Corning™), and the strainer caps subsequently replaced with regular round bottom polystyrene tube caps. FACS analysis of eGFP expression in NIH3T3 cells transduced with HMD-*NeuroD1* and HMD-*INS-FUR/NeuroD1* was performed on a BD LSR II™ in the Microbial Imaging Facility (UTS, Sydney, Australia) which possesses combined flow cytometry and high-content resolution imaging units. Flow cytometry data was analysed using BD FACSDiva™ software (Version 8.0.1). FACS analysis of mCherry expression in NIH3T3 cells transduced with HMD-*Pdx1* was performed on a BD LSR Fortessa™ at the Advanced Cytometry Facility (Centenary Institute, Sydney, Australia). Flow cytometry data was analysed using BD FACSDiva™ software (Version 8.0.1).

5.1.5 Gene modification of BMSC-*Luc2/CDUPRT* with lentiviral plasmids

5.1.5.1 Lentiviral transduction of BMSC-Luc2/CDUPRT

Mid-passage (P15-30) BMSC-*Luc2/CDUPRT* cells were cultured in T175 flasks as described in Section 2.1. In preparation for transduction, the cells were detached and seeded at $2x10^5$ cells per T25cm^2 flask in complete α-MEM containing 200µg/ml Hygromycin B and incubated overnight at 37ºC/5% CO_2. On the day of transduction the cells were washed twice

with 1x HBSS, and fresh complete α-MEM containing 200µg/ml Hygromycin B and 8µg/ml Polybrene was added to the cells. Concentrated viral supernatant was added to the cells at a multiplicity of infection (MOI) of 10 and the cells incubated overnight at 37ºC/5% CO_2. A negative control of $2x10^5$ untransduced BMSC-*Luc2/CDUPRT* was run alongside transduced BMSC-*Luc2/CDUPRT*. The variation of transductions with lentiviral vectors was as follows:

1. BMSC-*Luc2/CDUPRT* + HMD ($1.8x10^7$ TU) (Round 1 and 2)
2. BMSC-*Luc2/CDUPRT* + HMD-*INS-FUR* ($1.2x10^8$ TU) (Round 1 and 2)
3. BMSC-*Luc2/CDUPRT* + HMD-*INS-FUR/NeuroD1* (Round 1 and 2)
4. BMSC-*Luc2/CDUPRT* + HMD-*NeuroD1* (Round 1 and 2)
5. BMSC-*Luc2/CDUPRT* + HMD-*Pdx1* (Round 3)
6. BMSC-*Luc2/CDUPRT-INS-FUR* + HMD-*Pdx1* (Round 3)

The following day (16 hours) post-transduction, the medium containing the lentiviral vectors was discarded, the cells washed twice with 1x HBSS, the medium replenished with fresh complete α-MEM containing 200µg/ml Hygromycin B and the cells incubated for a further 72 hours at 37ºC/5% CO_2. Confirmation of successful transduction was performed via fluorescence microscopy of eGFP and mCherry expression.

In addition, a further set of transductions (Round 2) was performed where BMSC-*Luc2/CDUPRT* were cultured for a period of 2 weeks in complete high glucose DMEM (-bFGF) containing 200µg/ml Hygromycin B, followed by transduction with lentiviral vectors as described above. This was setup to observe the effect of high glucose and the absence of a fibroblast-stimulating growth factor on the differentiation of transduced BMSC-*Luc2/CDUPRT*. Further to this, BMSC-*Luc2/CDUPRT* and BMSC-*Luc2/CDUPRT-INS-FUR* were transduced with HMD-*Pdx1* (Round 3) (in complete α-MEM containing 200µg/ml

Hygromycin B and 8µg/ml Polybrene) as a consequence of the results obtained following the overexpression of *INS-FUR* and *NeuroD1* in BMSC-*Luc2/CDUPRT*.

5.1.5.2 FACS analysis and sorting of transduced BMSC-Luc2/CDUPRT

Transduced and untransduced (negative control) cells were cultured for 1 week post-transduction as described in Section 2.1. During this period, the media was changed and replenished twice to remove any remaining viral particles. On the day of FACS sorting, the transduced cells were washed twice with 1x HBSS, detached and resuspended in 1ml of cold 1x HBSS + 5% FCS. The cells were transferred to individual 5mL Round Bottom Polystyrene Test Tubes with Cell Strainer Snap Caps to dissociate cell aggregates, and the strainer caps subsequently replaced with regular round bottom polystyrene tube caps for transport to the Advanced Cytometry Facility (Centenary Institute, Sydney, Australia). $eGFP^+$ cells transduced with HMD, HMD-*INS-FUR*, HMD-*INS-FUR/NeuroD1* and HMD-*NeuroD1* were FACS sorted on the BD FACSAria™ II into 5mL Round Bottom Polystyrene Test Tubes containing 1ml of FCS. The tubes were kept on ice and a 100µl sample of each sorted $eGFP^+$ population was assessed for purity post sorting. The sorted $eGFP^+$ populations of cells were denoted as BMSC-*Luc2/CDUPRT-HMD*, BMSC-*Luc2/CDUPRT-INS-FUR*, BMSC-*Luc2/CDUPRT-INS-FUR/NeuroD1* and BMSC-*Luc2/CDUPRT-NeuroD1*.

$mCherry^+$ cells were sorted on the BD Influx™ into 5mL Round Bottom Polystyrene Test Tubes containing 1ml of FCS. The tubes were kept on ice and a 100µl sample of each sorted $mCherry^+$ population was assessed for purity post sorting. The sorted $mCherry^+$ populations of cells were denoted as BMSC-*Luc2/CDUPRT-Pdx1*. In addition, BMSC-*Luc2/CDUPRT-INS-FUR* cells that were transduced with HMD-*Pdx1* were sorted on the BD Influx™ as dual $eGFP^+/mCherry^+$ and were denoted as BMSC-*Luc2/CDUPRT-INS-FUR-Pdx1*.

5.1.5.3 Cell culture of transduced cells post-sorting

Post-sorting, half the volume of each sorted cell population that were transduced in complete α-MEM containing 200µg/ml Hygromycin B during Round 1 were returned to culture in individual T25cm2 flasks and maintained in complete α-MEM containing 200µg/ml Hygromycin B as described in Section 2.1, and the other half were maintained in complete high glucose DMEM (-bFGF) containing 200µg/ml Hygromycin B for a period of 4 weeks. Cells that were transduced in complete high glucose DMEM (-bFGF) containing 200µg/ml Hygromycin B during Round 2 and sorted as described in Section 5.1.5.3 were returned to culture in high glucose DMEM (-bFGF) containing 200µg/ml Hygromycin B for a period of 4 weeks. Cells that were transduced during Round 3 in complete α-MEM containing 200µg/ml Hygromycin B were returned to culture in complete α-MEM containing 200µg/ml Hygromycin B for a period of 4 weeks.

5.1.5.4 Cell proliferation assays

Cell proliferation assays were setup for each population of transduced cells as described in Sections 2.2.

5.1.6 Analysis of β-cell differentiation

5.1.6.1 Microscopic evaluation of morphological changes in transduced BMSC-Luc2/CDUPRT

Transduced and untransduced BMSC-*Luc2/CDUPRT* cells were assessed at 28 days post-transduction via light microscopy for observable morphological changes associated with β-cell differentiation. Images were acquired using a Leica© DM microscope (Leica

Microsystems©) and processed using image processing software Leica Application Suite (V4.4.0) (Leica Microsystems©).

5.1.6.2 Gene expression profiling of transduced BMSC-Luc2/CDUPRT

Gene expression profiling of transduced and untransduced BMSC-*Luc2/CDUPRT* was performed as described in Section 2.6. Specifically, RNA was extracted from transduced and untransduced cells at 28 days post-transduction, and utilised to generate cDNA for subsequent RT-PCR. The list of endogenous pancreatic genes assessed and the primers utilised are outlined in Table 3.3. In addition, specific primers were designed for the detection of the ectopically expressed *NeuroD1-T2A-eGFP* and codon-optimised *Pdx1* as outlined below. RT-PCR for *NeuroD1-T2A-eGFP* and codon-optimised *Pdx1* RT-PCR was run at 58ºC and 60ºC respectively for 40 cycles, and generated 1081bp and 180bp respectively.

- *NeuroD1-T2A-eGFP* Forward: 5` TCAACCCTCGGACTTTCTTG 3`
- *NeuroD1-T2A-eGFP* Reverse: 5` ATGTTGTGGCGGATCTTGAAG 3`
- Codon-optimised *Pdx1* Forward: 5` CCCCCACAGTTCACATCTAGC 3`
- Codon-optimised *Pdx1* Reverse: 5` CTCTGTGCCGTTAGGGAATG 3`

5.1.6.3 In vitro chronic insulin secretion assay

To assess the ability of transduced BMSC-*Luc2/CDUPRT* to secrete *INS-FUR*, a 24-hour chronic insulin secretion assay was established. To determine the optimal concentration of cells required, $5x10^4$, $1x10^5$ and $5x10^5$ BMSC-*Luc2/CDUPRT-INS-FUR* cells/ml were resuspended in complete α-MEM containing 200µg/ml Hygromycin B, and 1ml of each concentration was seeded in duplicate in a 6-well plate and incubated for 24 hours at 37ºC/5% CO_2. The following day (post 24hours) the medium was harvested from each well,

transferred to a 1.5ml microfuge tube and stored at -20°C until the insulin concentration of the samples was analysed.

Following determination of the optimal seeding concentration of cells, the assay was repeated as above by seeding $1x10^5$ cells/well of BMSC-*Luc2/CDUPRT*, BMSC-*Luc2/CDUPRT-INS-FUR*, BMSC-*Luc2/CDUPRT-INS-FUR/NeuroD1*, BMSC-*Luc2/CDUPRT-NeuroD1*, BMSC-*Luc2/CDPRT-Pdx1* and BMSC-*Luc2/CDUPRT-INS-FUR-Pdx1* in triplicate (n=4). The insulin concentration of the harvested samples was assessed as described in Section 2.7.

5.1.6.4 In vitro acute stimulation insulin secretion assay

BMSC-*Luc2/CDUPRT* transduced to express *INS-FUR* and *NeuroD1* were assessed for their ability to secrete insulin in response to acute glucose stimulation. Untransduced BMSC-*Luc2/CDUPRT* cells were assessed as a negative control. Cells were seeded in complete α-MEM containing 200µg/ml Hygromycin B at a concentration of $1x10^5$ cells/well in triplicate of a 6 well-plate (n=3). Following cell attachment (~4-6 hours), the cells were washed twice with basal medium (0.14M NaCl, 2.7mM KCl, 1.5mM KH_2PO_4, 10mM Na_2PO_4, 0.9mM $CaCl_2$, 0.5mM $MgCl_2$, 27mM $NaHCO_3$, 20mM N-(2-hydroxyethyl) piperazine-N'-(2-ethanesulphonic acid) HEPES, 2g/L BSA and 1.5mM D-Glucose, pH 7.4). The cells were subsequently incubated with 1ml of basal medium for two sequential periods of 1 hour at 37°C/5% CO_2. After each hour the medium was collected (labelled basal 1 and basal 2) and replenished, allowing for a basal level of insulin secretion to be established. The cells were subsequently stimulated with basal media containing 20mM D-Glucose for 1 hour and the medium collected and labelled "stimulation". A final basal incubation (basal 3) was performed to determine if insulin secretion returned to basal levels following the removing of the glucose stimulus. The samples were transferred to 1.5ml microfuge tubes and stored at -20°C until the insulin concentration was analysed as described in Section 2.7.

5.1.6.5 Quantification of insulin storage within secretory granules

BMSC-*Luc2/CDUPRT* transduced to express *INS-FUR* and *NeuroD1* were assessed for their ability to store insulin within storage granules. Untransduced BMSC-*Luc2/CDUPRT* cells were assessed as a negative control. Cells were grown in T175 flasks in α-MEM containing 200µg/ml Hygromycin B at 37ºC/5% CO_2. Insulin storage was subsequently determined following a 48-hour insulin extraction of $1x10^6$ cells (n=4) per cell population. Briefly, $1x10^6$ cells were resuspended in 400µl of acid/ethanol (0.18M HCl in 70% ethanol) for 48 hours at 4ºC. Insulin content was thereafter quantified as described in Section 2.7.

5.1.7 Generation of BMSC-*Luc2/CDUPRT-INS-FUR* spheroids

5.1.7.1 Spheroid cell culture

Mid-passage (P15-30) parental BMSC-*Luc2/CDUPRT*, BMSC-*Luc2/CDUPRT-HMD* and BMSC-*Luc2/CDUPRT-INS-FUR* were expanded in culture as described in Section 2.1. To induce aggregation the cells were washed twice with 1x HBSS, detached and resuspended to a concentration of $1x10^6$ cells/ml in serum-free DMEM/F12 (17.5mM D-glucose, 1% BSA, 1% 100x insulin-transferrin-selenium and 1% 100x P/S). $1x10^6$ cells were seeded in a well of a Corning™ Cellstar™ Ultra-low attachment 6-well plate (Sigma-Aldrich©) and incubated overnight at 37ºC/5% CO_2. Light and fluorescent images of spheroids were acquired 16-24 hours post seeding using a Leica© DM microscope (Leica Microsystems©) and processed using image processing software Leica Application Suite (V4.4.0) (Leica Microsystems©).

5.1.7.2 Time-lapse microscopy

Mid-passage (P15-30) BMSC-*Luc2/CDUPRT-INS-FUR* were seeded in a well of a Corning™ Cellstar™ Ultra-low attachment 6-well plate as described in Section 5.1.7.1. Prior to the

commencement of the time-lapse imaging, the spheroids were incubated with ReadyProbes® Cell Viability Imaging Kit, Blue/Red (Thermofisher©). Briefly, NucBlue® Live reagent and propidium iodide (PI) were added to freshly seeded cells at a concentration of 2 drops/ml of media. The 6-well plate was subsequently transferred to the incubation chamber of a Nikon A1 confocal microscope (Nikon©) maintained at 37ºC/5% CO_2 for 16 hours, during which time light and fluorescent images were obtained at 30 min intervals. Fluorescent images of nuclei, *INS-FUR*-expressing BMSCs and dead cells were captured using DAPI, GFP and Texas Red filters respectively. Acquired images were processed and analysed on NIS-Elements Advanced Research (Nikon©) software.

5.1.8 Reversal of diabetes in STZ-diabetic NOD/*Scid* mice

5.1.8.1 Sourcing of animals

Twenty-five female NOD/*Scid* mice at six weeks of age (19-23g) were sourced from the Animal Resources Centre (WA, Australia). They were housed within the Ernst Facility at UTS in a polycarbonate green line IVC system, with corncob bedding, irradiated rat and mouse feed (Gordon's Specialty Stock Feeds) and unlimited RO water. All bedding and housing equipment was autoclaved prior to use. The temperature and humidity of the animal rooms was maintained within 22-24ºC and 40-60% respectively. A maximum of five animals were housed per cage and monitored daily by the Ernst Facility technicians until they were required for experimental work, after which animals were monitored daily by the researcher and Ernst Facility technicians.

All animal work was approved by the UTS Animal Care and Ethics Committee (ACEC 2011-447A; ACEC 2009-244A) and complied with the Australian code for the care and use of animals for scientific purposes[328].

5.1.8.2 Preparation of STZ for diabetes induction

Acetate buffer was prepared by diluting 17.4M glacial acetic acid to 0.1M (pH 5.2) with dH_2O to a final volume of 100ml. Sodium acetate anhydrous (166mg) was dissolved in 0.1M (pH 5.2) glacial acetic acid and filtered through a 0.2µM Minisart® syringe filter (Merk-Millipore©). Acetate buffer was subsequently stored in 5ml aliquots at -20°C until required for preparation of STZ solution, which was performed on the day of diabetes induction.

On the day of diabetes induction, a 5ml aliquot of acetate buffer was thawed and a 20mg/ml solution of STZ was prepared by dissolving 80mg of STZ (Alexis® Biochemicals) in 4ml acetate buffer. The STZ solution was filtered through a 0.2µM Minisart® syringe filter and kept on ice until injection into NOD/*Scid* mice for diabetes induction.

5.1.8.3 STZ induction of diabetes in NOD/Scid mice

On the day of diabetes induction, eighteen NOD/*Scid* mice had body weights and blood glucose concentration measured prior to injection of STZ solution. Body weight measurements were utilised to determine the volume of STZ solution to administer per animal, with each animal receiving 170mg/kg of STZ solution (20mg/ml) via intraperitoneal injection using a 0.5ml Ultra-Fine Insulin Syringe (BD Medical®) and 26 Gauge PrecisionGlide™ needle. All animals, including non-diabetic controls, had their body weight and blood glucose concentration measured daily thereafter to monitor for the development of hyperglycaemia. Animals that did not develop hyperglycaemia (blood glucose concentration >8mmol/L) within 1-week post STZ-injection received a second low dose (40mg/kg) STZ-injection to induce diabetes. Only animals that displayed hyperglycaemia (blood glucose concentration >8mmol/L) for a period of four consecutive days were considered diabetic and utilised in *in vivo* experiments.

5.1.8.4 In vivo transplantation of BMSC-Luc2/CDUPRT-INS-FUR in STZ-diabetic NOD/Scid mice

Late passage (P40-60) BMSC-*Luc2/CDUPRT-INS-FUR* cells were expanded in culture as described in Section 2.1 to a total of 50 x T175 flasks for *in vivo* cell transplantation. On the day of cell transplantation, the cells were washed twice with 1x HBSS, detached and assessed for viability via Trypan Blue (0.4%) exclusion. A viability of >90% was established as the minimum cut-off for progressing with cell transplantation. The cells were subsequently resuspended in 1x HBSS + 5% FCS to a concentration of $1x10^8$ cells/ml and maintained on ice until injections were performed.

Animals were divided into 4 groups (n=6) as outlined below:

1. Non-diabetic control (NOD/*Scid*)
2. Treated Diabetic (STZ-NOD/*Scid*) + $1x10^7$ BMSC-*Luc2/CDUPRT-INS-FUR*
3. Treated Diabetic (STZ-NOD/*Scid*) + $5x10^7$ BMSC-*Luc2/CDUPRT-INS-FUR*
4. Diabetic control (STZ-NOD/*Scid*)

Using 0.5ml Ultra-Fine Insulin Syringe (BD Medical®) and 23 Gauge PrecisionGlide™ needle, treated diabetic STZ-NOD/*Scid* mice received a single subcutaneous injection of BMSC-*Luc2/CDUPRT-INS-FUR* on the cervical posterior. The animals were returned to IVC cages according to their respective groups, with body weight and blood glucose concentration measurements obtained daily using a glucometer (Accu-Chek® Performa). Animals that displayed hypoglycaemia (blood glucose concentration <3mmol/L) or body weight loss (>10%) for two consecutive days were euthanised by CO_2 asphyxiation and cervical dislocation.

5.1.8.5 Intraperitoneal glucose tolerance test (IPGTT)

At 4 weeks post BMSC-*Luc2/CDUPRT-INS-FUR* transplantation, animals were fasted for a period of 6 hours with access to RO water. Following fasting, the animals' body weights were measured to determine the required volume of 50% liquid glucose (0.5g/ml) to administer per animal (2g/kg). The animals were transferred to a ZDS Qube Manifold 5 Station (Advanced Anesthesia Specialists®) and maintained under stable anaesthesia, with delivery of Isoflurane (VCA®) and O_2 throughout the procedure maintained at 2.5 L/min Isoflurane and 1.5 L/min O_2. Using 0.5ml Ultra-Fine Insulin Syringe (BD Medical®) and 26 Gauge PrecisionGlide™ needle, the mice received an intraperitoneal injection of 2g/kg 50% liquid glucose (0.5g/ml). The animals blood glucose concentrations were measured at t=0 and t=5, 15, 30, 60, 90 post injection. Following the IPGTT, the animals were euthanised by CO_2 asphyxiation and cervical dislocation, which coincided with the 4-week experimental endpoint.

5.2 Results

5.2.1 Generation of the HMD-*INS-FUR/NeuroD1* and HMD-*NeuroD1* lentiviral plasmids

The generation of the HMD-*NeuroD1* and HMD-*INS-FUR-NeuroD1* lentiviral plasmids was performed according to the cloning strategy outlined in Figure 5.5.

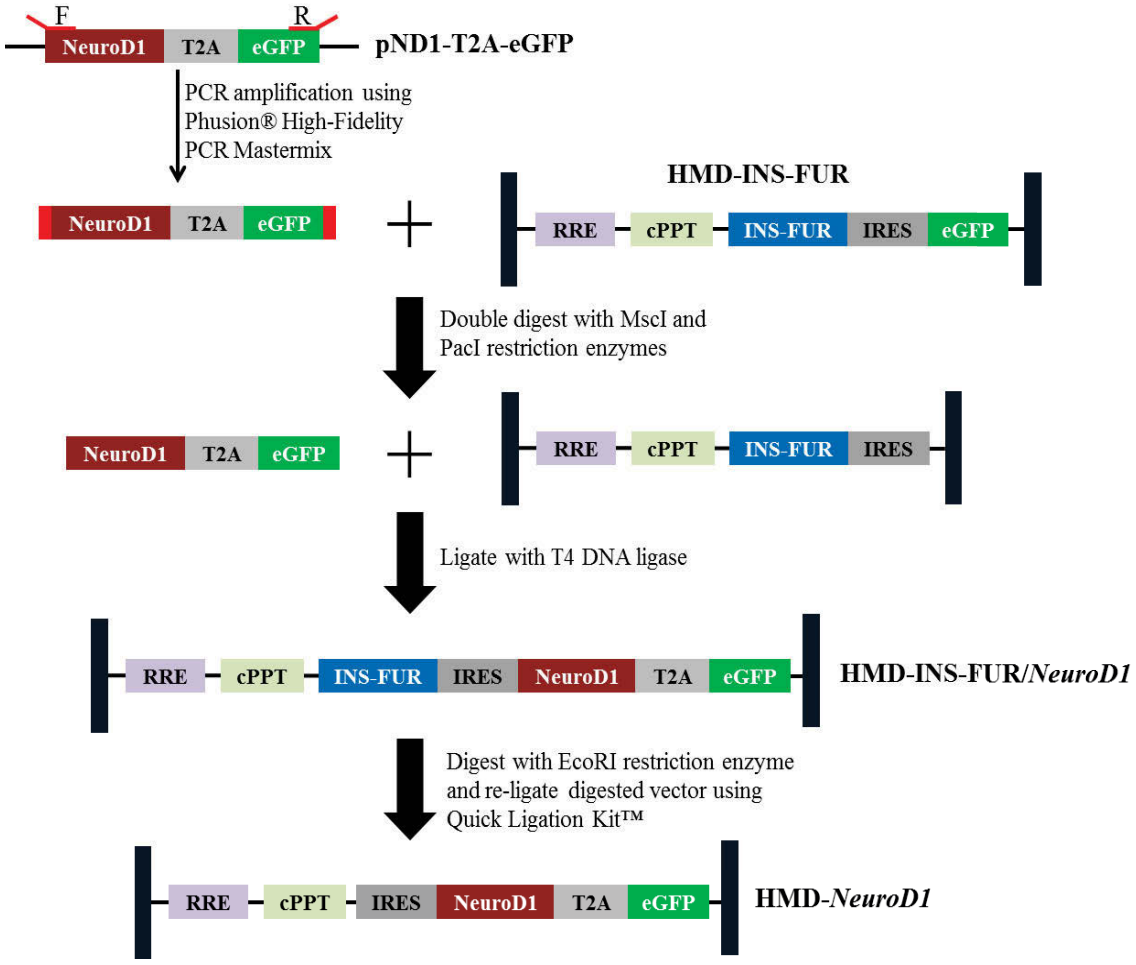

Figure 5.5: Cloning strategy for the generation of the HMD-*NeuroD1* and HMD-*INS-FUR-NeuroD1* lentiviral plasmids The *NeuroD1-T2A-eGFP* sequence PCR amplified from the pND1-T2A-eGFP and the HMD-*INS-FUR* plasmid were digested with MscI and PacI restriction enzymes. Ligation of the *NeuroD1-T2A-eGFP* sequence in the HMD-*INS-FUR* plasmid resulted in the generation of the HMD-*INS-FUR/NeuroD1* plasmid. The *INS-FUR* sequence was subsequently excised from the HMD-*INS-FUR/NeuroD1* plasmid and re-ligated to generate HMD-*NeuroD1*.

In order to clone the *NeuroD1-T2A-eGFP* sequence into the HMD-*INS-FUR* lentiviral plasmid, the *NeuroD1-T2A-eGFP* sequence was PCR amplified from the pND1-T2A-eGFP plasmid and digested with MscI and PacI restriction enzymes, the products of which were run on a 0.7% (w/v) agarose gel (Figure 5.6, Lane 2). The destination vector (HMD-*INS-FUR*) was similarly digested with MscI and PacI restriction enzymes, the products of which were run on a 0.7% (w/v) agarose gel (Figure 5.6, Lane 3). As can be seen from Figure 5.6, a single product of ~1900bp corresponding to the *NeuroD1-T2A-eGFP* fragment was amplified and successfully digested. The DNA staining intensity of the *NeuroD1-T2A-eGFP* fragment reflects the multiple PCR reactions that were run to increase the quantity of PCR amplified starting material for subsequent restriction digest. Following the digest of HMD-*INS-FUR* with MscI/PacI, fragments of ~780bp and ~9000bp were released, corresponding to the existing eGFP sequence and the remaining HMD-*INS-FUR* backbone. The gel purified *NeuroD1-T2A-eGFP* fragment and the HMD-*INS-FUR* backbone were subsequently run on a 1% (w/v) agarose gel to confirm the purity of the fragment extraction (Figure 5.7). The concentrations of purified *NeuroD1-T2A-eGFP* and HMD-*INS-FUR* backbone were ~800ng/µl and 500ng/µl respectively as quantified by NanoDrop™ 2000 spectrophotometry.

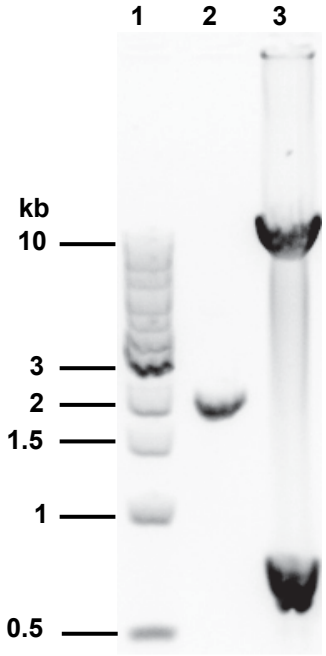

Figure 5.6: MscI/PacI restriction digest of *NeuroD1-T2A-eGFP* and HMD-*INS-FUR* *NeuroD1-T2A-eGFP* was PCR amplified from pND1-T2A-eGFP and digested with MscI/PacI, whilst HMD-*INS-FUR* plasmid was digested with MscI/PacI. Both were run on a 0.7% (w/v) agarose gel. Lane 1: 1kb DNA ladder (NEB), Lane 2: *NeuroD1-T2A-eGFP* (MscI/PacI digested), Lane 3: HMD-*INS-FUR* (MscI/PacI digested). All gels contained 0.5% (v/v) GelRed™ and were run at 90V for 90 min. The gel images were captured using an InGenius3® UV transilluminator.

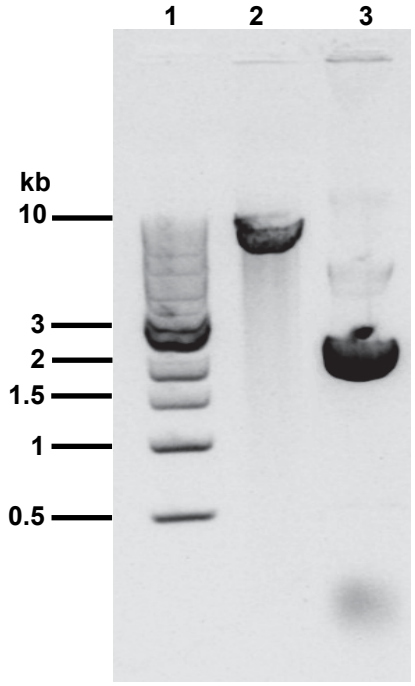

Figure 5.7: Gel extraction of MscI/PacI digested fragments The fragments corresponding to the HMD-*INS-FUR* (MscI/PacI cut) and the *NeuroD1-T2A-eGFP* sequence were gel purified and re-run on a 1% (w/v) agarose gel containing 0.05% GelRed™ at 90V for 90 min. The gel image was captured using an InGenius3® UV transilluminator. Lane 1: 1kb DNA ladder (NEB®), Lane 2: HMD-*INS-FUR* backbone (MscI/PacI cut), Lane 3: *NeuroD1-T2A-eGFP*.

The purified and dephosphorylated HMD-*INS-FUR* backbone (MscI/PacI cut) and *NeuroD1-T2A-eGFP* sequence were subsequently ligated as described in Section 5.1.1.4 and Figure 5.5. The ligation products were diluted 1 in 2 with dH_2O, transformed into One Shot® Stbl3 TOP10 *E. coli* and selected for antibiotic resistance on Ampicillin containing LB agar plates. Of the three insert:backbone molar ratios assessed during ligation, the molar ratios of 3:1 and 6:1 resulted in six and five colonies respectively, all of which expressed eGFP when assessed by fluorescence microscopy (data not shown). No colonies developed from the 10:1 ligation transformation, whilst one colony was observed on the negative control plate. Transformation with uncut HMD-*INS-FUR* resulted in >100 colonies.

To assess the success of *NeuroD1-T2A-eGFP* ligation into the HMD-*INS-FUR* plasmid, the eleven bacterial colonies that resulted from selective LB-agar growth were re-streaked onto new selective LB-agar plates to confirm true antibiotic resistance, of which all successfully developed clonal bacterial spread plates. A single colony from each clonal spread plate was grown overnight in selective LB media containing Ampicillin, and plasmid DNA subsequently isolated from all putative HMD-*INS-FUR/NeuroD1* clones. A diagnostic digest with MscI and PacI was performed to confirm successful ligation of the *NeuroD1-T2A-eGFP* sequence into the HMD-*INS-FUR* plasmid (Figure 5.8). As can be seen in Figure 5.8, seven of the eleven putative clones were positive for the incorporation of the *NeuroD1-T2A-eGFP* sequence. HMD-*INS-FUR/NeuroD1* clone 1 (Figure 5.8, Lane 2) was utilised for the subsequent generation of the HMD-*NeuroD1* plasmid and for lentiviral packaging.

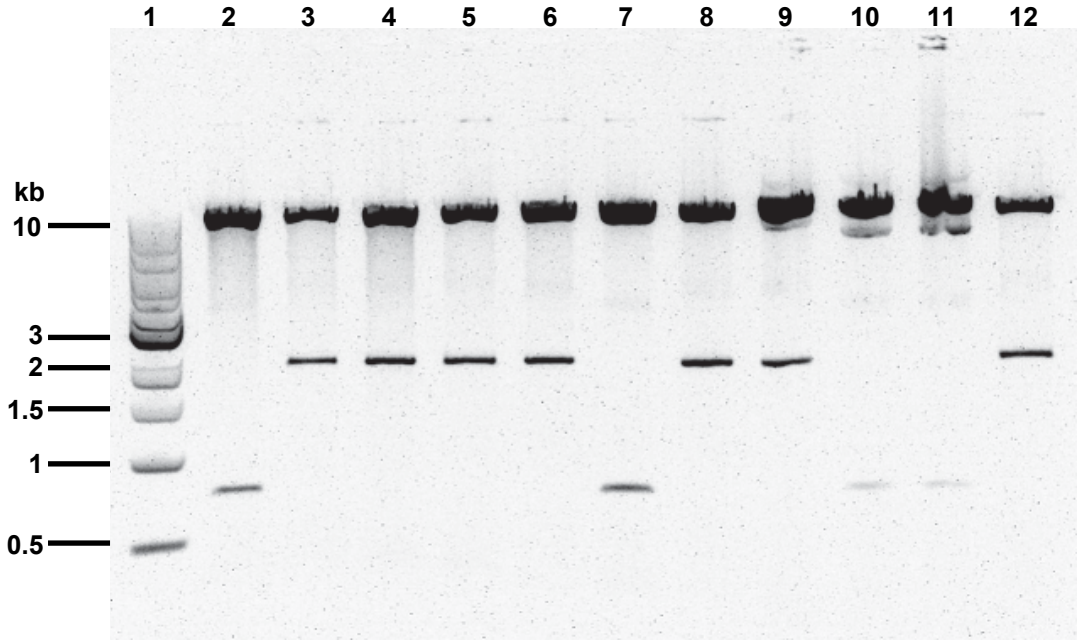

Figure 5.8: Diagnostic digest of putative HMD-*INS-FUR/NeuroD1* lentiviral plasmids Eleven putative HMD-*INS-FUR/NeuroD1* lentiviral plasmids were isolated from their respective overnight bacterial cultures and subsequently digested with MscI and PacI, and the products run on a 0.7% (w/v) agarose gel containing 0.5% (v/v) GelRed™ at 90V for 90 min. The gel image was captured using an InGenius3® UV transilluminator. Lane 1: 1kb DNA ladder (NEB), Lanes 2-12: Putative HMD-*INS-FUR/NeuroD1* clones #1-11 (MscI/PacI cut).

The *INS-FUR* sequence was subsequently excised from the HMD-*INS-FUR/NeuroD1* lentiviral plasmid following digestion with EcoRI-HF as outlined in Figure 5.5, the products of which were run on a 0.7% (w/v) agarose gel (Figure 5.9A). As can be seen from Figure 5.9A, fragments of ~400bp and ~10.8kb were observed corresponding to the *INS-FUR* gene and the HMD-*INS-FUR/NeuroD1* digested backbone. The digested HMD-*INS-FUR/NeuroD1* backbone was gel purified and re-ligated using the Quick Ligation Kit™. The ligation products were diluted 1 in 2 with dH_2O, transformed into One Shot® Stbl3 TOP10 *E. coli* and selected for antibiotic resistance on Ampicillin containing LB agar plates, from which >100 colonies were obtained.

To assess the success of HMD-*NeuroD1* re-ligation, five bacterial colonies that resulted from selective LB-agar growth were re-streaked onto new selective LB-agar plates to confirm true antibiotic resistance, of which all successfully developed clonal bacterial spread plates. A single colony from each clonal spread plate was grown overnight in selective LB media containing Ampicilin, and plasmid DNA subsequently isolated from all putative HMD-*NeuroD1* clones. A diagnostic digest with EcoRI-HF was performed to confirm successful re-ligation of the HMD-*NeuroD1* plasmid (Figure 5.9B). As can be seen in Figure 5.9B, all of the putative HMD-*NeuroD1* plasmids did not release the *INS-FUR* gene of ~400bp as would be expected if the HMD-*NeuroD1* backbone was successfully re-ligated. HMD-*NeuroD1* clone 1 (Figure 5.9B, Lane 2) was utilised for subsequent lentiviral packaging. The successfully generated HMD-*INS-FUR/NeuroD1* and HMD-*NeuroD1* lentiviral plasmid schematics are represented in Figure 5.10 and 5.11 respectively.

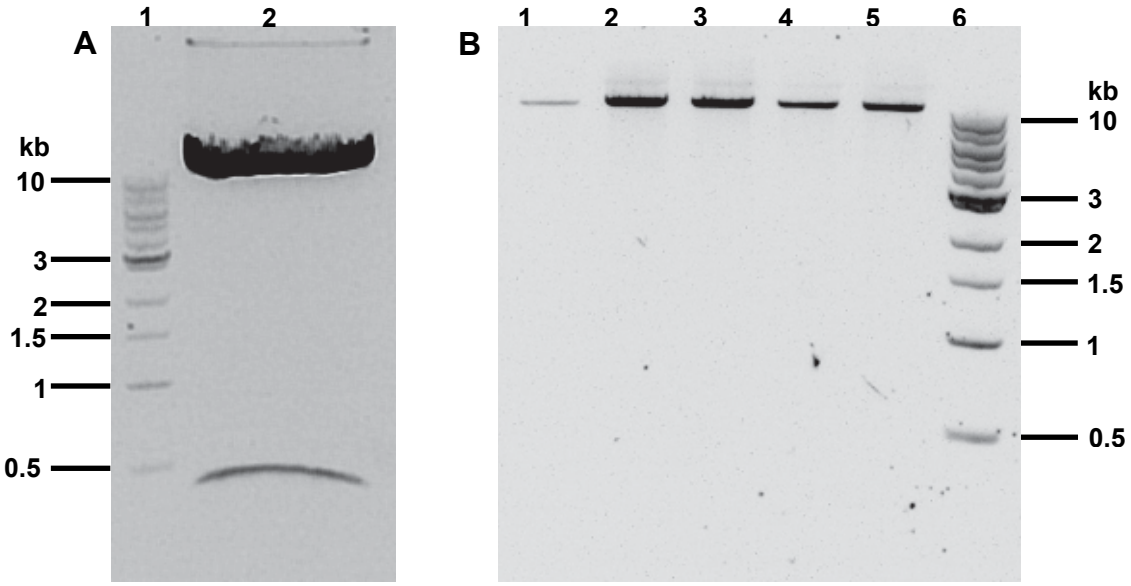

Figure 5.9: EcoRI-HF restriction digest of HMD-*INS-FUR/NeuroD1* and diagnostic digest of putative HMD-*NeuroD1* lentiviral plasmids (A) EcoRI-HF digest of HMD-*INS-FUR/NeuroD1* run on a 0.7% (w/v) agarose gel. Lane 1: 1kb DNA ladder (NEB), Lane 2: HMD-*INS-FUR/NeuroD1* (EcoRI-HF digested). (B) Diagnostic digest of putative HMD-NeuroD1 lentiviral plasmid clones run on a 0.7% (w/v) agarose gel. Lane 1-5: Putative HMD-NeuroD1 clones #1-5 (EcoRI-HF digested), Lane 6: 1kb DNA ladder (NEB). All gels contained 0.5% (v/v) GelRed™ and were run at 90V for 90 min. The gel images were captured using an InGenius3® UV transilluminator.

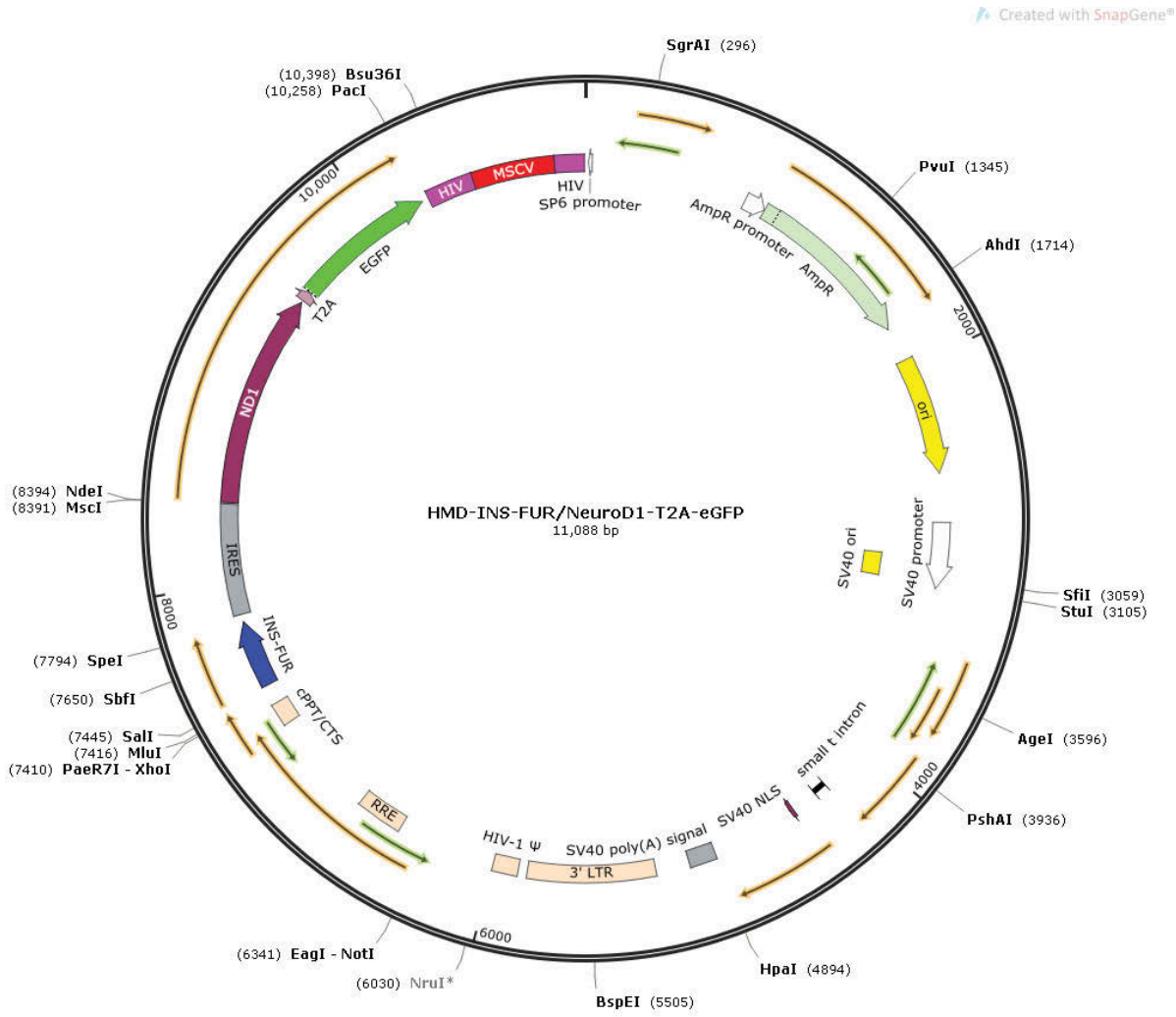

Figure 5.10: Diagrammatic representation of the HMD-*INS-FUR/NeuroD1* lentiviral plasmid *NeuroD1-T2A-eGFP* was cloned downstream of the IRES to replace eGFP. The IRES allows for co-expression of two genes of interest upstream (*INS-FUR*) and downstream (*NeuroD1-T2A-eGFP*). The eGFP fluorescent reporter is co-expressed with *NeuroD1* as a consequence of the T2A peptide which allows for two genes to be expressed from a single mRNA.

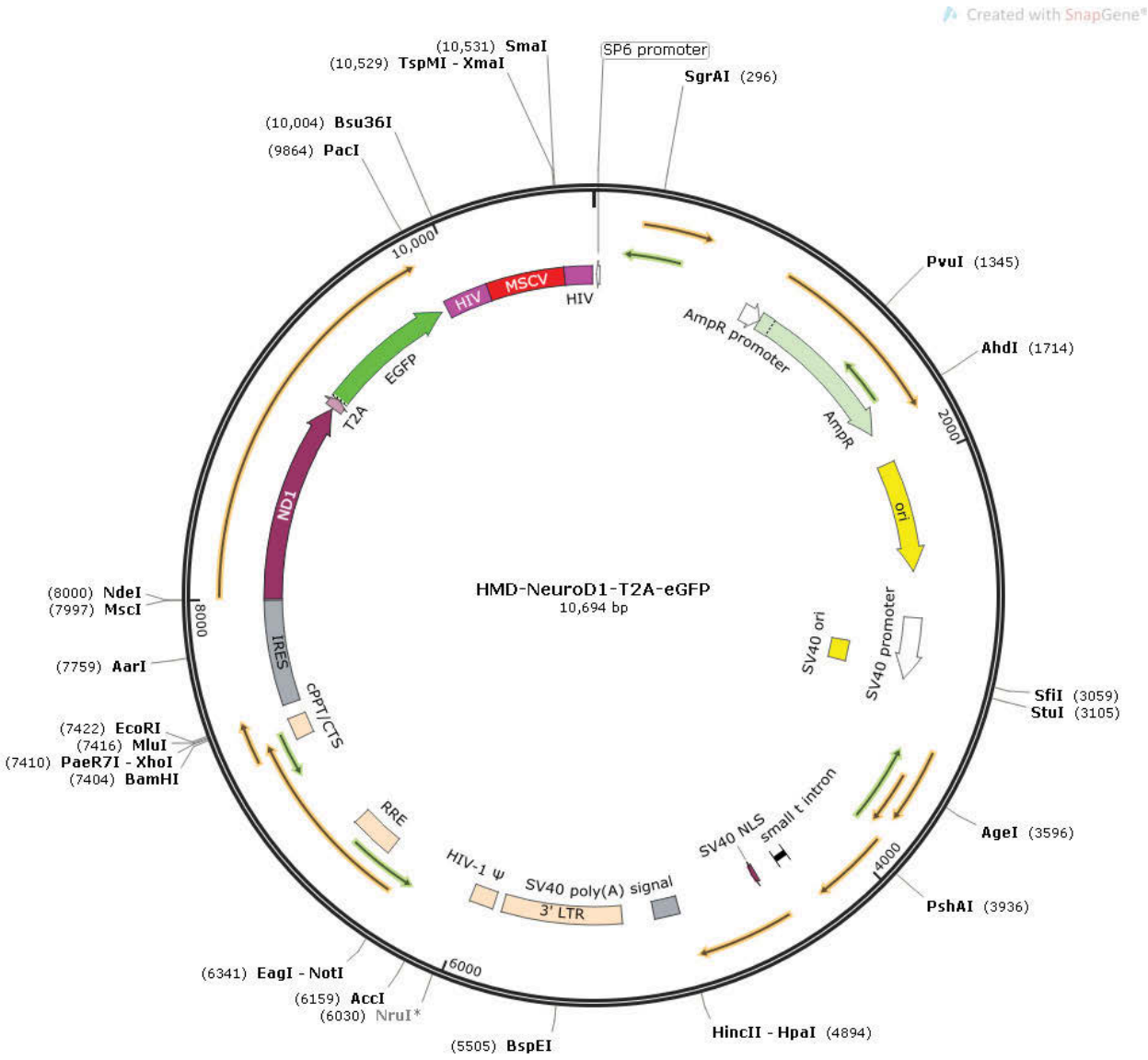

Figure 5.11: Diagrammatic representation of the HMD-*NeuroD1* lentiviral plasmid The *INS-FUR* gene was excised from the HMD-*INS-FUR/NeuroD1* lentiviral plasmid, and the resulting backbone re-ligated to generate HMD-*NeuroD1*. The eGFP fluorescent reporter is co-expressed with *NeuroD1* as a consequence of the T2A peptide which allows for two genes to be expressed from a single mRNA.

5.2.2 Generation of the HMD-*Pdx1* lentiviral plasmid

The generation of HMD-*Pdx1* was performed according to the schematic illustrated in Figure 5.12, where the existing IRES-eGFP sequence of the HMD lentiviral plasmid was excised and replaced with the *Pdx1-IRES-mCherry* sequence from the AAV-*Pdx1* plasmid.

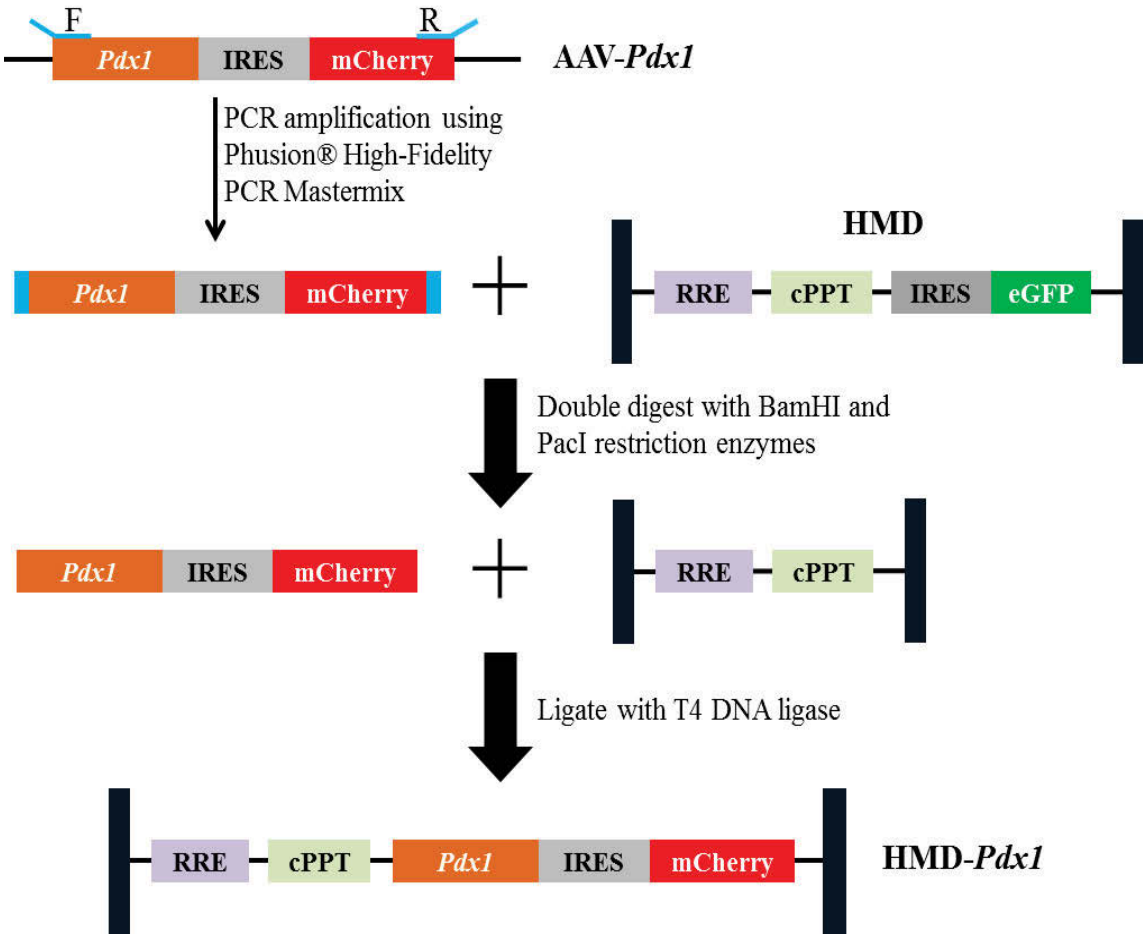

Figure 5.12: Cloning strategy for the generation of the HMD-*Pdx1* lentiviral plasmid The *Pdx1-IRES-mCherry* sequence PCR amplified from the AAV-Pdx1 plasmid and the HMD lentiviral plasmid were digested with BamHI-HF and PacI restriction enzymes. Ligation of the *Pdx1-IRES-mCherry* sequence in the HMD plasmid resulted in the generation of the HMD-*Pdx1* lentiviral plasmid.

In order to clone the *Pdx1-IRES-mCherry* sequence into the HMD lentiviral plasmid, the *Pdx1-IRES-mCherry* sequence was PCR amplified from the AAV-*Pdx1* plasmid and digested with BamHI-HF and PacI restriction enzymes, the products of which were run on a 0.7% (w/v) agarose gel (Figure 5.13, Lane 2). The destination vector (HMD) was similarly digested with BamHI-HF and PacI restriction enzymes, the products of which were run on a 0.7% (w/v) agarose gel (Figure 5.13, Lane 3). As can be seen from Figure 5.13, a single product of ~2000bp corresponding to the *Pdx1-IRES-mCherry* fragment was amplified and successfully digested. The U-shaped band formation of the *Pdx1-IRES-mCherry* fragment was an artifact of gel overloading. Following the digest of HMD with BamHI-HF/PacI, fragments of ~1300bp and ~8700bp were released, corresponding to the existing IRES-eGFP sequence and the remaining HMD backbone. The concentration of the purified *Pdx1-IRES-mCHerry* fragment and the HMD backbone were ~600ng/µl and 500ng/µl respectively as quantified by NanoDrop™ 2000 spectrophotometry.

The purified and dephosphorylated HMD backbone (BamHI-HF/PacI cut) and *Pdx1-IRES-mCherry* sequence were subsequently ligated as described in Section 5.1.2.3 and Figure 5.12. The ligation products were diluted 1 in 2 with dH_2O, transformed into One Shot® Stbl3 TOP10 *E. coli* and selected for antibiotic resistance on Ampicillin containing LB agar plates. Of the three insert:backbone molar ratios assessed during ligation, the molar ratio of 3:1 resulted in three colonies, of which two expressed mCherry and one eGFP when assessed by fluorescence microscopy (data not shown). No colonies developed from the 6:1, 10:1 and negative control ligation transformations. Transformation with uncut HMD resulted in >100 colonies.

To re-confirm the success of *Pdx1-IRES-mCherry* ligation into the HMD plasmid, the two mCherry-expressing colonies were re-streaked onto new selective LB-agar plates to confirm

true antibiotic resistance, both of which successfully developed clonal bacterial spread plates. A single colony from each clonal spread plate was grown overnight in selective LB media containing Ampicillin, and plasmid DNA subsequently isolated from all putative HMD-*Pdx1* clones. A diagnostic digest with BamHI-HF and PacI was performed to confirm successful ligation (Figure 5.14). As can be seen in Figure 5.14, the two putative colonies were positive for the incorporation of the *Pdx1-IRES-mCherry* sequence. HMD-*Pdx1* clone 1 (Figure 5.14, Lane 2) was utilised for the subsequent generation of the HMD-*Pdx1* plasmid and for lentiviral packaging. The successfully generated HMD-*Pdx1* schematic is represented in Figure 5.15.

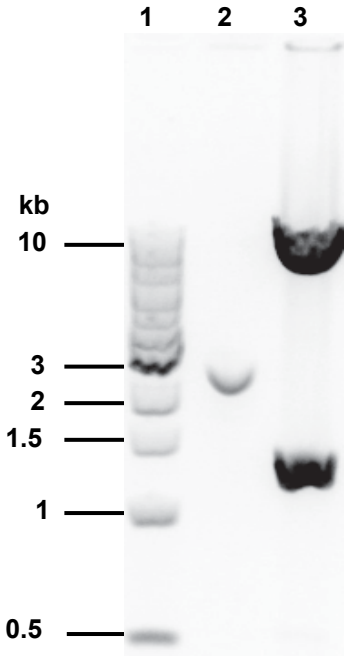

Figure 5.13: BamHI-HF/PacI restriction digest of *Pdx1-IRES-mCherry* and HMD *Pdx1-IRES-mCherry* was PCR amplified from AAV-*Pdx1* and digested with BamHI-HF/PacI. HMD was similarly digested. Both were run on a 0.7% (w/v) agarose gel. Lane 1: 1kb DNA ladder (NEB), Lane 2: *Pdx1-IRES-mCherry* (BamHI-HF/PacI digested), Lane 3: HMD (BamHI-HF/PacI digested). All gels contained 0.5% (v/v) GelRed™ and were run at 90V for 90 min. The gel images were captured using an InGenius3® UV transilluminator.

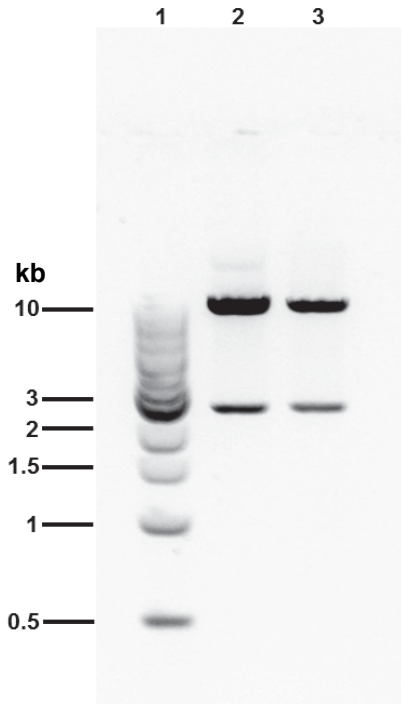

Figure 5.14: Diagnostic digest of putative HMD-*Pdx1* lentiviral plasmids Two putative HMD-*Pdx1* lentiviral plasmids were isolated from their respective overnight bacterial cultures and subsequently digested with BamHI-HF and PacI, and the products run on a 0.7% (w/v) agarose gel containing 0.5% (v/v) GelRed™ at 90V for 90 min. The gel image was captured using an InGenius3® UV transilluminator. Lane 1: 1kb DNA ladder (NEB), Lanes 2-3: Putative HMD-*Pdx1* clones #1-2 (BamHI-HF/PacI cut).

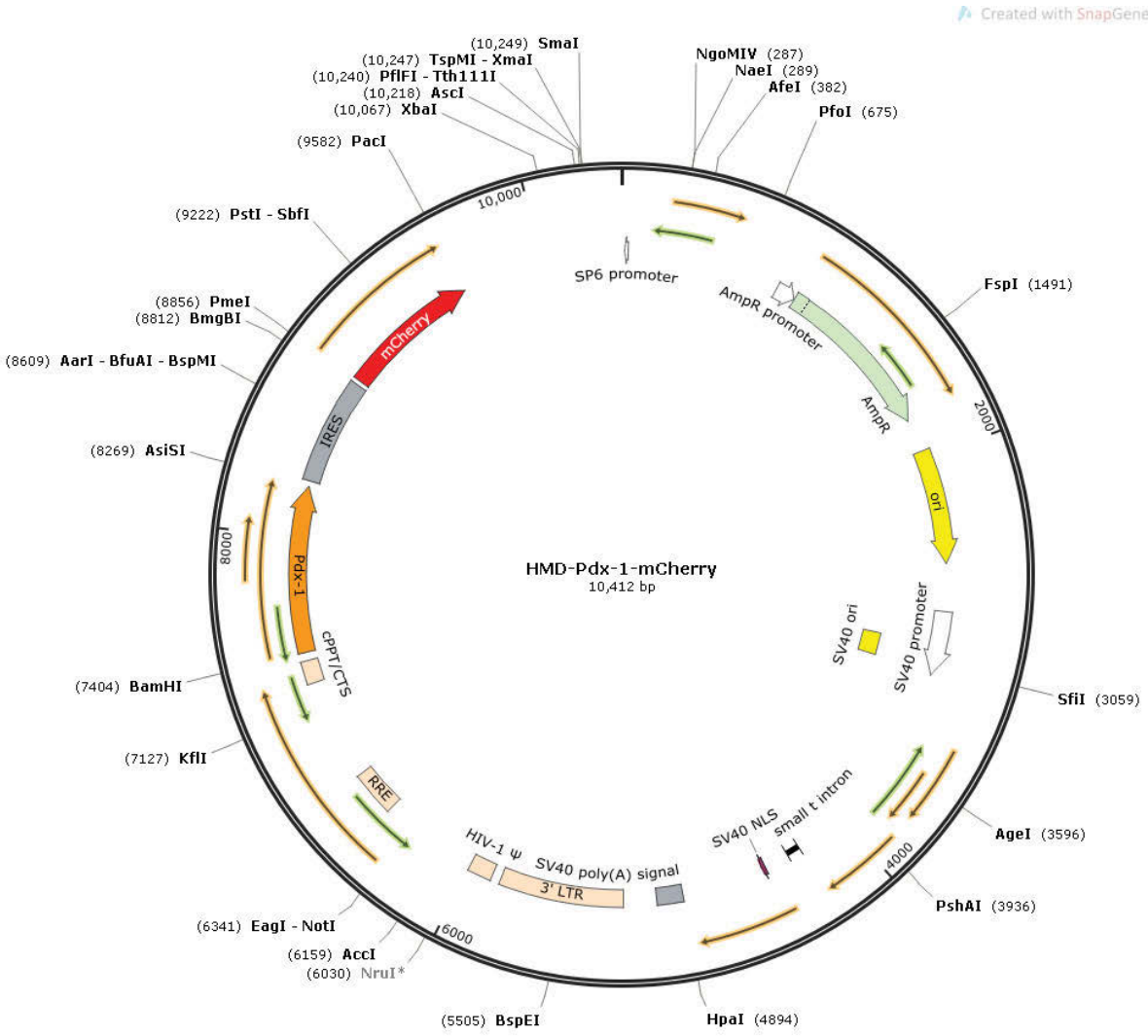

Figure 5.15: Diagrammatic representation of the HMD-*Pdx1* lentiviral plasmid The IRES-eGFP sequence was excised from the HMD lentiviral plasmid, and the *Pdx1-IRES-mCherry* sequence ligated into the HMD backbone to generate HMD-*Pdx1*. The mCherry fluorescent reporter allows for the determination of transduction efficiency and FACS of *Pdx1*-expressing cells.

5.2.3 Packaging and titration of lentiviral vectors HMD-*NeuroD1*, HMD-*INS-FUR/NeuroD1* and HMD-*Pdx1*

Lentiviral vectors were packaged in HEK293T cells (P5-10), and fluorescent images obtained on the Leica DM microscope at 24 and 48 hours post calcium phosphate precipitation. Cells transfected with the HMD-*NeuroD1* and HMD-*INS-FUR/NeuroD1* lentiviral plasmids that co-expressed eGFP were imaged using the Leica GFP filter set (BP 470/40). Cells transfected with the HMD-*Pdx1* lentiviral plasmid that co-expresses mCherry were imaged using the Leica Texas Red filter set (BP 560/40). As can be seen from Figure 5.16, increasing fluorophore expression can be observed from all lentiviral plasmids at 24 and 48 hours post transfection.

Viral supernatants were harvested at 36 hours post transfection and every 12 hours thereafter; pooled, and stored at 4^{o}C prior to purification. Following purification, viral supernatants were concentrated using Amicon Ultra 100 kDa filters and titrated using NIH3T3 (P5-10) cells. FACS analysis of transduced NIH3T3 cells determined the concentration of the packaged HMD-*NeuroD1*, HMD-*INS-FUR/NeuroD1* and HMD-*Pdx1* lentiviral vectors as $1.8x10^{6}$, $2.05x10^{6}$ and $1.4x10^{5}$ TU/ml respectively (Table 5.13). The concentration of the existing HMD and HMD-*INS-FUR* lentiviral vectors as produced and determined by Dr Binhai Ren were $1.8x10^{7}$ and $1.2x10^{8}$ TU/ml respectively.

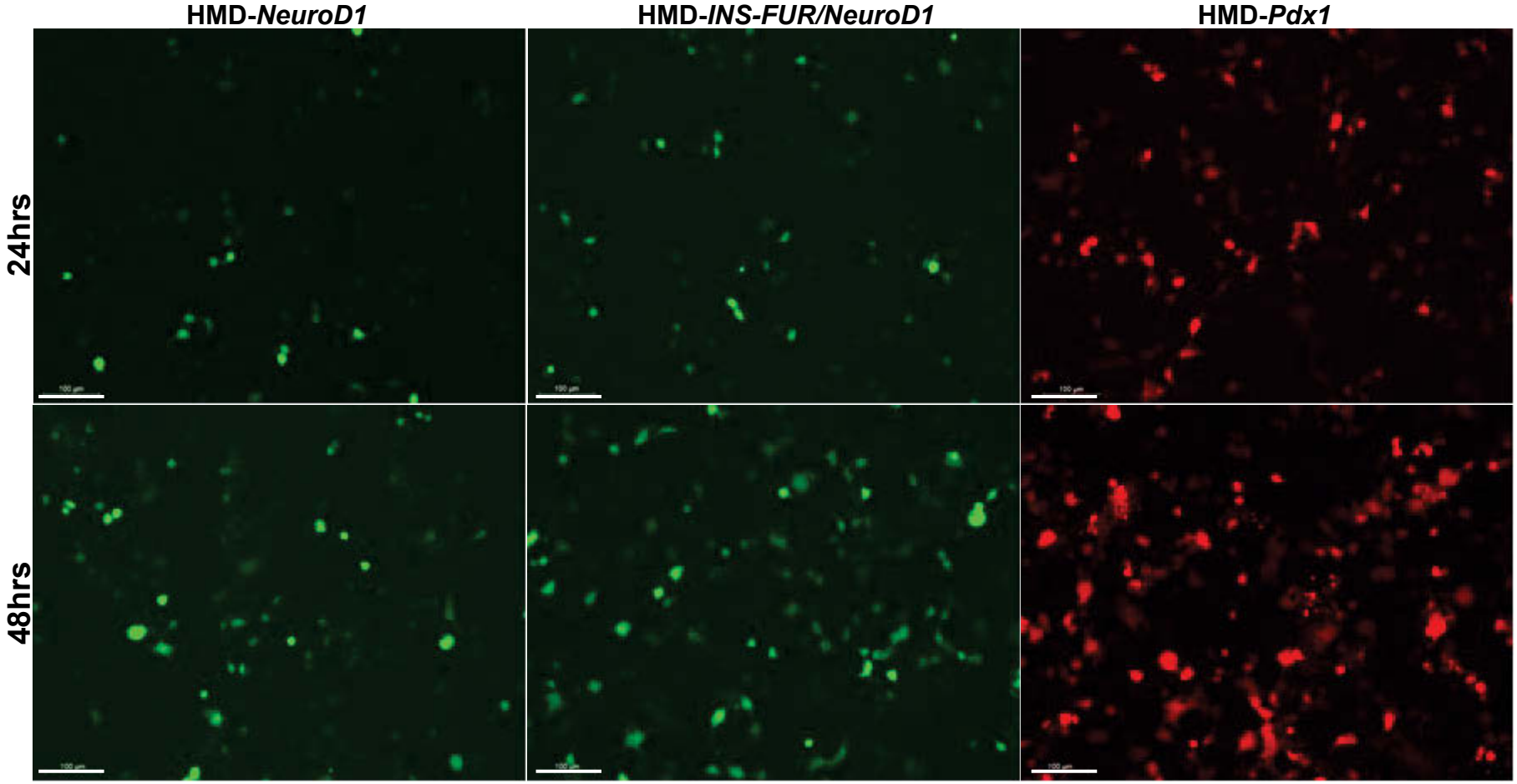

Figure 5.16: Fluorescence imaging of lentiviral packaging in HEK293T cells Fluorescence images were acquired at 24 and 48 hours post calcium phosphate precipitation of HEK293T cells (P5-10) with HMD-*NeuroD1*, HMD-*INS-FUR/NeuroD1* and HMD-*Pdx1* lentiviral plasmids. Images were acquired on the Leica DM microscope (Leica Microsystems) at 10x magnification using the GFP and Texas Red filter sets. 100µm scale.

Table 5.13: Determination of lentivirus concentration via FACS analysis of transduced NIH3T3 cells

	HMD-*NeuroD1* (% GFP^+)	HMD-*INS-FUR/NeuroD1* (% GFP^+)	HMD-*Pdx1* (% $mCherry^+$)
Untransduced	0.8 ± 0.2	0.9 ± 0.2	0.6 ± 0.1
1/2	30.3 ± 0.9	40.5 ± 0.9	8.5 ± 0.3
1/4	25.2 ± 0.7	28.8 ± 0.6	6 ± 0.3
1/8	15 ± 1.2	19.7 ± 0.4	3.8 ± 0.4
1/16	13 ± 1.7	15 ± 1	2.5 ± 0.4
1/32	10.2 ± 1.2	11.7 ± 1.3	1.6 ± 0.4
1/64	7.4 ± 0.8	9 ± 0.1	1 ± 0.1
1/128	7.5 ± 0.9	8.3 ± 0.8	0.6 ± 0.1
Concentration (TU/ml)	**$1.8x10^6$**	**$2.05x10^6$**	**$1.4x10^5$**

Values are average (%) ± SD (n=3). Cells highlighted in green were used to determine lentivirus concentration.

5.2.4 Lentiviral gene-modification of suicide BMSCs to express *INS-FUR* and murine *NeuroD1*

5.2.4.1 FACS sorting of suicide BMSCs lentivirally transduced to express INS-FUR and murine NeuroD1

Suicide BMSC-*F2/CDUPRT* cells were transduced with lentiviral vectors encoding the *INS-FUR* and murine *NeuroD1* genes as described in Section 5.1.5.1. The transduced cells were subsequently incubated for a period of 1 week, after which the transduced cells were analysed via FACS analysis and sorted into $eGFP^+$ populations corresponding to BMSC-*Luc2/CDUPRT-HMD*, BMSC-*Luc2/CDUPRT-INS-FUR*, BMSC-*Luc2/CDUPRT-NeuroD1* and BMSC-*Luc2/CDUPRT-INS-FUR/NeuroD1*. The FACS analysis plot represented in Figure 5.17 corresponds to suicide BMSC transduced during Round 1, which were the primary experimental conditions assessed. Transduced cells that were sorted during this FACS analysis were utilised in the downstream *in vivo* experiments. The cell acquisition and purity data for suicide BMSC transduced during Round 1 are detailed in Tables 5.14 and 5.15 respectively. The cell acquisition and purity data for suicide BMSC transduced during Round 2 in high glucose DMEM (-bFGF) are detailed in Tables 5.16 and 5.17 respectively. As can be seen from Tables 5.15 and 5.17, purity analysis showed that the purities of the sorted populations were lower than expected, a result of contaminating $eGFP^-$ cells and debris from FCS in the collection tubes.

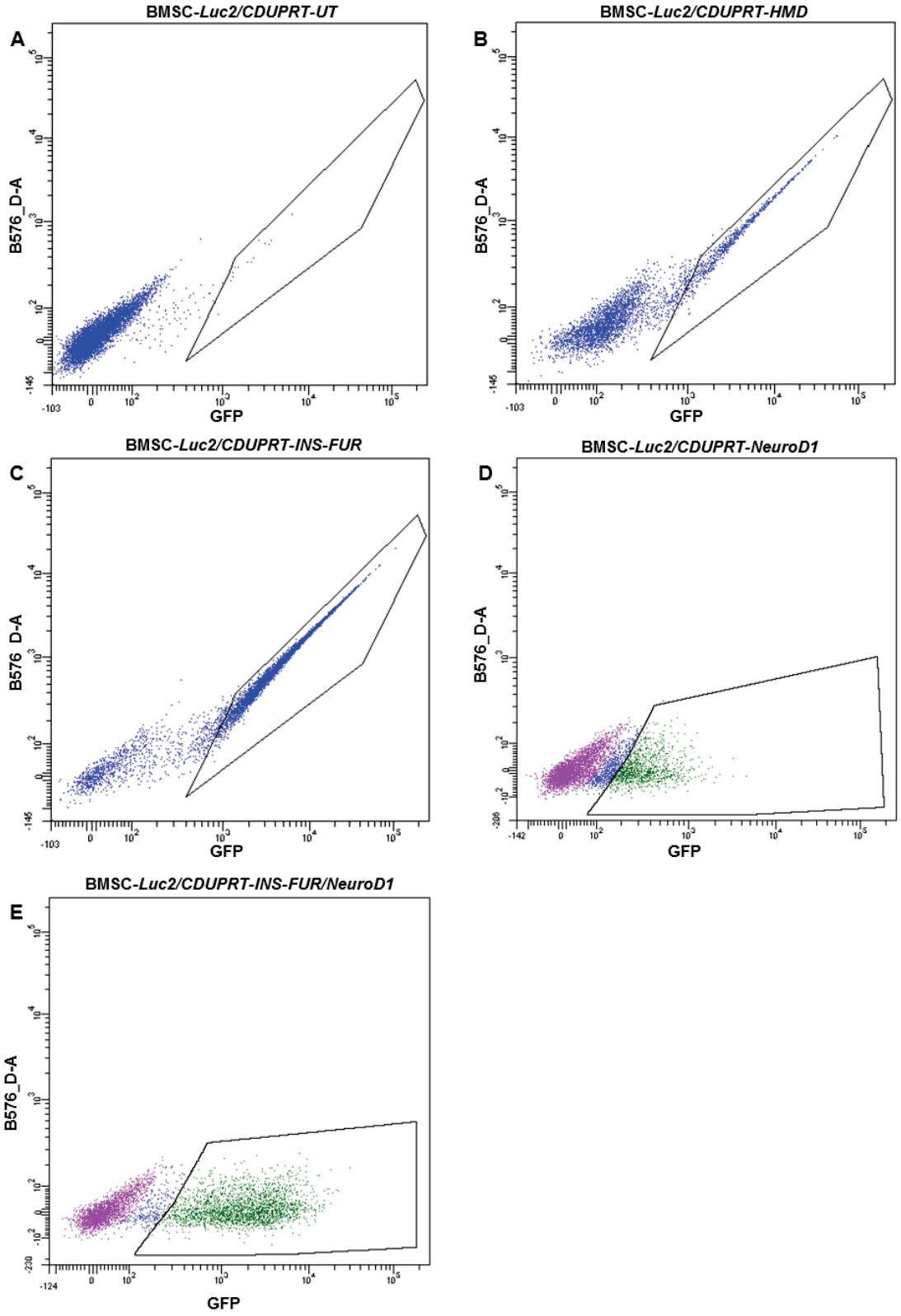

Figure 5.17: FACS analysis of suicide BMSCs transduced to express *INS-FUR* and *NeuroD1* (Round 1)

Following culture for 1 week, suicide BMSCs that were transduced with HMD, HMD-*INS-FUR*, HMD-*NeuroD1* and HMD-*INS-FUR/NeuroD1* (B-E) at an MOI of 10 were sorted into $eGFP^+$ populations. Untransduced suicide BMSCs were analysed as a negative control (A). Fluorescence dot plots of B576 D_A (y-axis) and GFP (x-axis) were used to identify $eGFP^+$ cells for cell sorting using the BD FACSAria™ II instrument.

Table 5.14: Cell acquisition analysis of transduced suicide BMSCs (Round 1)

Transduction	All events (%)	Viable cells (%)	Singlets (%)	GFP$^+$ (%)
Untransduced	10,000	8,996	8,755	15
	100	90.0	87.6	0.0
HMD	10,000	4,732	3,723	788
	100	47.3	37.2	7.9
HMD-*INS-FUR*	10,000	7,582	7,123	5,995
	100	75.8	71.2	60.0
HMD-*NeuroD1*	10,000	8,832	5,854	1,149
	100	88.3	58.5	11.5
HMD-*INS-FUR/NeuroD1*	10,000	6,081	5,297	2,465
	100	60.8	53.0	24.7

Untransduced and transduced suicide BMSCs were assessed for GFP expression via FACS analysis. The final percentages of each sorted cell population were determined as a fraction of the total cell count.

Table 5.15: Sorted cell purity analysis of transduced BMSCs (Round 1)

Sorted cells	All events (%)	Viable cells (%)	Singlets (%)	GFP$^+$ (%)
BMSC-*Luc2/CDUPRT-HMD*	147	80	72	45
	100	54.4	49.0	30.6
BMSC-*Luc2/CDUPRT-INS-FUR*	118	89	84	73
	100	75.4	71.2	49.7
BMSC-*Luc2/CDUPRT-NeuroD1*	208	162	160	93
	100	77.9	76.9	44.7
BMSC-*Luc2/CDUPRT-INS-FUR/NeuroD1*	119	87	81	68
	100	73.1	68.1	57.1

Transduced suicide BMSCs were sorted in to four distinct GFP$^+$ cell populations via FACS analysis. The final purity percentages of each sorted cell population were determined as a fraction of the total cell count.

Table 5.16: Cell acquisition analysis of transduced suicide BMSCs (Round 2)

Transduction	All events (%)	Viable cells (%)	Singlets (%)	GFP$^+$ (%)
Untransduced	10,000	7,259	5,978	4
	100	72.6	59.8	0.0
HMD	10,000	8,476	6,624	6,480
	100	84.8	66.2	64.8
HMD-*INS-FUR*	10,000	7,630	5,662	5,127
	100	76.3	56.6	51.3
HMD-*NeuroD1*	10,000	8,767	6,904	1,047
	100	87.7	69.0	10.5
HMD-*INS-FUR/NeuroD1*	10,000	8,552	7,115	3,383
	100	85.5	71.2	33.9

Untransduced and transduced suicide BMSCs were assessed for GFP expression via FACS analysis. The final percentages of each sorted cell population were determined as a fraction of the total cell count.

Table 5.17: Sorted cell purity analysis of transduced BMSCs (Round 2)

Sorted cells	All events (%)	Viable cells (%)	Singlets (%)	GFP$^+$ (%)
BMSC-*Luc2/CDUPRT-HMD*	243	198	181	160
	100	81.5	74.5	65.8
BMSC-*Luc2/CDUPRT-INS-FUR*	184	118	111	83
	100	64.1	60.3	45.1
BMSC-*Luc2/CDUPRT-NeuroD1*	127	101	94	28
	100	79.5	74.0	22.0
BMSC-*Luc2/CDUPRT-INS-FUR/NeuroD1*	284	213	196	142
	100	75.0	69.0	50.0

Transduced suicide BMSCs were sorted in to four distinct GFP$^+$ cell populations via FACS analysis. The final purity percentages of each sorted cell population were determined as a fraction of the total cell count.

A comparison of BMSC transduction efficiencies (Figure 5.18) during Round 1 and Round 2 showed that transduction with the existing HMD and HMD-*INS-FUR* lentiviral vectors resulted in higher transduction efficiencies in comparison to the newly generated HMD-*NeuroD1* and HMD-*INS-FUR/NeuroD1* lentiviral vectors. However, Round 1 transduction with HMD was unexpectedly low in comparison to its Round 2 counterpart, likely a result of human error. There were no differences in the lentiviral transduction efficiencies of BMSCs between Round 1 and Round 2 with respect to the HMD-*INS-FUR*, HMD-*NeuroD1* and HMD-*INS-FUR/NeuroD1* lentiviral vectors.

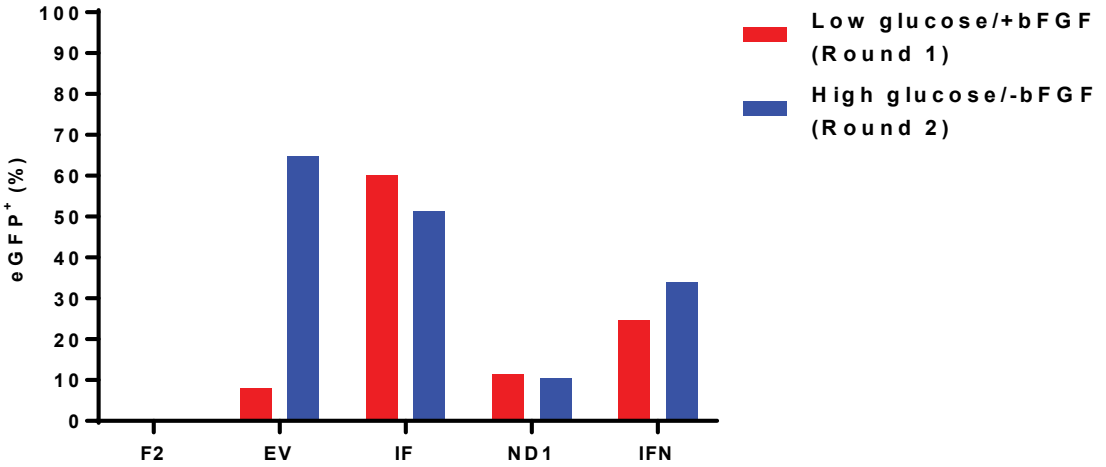

Figure 5.18: Effect of media composition on the transduction efficiency of suicide BMSCs Suicide BMSCs were transduced with lentiviral vectors in the presence of low glucose/+bFGF (red) and high glucose/-bFGF (blue) containing media (n=1). A comparison of transduction efficiency with each lentiviral vector HMD (EV), HMD-*INS-FUR* (IF), HMD-*NeuroD1* (ND1) and HMD-*INS-FUR/NeuroD1* (IFN) is represented as percentage of $eGFP^+$ cells. Untransduced suicide BMSCs are represented as the negative control (F2).

The sorted cells were returned to culture and imaged under fluorescence microscopy (Figure 5.19), showing the intensity of eGFP expression in transduced suicide BMSCs. As can be seen, eGFP expression in suicide BMSCs transduced with the newly generated HMD-*NeuroD1* and HMD-*INS-FUR/NeuroD1* was lower than in cells transduced with the existing HMD and HMD-*INS-FUR* lentiviral vectors.

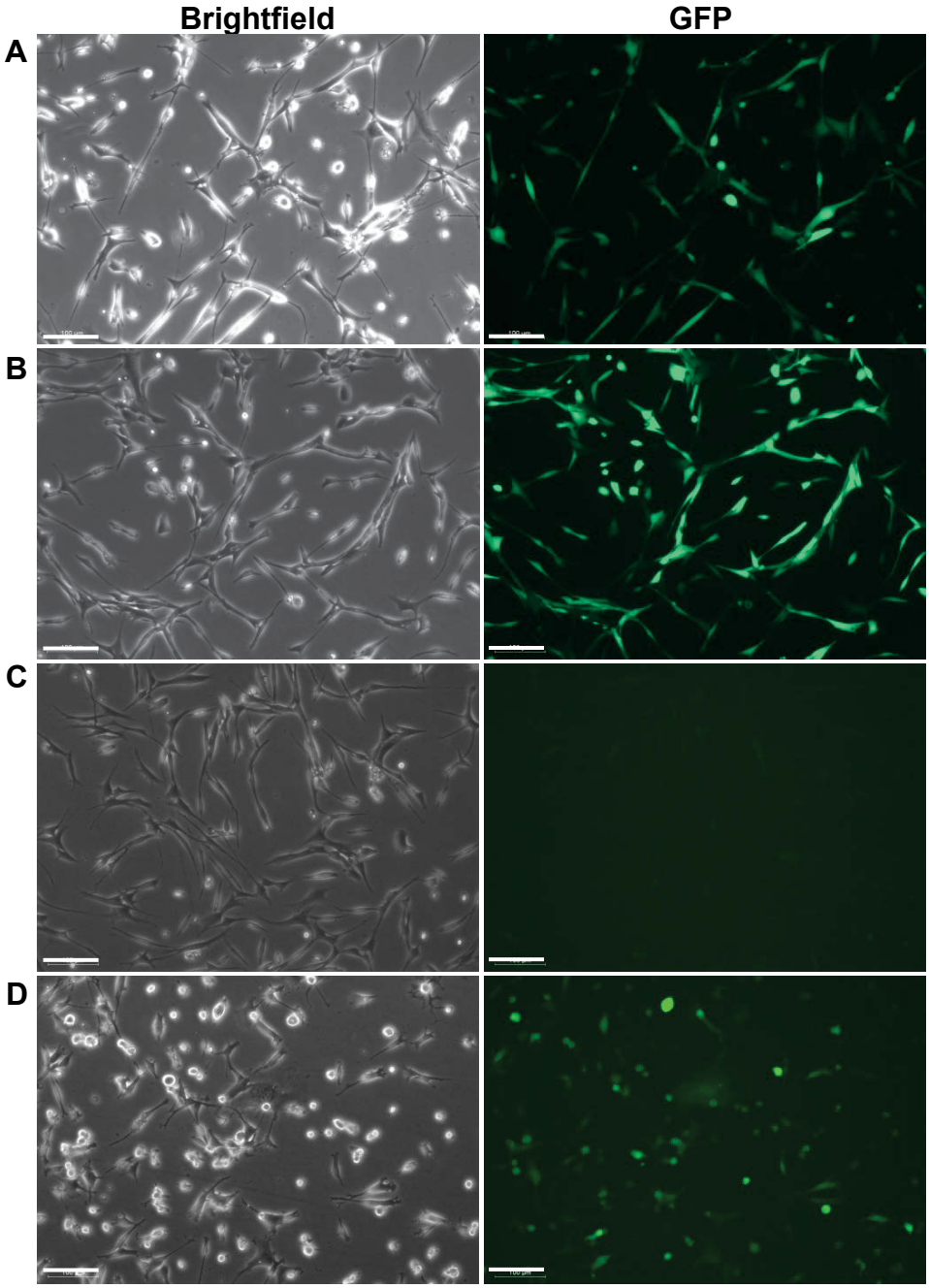

Figure 5.19: Fluorescence imaging of suicide BMSCs transduced to express *INS-FUR* and *NeuroD1* BMSC-*Luc2/CDUPRT-HMD* (A), BMSC-*Luc2/CDUPRT-INS-FUR* (B), BMSC-*Luc2/CDUPRT-NeuroD1* (C) and BMSC-*Luc2/CDUPRT-INS-FUR/NeuroD1* (D) were returned to culture post-sorting and imaged for GFP expression (Day 7 post transduction) on the on the Leica DM microscope (Leica Microsystems) at 10x magnification under brightfield and GFP fluorescence filter sets. Scale 100µm.

5.2.4.2 Morphological characterisation of INS-FUR and NeuroD1-expressing suicide BMSCs

Suicide BMSCs that were transduced in Round 1 were returned to culture in complete α-MEM and cultured for 4 weeks, after which the cells were imaged and RNA samples acquired for gene expression profiling (Figure 5.20A). Suicide BMSCs transduced during Round 1 that were returned to culture in high glucose DMEM (-bFGF) were imaged and RNA samples acquired at 1, 2 and 4 weeks post-media change for gene expression profiling (Figure 5.20B). Suicide BMSCs that were pre-conditioned in high glucose DMEM (-bFGF) and transduced during the Round 2 transductions were returned to culture in high glucose DMEM (-bFGF) for 4 weeks, after which the cells were imaged and RNA samples acquired for gene expression profiling (Figure 5.20C).

As can be seen from Figure 5.20, suicide BMSCs transduced with all lentiviral vectors in complete α-MEM retained a fibroblast-like morphology in comparison to their untransduced counterparts, demonstrating no change in morphology due to transgene over-expression (Figure 5.20A). By comparison, untransduced and transduced suicide BMSCs that were returned to culture in high glucose DMEM (-bFGF) developed a cuboidal morphology. These results indicated that the change in morphology from fibroblast-like to cuboidal was a consequence of the change of culture conditions to high glucose DMEM (-bFGF), rather than of transgene over-expression (Figure 5.20B). Suicide BMSCs transduced following pre-conditioning in high glucose DMEM (-bFGF) displayed a similar cuboidal morphology to those that were switched to high glucose DMEM (-bFGF) at 28 days post-transduction, yet also displayed no difference in morphology to their untransduced counterparts (Figure 5.20C). This suggests bFGF may be a possible contributor to the maintenance of the fibroblast-like morphology of transduced cells when cultured in the presence of bFGF. In

summary, across all media conditions assessed for the transduction of suicide BMSCs with lentiviral vectors, no difference in morphology was observed due to the over-expression of *INS-FUR* or *NeuroD1*.

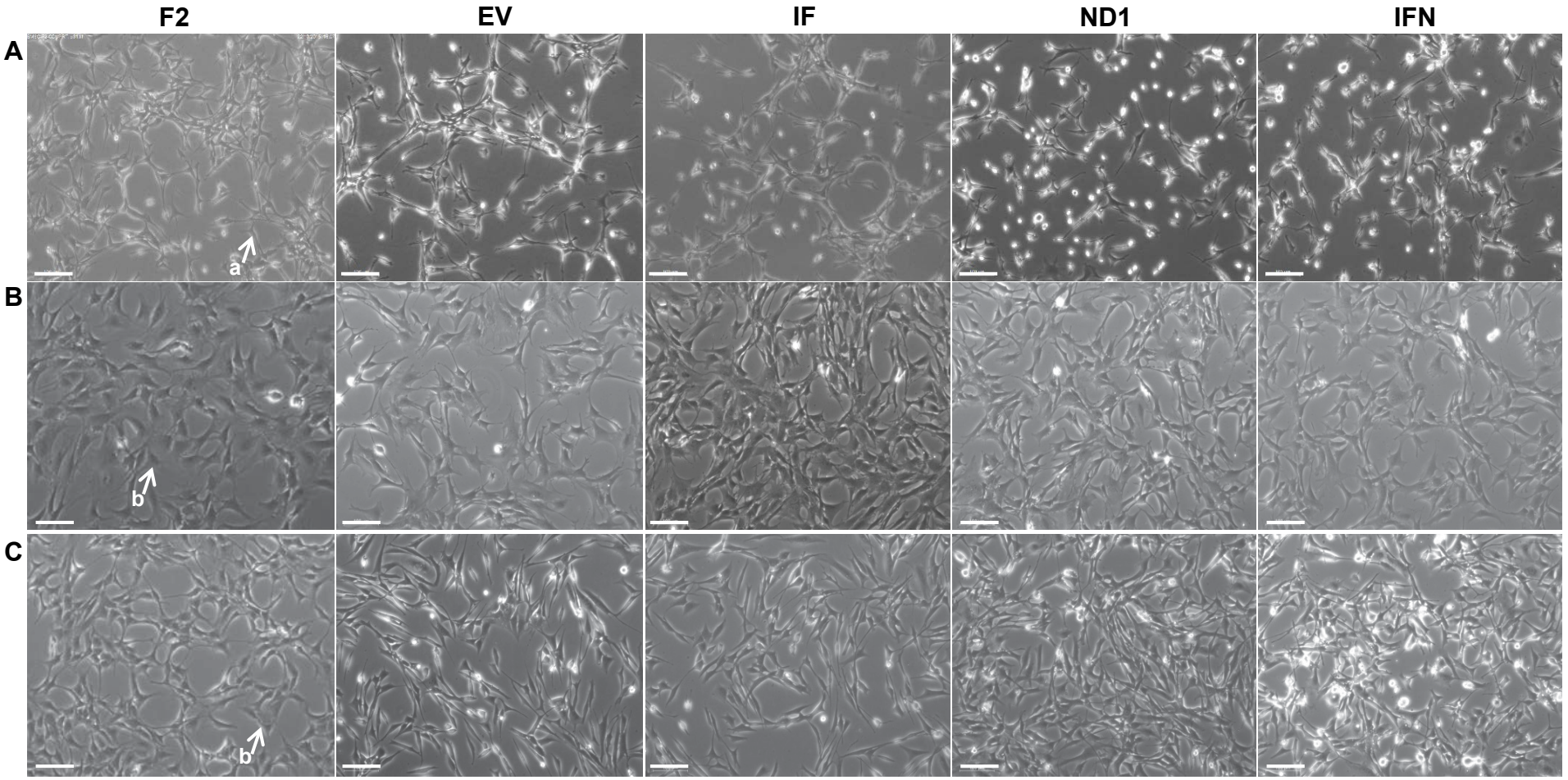

Figure 5.20: Morphological characterisation of suicide BMSCs post transduction with *INS-FUR* and *NeuroD1* Brightfield microscopy of suicide BMSC (F2) that were transduced with HMD (EV), HMD-*INS-FUR* (IF), HMD-*NeuroD1* (ND1) and HMD-*INS-FUR/NeuroD1* (IFN) in complete α-MEM (Round 1) (A), in complete α-MEM (Round 1) and returned to culture in high glucose DMEM (-bFGF) (B) and high glucose DMEM (Round 2) (-bFGF) (C) at 28 days post transduction. The Images were acquired on a Leica DM microscope (Leica Microsystems) at 10x magnification under brightfield setting. Arrowheads indicate morphology of parental suicide BMSC in complete α-MEM (a) and in high glucose DMEM (-bFGF) (b). Scale 100μm.

5.2.4.3 Gene expression profiling of INS-FUR and NeuroD1-expressing suicide BMSCs

To determine whether over-expression of *INS-FUR* and *NeuroD1* in suicide BMSCs resulted in pancreatic transdifferentiation, gene expression profiling of transduced suicide BMSCs at 28 days post-transduction was performed to characterise the cells' pancreatic gene expression profile (Figure 5.21). The upper-hierarchy transcription factors involved in early pancreatic cell development such as *Pdx-1*, and endogenous and exogenous *NeuroD1*, as well as the β-cell specific transcription factor *Nkx6.1* were assessed. In addition, genes involved in insulin secretion such *Scl2a2*, *Ins1* and *Ins2* were assessed.

As can be seen from Figure 5.21A, exogenous murine *NeuroD1* that was over-expressed in suicide BMSC was detected at 28 days post-transduction both in cells transduced in complete α-MEM (Round 1) and in high glucose DMEM (-bFGF) (Round 2). As expected, exogenous *NeuroD1* was not detected in the parental suicide BMSCs, suicide BMSC transduced with HMD and HMD-*INS-FUR*, and the positive control (mouse pancreas). Interestingly, exogenous *NeuroD1* expression resulted in endogenous *NeuroD1* expression. However, neither *Pdx1*, *Nkx6.1*, *Scl2a2*, *Ins1* nor *Ins2* were detected in parental and transduced suicide BMSCs, confirming a lack of pancreatic transdifferentiation. Suicide BMSCs transduced in complete α-MEM and returned to culture in high glucose DMEM (-bFGF) demonstrated a similar gene expression profile (Figure 5.21) as those the cells profiled in Figure 5.21B. Differences were observed with diminished expression of endogenous *NeuroD1* in cells switched to high glucose DMEM (-bFGF) post-transduction in comparison to those pre-conditioned, transduced and returned to culture in the same media formulation; and the transient detection of *Nkx6.1* in suicide BMSC transduced with *NeuroD1* alone at Day 28.

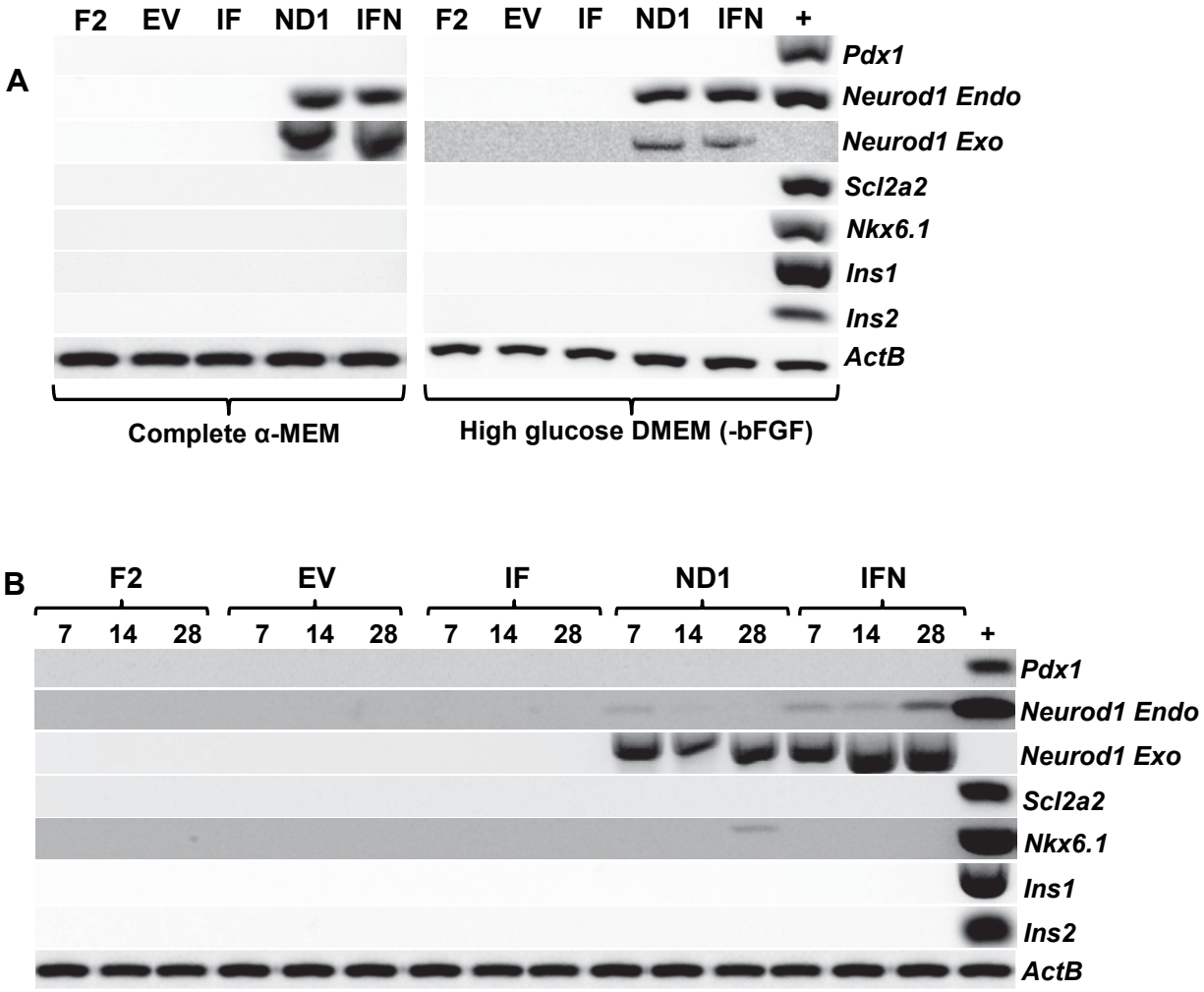

Figure 5.21: Gene expression profiling of *INS-FUR* and *NeuroD1*-expressing suicide BMSCs cDNA was synthesised from RNA extracted from untransduced suicide BMSCs (F2) and transduced with HMD (EV), HMD-*INS-FUR* (IF), HMD-*NeuroD1* (ND1) and HMD-*INS-FUR/NeuroD1* (IFN) in either complete α-MEM or high glucose DMEM (-bFGF) (A) at 28 days post-transduction; or switched to high glucose DMEM (-bFGF) (B) at 7, 14 and 28 days post-transduction. Mouse pancreas (+) was used as a positive control. All products were run on a 1% (w/v) agarose gel containing 0.5% (v/v) GelRed™ at 90V for 90 min, and were visualised on the InGenius3® UV transilluminator.

5.2.4.4 Insulin secretion and storage assays

Suicide BMSCs transduced during Round 1 (which were the primary conditions under investigation) were assessed for their ability to secrete insulin in a chronic (Figure 5.22) and acute-regulated manner (Figure 5.23) as described in Section 5.1.6.3 and 5.1.6.4 respectively. As can be seen from Figure 5.22, a significant quantity of secreted human insulin was detected in the culture medium of suicide BMSCs transduced with HMD-*INS-FUR* ($p<0.001$) and HMD-*INS-FUR-NeuroD1* ($p<0.05$) in comparison to untransduced suicide BMSC, where insulin was not detected. Similarly, no insulin was detected in culture medium from suicide BMSCs transduced with HMD and HMD-*NeuroD1*. As expected, there was a significant difference in the quantity of insulin secreted between BMSC-*Luc2/CDUPRT-INS-FUR* and BMSC-*Luc2/CDUPRT-INS-FUR/NeuroD1*, which directly correlated with a difference in the level of fluorescent reporter expression. The detected insulin was a consequence of the over-expression of *INS-FUR* rather than of endogenous mouse insulin expression, which was confirmed to not be expressed in suicide BMSCs transduced to express both *INS-FUR* and *NeuroD1* via RT-PCR (Figure 5.21).

Acute stimulation assays were performed as described in Section 5.1.6.4, and secreted insulin subsequently quantified as described in Section 2.7. As can be seen from Figure 5.23, an increase in insulin secretion following the addition of a 20mM glucose stimulus was not observed in either of the suicide BMSCs transduced to express *INS-FUR*. In addition to the significant difference in hourly insulin secretion detected between BMSC-*Luc2/CDUPRT-INS-FUR* and BMSC-*Luc2/CDUPRT-INS-FUR/NeuroD1* ($p<0.001$), there is also a significant decrease in hourly insulin secretion across cell lines between basal 1, 2, stimulus and basal 3 ($p<0.001$). The lack of stimulated insulin secretion was expected due to the lack of *Slc2a2* detected via RT-PCR (Figure 5.21).

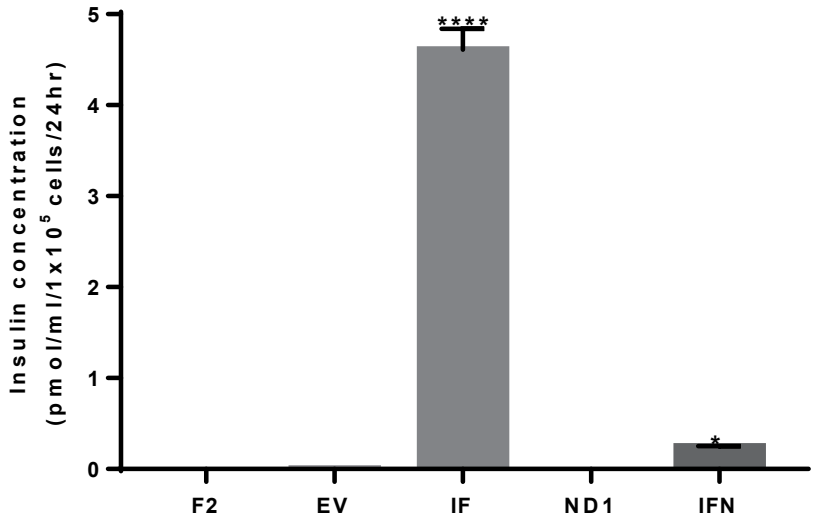

Figure 5.22: Chronic insulin secretion from suicide BMSCs transduced to express *INS-FUR* and *NeuroD1* Suicide BMSCs that were untransduced (F2) and transduced with HMD (EV), HMD-*INS-FUR* (IF), HMD-*NeuroD1* (ND1) and HMD-*INS-FUR/NeuroD1* (IFN) were plated at $1x10^5$ cells/well of a 6-well in triplicate (n=4). Culture medium was obtained 24 hours post-seeding and human insulin was quantified via ARCHITECT™ i4000SR Immunoassay Analyser (Abbott Diagnostics©). Data is represented as mean ± SD. A one-way ANOVA with Sidak's post-hoc test was performed, * $p<0.05$.

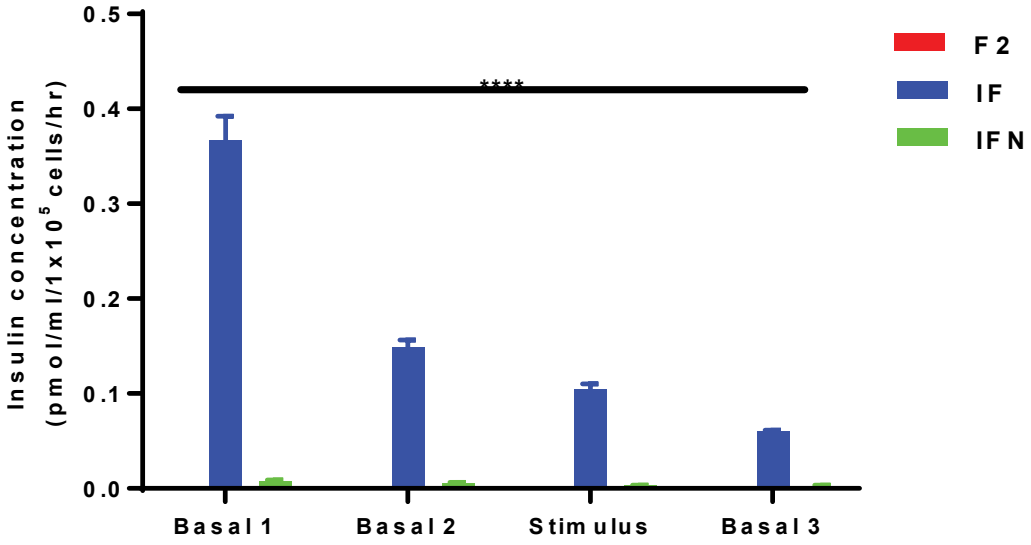

Figure 5.23: Acute stimulated insulin secretion from suicide BMSCs transduced to express *INS-FUR* and *NeuroD1* Suicide BMSCs that were untransduced (F2) and transduced with HMD-*INS-FUR* (IF), and HMD-*INS-FUR/NeuroD1* (IFN) were plated at $1x10^5$ cells/well of a 6-well in triplicate (n=3). Culture medium was obtained hourly post incubation with basal and stimulus (20mM glucose) medium, and human insulin quantified via ARCHITECT™ i4000SR Immunoassay Analyser (Abbott Diagnostics©). Data is represented as mean ± SD. A two-way ANOVA with Tukey's post-hoc test was performed, * $p<0.05$.

The ability of β-cells to secrete insulin in response to a glucose stimulus is in part possible due to their ability to store insulin within secretory granules. Storage of insulin within granules facilitates a rapid insulin secretion response in the presence of fluctuating glucose concentrations. As a result, detection of insulin stored within secretory granules provides evidence of the cells ability to secrete insulin in response to a glucose stimulus. In the absence of secretory granules, the ability of a cell to secrete insulin in response to a glucose stimulus would be tightly linked to the regulatory processes involved in the transcription and translation of mature insulin, which is a timely process that would not facilitate rapid insulin secretion. Therefore, the results of the acute stimulation obtained in Figure 5.23 provide preliminary evidence for the absence of secretory granules in BMSC transduced to express *INS-FUR* and *NeuroD1*. To confirm these results, quantification of insulin stored within secretory granules (Figure 5.24) was performed as described in Section 5.1.6.5.

As can be seen in Figure 5.24, very little insulin was detected in suicide BMSCs transduced to express *INS-FUR* and *INS-FUR/NeuroD1* in comparison to the quantity of insulin secreted over a 24-hour period. In fact, the quantity of insulin detected following acid/ethanol extraction constitutes ~1% of the total quantity of insulin secreted over 24 hours. This suggests that insulin was not stored within secretory granules, and confirms the lack of glucose-stimulated insulin secretion demonstrated in Figure 5.23 and absence of β-cell differentiation. The insulin detected in these assays is therefore likely an artefact of free cytoplasmic insulin rather than insulin stored within secretory granules.

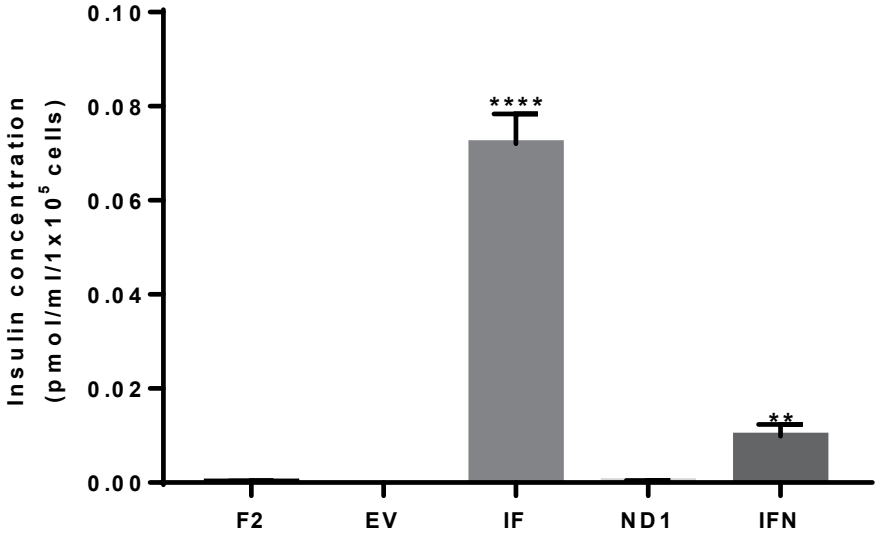

Figure 5.24: Insulin storage in transduced suicide BMSCs Untransduced suicide BMSCs (F2) and suicide BMSC transduced with HMD (EV), HMD-*INS-FUR* (IF), HMD-*NeuroD1* (ND1) and HMD-*INS-FUR/NeuroD1* (IFN) ($1x10^6$ cells/assay) (n=4) were incubated for 48 hours in acid/ethanol, and insulin in the supernatants quantified via ARCHITECT™ i4000SR Immunoassay Analyser (Abbott Diagnostics©). Data is represented as mean ± SD (n=3). A one-way ANOVA with Dunnett's post-hoc was performed, * $p<0.05$.

5.2.4.5 BMSC proliferation following lentiviral transduction

Cell proliferation assays were performed using mid-passage suicide BMSCs that were transduced during Round 1 as described in Section 2.2. As can be seen in Figure 5.25, there was no significant difference in the proliferation of transduced suicide BMSCs in comparison to their parental counterpart.

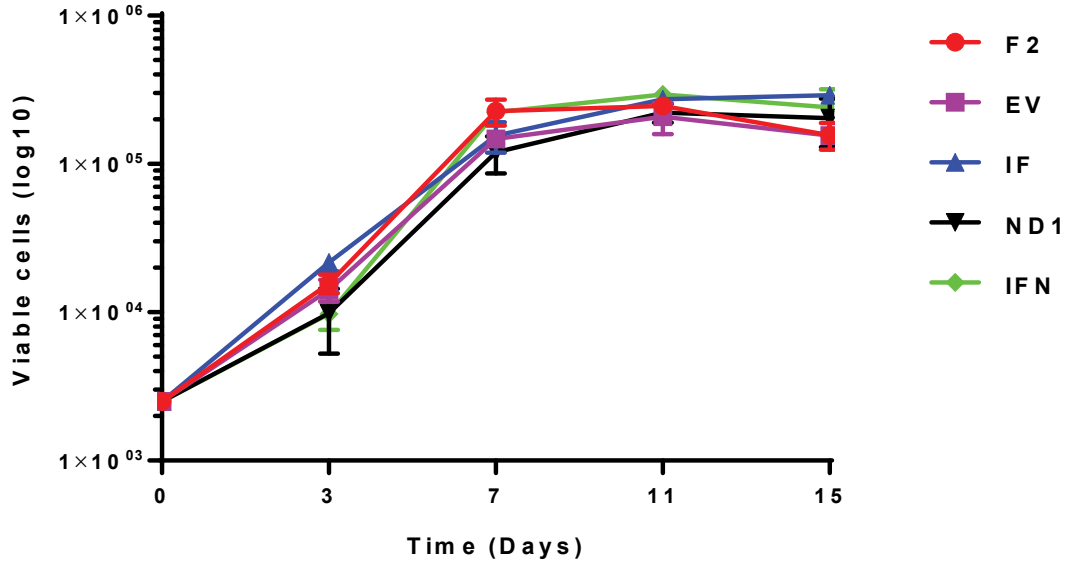

Figure 5.25: Cell proliferation of transduced suicide BMSCs Untransduced suicide BMSCs (F2) and suicide BMSC transduced with HMD (EV), HMD-*INS-FUR* (IF), HMD-*NeuroD1* (ND1) and HMD-*INS-FUR/NeuroD1* (IFN) were seeded at 2.5x10^3 cells/well in triplicate of a 24-well plate (n=3), and viable cells were counted via Trypan blue exclusion at Days 0, 3, 7, 11 and 15. Data is represented as mean ± SD (n=3). A two-way ANOVA with Tukey's post-hoc was performed, * $p<0.05$.

5.2.5 Lentiviral gene-modification of suicide BMSCs to express murine codon-optimised *Pdx1*

5.2.5.1 FACS sorting suicide BMSCs lentivirally transduced to express murine codon-optimised Pdx1

Following the morphological and genetic characterisation of suicide BMSC transduced during Round 1 and 2 that showed a lack of pancreatic transdifferentiation, BMSC-*Luc2/CDUPRT-INS-FUR* and their parental counterparts (BMSC-*Luc2/CDUPRT*) were further transduced with a lentiviral vector encoding the murine *Pdx1* gene (HMD-*Pdx1*) as described in Section 5.1.5.1. BMSC-*Luc2/CDUPRT-INS-FUR* cells were chosen as targets for *Pdx-1* over-expression due to the increased quantities of *INS-FUR* that were secreted from these cells in comparison to BMSC-*Luc2/CDUPRT-INS-FUR/NeuroD1*. The transduced cells were subsequently incubated for 1 week, after which the transduced cells were analysed via FACS analysis and sorted into $mCherry^+$ and $GFP^+/mCherry^+$ populations corresponding to BMSC-*Luc2/CDUPRT-Pdx1* and BMSC-*Luc2/CDUPRT-INS-FUR-Pdx1* (Figure 5.26). The cell acquisition and purity data for suicide BMSC transduced with HMD-*Pdx1* are detailed in Tables 5.18 and 5.19 respectively.

As can be seen in Table 5.18, parental suicide BMSC and BMSC-*Luc2/CDUPRT-INS-FUR* transduced with HMD-*Pdx1* display transduction efficiencies of 36.0% and 30.4% respectively, of which 20.3% were $GFP^+/mCherry^+$ in the former population. Purity analysis following sorting of BMSC-*Luc2/CDUPRT-Pdx1* and BMSC-*Luc2/CDUPRT-INS-FUR-Pdx1* into distinct populations showed purities of 97.0 and 88.6% respectively. The sorted cells were returned to culture in complete α-MEM and imaged under brightfield and

fluorescence settings (Figure 5.27), showing the intensity and co-expression of eGFP and mCherry in transduced suicide BMSC.

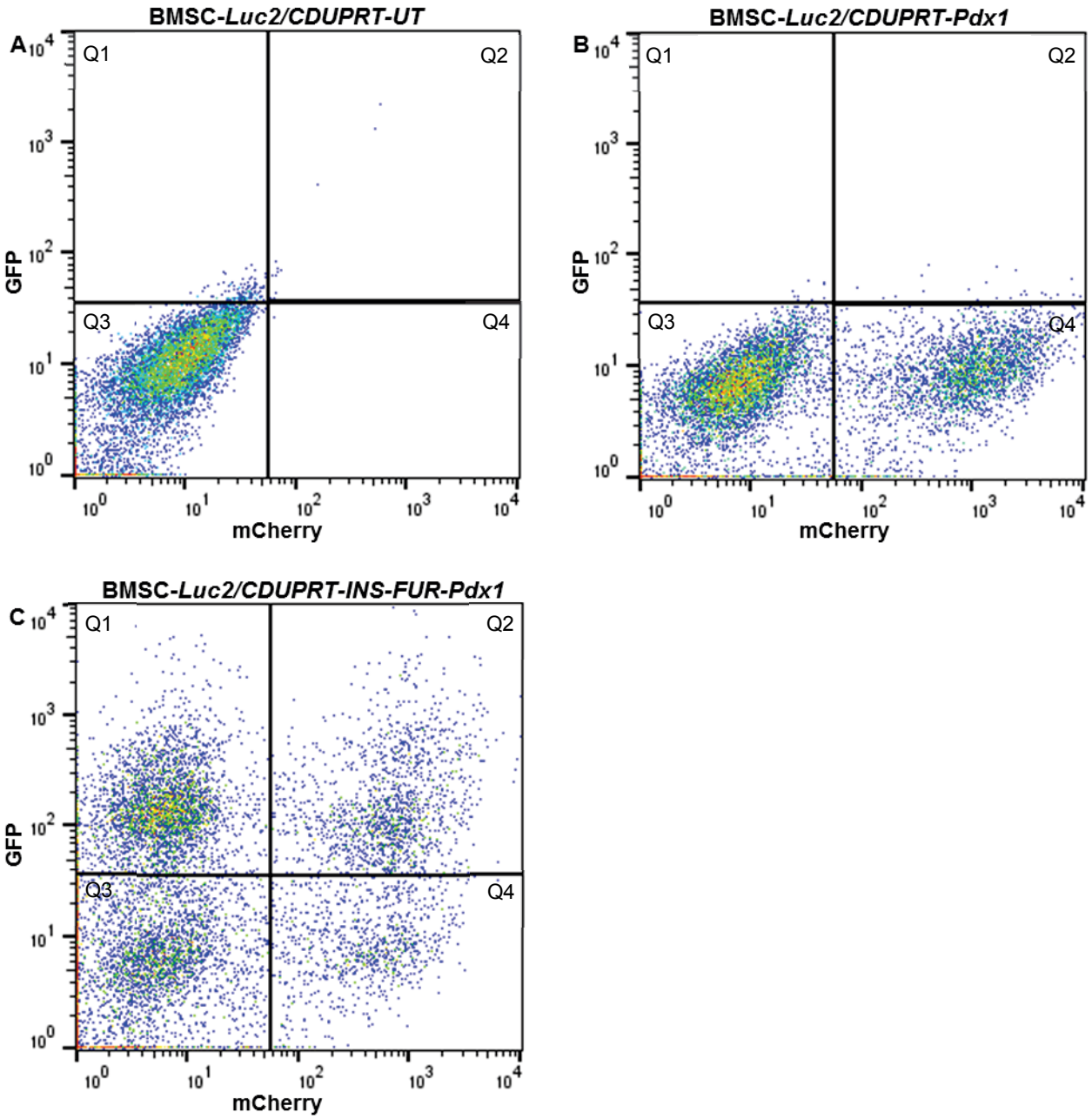

Figure 5.26: Transduction of suicide BMSCs with *Pdx1*-expressing lentiviral vector Following culture for 1 week, BMSC-*F2/CDUPRT* (B) and BMSC-*F2/CDUPRT-INS-FUR* (C) that were transduced with HMD-*Pdx1* at an MOI of 10 were sorted into mCherry$^+$ (Q4) and eGFP$^+$/mCherry$^+$ (Q2) populations respectively. Untransduced suicide BMSCs were analysed as a negative control (A). Fluorescence dot plots of GFP (y-axis) and mCherry (x-axis) were used to identify eGFP$^+$/mCherry$^+$ cells for cell sorting using the BD FACSAria™ II instrument.

Table 5.18: Cell acquisition analysis of suicide BMSCs transduced with *Pdx1*

Transduction	All events (%)	Viable cells (%)	Singlets (%)	GFP$^+$ (%)	mCherry$^+$ (%)	GFP$^+$/mCherry$^+$ (%)
Untransduced BMSC-*Luc2/CDUPRT*	10,000	8,041	7,887	149	1	15
	100	80.4	98.1	0.02	0.0	0.2
BMSC-*Luc2/CDUPRT* + HMD-*Pdx1*	10,000	8,623	8,568	17	3,081	28
	100	86.2	99.4	0.0	36.0	0.0
BMSC-*Luc2/CDUPRT-INS-FUR* + HMD-*Pdx1*	10,000	7,444	7,384	3,559	2,245	1,500
	100	74.4	99.2	48.2	30.4	20.3

Transduced suicide BMSCs were divided into three groups for FACS analysis: Untransduced BMSC-*Luc2/CDUPRT*, BMSC-*Luc2/CDUPRT* transduced with HMD-*Pdx1* and BMSC-*Luc2/CDUPRT-INS-FUR* transduced with HMD-*Pdx1*. BMSC-*Luc2/CDUPRT-Pdx1* and BMSC-*Luc2/CDUPRT-INS-FUR-Pdx1* were sorted dependent on their fluorescent profiles as mCherry$^+$ (red) and GFP$^+$/mCherry$^+$ (orange) respectively. The final percentages of each sorted cell population were determined as a fraction of the total cell count.

Table 5.19: Sorted cell purity analysis of suicide BMSCs transduced with *Pdx1*

Sorted cells	All events (%)	Viable cells (%)	Singlets (%)	GFP$^+$ (%)	mCherry$^+$ (%)	GFP$^+$/mCherry$^+$ (%)
BMSC-*Luc2/CDUPRT-Pdx1*	1000	930	916	0	888	5
	100	93	98.5	0	97.0	0.5
BMSC-*Luc2/CDUPRT-INS-FUR-Pdx1*	1014	955	941	43	801	834
	100	94.2	98.5	4.6	85.1	88.6

Transduced suicide BMSCs were sorted in to two distinct mCherry$^+$ (red) and GFP$^+$/mCherry$^+$ (orange) cell populations via FACS analysis. The final purity percentages of each sorted cell population were determined as a fraction of the total cell count.

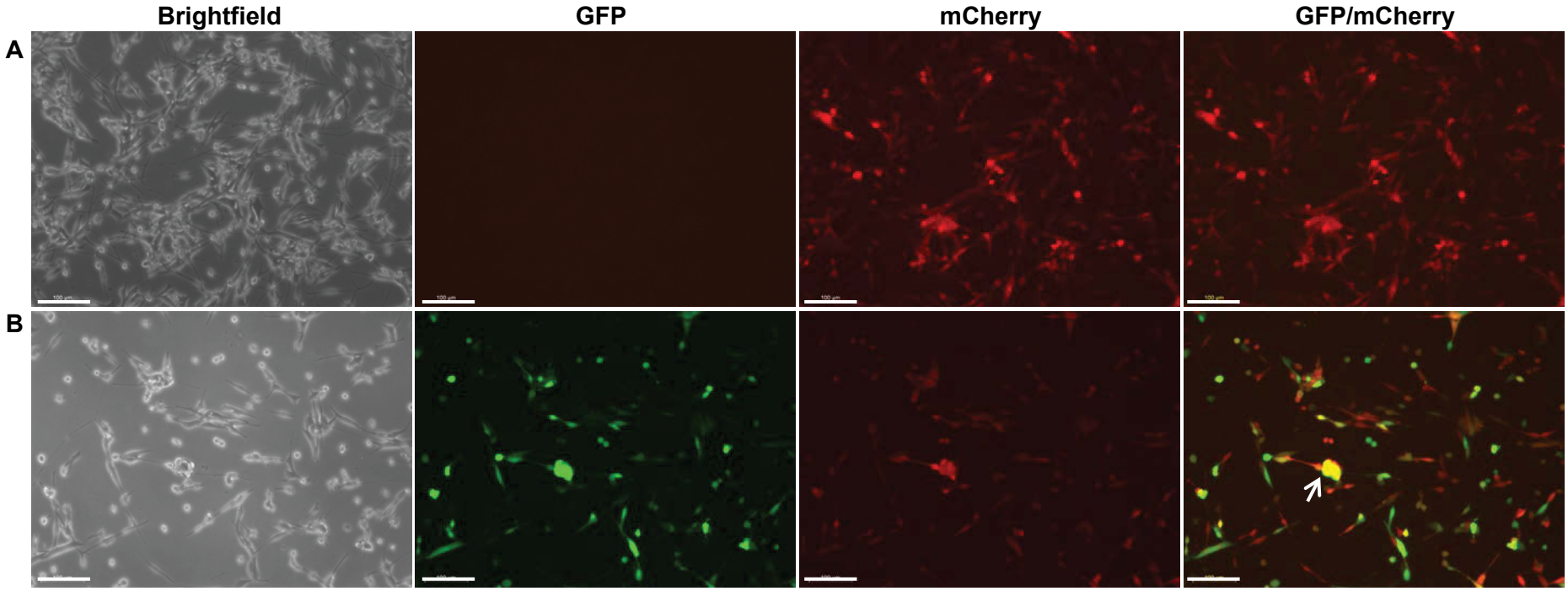

Figure 5.27: Fluorescence imaging of suicide BMSCs transduced to express *Pdx1* BMSC-*Luc2/CDUPRT-Pdx1* (A) and BMSC-*Luc2/CDUPRT-INS-FUR-Pdx1*(B) were returned to culture post-sorting and imaged for GFP and mCherry expression (Day 7 post transduction) on the Leica DM microscope (Leica Microsystems) at 10x magnification under brightfield and GFP fluorescence filter sets. Composite GFP/mCherry images were generated using ImageJ software. Arrowhead indicates overlapping GFP/mCherry expression (yellow) in BMSC-*Luc2/CDUPRT-INS-FUR-Pdx1*. Scale 100µm.

5.2.5.2 Morphological characterisation of INS-FUR and Pdx1-expressing suicide BMSCs

Suicide BMSCs that were transduced during Round 3 transductions with HMD-*Pdx1* were returned to culture in complete α-MEM and cultured for 4 weeks, after which the cells were imaged and RNA samples acquired for gene expression profiling (Figure 5.29). As can be seen from Figure 5.28, parental suicide BMSCs and suicide BMSCs expressing *INS-FUR* transduced with HMD-*Pdx1* retained a similar fibroblast-like morphology at 28 days post transduction in comparison to their untransduced parental counterparts. Cell cycle stage and confluency associated differences in morphology can also be observed between cell populations.

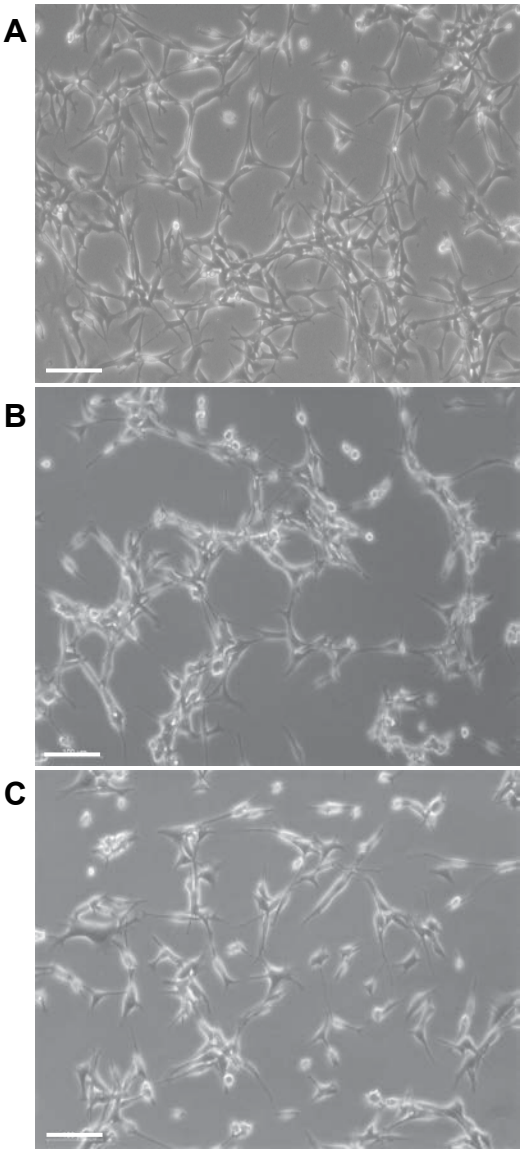

Figure 5.28: Morphological characterisation of suicide BMSCs post transduction with *Pdx1* Untransduced suicide BMSCs (A), and suicide BMSCs (B) and suicide BMSC-*INS-FUR* (C) were transduced with HMD-*Pdx1* and returned to culture in complete α-MEM for 28 days, after which brightfield images were acquired. The images were acquired on a Leica DM microscope (Leica Microsystems) at 10x magnification. Scale 100µm.

5.2.5.3 Gene expression profiling of INS-FUR and Pdx1-expressing suicide BMSCs

Suicide BMSCs transduced to over-express codon-optimised murine *Pdx1* indicated that pancreatic transdifferentiation did not occur. To confirm this observation, gene expression profiling of BMSCs transduced with HMD-*Pdx1* at 28 days post-transduction was performed to characterise the cells' pancreatic gene expression profile (Figure 5.29). The upper-hierarchy transcription factors involved in early pancreatic cell development such as *Pdx-1* (endogenous and exogenous) and *NeuroD1*, and genes involved in insulin secretion such *Scl2a2*, *Ins1* and *Ins2* were assessed.

As can be seen from Figure 5.29, exogenous murine codon-optimised *Pdx1* that was over-expressed in suicide BMSCs was detected at 28 days post-transduction. As expected, exogenous codon-optimised *Pdx1* was not detected in the positive control (mouse pancreas). Interestingly, in contrast to the previous results with respect to over-expression of exogenous *NeuroD1* in suicide BMSCs, over-expression of exogenous *Pdx1* did not result in endogenous *Pdx1* expression. In addition, *NeuroD1*, *Scl2a2*, *Ins1* or *Ins2* were detected in transduced suicide BMSCs, confirming a lack of pancreatic transdifferentiation.

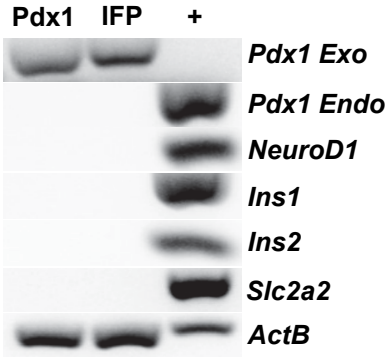

Figure 5.29: Gene expression profiling of *INS-FUR* and *Pdx1*-expressing suicide BMSCs cDNA was synthesised from RNA extracted from suicide BMSCs (*Pdx1*) and BMSC-*Luc2/CDUPRT-INS-FUR* (IFP) transduced with HMD-*Pdx1* respectively in complete α-MEM at 28 days post-transduction. Mouse pancreas (+) was used as a positive control. All products were run on a 1% (w/v) agarose gel containing 0.5% (v/v) GelRed™ at 90V for 90 min, and were visualised on the InGenius3® UV transilluminator.

5.2.5.4 Chronic insulin secretion assay

Parental suicide BMSCs and those engineered to over-express *INS-FUR* that were subsequently engineered to express murine codon-optimised *Pdx1* were assessed for their ability to chronically secrete human insulin via quantitation of secreted insulin over a 24 hour period as described in Section 5.1.6.3 and Section 2.7. As can be seen from Figure 5.30, a significant quantity of secreted human insulin was detected in the culture medium of suicide BMSCs expressing *INS-FUR* and *Pdx1* ($p<0.001$) in comparison to untransduced and suicide BMSCs expressing *Pdx*1 alone, where no insulin was detected. As with the previous assays, detected insulin was a consequence of the over-expression of *INS-FUR* rather than of endogenous mouse insulin expression, which was not expressed in suicide BMSCs transduced to express both *INS-FUR* and *Pdx1* via RT-PCR. Acute stimulation and insulin storage assays were not performed with suicide BMSCs expressing *Pdx1* and *INS-FUR*, as no evidence of pancreatic transdifferentiation characterised by expression of pancreatic transcription factors was detected by RT-PCR.

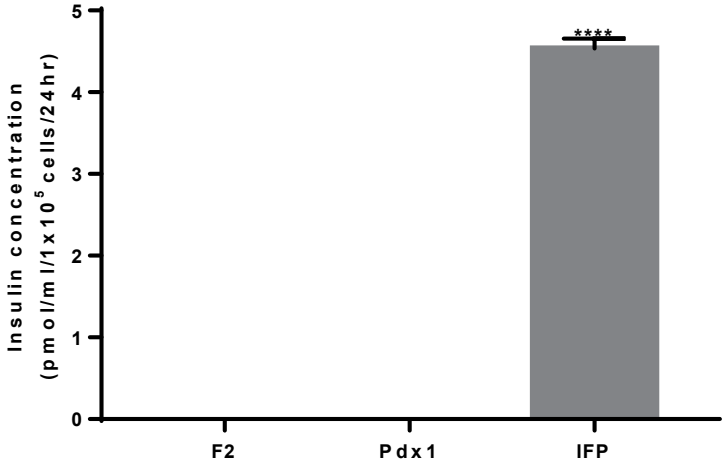

Figure 5.30: Chronic insulin secretion from suicide BMSCs transduced to express *INS-FUR* and *Pdx1*

Untransduced suicide BMSCs (UT), suicide BMSCs transduced with HMD-*Pdx1* (Pdx1) and suicide BMSCs expressing *INS-FUR* transduced with HMD-*Pdx1* (IFP) were plated at $1x10^5$ cells/well of a 6-well in triplicate (n=4). Culture medium was obtained 24 hours post-seeding and human insulin was quantified via ARCHITECT™ i4000SR Immunoassay Analyser (Abbott Diagnostics©). Data is represented as mean ± SD. A one-way ANOVA with Sidak's post-hoc test was performed, * $p<0.05$.

In summary, BMSCs engineered to over-express *INS-FUR* secreted significant amounts of insulin in an unregulated constitutive manner. The over-expression of the β-cell transcription factors *NeuroD1* and *Pdx1* did not result in pancreatic transdifferentiation with storage of insulin, and thus no glucose-responsive insulin secretion was demonstrated. Due to the higher quantities of insulin secreted from suicide BMSCs expressing *INS-FUR* alone in comparison to those co-expressing pancreatic transcription factors, BMSC-*Luc2/CDUPRT-INS-FUR* were utilised in subsequent cell aggregation and *in vivo* experiments.

The purpose of the cell aggregation study was to determine whether BMSCs undergo spheroid formation in a similar manner to human islet-derived progenitor cells (hIPCs), which were a primary cell line of interest in our laboratory. hIPCs are mesenchymal-like primary cells derived from the *ex vivo* culture of pancreas explants, that when cultured through a 14 day chemically-defined differentiation protocol form islet cell-like aggregates (ICAs) containing cells that express human *Ins*, *Pdx1*, *Slc2a2* and *Sst*[382]. However, ICAs secrete small quantities of insulin that would not be sufficient to reverse hyperglycaemia. Considering the mesenchymal similarity of BMSCs and hIPCs, BMSCs over-expressing *INS-FUR* were considered as a more suitable target for ICA formation and differentiation. Prior to culturing BMSC-*Luc2/CDUPRT-INS-FUR* cells through the 14-day differentiation protocol, their ability to form ICA-like spheroids was assessed. Mr. Vijit Saini (an undergraduate Honours student) assisted with the assessment of *BMSC-Luc2/CDUPRT-INS-FUR* differentiation into mature ICAs by culturing BMSC-*Luc2/CDUPRT-INS-FUR* spheroids through the 14-day differentiation protocol.

5.2.6 Spheroid formation of suicide BMSCs expressing *INS-FUR*

The ability of parental suicide BMSCs and those transduced to over-express *INS-FUR* to form spheroids similar to islet-cell aggregates in culture was assessed via brightfield and fluorescence microscopy (Figure 5.31). As can be seen in Figure 5.31A, following over-night (24 hours) culture in low-attachment culture plates, both parental suicide BMSCs and those transduced with HMD and HMD-*INS-FUR* tightly aggregated to form spheroids ranging in size from 50-200µm. In addition, spheroid formation did not affect fluorescent reporter expression. Triple-immunofluorescent staining of BMSC-*Luc2/CDUPRT-INS-FUR* spheroids at 24 hours post-seeding qualitatively showed the proportion of live/dead cells within formed spheroids (Figure 5.31B). As can be seen, a number of dead cells were observed within the formed spheroids. This was likely due to the adherent property of BMSCs and their preferential growth as adherent monolayers rather than in suspension, which resulted in an increase in cell death.

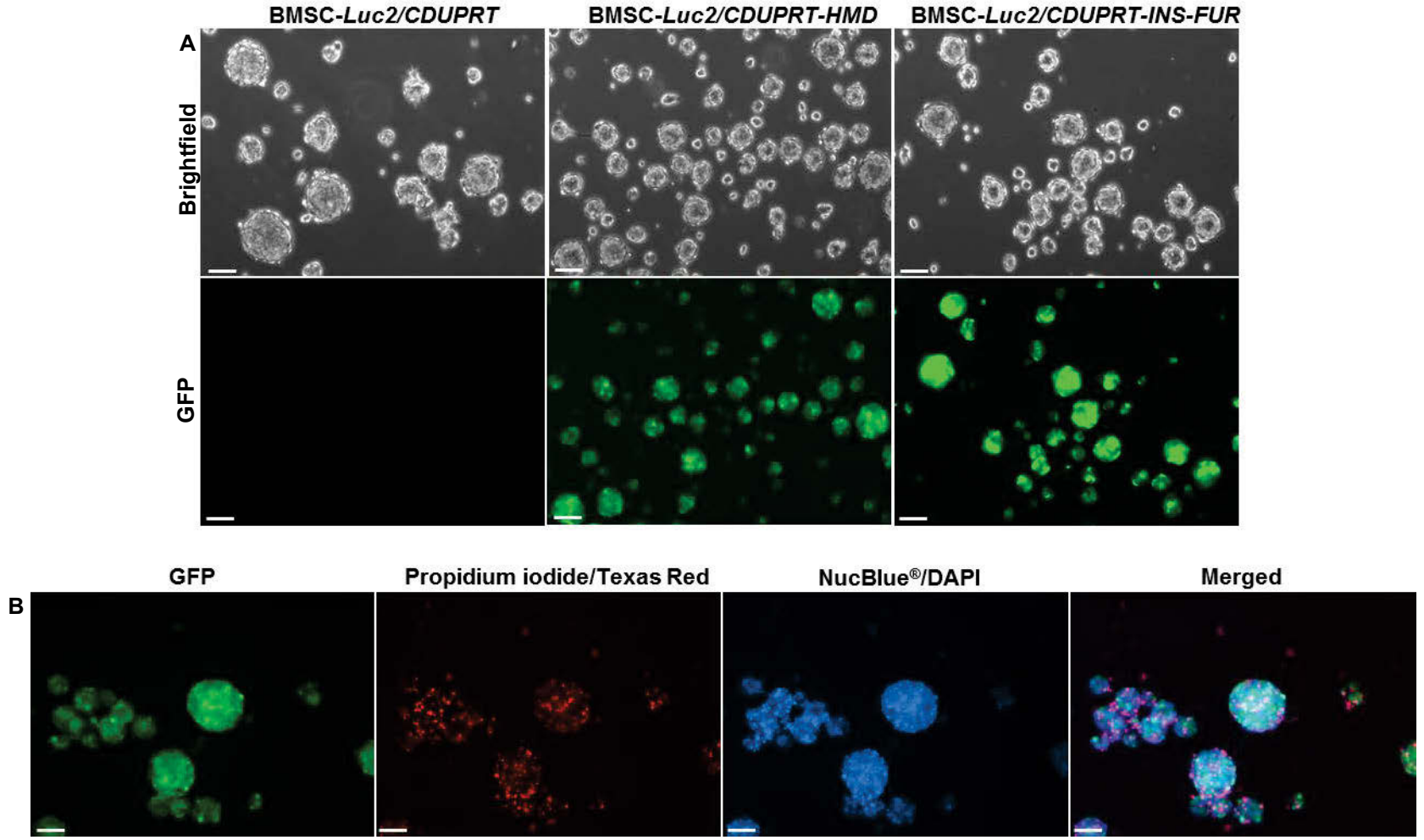

Figure 5.31: Suicide BMSC spheroid formation Parental suicide BMSCs and suicide BMSCs transduced with HMD and HMD-*INS-FUR* were seeded at $1x10^6$ cells/well of a low-attached 6-well plate in triplicate for 24 hours. Brightfield and GFP fluorescence images (A) were obtained at 24 hours post-seeding. Triple-immunofluorescent imaging of *INS-FUR* (GFP), dead cells (PI/Texas Red), live cells (NucBlue®/DAPI) highlight the co-localisation of fluorescent signal acquired from BMSC-*Luc2/CDUPRT-INS-FUR* spheroids (B). All images were acquired on the Leica DM microscope (Leica Microsystems) at 10x magnification. Scale 100µm.

A double-immunofluorescent time-lapse analysis of BMSC-*Luc2/CDUPRT-INS-FUR* spheroid formation (Figure 5.32) captured the period over which cell aggregation occurred. As can be seen in Figure 5.32, complete spheroid formation occurred by 12 hours post seeding (Figure 5.32M), during which time individual cells aggregated to form seed clusters of ~5-75µm (Figure 5.32D), and then fused over the following 9 hours to form mature spheroids of ~150-200µm. This was observed within the highlighted field of interest, which shows three seed clusters migrating in suspension and fusing to form a mature spheroid from t=0 to t=15 hours. PI staining visualised via immunofluorescence (Texas Red filter set) qualitatively showed the proportion of dead cells (red) within the seeded cell population over the 16-hour imaging period. As can be seen, there appeared to be an increased number of individual dead cells at t=0 in comparison to t=15 hours. PI stained dead cells appeared to move in suspension, specifically in conjunction with live cells and as aggregation targets mature spheroids. As a result, the majority of dead cells after 16 hours are localised within spheroids rather than as individual cells in suspension.

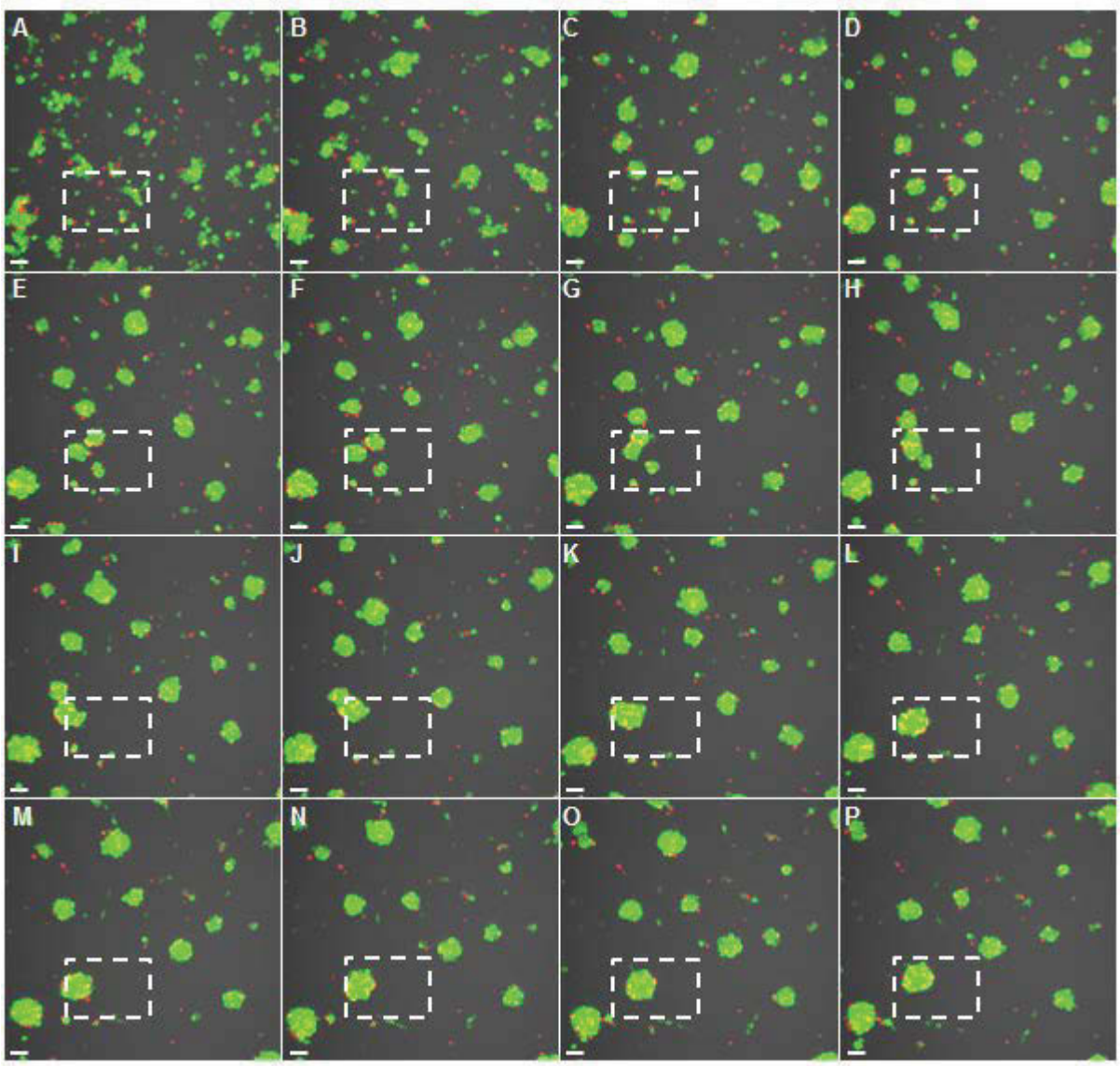

Figure 5.32: Time-lapse imaging of spheroid formation BMSC-*Luc2/CDUPRT-INS-FUR* were seeded at $1x10^6$ cells/well of a low-attachment 6-well plate, stained with ReadyProbes® propodium iodide (2 drops/ml) and incubated in the incubation chamber of the Nikon A1 confocal microscope (Nikon©). Double-fluorescent images (GFP and Texas Red) represented were acquired at one hour intervals from t=0 to t=15 (A-P). Field of interest (white dotted box) highlights the movement and aggregation of seed clusters in suspension to form a mature spheroid. Images were acquired at 10x magnification. Scale 100µm.

5.2.7 *In vivo* transplant of BMSC-*Luc2/CDUPRT-INS-FUR* in STZ-diabetic NOD/*Scid* mice

NOD/*Scid* mice were rendered diabetic as described in Section 5.1.8.3 via intraperitoneal injection of STZ (170mg/kg). Hyperglycaemia induced via STZ injection in all induced animals was observed within 3-6 days post injection, and on Day 8 post STZ-injection the animals received a subcutaneous transplant of either $1x10^7$ (n=5) or $5x10^7$ (n=5) cells/injection behind the neck. Blood glucose concentration (Figure 5.33) and body weight (Figure 5.34) was measured daily for up to 28 days post cell transplantation. As can be seen from Figure 5.33, immediately following transplantation of $1x10^7$ and $5x10^7$ cells (Day 9), there was a significant decrease in blood glucose concentrations compared to pre-transplantation, albeit still significantly higher than normal controls ($p<0.001$; $1x10^7$ cells and $p<0.05$; $5x10^7$ cells). The reduction in blood glucose concentration following transplantation of $5x10^7$ cells persisted for ~15 days post transplantation, after which blood glucose concentrations returned to pre-transplant values and significance in comparison to normal controls ($p<0.001$). By comparison, the reduction in blood glucose concentration in animals treated with $1x10^7$ cells remained significantly higher than normal controls ($p<0.001$) for the duration of the experiment. Most importantly, animals treated with either $1x10^7$ or $5x10^7$ cells did not normalise blood glucose at any time.

In addition, there was a significant difference in the body weights of treated animals ($p<0.001$; $5x10^7$, $p<0.01$; $1x10^7$) in comparison to normal controls pre and post transplantation despite random allocation of animals to the different groups (Table 5.21). However, as can be seen in Figure 5.34, there was a similar increasing trend in the body weights of diabetic and treated animals post transplantation. At no point was a significant decrease in body weight observed over the course of the experiment.

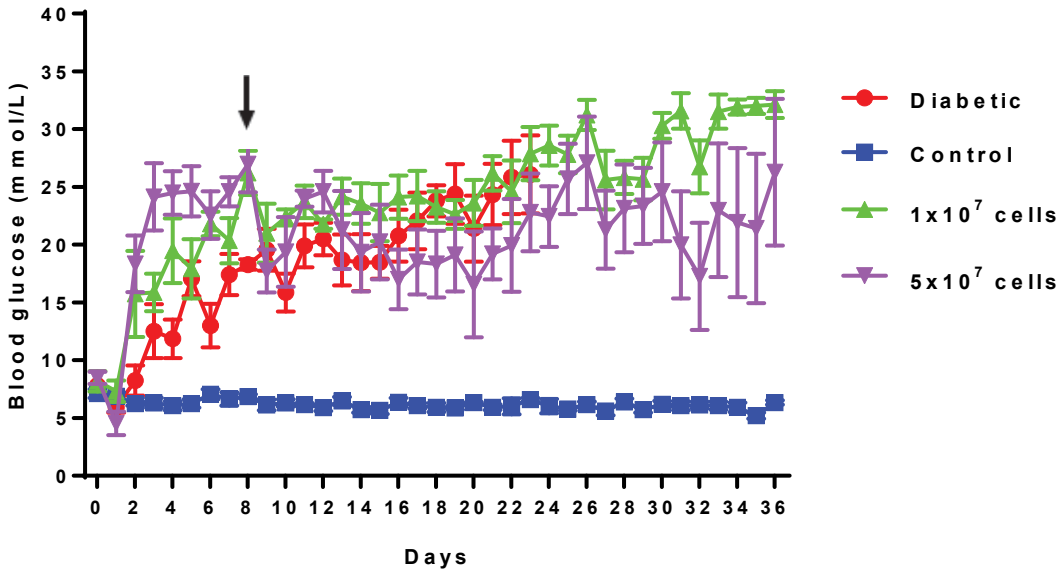

Figure 5.33: Blood glucose concentration of treated STZ-NOD/*Scid* mice NOD/*Scid* mice had diabetes induced following a peritoneal injection of STZ (170mg/kg), after which diabetic animals received either $1x10^7$ (n=5) or $5x10^7$ (n=5) BMSC-*Luc2/CDUPRT-INS-FUR* subcutaneously behind the neck. Diabetic (n=5) and normal control (n=5) animals were assessed in comparison. The arrowhead indicates the day on which cells were transplanted (Day 8 post STZ-injection). Blood glucose measurements were recorded daily post STZ-injection for the duration of the experiment (36 days). Data is represented as mean ± SEM. A two-way ANOVA was performed with Sidak's post-hoc, * $p<0.05$.

Table 5.20: Comparison of significance in blood glucose concentration following cell transplant

	Days																		
	0	1	2	3	4	5	6	7	8	9	10	11	12	13	14	15	16	17	18
Diabetic	ns	ns	ns	ns	ns	****	ns	****	****	****	***	****	****	****	****	****	****	****	****
1x10^7	ns	ns	****	****	****	****	****	****	****	****	****	****	****	****	****	****	****	****	****
5x10^7	ns	ns	*	****	****	****	***	****	****	*	**	****	****	**	**	**	ns	*	*
		19	20	21	22	23	24	25	26	27	28	29	30	31	32	33	34	35	36
Diabetic		****	****	****	****	****	-	-	-	-	-	-	-	-	-	-	-	-	-
1x10^7		****	****	****	****	****	****	****	****	****	****	****	****	****	****	****	****	****	****
5x10^7		**	ns	**	**	***	***	****	****	***	****	****	****	**	ns	****	***	***	****

A two-way ANOVA with Sidak's post-hoc was performed comparing blood glucose concentrations of diabetic and treated animals in comparison to normal animals for the duration of the experiment. Data is represented as significance, * $p<0.05$.

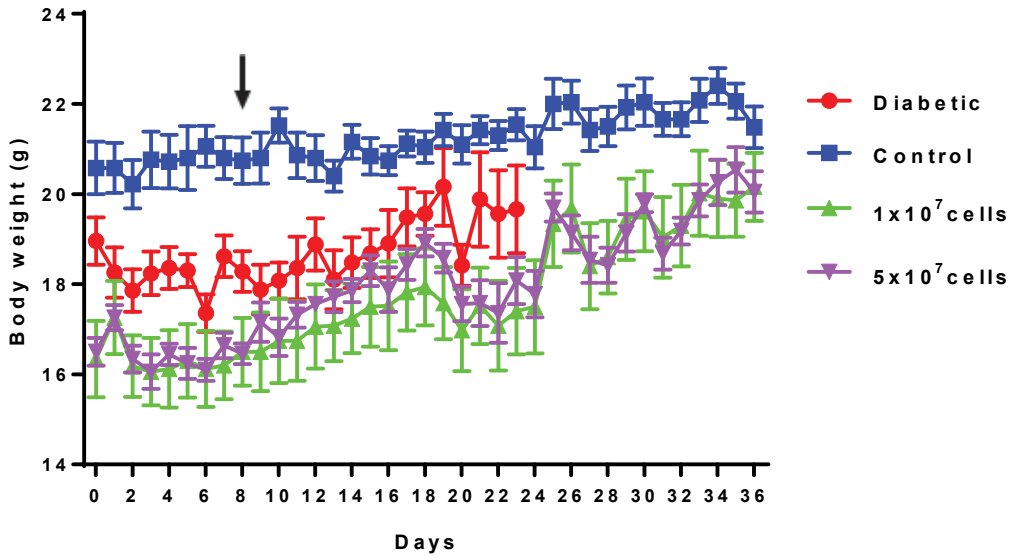

Figure 5.34: Body weight of treated STZ-NOD/*Scid* mice NOD/*Scid* mice had diabetes induced following a peritoneal injection of STZ (170mg/kg), after which diabetic animals received either $1x10^7$ (n=5) or $5x10^7$ (n=5) BMSC-*Luc2/CDUPRT-INS-FUR* subcutaneously behind the neck. Diabetic (n=5) and normal control (n=5) animals were assessed in comparison. The arrowhead indicates the day on which cells were transplanted (Day 8 post STZ-injection). Body weight measurements were recorded daily post STZ-injection for the duration of the experiment (36 days). Data is represented as mean ± SEM. A two-way ANOVA was performed with Sidak's post-hoc, * $p<0.05$.

Table 5.21: Comparison of significance in body weight following cell transplant

	Days																		
	0	1	2	3	4	5	6	7	8	9	10	11	12	13	14	15	16	17	18
Diabetic	ns	ns	ns	*	ns	*	***	ns	*	**	***	*	ns	ns	*	ns	ns	ns	ns
$1x10^7$	***	*	**	***	***	***	****	***	***	***	****	**	**	*	**	*	*	*	ns
$5x10^7$	****	****	****	****	****	****	****	****	****	****	****	****	****	***	****	**	***	***	*
		19	20	21	22	23	24	25	26	27	28	29	30	31	32	33	34	35	36
Diabetic		ns	*	ns	ns	ns	-	-	-	-	-	-	-	-	-	-	-	-	-
$1x10^7$		**	**	**	***	**	*	ns	ns	ns	ns	ns	ns	ns	ns	ns	ns	ns	ns
$5x10^7$		***	****	****	****	****	****	**	****	****	****	***	**	****	**	**	*	ns	ns

A two-way ANOVA with Sidak's post-hoc was performed comparing body weights of diabetic and treated animals in comparison to normal animals for the duration of the experiment. Data is represented as significance, * $p<0.05$.

Of the five diabetic animals that received $5x10^7$ cells, one animal's blood glucose decreased to within 5-10mmol/L six days post cell transplantation and maintained normoglycaemia for a period of three weeks, after which the animal was found deceased unexpectedly. A second animal that received $5x10^7$ cells had blood glucose levels reduced to 5-10mmol/L three weeks post transplantation, after which blood glucose continued to decrease to below 2mmol/L at which point the animal was sacrificed. However, prior to sacrificing, treated animals were tested for glucose tolerance via an IPGTT (Figure 5.35). As can be seen from Figure 5.35, treated animals receiving $5x10^7$ cells (n=3) displayed an abnormal glucose tolerance in comparison to normal control. The high degree of error in the treated group's glucose tolerance was due to one treated animal beginning the IPGTT at a significantly lower blood glucose concentration than the other treated animals, a consequence of the cell transplant having successfully reduced blood glucose levels. Consequently, this resulted in no significant difference in the treated mean blood glucose values in comparison to control animals by two-way ANOVA. Although this is not representative of normal glucose tolerance, as blood glucose levels remain high in the treated group compared to the control at 90 min post glucose bolus.

Organs harvested from the animal that was unexpectedly discovered deceased included the lungs, heart, liver and spleen, which underwent external histological assessment by Cerberus Sciences©. The results of the report showed no abnormalities in the lung or heart. The liver presented with a few dilated portal veins; whilst the spleen was congested, and displayed extramedullary haemopoeisis and follicular depletion. In addition, the transplanted cells recovered from the transplant site behind the neck as a mass were histologically processed. The results indicated that the cell mass was a mesenchymal tumour composed of a heterogeneous population of elongated, spindle-shaped cells with greatly varying nuclear size and shape, and a variable amount of eosinophilic cytoplasm. A high mitotic rate was

observed. Some cells were large and muscle-like (strap cells), while others were more ovoid in shape with nuclear caps at one end (racket cells); in these cells, the nuclei were often bizarre in appearance. The report indicated that the mesenchymal tumour resembled a rhabdomyosarcoma, or malignant tumour of skeletal muscle origin.

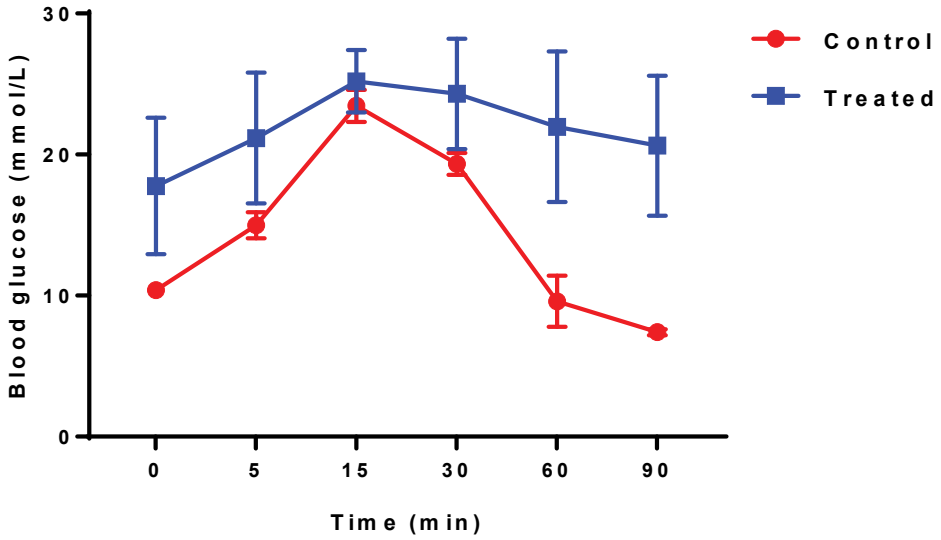

Figure 5.35: IPGTT in treated STZ-diabetic NOD/*Scid* mice An IPGTT was performed on normal animals (n=5) and animals that received a subcutaneous injection of $5x10^7$ cells (n=3). Animals were fasted for 6 hours and subsequently received an intraperitoneal bolus of 50% liquid glucose (0.5g/ml) at 2g/kg. Blood glucose measurements were obtained at 0, 5, 15, 30, 60 and 90min post glucose injection. Data is represented as mean ± SEM. A two-way ANOVA with Sidak's post-hoc test was performed, * $p<0.05$.

5.3 Discussion

Previous studies using non-pancreatic tissues/cells as targets for T1D gene therapy has yielded encouraging results as detailed in Section 1.5.7. However, translation of these findings into the clinical setting has proved challenging due to the nature of the target cells (i.e. tumourigenic cells lines, ESC safety profile), the requirement of immune suppression or encapsulation for transplantation, variability in the differentiated target cell phenotype and function, and difficulties in generating sufficient quantities of target cells for differentiation[383, 384]. To overcome many of these limitations, MSCs have been considered as an attractive alternative target cell due to their ease of gene modification, immunomodulatory properties and ability to be culture-expanded *ex vivo*. However, BMSCs constitute a small proportion of the heterogeneous population of cells within the bone marrow. As a result, obtaining sufficient quantities of BMSCs at early passage is challenging and would not be clinically scalable. In addition, early-passage stem cells (whether MSCs, ESCs or iPSCs) once terminally differentiated into replacement β-cells, would reduce their rate of proliferation[385], thus limiting the number of terminally-differentiated, functional replacement β-cells available for transplantation. As a result, *ex vivo* culture-expanded murine BMSCs were assessed for their ability to differentiate into IPCs via the lentiviral over-expression of pancreatic transcription factors *NeuroD1* and *Pdx1*, and the modified pancreatic hormone *INS-FUR*, as a means of overcoming the limitation of early-passage shortage of primary stem cells.

5.3.1 Lentiviral transduction of BMSCs

The murine *NeuroD1* and the codon-optimised murine *Pdx1* genes were successfully cloned into the existing HMD and HMD-*INS-FUR* lentiviral plasmids for their assessment as

mediators of β-cell differentiation in BMSCs. The co-expression of eGFP and mCherry fluorescent reporters facilitated the analysis of lentiviral transduction efficiency and enrichment of positively transduced BMSCs via FACS for downstream cell culture and analysis of β-cell differentiation. The existing HMD and HMD-*INS-FUR* lentiviral vectors were packaged and concentrated by Dr Binhai Ren for previous *in vivo* studies performed in our laboratory. Specifically, the HMD and HMD-*INS-FUR* lentiviral vectors were packaged in cell factories to accumulate large volumes of viral supernatant, and subsequently concentrated for *in vivo* purposes via tangential flow filtration (TFF)[77, 133]. The remaining lentiviral vector preparations from these previous studies was stored at -80ºC, and subsequently used for *in vitro* transduction of BMSCs in this study. By comparison to the HMD-*NeuroD1*, HMD-*INS-FUR/NeuroD1* and HMD-*Pdx1* lentiviral vectors packaged during this study for *in vitro* purposes, the HMD and HMD-*INS-FUR* vector preparations were of much higher titer; a direct consequence of the scale of vector production and purification by TFF.

BMSCs were transduced with each lentiviral vector at an MOI of 10, and as shown in Figure 5.18, there were titer-related differences in the transduction efficiencies of BMSCs. The high titer HMD and HMD-*INS-FUR* lentiviral vectors resulted in comparable transduction efficiencies of ~50-60%. By comparison, the HMD-*NeuroD1* and HMD-*INS-FUR/NeuroD1* lentiviral vectors demonstrated lower BMSC transduction efficiency of ~10-30%. In addition, it was demonstrated that high glucose concentration and the addition of bFGF did not have an effect on the transduction efficiency of BMCSs. The results of lentiviral transduction of BMSCs in this study are comparable to similar studies utilising lentiviral vectors to gene modify MSCs[386-388]. In addition, as would be expected an increase in transduction efficiency was observed with an increase in MOI, suggesting that at higher MOIs, improved transduction efficiency of BMSCs could have been achieved in this study. The cumulative

results of lentiviral transduction of MSCs reported in this study and in the literature demonstrate that lentiviral vectors are the method of choice for MSC gene modification. Nucleofection was initially used in this study as a means of genetically modifying murine BMSCs due to its reported success in previous work conducted by Martiniello-Wilks *et al*[389]. However, a direct comparison of non-viral and viral methods of gene transfer in rat MSCs highlights the improved transduction efficiency and level of transgene expression in MSCs using lentiviral vectors[390]. In fact, a comparison of the two methods of gene-modification utilised in this study (nucleofection and lentiviral gene transfer) demonstrates the advantages of lentiviral gene transfer over nucleofection. In particular, the ease of generating stable transgene-expressing cell lines with fewer physico-chemical limitations observed with nucleofection. Consequently, if the experiments were to be repeated, lentiviral transduction would be the method of choice for all BMSC gene modification.

5.3.2 *NeuroD1*, *Pdx1* and *INS-FUR* as mediators of β-cell differentiation in *ex vivo* expanded BMSCs

The use of the β-cell transcription factors *NeuroD1*[163, 183, 190] and *Pdx1*[78, 87, 183, 93, 184-187] as mediators of β-cell transdifferentiation in non-pancreatic tissues has been performed in a number of studies. At the commencement of this study, *NeuroD1* was yet to be assessed as a mediator of β-cell differentiation in MSCs. Considering the success of *NeuroD1* as a mediator of β-cell differentiation in non-pancreatic tissues and the lack of research on its effects in MSCs, elucidating the potential of *NeuroD1* to induce β-cell differentiation of MSCs was determined to be of significant interest.

Murine BMSCs were therefore transduced using lentiviral vectors in the first instance to over-express murine *NeuroD1* and *INS-FUR*. A preliminary indicator of β-cell differentiation

from a morphological perspective is the observation of a cuboidal phenotype, followed by stage-specific aggregation of individual cells into islet-like aggregates[391]. Surprisingly, over-expression of *NeuroD1* and *INS-FUR* did not result in any observed morphological changes of transduced BMSCs associated with β-cell differentiation. In addition, gene expression profiling confirmed a lack of β-cell differentiation in transduced BMSCs due to the absence of expression of endogenous pancreatic transcription factors and insulin. However, exogenous expression of *NeuroD1* resulted in the expression of endogenous *NeuroD1*, indicating a potential role of *NeuroD1* in the auto-regulation of its expression. This study is the first study to identify a potential role of *NeuroD1* as an auto-regulator. Alternatively, exogenous *NeuroD1* expression may have initiated differentiation of a neuronal phenotype as has been reported in ESCs[392], however transduced BMSCs did not display a neuronal phenotype, nor was gene expression profiling of genes involved in neuronal development performed to confirm this possibility. However, a recent study by Qing-Song et al, that assessed the effect of *Pdx1*, *NeuroD1* and *MafA* over-expression in BMSCs showed that *NeuroD1* was a weak inducer of endogenous *Pdx1* and *Ins2* expression, and that only in combination with *Pdx1* and *MafA* was there significant induction of β-cell differentiation and insulin secretion[393].

The lack of β-cell differentiation following BMSC transduction with *NeuroD1* was surprising considering its success in other non-pancreatic tissues. A potential explanation for this observation was the use of bFGF in the culture of transduced BMSCs, which may have inhibited the inductive effects of *NeuroD1* by promoting a fibroblast-like morphology. As such, the transduction of BMSCs was repeated in the absence of bFGF, the results of which excluded an inhibitory effect of bFGF on β-cell differentiation. Despite the lack of β-cell differentiation, *INS-FUR* and *NeuroD1/INS-FUR* transduced BMSCs were capable of synthesising and secreting significant quantities of human insulin. However, both *INS-FUR*

and *NeuroD1/INS-FUR*-expressing BMSCs were not glucose-responsive and secreted insulin in a constitutive manner, which is an undesirable feature for a potential β-cell replacement therapy.

A number of studies have shown that *Pdx1* over-expression in MSCs induces β-cell differentiation characterised by the expression of pancreatic transcription factors and insulin secretion[94, 123, 192-195, 196, 92, 197, 198]. As such, and considering the lack of β-cell differentiation mediated by *NeuroD1* over-expression, culture-expanded native BMSCs and BMSCs expressing *INS-FUR* were subsequently transduced with codon-optimised murine *Pdx1* with the hope of inducing β-cell differentiation. Surprisingly, the lack of β-cell differentiation following over-expression of *Pdx1* in native BMSCs and BMSCs expressing *INS-FUR* indicated that culture-expanded BMSCs were defective in their ability to differentiate into IPCs. Upon further examination of the literature, all reported studies of successful differentiation of MSCs into replacement β-cells (both chemically-induced and viral-mediated) were performed using early-passage MSCs.

Collectively, this study (and those previously mentioned), suggest that a combination of pancreatic transcription factors, in combination with *INS-FUR*, may be a more suitable gene therapy regimen for the differentiation of BMSCs into IPCs. However, of critical importance for successful differentiation is the passage at which BMSCs are induced to undergo differentiation. This study highlighted the limitations of targeting culture-expanded BMSCs for β-cell differentiation, specifically their loss of differentiation potential with increasing passage. Although this study demonstrated that at late passage BMSCs are capable of undergoing intrinsic adipogenic and osteogenic differentiation, their propensity for doing so decreased with passage. Ideally, determining the specific passage at which loss of differentiation potential is first observed would provide a time frame for the optimal targeting

of BMSCs for differentiation. It is therefore fitting to speculate that the potential for BMSCs to undergo differentiation towards alternative cell lineages (endodermal in this instance), is diminished with increasing passage. Therefore, targeting of BMSCs for differentiation into β-cells should be performed immediately following isolation and enrichment.

5.3.3 BMSC spheroid formation as a model for islet-cell aggregation

A preliminary study conducted during this project was the assessment of BMSCs expressing *INS-FUR* to undergo islet-like spheroid formation as reported in a previous study utilising PANC-1 cells and hiPCs[382]. The aggregation of hiPCs is an essential process in their subsequent differentiation into islet-like aggregates capable of secreting insulin in a glucose-responsive manner. However, islet-like aggregates derived from hiPCs synthesise and secrete small quantities of insulin that would not be sufficient to reverse diabetes upon transplantation. Thus, our laboratory was interested in determining whether BMSCs expressing *INS-FUR* could be differentiated into similar islet-like aggregates when subjected to a similar chemical-differentiation protocol, a study conducted with assistance of Mr. Saini. However, prior to culturing *INS-FUR*-expressing BMSCs through the complete differentiation protocol, their ability to undergo spheroid formation was first assessed. The results of this study showed that both native BMSCs and *INS-FUR*-expressing BMSCs underwent spheroid formation similar to those derived from hiPCs. However, during the overnight aggregation period (~12-16 hours), an increase in the number of dead cells was observed with increasing time. This was likely due to the adherent property of MSCs, which dictates their preference for adherent tissue culture as opposed to suspension culture.

Despite the success in generating spheroids derived from BMSCs expressing *INS-FUR*, it remains to be seen whether they also undergo differentiation into islet-like aggregates that

express pancreatic transcription factors with regulated insulin secretion. Considering the demonstrated diminished ability of culture-expanded BMSCs to undergo differentiation into β-cells following the expression of pancreatic transcription factors known to induce pancreatic differentiation, it is fitting to hypothesise that culture-expanded BMSCs will not undergo islet-cell differentiation after having formed spheroids and cultured through the specific chemically-defined differentiation protocol described in Hardikar et al[382]. However, as previously mentioned, this could be overcome by using early passage BMSCs.

5.3.4 *INS-FUR*-expressing BMSCs fail to reverse diabetes in STZ-NOD/*Scid* mice

Effective reduction in blood glucose levels is also dependent on the site of cell transplantation. Transplantation sites with poor access to vascular networks are associated with negative transplant outcomes, in particular with relation to correction of hyperglycaemia and graft survival[394]. BMSC persistence studies discussed in Chapter 4 support this observation, with poor BMSC survival following subcutaneous transplantation. However, previous studies conducted in our laboratory have shown that transplantation of liver-derived IPCs behind the neck result in long-term correction of hyperglycaemia[76, 118, 163]. The improved graft survival in these studies was however likely due to the fact that the cells in question had shown significant pancreatic transdifferenciation with both storage of insulin and its secretion in a regulated manner to glucose and other secretogogues. They were also cell lines which may have proliferated in the animal models secreting increased levels of insulin over the experimental period. As a result of the successful correction of hyperglycaemia in these previous studies, the same site was chosen for the transplantation of BMSCs in the current study.

With the *in vitro* characterisation of culture-expanded BMSCs expressing *NeuroD1*, *INS-FUR* and *Pdx1* demonstrating a lack of β-cell transdifferentiation showing no expression of β-cell transcription factors or regulated insulin secretion, BMSCs expressing *INS-FUR* were determined to be the most suitable candidates for transplantation into STZ-NOD/*Scid* mice due to their enhanced insulin secretion in comparison to the other transduced BMSCs. A previous study showed that *in vivo* transplantation is required for functional β-cell maturation[395], therefore *INS-FUR*-expressing BMSCs were assessed for their ability to reverse diabetes following transplantation into STZ-NOD/*Scid* mice. The results of this study showed that a transplantation of $5x10^7$ cells was able to reduce blood glucose levels immediately following transplantation to ~15-20mmol/L (Figure 5.32), however blood glucose levels were not reduced to within the normal physiological range (5-7mmol/L). The reduction in blood glucose concentration was maintained for ~2 weeks, after which blood glucose concentrations began to steadily increase. The increase in blood glucose correlated with the results of the persistence studies conducted in Chapter 4, which showed that in NOD/*Scid* mice, death of transplanted BMSCs began at ~2-3 weeks post transplantation. Consequently, the increase in blood glucose observed in this study was likely a direct consequence of cell death. By comparison to the high cell dose, no decrease in blood glucose levels was observed following transplantation of $1x10^7$ cells. The failure to reduce blood glucose levels to within the normal range could be a result of the severe diabetes induced in the NOD/*Scid* mice, thereby rendering a reduction in blood glucose to within the normal range more challenging.

In addition, an IPGTT was performed on treated animals at 4 weeks post-transplantation to determine their ability to tolerate a bolus of glucose. As expected the treated animals displayed an impaired glucose tolerance in comparison to normal controls, indicating that the transplant had not improved their ability to manage acute episodes of hyperglycaemia,

showing no indication that the *in vivo* environment had stimulated any process that resulted in pancreatic transdifferentiation. By comparison, constitutive secretion of insulin from mouse livers transduced with *INS-FUR*, whilst not inducing normal glucose tolerance did maintain animal blood glucose levels in the 8-10 mmol/L range for several months, with relatively healthy animals[116, 133]. Following graft removal, histological analysis also revealed that the transplanted BMSCs had formed mesenchymal tumours, a deleterious outcome for any potential cell therapy. This is in contrast to many pre-clinical and clinical studies reporting the safety of MSCs[396-398]. However, species-specific differences may contribute to the increased propensity of murine MSCs to form tumours in comparison to human MSCs[399-401]. More importantly, the requirement for *ex vivo* expansion in this study increases the risk of acquired mutations that may have led to BMSC transformation. This highlights the age-dependent utility of MSCs for their use in regenerative medicine, and in particular as targets for gene therapy.

In summary, culture-expanded BMSCs were successfully transduced to over-express the pancreatic transcription factors *NeuroD1* and *Pdx1*, which failed to induce β-cell differentiation. BMSCs transduced to express *INS-FUR* were capable of synthesising and secreting significant quantities of bioactive insulin, however these cells were not glucose-responsive and secreted insulin in a constitutive manner. The lack of β-cell differentiation was due to the reduced differentiation potential of culture-expanded BMSCs, which were likely to also have lost other intrinsic functions. Upon transplantation in STZ-NOD/*Scid* mice, *INS-FUR*-expressing BMSCs were capable of reducing blood glucose levels for a period of 2 weeks (albeit not to within the normal physiological range). The animals receiving cell transplants displayed abnormal glucose tolerance and at least one of the cell grafts developed into a mesenchymal tumour. Cumulatively, this data suggests that culture-expanded BMSCs are not an ideal candidate for T1D gene therapy, and although early

passage BMSCs may be a more suitable target, the inability to culture sufficient numbers at low passage makes this approach problematic for large-scale production needed for gene therapy.

Chapter 6

General Discussion

Introduction

The overall aim of the studies presented in this thesis was to generate an alternative cell replacement therapy via gene therapy for the treatment of T1D. MSCs were conceived as a promising target cell for this purpose due to their ease of isolation and gene modification, capacity to be cultured *ex vivo*, and their ability to differentiate towards both the endodermal and mesodermal lineages.

In this study, MSCs were successfully isolated from the bone marrow of NOD mice, and were shown to possess the well-established functional properties of MSCs. In addition, BMSCs demonstrated high-levels of stable transgene expression following gene-modification via both nucleofection and lentiviral transduction. Nucleofection was successfully utilised to express the *Luc2* and *CDUPRT* genes in *ex vivo* expanded BMSCs, after which 5-FC cytotoxicity assays revealed functional *CDUPRT* suicide gene activity *in vitro*. Lentiviral transduction was successfully utilised to over-express *INS-FUR*, *NeuroD1* and *Pdx1* in *ex vivo* expanded BMSCs, after which it was demonstrated that although *INS-FUR*-expressing BMSCs secreted significant quantities of mature human insulin, the over-expression of *NeuroD1* and *Pdx1* did not result in β-cell differentiation characterised by a lack of β-cell transcription factor expression or regulated insulin secretion. The cumulative results of these studies suggested that *ex vivo* culture-expanded BMSCs were not suitable targets for T1D gene therapy, and that a number of limitations associated with their *ex vivo* expansion ultimately diminished their utility for gene therapy purposes in general.

The remainder of this chapter discusses the limitations of BMCSs as targets for T1D gene and cell therapy identified in this study, and suggests the application of novel technologies that were unavailable at the commencement of this study to overcome these challenges.

6.1 Limitations of *ex vivo* culture expanded BMSCs as targets for T1D gene therapy

For the purposes of this study, *ex vivo* culture expansion of BMSCs was required to generate sufficient quantities of cells for subsequent gene-modification and differentiation into IPCs. This was due to the fact that BMSCs constitute a very small proportion of the total cell population within the bone marrow, and that they also undergo senescence at early passage which significantly inhibited our capacity to rapidly generate large cell quantities. As a consequence, age-related loss of MSC characteristics as demonstrated in this study was likely to be the predominating reason for the lack of success with respect to BMSC survival, differentiation and reversal of diabetes. Although the methods used in this study were suitable to isolate and enrich for a population of cells that displayed many of the characteristic phenotypic and functional properties of MSCs, the results of this study highlighted the limitations of culture-expanded BMSCs as targets for T1D gene therapy.

The lack of immuno-phenotyping, amongst other assays, limited the specific characterisation of culture expanded BMSCs. This highlighted the need for ongoing genetic, phenotypic and functional characterisation of MSCs at multiple stages of MSC therapy development, in particular throughout *ex vivo* culture and manipulation. As a result, changes in MSC characteristics could be identified earlier. However, the results of murine MSC research are not truly representative of human MSCs due to a number of species and strain-specific differences such as the difficulty in growing murine MSCs during early passage without the use of growth factors or co-culture with hematopoietic cells[402, 403], surface marker expression[331, 404], proliferation and differentiation potential[405, 406] and the tendency of murine MSCs tendency to transform *ex vivo*[399-401].

As mentioned previously, MSC research is confounded by accumulating evidence of variation in MSC characterisation and function. Therefore, a broad classification system is destined to continue to yield conflicting data; and highlights the need to generate species, strain and tissue-specific MSC classifications. In spite of this clear necessity, our limited understanding of the role of MSCs *in vivo* will ultimately hamper our ability to connect the *in vivo* situation with that observed *in vitro*. As a result, research conducted to comprehensively understand and clarify these key points may assist in advancing MSC-derived therapies for the treatment of human disease.

With respect to assessing combinatorial gene and MSC therapy for the treatment of T1D, the use of murine MSCs is not the best model due to the aforementioned reasons. Clinically, human MSCs would be the eventual targets for T1D gene therapy; therefore human MSCs are the appropriate target cells to assess in pre-clinical studies. However, a cell replacement therapy for T1D requires large numbers of cells for transplantation, and as such a number of hurdles remain to be overcome for MSCs to become a realistic gene therapy target for T1D. These hurdles include:

1. Scale-up of initial MSC numbers for subsequent genetic modification and differentiation into IPCs without compromising MSC function.
2. Prevention or circumvention of extended cell culture or age-related changes (especially loss of differentiation potential), which severely diminishes their utility as gene therapy targets.
3. Improving efficiency of gene-modification to maximise the quantity of differentiated IPCs.
4. Abrogating recurrent autoimmunity to autologous MSC-derived IPCs.

6.2 Future Directions

The results of this study highlighted that the extended cell culture or age-related limitations of MSCs must be considered prior to targeting MSCs for the application of novel gene therapies. To address this issue, gene modification of MSCs should occur immediately following MSC isolation. This would improve the likelihood of extending their intrinsic properties, and also their potential differentiation into β-cells. The results from this study do not conclusively exclude the potential of *NeuroD*1 or *Pdx1* to induce β-cell differentiation in MSCs due to the late passage at which gene-modification was performed. As a result, was this study to be repeated, the utilisation of the deactivated clustered regularly interspaced short palindromic repeat (CRISPR) system[407, 408] to activate endogenous *NeuroD1* expression in P1-5 MSCs could yield results that more reliably indicate the success of *NeuroD1* in inducing β-cell differentiation. In addition, the deactivated CRISPR system would easily allow for the assessment of alternative β-cell transcription factors without the need to introduce full-length cDNA. This overcomes the transduction efficiency limitation of lentiviral vectors, which decreases with increasing insert size.

Early studies showed that single sgRNAs targeted to the promoter region of target genes activate negligible levels of endogenous gene expression. However, multiplexing with three or more sgRNAs results in synergistic activation of target genes with significant increases in gene expression. More importantly, sgRNA multiplexing can be designed for multiple gene activation thereby eliminating the need to deliver multiple transcription factor cDNAs for robust gene expression to induce differentiation[409]. Improvement in dCas9-transcriptional activator fusions have led to novel gene activators with enhanced activation capabilities compared to early dCas9-VP64 activators. Fusions of dCas9 to multiple co-activators such as the VPR domain (consisting of VP64, p65 and Rta), or specifically engineered dCas9

proteins that utilise modified sgRNAs in conjunction with a synergistic activator complex have been shown to induce robust gene activation[410]. In fact, several recent studies have demonstrated CRISPR-mediated activation of endogenous gene expression for controlled differentiation into diverse cell types[411-413].

By utilising dCas9 activators and multiple sgRNAs to target the endogenous activation of pancreatic transcription factors and/or MSC chemokine receptors in MSCs, it may be possible to direct the differentiation of MSCs into surrogate IPCs capable of maintaining their immunomodulatory properties through *ex vivo* expansion and transplantation (Figure 6.1). To this end, one study in particular has demonstrated success in activating endogenous human insulin transcription utilising the dCas9-VP160 fusion and multiple insulin promoter targeting sgRNAs in HEK293T, Hela and human fibroblasts[414]. The success of this study supports the proposed novel application of activating transcription of endogenous genes involved in pancreatic development such as *Pdx1*, *Neurod1* and *MafA* as mediators of β-cell differentiation in MSCs. In addition, this strategy could be combined with the targeted activation and maintenance of genes involved in MSC immunomodulation such as chemokine receptors and soluble factor production.

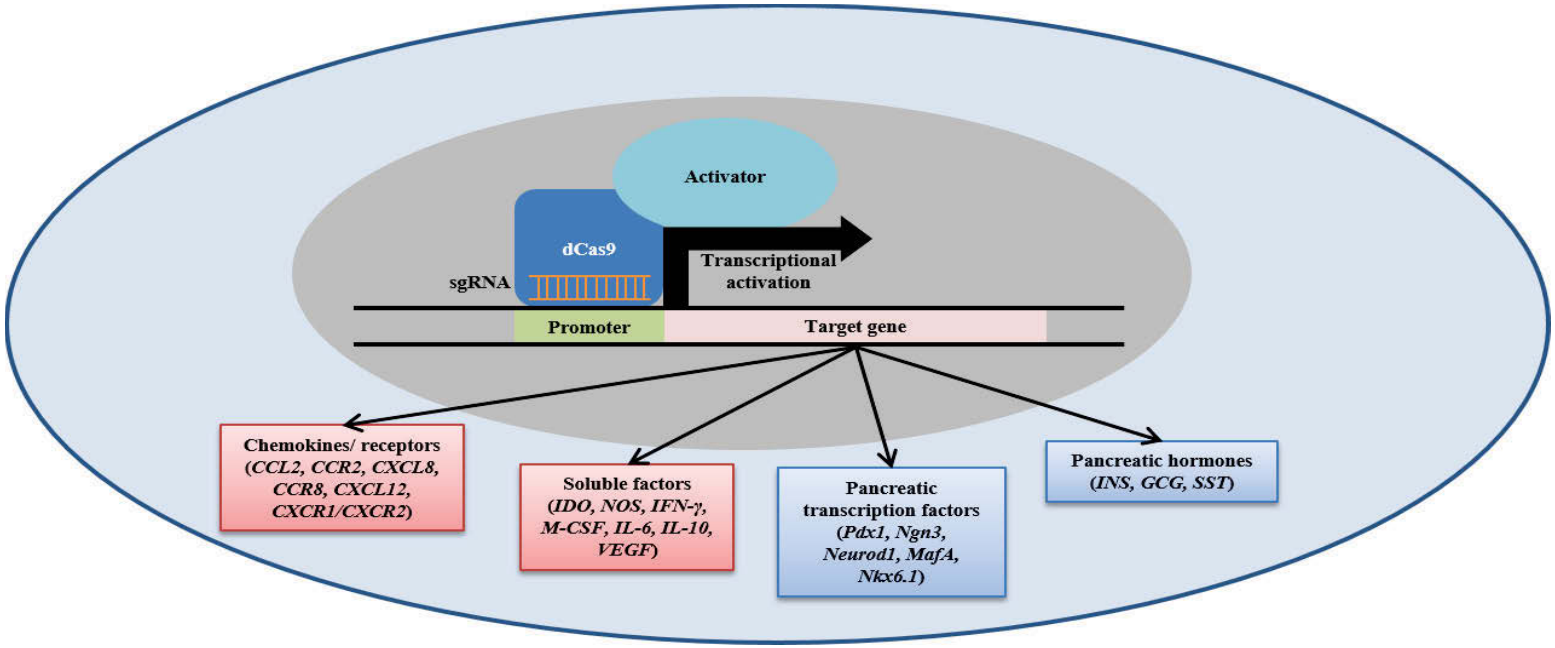

Figure 6.1: CRISPR-mediated generation of IPCs and enhanced MSC-derived immunotherapies Expression of the nuclease-deficient dCas9 fused to a transcriptional activator in MSCs facilitates the activation of endogenous gene expression. To drive the differentiation of MSCs into IPCs (*blue boxes*), sgRNAs targeting the promoter of target genes such as *Pdx-1*, *NeuroD1*, *MafA*, etc., are delivered to MSCs expressing the dCas9-transcription activator fusion. Additional sgRNAs targeting the promoter of genes involved in MSC immunomodulation (*red boxes*) are delivered in combination to maintain the immunomodulatory phenotype of MSCs through multiple cell expansions for the development of therapeutic doses of cell therapy. *CCL* chemokine ligand, *CXCR* chemokine receptor, *dCas9* nuclease-deficient CRISPR-associated protein 9, *GCG* glucagon, *IDO* indoleamine 2,3-deoxygenase, *IFN* interferon, *IL* interleukin, *INS* insulin, *MafA* v-maf musculoaponeurotic fibrosarcoma A, *M-CSF* macrophage colony stimulating factor, *Neurod1* neuronal differentiation 1, *Ngn3* neurogenin 3, *Nkx6.1* NK6 homeobox 1, *NOS* nitric oxide synthase, *Pdx1* pancreatic and duodenal homeobox 1, *sgRNA* short guide RNA, *SST* somatostatin, *VEGF* vascular endothelial growth factor

Nonetheless, despite the demonstrated success in targeting early passage MSCs for differentiation into β-cells[94, 123, 192-195, 196, 92, 197, 198], the overwhelming challenge remains our inability to produce sufficient quantities of transplantable β-cells from MSCs due to the small cellular fraction they represent. Although sourcing MSCs from alternative tissues richer in the abundance of MSCs such as adipose tissue is a popular alternative, their tissue-specific functional differences may limit their propensity/or efficiency to be differentiated into β-cells. *Ex vivo* expansion as a means of overcoming the challenge of MSC shortages proved unsuccessful in this study, as it highlighted MSC age-related deficiencies. Extending the life-span (and potentially the early passage characteristics) of MSCs via the conditional over-expression of genes involved in immortalisation such as the simian virus 40 (SV40T) antigen[415] or human telomerase reverse transcriptase (hTERT)[416] has been shown to overcome the senescence-related limitations of MSCs, whilst demonstrating the maintenance of early passage MSC phenotype and multi-lineage differentiation potential. As a result, MSC immortalisation would allow for the *ex vivo* expansion of MSCs (without the loss of their intrinsic properties), whilst producing sufficient starting quantities of target cells to differentiate into β-cells.

However, the immortalisation of primary stem cells remains controversial as the immortalised cells have the potential to spontaneously transform into malignant cells. Therefore, novel bioprocessing methods such as bioreactors (which remove the transformation-associated risk of immortalised cells) represent a tool that may allow for the optimisation and development of efficient, cost-effective, and easily scalable expansion of MSCs at early passage for human therapy[417, 418]. The integration of viral-mediated gene modification and large-scale MSC production in a combined bioreactor system could potentially represent a new frontier for human T1D gene and cell therapy.

In conclusion, gene and cell therapy for the treatment of T1D is an encouraging alternative to current treatment options. Through careful *in vitro* and pre-clinical experimental design (in particular acknowledging the benefits and limitations of particular cell types), and by implementing the aforementioned strategies, the use of MSCs as targets for T1D gene and cell therapy may become a realistic outcome.

References

1. Margulies D, Ergun-longmire B, Ten S, Maclaren N. *Pediatric Endocrinology, In Chapter 5: Diabetes Mellitus*, New, M., Ed., 2010.

2. van Belle TL, Coppieters KT, von Herrath MG. Type 1 diabetes: etiology, immunology, and therapeutic strategies. *Physiol Rev* 2011; **91**(1)**:** 79-118.

3. Atkinson MA, Maclaren NK. The Pathogenesis of Insulin-Dependent Diabetes Mellitus. *The New England Journal of Medicine* 1994; **19**(331)**:** 1428-1436.

4. Melendez-Ramirez LY, Richards RJ, Cefalu WT. Complications of Type 1 Diabetes. *Endocrinology and metabolism clinics of North America* 2010; **39**(3)**:** 625-640.

5. Cryer PE, Davis SN, Shamoon H. Hypoglycemia in Diabetes. *Diabetes Care* 2003; **26**(6)**:** 1902-1912.

6. Marzorati S, Melzi R, Citro A, Cantarelli E, Mercalli A, Scavini M *et al.* Engraftment Versus Immunosuppression: Cost-Benefit Analysis of Immunosuppression After Intrahepatic Murine Islet Transplantation. *Transplantation* 2014; **97**(10)**:** 1019-1026.

7. Weisman A, Bai J-W, Cardinez M, Kramer CK, Perkins BA. Effect of artificial pancreas systems on glycaemic control in patients with type 1 diabetes: a systematic review and meta-analysis of outpatient randomised controlled trials. *The Lancet Diabetes & Endocrinology* 2017; **5**(7)**:** 501-512.

8. AIHW. *Cardiovascular disease, diabetes and chronic kidney disease: Australian facts: prevalence and incidence*. Canberra: AIHW, 2014.

9. Federation ID. *IDF Diabetes Atlas*, 6th Edition edn Brussels, Belgium: International Diabetes Federation, 2013.

10. Mokdad AH, Ford ES, Bowman BA, et al. Prevalence of obesity, diabetes, and obesity-related health risk factors, 2001. *JAMA* 2003; **289**(1)**:** 76-79.

11. Howard BV. Dietary fat as a risk factor for type 2 diabetes. *Annals of the New York Academy of Sciences* 2002; **967:** 324-328.

12. Hamasaki H. Daily physical activity and type 2 diabetes: A review. *World Journal of Diabetes* 2016; **7**(12)**:** 243-251.

13. Hariri S, Yoon PW, Qureshi N, Valdez R, Scheuner MT, Khoury MJ. Family history of type 2 diabetes: a population-based screening tool for prevention? *Genetics in medicine : official journal of the American College of Medical Genetics* 2006; **8**(2)**:** 102-108.

14. Deeb SS, Fajas L, Nemoto M, Pihlajamaki J, Mykkanen L, Kuusisto J *et al.* A Pro12Ala substitution in PPARgamma2 associated with decreased receptor activity, lower body mass index and improved insulin sensitivity. *Nature genetics* 1998; **20**(3)**:** 284-287.

15. Gloyn AL, Weedon MN, Owen KR, Turner MJ, Knight BA, Hitman G *et al.* Large-scale association studies of variants in genes encoding the pancreatic beta-cell KATP channel subunits Kir6.2 (KCNJ11) and SUR1 (ABCC8) confirm that the KCNJ11 E23K variant is associated with type 2 diabetes. *Diabetes* 2003; **52**(2)**:** 568-572.

16. Tong Y, Lin Y, Zhang Y, Yang J, Zhang Y, Liu H *et al.* Association between TCF7L2 gene polymorphisms and susceptibility to type 2 diabetes mellitus: a large Human Genome Epidemiology (HuGE) review and meta-analysis. *BMC medical genetics* 2009; **10:** 15.

17. Mahajan A, Go MJ, Zhang W, Below JE, Gaulton KJ, Ferreira T *et al.* Genome-wide trans-ancestry meta-analysis provides insight into the genetic architecture of type 2 diabetes susceptibility. *Nature genetics* 2014; **46**(3)**:** 234-244.

18. Cho YS, Chen CH, Hu C, Long J, Ong RT, Sim X *et al.* Meta-analysis of genome-wide association studies identifies eight new loci for type 2 diabetes in east Asians. *Nature genetics* 2011; **44**(1)**:** 67-72.

19. Dunn CJ, Peters DH. Metformin. A review of its pharmacological properties and therapeutic use in non-insulin-dependent diabetes mellitus. *Drugs* 1995; **49**(5)**:** 721-749.

20. Marble A. Glibenclamide, a new sulphonylurea: whither oral hypoglycaemic agents? *Drugs* 1971; **1**(2)**:** 109-115.

21. Gangji AS, Cukierman T, Gerstein HC, Goldsmith CH, Clase CM. A Systematic Review and Meta-Analysis of Hypoglycemia and Cardiovascular Events. *A comparison of glyburide with other secretagogues and with insulin* 2007; **30**(2)**:** 389-394.

22. Shaw J, Tanamas S. *Diabetes: the silent pandemic and its impact on Australia*. Diabetes Australia, 2012.

23. Colagiuri S, Colagiuri R, Conway B, Davey P, Grainger D. *DiabCo$t Australia: Assessing the burden of Type 2 diabetes in Australia*, 2003.

24. Colagiuri S, Brnabic, A., Gomez, M., Fitzgerald, B.,, Buckley AC, R. *DiabCo$t Australia Type 1: Assessing the burden of Type 1 Diabetes in Australia*. Canberra: Diabetes Australia, 2009a.

25. Eisenbarth GS. Type I Diabetes Mellitus. *New England Journal of Medicine* 1986; **314**(21)**:** 1360-1368.

26. Nerup J, Platz P, Andersen OO, Christy M, Lyngsoe J, Poulsen JE *et al.* HL-A Antigens and Diabetes Mellitus. *The Lancet* 1974; **304**(7885)**:** 864-866.

27. Cudworth AG, Woodrow JC. Evidence for HL-A-linked genes in "juvenile" diabetes mellitus. *Br Med J* 1975; **3**(5976)**:** 133-135.

28. Todd JA, Acha-Orbea H, Bell JI, Chao N, Fronek Z, Jacob CO *et al.* A molecular basis for MHC class II--associated autoimmunity. *Science* 1988; **240**(4855)**:** 1003-1009.

29. Farid NR, Sampson L, Noel P, Barnard JM, Davis AJ, Hillman DA. HLA-D–related (DRw) Antigens in Juvenile Diabetes Mellitus. *Diabetes* 1979; **28**(6)**:** 552-557.

30. Owerbach D, Lernmark A, Platz P, Ryder LP, Rask L, Peterson PA *et al.* HLA-D region beta-chain DNA endonuclease fragments differ between HLA-DR identical healthy and insulin-dependent diabetic individuals. *Nature* 1983; **303**(5920)**:** 815-817.

31. Lernmark A. Molecular biology of IDDM. *Diabetologia* 1994; **37 Suppl 2:** 73-81.

32. Lie BA, Todd JA, Pociot F, Nerup J, Akselsen HE, Joner G *et al.* The predisposition to type 1 diabetes linked to the human leukocyte antigen complex includes at least one non-class II gene. *American Journal of Human Genetics* 1999; **64**(3)**:** 793-800.

33. Nejentsev S, Howson JMM, Walker NM, Szeszko J, Field SF, Stevens HE *et al.* Localization of type 1 diabetes susceptibility to the MHC class I genes HLA-B and HLA-A. *Nature* 2007; **450**(7171)**:** 887-892.

34. Panagiotopoulos C, Qin H, Tan R, Verchere CB. Identification of a beta-cell-specific HLA class I restricted epitope in type 1 diabetes. *Diabetes* 2003; **52**(11)**:** 2647-2651.

35. Marron MP, Graser RT, Chapman HD, Serreze DV. Functional evidence for the mediation of diabetogenic T cell responses by HLA-A2.1 MHC class I molecules through transgenic expression in NOD mice. *Proc Natl Acad Sci U S A* 2002; **99**(21)**:** 13753-13758.

36. Rotwein P, Yokoyama S, Didier DK, Chirgwin JM. Genetic analysis of the hypervariable region flanking the human insulin gene. *American Journal of Human Genetics* 1986; **39**(3)**:** 291-299.

37. Bell GI, Karam JH, Rutter WJ. Polymorphic DNA region adjacent to the 5' end of the human insulin gene. *Proc Natl Acad Sci U S A* 1981; **78**(9)**:** 5759-5763.

38. Todd JA. Genetic analysis of type 1 diabetes using whole genome approaches. *Proc Natl Acad Sci U S A* 1995; **92**(19)**:** 8560-8565.

39. Bottini N, Musumeci L, Alonso A, Rahmouni S, Nika K, Rostamkhani M *et al.* A functional variant of lymphoid tyrosine phosphatase is associated with type I diabetes. *Nature genetics* 2004; **36**(4)**:** 337-338.

40. Bottini N, Vang T, Cucca F, Mustelin T. Role of PTPN22 in type 1 diabetes and other autoimmune diseases. *Seminars in immunology* 2006; **18**(4)**:** 207-213.

41. Wenzlau JM, Juhl K, Yu L, Moua O, Sarkar SA, Gottlieb P *et al.* The cation efflux transporter ZnT8 (Slc30A8) is a major autoantigen in human type 1 diabetes. *Proc Natl Acad Sci U S A* 2007; **104**(43)**:** 17040-17045.

42. Gillespie KM, Bain SC, Barnett AH, Bingley PJ, Christie MR, Gill GV *et al.* The rising incidence of childhood type 1 diabetes and reduced contribution of high-risk HLA haplotypes. *Lancet* 2004; **364**(9446)**:** 1699-1700.

43. Yoon JW, Onodera T, Notkins AL. Virus-induced diabetes mellitus. XV. Beta cell damage and insulin-dependent hyperglycemia in mice infected with coxsackie virus B4. *The Journal of experimental medicine* 1978; **148**(4)**:** 1068-1080.

44. Foulis AK, Farquharson MA, Cameron SO, McGill M, Schönke H, Kandolf R. A search for the presence of the enteroviral capsid protein VP1 in pancreases of patients with Type 1 (insulin-dependent) diabetes and pancreases and hearts of infants who died of coxsackieviral myocarditis. *Diabetologia* 1990; **33**(5)**:** 290-298.

45. Richardson SJ, Willcox A, Bone AJ, Foulis AK, Morgan NG. The prevalence of enteroviral capsid protein vp1 immunostaining in pancreatic islets in human type 1 diabetes. *Diabetologia* 2009; **52**(6)**:** 1143-1151.

46. Dotta F, Censini S, van Halteren AGS, Marselli L, Masini M, Dionisi S *et al.* Coxsackie B4 virus infection of β cells and natural killer cell insulitis in recent-onset type 1 diabetic patients. *Proceedings of the National Academy of Sciences of the United States of America* 2007; **104**(12)**:** 5115-5120.

47. Tracy S, Drescher KM, Chapman NM, Kim KS, Carson SD, Pirruccello S *et al.* Toward testing the hypothesis that group B coxsackieviruses (CVB) trigger insulin-dependent diabetes: inoculating nonobese diabetic mice with CVB markedly lowers diabetes incidence. *J Virol* 2002; **76**(23)**:** 12097-12111.

48. Honeyman MC, Coulson BS, Stone NL, Gellert SA, Goldwater PN, Steele CE *et al.* Association between rotavirus infection and pancreatic islet autoimmunity in children at risk of developing type 1 diabetes. *Diabetes* 2000; **49**(8)**:** 1319-1324.

49. Pak CY, Eun HM, McArthur RG, Yoon JW. Association of cytomegalovirus infection with autoimmune type 1 diabetes. *Lancet* 1988; **2**(8601)**:** 1-4.

50. Kasuga A, Harada R, Saruta T. Insulin-dependent diabetes mellitus associated with parvovirus B19 infection. *Annals of internal medicine* 1996; **125**(8)**:** 700-701.

51. Jordan GW, Cohen SH. Encephalomyocarditis virus-induced diabetes mellitus in mice: model of viral pathogenesis. *Reviews of infectious diseases* 1987; **9**(5)**:** 917-924.

52. Bach J-F. The Effect of Infections on Susceptibility to Autoimmune and Allergic Diseases. *New England Journal of Medicine* 2002; **347**(12)**:** 911-920.

53. Brugman S, Klatter F, Visser J, Wildeboer-Veloo A, Harmsen H, Rozing J *et al.* Antibiotic treatment partially protects against type 1 diabetes in the Bio-Breeding diabetes-prone rat. Is the gut flora involved in the development of type 1 diabetes? *Diabetologia* 2006; **49**(9)**:** 2105-2108.

54. Calcinaro F, Dionisi S, Marinaro M, Candeloro P, Bonato V, Marzotti S *et al.* Oral probiotic administration induces interleukin-10 production and prevents spontaneous autoimmune diabetes in the non-obese diabetic mouse. *Diabetologia* 2005; **48**(8)**:** 1565-1575.

55. Rosu V, Ahmed N, Paccagnini D, Gerlach G, Fadda G, Hasnain SE *et al.* Specific Immunoassays Confirm Association of Mycobacterium avium paratuberculosis with Type-1 but Not Type-2 Diabetes Mellitus. *PLoS ONE* 2009; **4**(2)**:** e4386.

56. Karjalainen J, Martin JM, Knip M, Ilonen J, Robinson BH, Savilahti E *et al.* A bovine albumin peptide as a possible trigger of insulin-dependent diabetes mellitus. *N Engl J Med* 1992; **327**(5)**:** 302-307.

57. Klemetti P, Savilahti E, Ilonen J, Akerblom HK, Vaarala O. T-cell reactivity to wheat gluten in patients with insulin-dependent diabetes mellitus. *Scand J Immunol* 1998; **47**(1)**:** 48-53.

58. Norris JM, Barriga K, Klingensmith G, Hoffman M, Eisenbarth GS, Erlich HA *et al.* Timing of initial cereal exposure in infancy and risk of islet autoimmunity. *Jama* 2003; **290**(13)**:** 1713-1720.

59. Kukreja A, Maclaren NK. Autoimmunity and diabetes. *The Journal of clinical endocrinology and metabolism* 1999; **84**(12)**:** 4371-4378.

60. Stassi G, De Maria R, Trucco G, Rudert W, Testi R, Galluzzo A *et al.* Nitric oxide primes pancreatic beta cells for Fas-mediated destruction in insulin-dependent diabetes mellitus. *The Journal of experimental medicine* 1997; **186**(8)**:** 1193-1200.

61. Redd S, Ginn S, Ross JM. Fas and Fas ligand immunolocalization in pancreatic islets of NOD mice during spontaneous and cyclophosphamide-accelerated diabetes. *The Histochemical journal* 2002; **34**(1-2)**:** 1-12.

62. Association AD. Standards of Medical Care in Diabetes—2015 Abridged for Primary Care Providers. *Clinical Diabetes* 2015; **33**(2)**:** 97-111.

63. Fowler MJ. Microvascular and Macrovascular Complications of Diabetes. *Clinical Diabetes* 2008; **26**(2)**:** 77-82.

64. Keenan HA, Costacou T, Sun JK, Doria A, Cavellerano J, Coney J *et al.* Clinical Factors Associated With Resistance to Microvascular Complications in Diabetic Patients of Extreme Disease Duration. *The 50-year Medalist Study* 2007; **30**(8)**:** 1995-1997.

65. Gabbay KH. Hyperglycaemia, Polyol Metabolism, and Complications Of Diabetes-Mellitus. *Annual Review of Medicine* 1975; **26:** 521-536.

66. Fong DS, Aiello LP, Ferris FL, Klein R. Diabetic Retinopathy. *Diabetes Care* 2004; **27**(10)**:** 2540-2553.

67. Aiello LP, Pierce EA, Foley ED, Takagi H, Chen H, Riddle L *et al.* Suppression of retinal neovascularization in vivo by inhibition of vascular endothelial growth factor (VEGF) using soluble VEGF-receptor chimeric proteins. *Proc Natl Acad Sci U S A* 1995; **92**(23)**:** 10457-10461.

68. Gross JL, de Azevedo MJ, Silveiro SP, Canani LH, Caramori ML, Zelmanovitz T. Diabetic Nephropathy: Diagnosis, Prevention, and Treatment. *Diabetes Care* 2005; **28**(1)**:** 164-176.

69. Boulton AJM, Vinik AI, Arezzo JC, Bril V, Feldman EL, Freeman R *et al.* Diabetic Neuropathies. *A statement by the American Diabetes Association* 2005; **28**(4)**:** 956-962.

70. Paterson AD, Rutledge BN, Cleary PA, Lachin JM, Crow RS. The Effect of Intensive Diabetes Treatment on Resting Heart Rate in Type 1 Diabetes. *The Diabetes Control and Complications Trial/Epidemiology of Diabetes Interventions and Complications Study* 2007; **30**(8)**:** 2107-2112.

71. Nathan DM, Cleary PA, Backlund JYC, Genuth SM, Lachin JM, Orchard TJ *et al.* Intensive diabetes treatment and cardiovascular disease in patients with type 1 diabetes. *New England Journal of Medicine* 2005; **353**(25)**:** 2643-2653.

72. Hirshberg B, Rother KI, Digon BJ, 3rd, Lee J, Gaglia JL, Hines K *et al.* Benefits and risks of solitary islet transplantation for type 1 diabetes using steroid-sparing immunosuppression: the National Institutes of Health experience. *Diabetes Care* 2003; **26**(12)**:** 3288-3295.

73. Deng YM, Tuch BE, Rawlinson WD. Transmission of porcine endogenous retroviruses in severe combined immunodeficient mice xenotransplanted with fetal porcine pancreatic cells. *Transplantation* 2000; **70**(7)**:** 1010-1016.

74. Hering BJ, Wijkstrom M, Graham ML, Hardstedt M, Aasheim TC, Jie T *et al.* Prolonged diabetes reversal after intraportal xenotransplantation of wild-type porcine islets in immunosuppressed nonhuman primates. *Nat Med* 2006; **12**(3)**:** 301-303.

75. Stewart C, Taylor NA, Green IC, Docherty K, Bailey CJ. Insulin-releasing pituitary cells as a model for somatic cell gene therapy in diabetes mellitus. *Journal of Endocrinology* 1994; **142**(2)**:** 339-343.

76. Tuch BE, Szymanska B, Yao M, Tabiin MT, Gross DJ, Holman S *et al.* Function of a genetically modified human liver cell line that stores, processes and secretes insulin. *Gene Ther* 2003; **10**(6)**:** 490-503.

77. Ren B, O'Brien BA, Swan MA, Koina ME, Nassif N, Wei MQ *et al.* Long-term correction of diabetes in rats after lentiviral hepatic insulin gene therapy. *Diabetologia* 2007; **50**(9)**:** 1910-1920.

78. Ferber S, Halkin A, Cohen H, Ber I, Einav Y, Goldberg I *et al.* Pancreatic and duodenal homeobox gene 1 induces expression of insulin genes in liver and ameliorates streptozotocin-induced hyperglycemia. *Nat Med* 2000; **6**(5)**:** 568-572.

79. Barnes AJ, Bloom SR. Pancreatectomised man: A mode for diabetes without glucagon. *The Lancet* 1976; **307**(7953)**:** 219-221.

80. Bono VH, Jr. Review of mechanism of action studies of the nitrosoureas. *Cancer treatment reports* 1976; **60**(6)**:** 699-702.

81. Dekel Y, Glucksam Y, Elron-Gross I, Margalit R. Insights into modeling streptozotocin-induced diabetes in ICR mice. *Lab animal* 2009; **38**(2)**:** 55-60.

82. Leiter EH. Multiple low-dose streptozotocin-induced hyperglycemia and insulitis in C57BL mice: influence of inbred background, sex, and thymus. *Proc Natl Acad Sci USA* 1982; **79**(2)**:** 630-634.

83. Nerup J, Mandrap-Poulsen T, Helqvist S, Andersen HU, Pociot F, Reimers JI *et al.* On the pathogenesis of IDDM. *Diabetologia* 1994; **37**(2)**:** S82-S89.

84. Szkudelski T. The mechanism of alloxan and streptozotocin action in B cells of the rat pancreas. *Physiological research / Academia Scientiarum Bohemoslovaca* 2001; **50**(6)**:** 537-546.

85. Grossman EJ, Lee DD, Tao J, Wilson RA, Park S-Y, Bell GI *et al.* Glycemic Control Promotes Pancreatic Beta-Cell Regeneration in Streptozotocin-Induced Diabetic Mice. *PLoS ONE* 2010; **5**(1)**:** e8749.

86. Hanafusa T, Miyagawa J, Nakajima H, Tomita K, Kuwajima M, Matsuzawa Y *et al.* The NOD mouse. *Diabetes research and clinical practice* 1994; **24 Suppl:** S307-311.

87. Yoon JW, Jun HS. Cellular and molecular pathogenic mechanisms of insulin-dependent diabetes mellitus. *Annals of the New York Academy of Sciences* 2001; **928:** 200-211.

88. Yang Y, Santamaria P. Lessons on autoimmune diabetes from animal models. *Clin Sci* 2006; **110**(6)**:** 627-639.

89. Zhao Y, Jiang Z, Zhao T, Ye M, Hu C, Yin Z *et al.* Reversal of type 1 diabetes via islet beta cell regeneration following immune modulation by cord blood-derived multipotent stem cells. *BMC medicine* 2012; **10**(1)**:** 3.

90. Zhao Y, Lin B, Darflinger R, Zhang Y, Holterman MJ, Skidgel RA. Human Cord Blood Stem Cell-Modulated Regulatory T Lymphocytes Reverse the Autoimmune-Caused Type 1 Diabetes in Non-obese Diabetic (NOD) Mice. *PLoS ONE* 2009; **4**(1)**:** e4226.

91. Roep BO, Tree TIM. Immune modulation in humans: implications for type 1 diabetes mellitus. *Nat Rev Endocrinol* 2014; **10**(4)**:** 229-242.

92. Kajiyama H, Hamazaki TS, Tokuhara M, Masui S, Okabayashi K, Ohnuma K *et al.* Pdx1-transfected adipose tissue-derived stem cells differentiate into insulin-producing cells in vivo and reduce hyperglycemia in diabetic mice. *Int J Dev Biol* 2010; **54**(4)**:** 699-705.

93. Fodor A, Harel C, Fodor L, Armoni M, Salmon P, Trono D *et al.* Adult rat liver cells transdifferentiated with lentiviral IPF1 vectors reverse diabetes in mice: an ex vivo gene therapy approach. *Diabetologia* 2007; **50**(1)**:** 121-130.

94. Karnieli O, Izhar-Prato Y, Bulvik S, Efrat S. Generation of insulin-producing cells from human bone marrow mesenchymal stem cells by genetic manipulation. *STEM CELLS* 2007; **25**(11)**:** 2837-2844.

95. Driver JP, Serreze DV, Chen YG. Mouse models for the study of autoimmune type 1 diabetes: a NOD to similarities and differences to human disease. *Seminars in immunopathology* 2011; **33**(1)**:** 67-87.

96. Rossini AA, Handler ES, Mordes JP, Greiner DL. Human Autoimmune Diabetes Mellitus: Lessons from BB Rats and NOD Mice—Caveat Emptor. *Clinical Immunology and Immunopathology* 1995; **74**(1)**:** 2-9.

97. Prochazka M, Serreze DV, Frankel WN, Leiter EH. NOR/Lt Mice: MHC-Matched Diabetes-Resistant Control Strain for NOD Mice. *Diabetes* 1992; **41**(1)**:** 98-106.

98. Nakhooda AF, Like AA, Chappel CI, Murray FT, Marliss EB. The spontaneously diabetic Wistar rat. Metabolic and morphologic studies. *Diabetes* 1977; **26**(2)**:** 100-112.

99. Mordes JP, Bortell R, Blankenhorn EP, Rossini AA, Greiner DL. Rat models of type 1 diabetes: genetics, environment, and autoimmunity. *ILAR journal / National Research Council, Institute of Laboratory Animal Resources* 2004; **45**(3)**:** 278-291.

100. Lenzen S, Tiedge M, Elsner M, Lortz S, Weiss H, Jörns A *et al.* The LEW.1AR1/Ztm-iddm rat: a new model of spontaneous insulin-dependent diabetes mellitus. *Diabetologia* 2001; **44**(9)**:** 1189-1196.

101. Kramer JW, Nottingham S, Robinette J, Lenz G, Sylvester S, Dessouky MI. Inherited, early onset, insulin-requiring diabetes mellitus of Keeshond dogs. *Diabetes* 1980; **29**(7)**:** 558-565.

102. Howard CF. Spontaneous Diabetes in Macaca Nigra. *Diabetes* 1972; **21**(11)**:** 1077-1090.

103. Mathews CE, Langley SH, Leiter EH. New mouse model to study islet transplantation in insulin-dependent diabetes mellitus. *Transplantation* 2002; **73**(8)**:** 1333-1336.

104. Yoon J-W, London WT, Curfman BL, Brown RL, Notkins AL. Coxsackie Virus B4 Produces Transient Diabetes in Nonhuman Primates. *Diabetes* 1986; **35**(6)**:** 712-716.

105. Craighead JE, McLane MF. Diabetes Mellitus: Induction in Mice by Encephalomyocarditis Virus. *Science* 1968; **162**(3856)**:** 913-914.

106. Guberski D, Thomas V, Shek W, Like A, Handler E, Rossini A *et al.* Induction of type I diabetes by Kilham's rat virus in diabetes-resistant BB/Wor rats. *Science* 1991; **254**(5034)**:** 1010-1013.

107. Laub O, Rutter WJ. Expression of the human insulin gene and cDNA in a heterologous mammalian system. *Journal of Biological Chemistry* 1983; **258**(10)**:** 6043-6050.

108. Iwata H, Ogawa N, Takagi T, Mizoguchi J. Preparation of Insulin-Releasing Chinese Hamster Ovary Cell by Transfection of Human Insulin Gene. In: *Polymers of Biological and Biomedical Significance*, vol. 540. American Chemical Society, 1993, pp 306-313.

109. Zaret KS, Grompe M. Generation and Regeneration of Cells of the Liver and Pancreas. *Science* 2008; **322**(5907)**:** 1490-1494.

110. Stewart C, Taylor NA, Green JC, Docherty K, Bailey CJ. Insulin-releasing pituitary cells as a model for somatic cell gene therapy in diabetes mellitus. *Journal of Endocrinology* 1994; **142**(2)**:** 339-343.

111. Hughes SD, Quaade C, Johnson JH, Ferber S, Newgard CB. Transfection of AtT-20ins cells with GLUT-2 but not GLUT-1 confers glucose-stimulated insulin secretion. Relationship to glucose metabolism. *Journal of Biological Chemistry* 1993; **268**(20)**:** 15205-15212.

112. Barry SC, Ramesh N, Lejnieks D, Simonson WT, Kemper L, Lernmark A *et al.* Glucose-regulated insulin expression in diabetic rats. *Hum Gene Therapy* 2001; **12**(2)**:** 131-139.

113. Mas A, Montané J, Anguela XM, Muñoz S, Douar AM, Riu E *et al.* Reversal of Type 1 Diabetes by Engineering a Glucose Sensor in Skeletal Muscle. *Diabetes* 2006; **55**(6)**:** 1546-1553.

114. Zaret KS. Genetic programming of liver and pancreas progenitors: lessons for stem-cell differentiation. *Nat Rev Genet* 2008; **9**(5)**:** 329-340.

115. Vollenweider F, Irminger JC, Gross DJ, Villa-Komaroff L, Halban PA. Processing of proinsulin by transfected hepatoma (FAO) cells. *The Journal of biological chemistry* 1992; **267**(21)**:** 14629-14636.

116. Elsner M, Terbish T, Jorns A, Naujok O, Wedekind D, Hedrich H-J *et al.* Reversal of Diabetes Through Gene Therapy of Diabetic Rats by Hepatic Insulin Expression via Lentiviral Transduction. *Molecular therapy : the journal of the American Society of Gene Therapy* 2012; **20**(5)**:** 918-926.

117. Short DK, Okada S, Yamauchi K, Pessin JE. Adenovirus-mediated transfer of a modified human proinsulin gene reverses hyperglycemia in diabetic mice. *The American journal of physiology* 1998; **275**(5 Pt 1)**:** E748-756.

118. Lawandi J, Tao C, Ren B, Williams P, Ling D, Swan MA *et al.* Reversal of diabetes following transplantation of an insulin-secreting human liver cell line: Melligen cells. *Molecular Therapy — Methods & Clinical Development* 2015; **2:** 15011.

119. Morgan RA, Anderson WF. Human gene therapy. *Annu Rev Biochem* 1993; **62:** 191-217.

120. Bushman FD. Retroviral integration and human gene therapy. *The Journal of Clinical Investigation* 2007; **117**(8)**:** 2083-2086.

121. Cavazzana-Calvo M, Hacein-Bey S, de Saint Basile G, Gross F, Yvon E, Nusbaum P *et al.* Gene therapy of human severe combined immunodeficiency (SCID)-X1 disease. *Science* 2000; **288**(5466)**:** 669-672.

122. Laufs S, Nagy KZ, Giordano FA, Hotz-Wagenblatt A, Zeller WJ, Fruehauf S. Insertion of Retroviral Vectors in NOD/SCID Repopulating Human Peripheral Blood Progenitor Cells Occurs Preferentially in the Vicinity of Transcription Start Regions and in Introns. *Molecular therapy : the journal of the American Society of Gene Therapy* 2004; **10**(5)**:** 874-881.

123. Li Y, Zhang R, Qiao H, Zhang H, Wang Y, Yuan H *et al.* Generation of insulin-producing cells from PDX-1 gene-modified human mesenchymal stem cells. *Journal of Cellular Physiology* 2007; **211**(1)**:** 36-44.

124. Volpers C, Kochanek S. Adenoviral vectors for gene transfer and therapy. *The Journal of Gene Medicine* 2004; **6**(S1)**:** S164-S171.

125. Wold WS, Doronin K, Toth K, Kuppuswamy M, Lichtenstein DL, Tollefson AE. Immune responses to adenoviruses: viral evasion mechanisms and their implications for the clinic. *Curr Opin Immunol* 1999; **11**(4)**:** 380-386.

126. McCaffrey AP, Fawcett P, Nakai H, McCaffrey RL, Ehrhardt A, Pham TT *et al.* The host response to adenovirus, helper-dependent adenovirus, and adeno-associated virus in mouse liver. *Molecular therapy : the journal of the American Society of Gene Therapy* 2008; **16**(5)**:** 931-941.

127. Alba R, Bosch A, Chillon M. Gutless adenovirus: last-generation adenovirus for gene therapy. *Gene Therapy* 2005; **12:** 18-27.

128. Zhou HS, Liu DP, Liang CC. Challenges and strategies: the immune responses in gene therapy. *Med Res Rev* 2004; **24**(6)**:** 748-761.

129. Muzyczka N. Use of Adeno-Associated Virus as a General Transduction Vector for Mammalian Cells. In: Muzyczka N (ed) *Viral Expression Vectors*, vol. 158. Springer Berlin Heidelberg, 1992, pp 97-129.

130. Sugiyama A, Hattori S, Tanaka S, Isoda F, Kleopoulos S, Rosenfeld M *et al.* Defective adenoassociated viral-mediated transfection of insulin gene by direct injection into liver parenchyma decreases blood glucose of diabetic mice. *Horm Metab Res* 1997; **29**(12)**:** 599-603.

131. Yoon JW, Jun HS. Recent advances in insulin gene therapy for type 1 diabetes. *Trends in Molecular Medicine* 2002; **8**(2)**:** 62-68.

132. Zufferey R, Dull T, Mandel RJ, Bukovsky A, Quiroz D, Naldini L *et al.* Self-inactivating lentivirus vector for safe and efficient in vivo gene delivery. *J Virol* 1998; **72**(12)**:** 9873-9880.

133. Ren B, O'Brien BA, Byrne MR, Ch'ng E, Gatt PN, Swan MA *et al.* Long-term reversal of diabetes in non-obese diabetic mice by liver-directed gene therapy. *J Gene Med* 2013; **15**(1)**:** 28-41.

134. Gerace D, Ren B, Hawthorne WJ, Byrne MR, Phillips PM, O'Brien BA *et al.* Pancreatic Transdifferentiation in Porcine Liver Following Lentiviral Delivery of Human Furin–Cleavable Insulin. *Transplantation Proceedings* 2013; **45**(5)**:** 1869-1874.

135. Shanmukhappa K, Mourya R, Sabla GE, Degen JL, Bezerra JA. Hepatic to pancreatic switch defines a role for hemostatic factors in cellular plasticity in mice. *Proc Natl Acad Sci U S A* 2005; **102**(29)**:** 10182-10187.

136. Han J, McLane B, Kim E-H, Yoon J-W, Jun H-S. Remission of Diabetes by Insulin Gene Therapy Using a Hepatocyte-specific and Glucose-responsive Synthetic Promoter. *Molecular therapy : the journal of the American Society of Gene Therapy* 2011; **19**(3)**:** 470-478.

137. Hsu P-J, Kotin R, Yang Y-W. Glucose- and Metabolically Regulated Hepatic Insulin Gene Therapy for Diabetes. *Pharm Res* 2008; **25**(6)**:** 1460-1468.

138. Brunner Y, Coute Y, Iezzi M, Foti M, Fukuda M, Hochstrasser DF *et al.* Proteomics Analysis of Insulin Secretory Granules. *Molecular & Cellular Proteomics* 2007; **6:** 1007-1017.

139. Lee HC, Kim SJ, Kim KS, Shin HC, Yoon JW. Remission in models of type 1 diabetes by gene therapy using a single-chain insulin analogue. *Nature* 2000; **408**(6811)**:** 483-488.

140. Thule PM, Liu J, Phillips LS. Glucose regulated production of human insulin in rat hepatocytes. *Gene Therapy* 2000; **7:** 205-214.

141. Thule PM, Liu J. Regulated hepatic insulin gene therapy of STZ-diabetic rats *Gene Therapy* 2000; **7:** 1744-1752.

142. Mitanchez D, Doiron B, Chen R, Kahn A. Glucose-Stimulated Genes and Prospects of Gene Therapy for Type I Diabetes. *Endocrine Reviews* 1997; **18**(4)**:** 520-540.

143. Chen R, Meseck M, McEvoy RC, Woo SL. Glucose-stimulated and self-limiting insulin production by glucose 6-phosphatase promoter driven insulin expression in hepatoma cells. *Gene Ther* 2000; **7**(21)**:** 1802-1809.

144. Chen NK, Tan SY, Udolph G, Kon OL. Insulin expressed from endogenously active glucose-responsive EGR1 promoter in bone marrow mesenchymal stromal cells as diabetes therapy. *Gene Ther* 2010; **17**(5)**:** 592-605.

145. Harada S, Smith RM, Smith JA, Shah N, Hu DQ, Jarett L. Insulin-induced egr-1 expression in Chinese hamster ovary cells is insulin receptor and insulin receptor substrate-1 phosphorylation-independent. Evidence of an alternative signal transduction pathway. *The Journal of biological chemistry* 1995; **270**(44)**:** 26632-26638.

146. Rees DA, Alcolado JC. Animal models of diabetes mellitus. *Diabetic medicine : a journal of the British Diabetic Association* 2005; **22**(4)**:** 359-370.

147. Sander M, Griffen SC, Huang J, German MS. A novel glucose-responsive element in the human insulin gene functions uniquely in primary cultured islets. *Proc Natl Acad Sci USA* 1998; **95**(20)**:** 11572-11577.

148. Burkhardt BR, Loiler SA, Anderson JA, Kilberg MS, Crawford JM, Flotte TR *et al.* Glucose-responsive expression of the human insulin promoter in HepG2 human hepatoma cells. *Annals of the New York Academy of Sciences* 2003; **1005:** 237-241.

149. Burkhardt BR, Yang MC, Robert CE, Greene SR, McFadden KK, Yang J *et al.* Tissue-specific and glucose-responsive expression of the pancreatic derived factor (PANDER) promoter. *Biochim Biophys Acta* 2005; **1730**(3)**:** 215-225.

150. Kojima H, Fujimiya M, Matsumura K, Younan P, Imaeda H, Maeda M *et al.* NeuroD-betacellulin gene therapy induces islet neogenesis in the liver and reverses diabetes in mice. *Nat Med* 2003; **9**(5)**:** 596-603.

151. Nathwani AC, Tuddenham EG, Rangarajan S, Rosales C, McIntosh J, Linch DC *et al.* Adenovirus-associated virus vector-mediated gene transfer in hemophilia B. *N Engl J Med* 2011; **365**(25)**:** 2357-2365.

152. Lisowski L, Dane AP, Chu K, Zhang Y, Cunningham SC, Wilson EM *et al.* Selection and evaluation of clinically relevant AAV variants in a xenograft liver model. *Nature* 2014; **506**(7488)**:** 382-386.

153. Apelqvist A, Li H, Sommer L, Beatus P, Anderson DJ, Honjo T *et al.* Notch signalling controls pancreatic cell differentiation. *Nature* 1999; **400**(6747)**:** 877-881.

154. Sommer L, Ma Q, Anderson DJ. neurogenins, a novel family of atonal-related bHLH transcription factors, are putative mammalian neuronal determination genes that reveal progenitor cell heterogeneity in the developing CNS and PNS. *Mol Cell Neurosci* 1996; **8**(4)**:** 221-241.

155. Shanmukhappa K, Mourya R, Sabla GE, Degen JL, Bezerra JA. Hepatic to pancreatic switch defines a role for hemostatic factors in cellular plasticity in mice. *Proceedings of the National Academy of Sciences of the United States of America* 2005; **102**(29)**:** 10182-10187.

156. Kim S, Shin J-S, Kim H-J, Fisher RC, Lee M-J, Kim C-W. Streptozotocin-induced diabetes can be reversed by hepatic oval cell activation through hepatic transdifferentiation and pancreatic islet regeneration. *Lab Invest* 2007; **87**(7)**:** 702-712.

157. Yang L, Li S, Hatch H, Ahrens K, Cornelius JG, Petersen BE *et al.* In vitro trans-differentiation of adult hepatic stem cells into pancreatic endocrine hormone-producing cells. *Proc Natl Acad Sci U S A* 2002; **99**(12)**:** 8078-8083.

158. Tatake RJ, O'Neill MM, Kennedy CA, Reale VD, Runyan JD, Monaco K-AD *et al.* Glucose-regulated insulin production from genetically engineered human non-beta cells. *Life Sciences* 2007; **81**(17–18)**:** 1346-1354.

159. Tudurí E, Bruin JE, Kieffer TJ. Restoring insulin production for type 1 diabetes. *Journal of Diabetes* 2012; **4**(4)**:** 319-331.

160. Tabiin MT, Tuch BE, Bai L, Han XG, Simpson AM. Susceptibility of insulin-secreting hepatocytes to the toxicity of pro-inflammatory cytokines. *Journal of autoimmunity* 2001; **17**(3)**:** 229-242.

161. Tuch BE, Beynon S, Tabiin MT, Sassoon R, Goodman RJ, Simpson AM. Effect of beta-cell toxins on genetically engineered insulin-secreting cells. *Journal of autoimmunity* 1997; **10**(3)**:** 239-244.

162. Tabiin MT, White CP, Morahan G, Tuch BE. Insulin expressing hepatocytes not destroyed in transgenic NOD mice. *J Autoimmune Dis* 2004; **1**(1)**:** 3.

163. Ren B, Tao C, Swan MA, Joachim N, Martiniello-Wilks R, Nassif NT *et al.* Pancreatic Transdifferentiation and Glucose-Regulated Production of Human Insulin in the H4IIE Rat Liver Cell Line. *International Journal of Molecular Sciences* 2016; **17**(4)**:** 534.

164. Chakrabarti SK, Mirmira RG. Transcription factors direct the development and function of pancreatic beta cells. *TRENDS in Endocrinology and Metabolism* 2003; **14**(2)**:** 78-84.

165. Gerace D, Martiniello-Wilks R, O'Brien BA, Simpson AM. The use of β-cell transcription factors in engineering artificial β-cells from non-pancreatic tissue. *Gene Ther* 2015; **22**(1)**:** 1-8.

166. Ang SL, Wierda A, Wong D, Stevens KA, Cascio S, Rossant J *et al.* The formation and maintenance of the definitive endoderm lineage in the mouse: involvement of HNF3/forkhead proteins. *Development* 1993; **119**(4)**:** 1301-1315.

167. Korolija M, Hadzija MP, Hadzija M. Molecular mechanism in Beta-cell development: The role of Pdx1, Ngn3 and Pax4 proteins. *Periodicum Biologorum* 2009; **111**(1)**:** 59-63.

168. Melloul D, Marshak S, Cerasi E. Regulation of pdx-1 gene expression. *Diabetes* 2002; **51**(3)**:** S320-325.

169. Jonsson J, Carlsson L, Edlund T, Edlund H. Insulin-promoter-factor 1 is required for pancreas development in mice. *Nature* 1994; **371**(6498)**:** 606-609.

170. Offield MF, Jetton TL, Labosky PA, Ray M, Stein RW, Magnuson MA *et al.* PDX-1 is required for pancreatic outgrowth and differentiation of the rostral duodenum. *Development* 1996; **122**(3)**:** 983-995.

171. Gu G, Dubauskaite J, Melton DA. Direct evidence for the pancreatic lineage: NGN3+ cells are islet progenitors and are distinct from duct progenitors. *Development* 2002; **129**(10)**:** 2447-2457.

172. Gazave E, Lapebie P, Richards G, Brunet F, Ereskovsky A, Degnan B *et al.* Origin and evolution of the Notch signalling pathway: an overview from eukaryotic genomes. *BMC Evolutionary Biology* 2009; **9**(1)**:** 249.

173. Gradwohl G, Dierich A, LeMeur M, Guillemot F. Neurogenin3 is required for the development of the four endocrine cell lineages of the pancreas. *Proc Natl Acad Sci U S A* 2000; **97**(4)**:** 1607-1611.

174. Gasa R, Mrejen C, Lynn FC, Skewes-Cox P, Sanchez L, Yang KY *et al.* Induction of pancreatic islet cell differentiation by the neurogenin-neuroD cascade. *Differentiation* 2008; **76**(4)**:** 381-391.

175. Naya FJ, Huang HP, Qiu Y, Mutoh H, DeMayo FJ, Leiter AB *et al.* Diabetes, defective pancreatic morphogenesis, and abnormal enteroendocrine differentiation in BETA2/neuroD-deficient mice. *Genes Dev* 1997; **11**(18)**:** 2323-2334.

176. St-Onge L, Sosa-Pineda B, Chowdhury K, Mansouri A, Gruss P. Pax6 is required for differentiation of glucagon-producing alpha-cells in mouse pancreas. *Nature* 1997; **387**(6631)**:** 406-409.

177. Sander M, Griffen SC, Huang J, German MS. A novel glucose-responsive element in the human insulin gene functions uniquely in primary cultured islets. *Proc Natl Acad Sci U S A* 1998; **95**(20)**:** 11572-11577.

178. Sander N, Sussel L, Conners J, Scheel D, Kalamaras J, Dela Cruz F *et al.* Homeobox gene Nkx6.1 lies downstream of Nkx2.2 in the major pathway of beta-cell formation in the pancreas. *Development* 2000; **127**(24)**:** 5533-5540.

179. Kaneto H, Matsuoka T-a, Nakatani Y, Miyatsuka T, Matsuhisa M, Hori M *et al.* A Crucial Role of MafA as a Novel Therapeutic Target for Diabetes. *Journal of Biological Chemistry* 2005; **280**(15)**:** 15047-15052.

180. Glauser DA, Schlegel W. The emerging role of FOXO transcription factors in pancreatic β cells. *Journal of Endocrinology* 2007; **193**(2)**:** 195-207.

181. Cerf ME. Transcription factors regulating beta-cell function. *European Journal of Endocrinology* 2006; **155**(5)**:** 671-679.

182. Melloul D, Marshak S, Cerasi E. Regulation of insulin gene transcription. *Diabetologia* 2002; **45**(3)**:** 309-326.

183. Kojima H, Fujimiya M, Matsumura K, Younan P, Imaeda H, Maeda M *et al.* NeuroD-betacellulin gene therapy induces islet neogenesis in the liver and reverses diabetes in mice. *Nature Medicine* 2003; **9**(5)**:** 596-603.

184. Ber I, Shternhall K, Perl S, Ohanuna Z, Goldberg I, Barshack I *et al.* Functional, persistent, and extended liver to pancreas transdifferentiation. *Journal of Biological Chemistry* 2003; **278**(34)**:** 31950-31957.

185. Wang AY, Ehrhardt A, Xu H, Kay MA. Adenovirus transduction is required for the correction of diabetes using Pdx-1 or Neurogenin-3 in the liver. *Mol Ther* 2007; **15**(2)**:** 255-263.

186. Sapir T, Shternhall K, Meivar-Levy I, Blumenfeld T, Cohen H, Skutelsky E *et al.* Cell-replacement therapy for diabetes: Generating functional insulin-producing tissue from adult human liver cells. *Proceedings of the National Academy of Sciences* 2005; **102**(22)**:** 7964-7969.

187. Nagaya M, Katsuta H, Kaneto H, Bonner-Weir S, Weir GC. Adult mouse intrahepatic biliary epithelial cells induced in vitro to become insulin-producing cells. *J Endocrinol* 2009; **201**(1)**:** 37-47.

188. Taniguchi H, Yamato E, Tashiro F, Ikegami H, Ogihara T, Miyazaki J. beta-cell neogenesis induced by adenovirus-mediated gene delivery of transcription factor pdx-1 into mouse pancreas. *Gene Ther* 2003; **10**(1)**:** 15-23.

189. Yoshida S, Kajimoto Y, Yasuda T, Watada H, Fujitani Y, Kosaka H *et al.* PDX-1 Induces Differentiation of Intestinal Epithelioid IEC-6 Into Insulin-Producing Cells. *Diabetes* 2002; **51**(8)**:** 2505-2513.

190. Noguchi H, Xu G, Matsumoto S, Kaneto H, Kobayashi N, Bonner-Weir S *et al.* Induction of pancreatic stem/progenitor cells into insulin-producing cells by adenoviral-mediated gene transfer technology. *Cell Transplant* 2006; **15**(10)**:** 929-938.

191. Zhou Q, Brown J, Kanarek A, Rajagopal J, Melton DA. In vivo reprogramming of adult pancreatic exocrine cells to β-cells. *Nature* 2008; **455**(7213)**:** 627-632.

192. Sun J, Yang Y, Wang X, Song J, Jia Y. Expression of Pdx-1 in bone marrow mesenchymal stem cells promotes differentiation of islet-like cells in vitro. *Sci China C Life Sci* 2006; **49**(5)**:** 480-489.

193. Limbert C, Path G, Ebert R, Rothhammer V, Kassem M, Jakob F *et al.* PDX1- and NGN3-mediated in vitro reprogramming of human bone marrow-derived mesenchymal stromal cells into pancreatic endocrine lineages. *Cytotherapy* 2011; **13**(7)**:** 802-813.

194. Moriscot C, de Fraipont F, Richard M-J, Marchand M, Savatier P, Bosco D *et al.* Human Bone Marrow Mesenchymal Stem Cells Can Express Insulin and Key Transcription Factors of the Endocrine Pancreas Developmental Pathway upon Genetic and/or Microenvironmental Manipulation In Vitro. *STEM CELLS* 2005; **23**(4)**:** 594-603.

195. Li L, Li F, Qi H, Feng G, Yuan K, Deng H *et al.* Coexpression of Pdx1 and betacellulin in mesenchymal stem cells could promote the differentiation of nestin-positive epithelium-like progenitors and pancreatic islet-like spheroids. *Stem Cells Dev* 2008; **17**(4)**:** 815-823.

196. He D, Wang J, Gao Y, Zhang Y. Differentiation of PDX1 gene-modified human umbilical cord mesenchymal stem cells into insulin-producing cells in vitro. *Int J Mol Med* 2011; **28**(6)**:** 1019-1024.

197. Baer PC. Adipose-derived stem cells and their potential to differentiate into the epithelial lineage. *Stem Cells Dev* 2011; **20**(10)**:** 1805-1816.

198. Lin G, Wang G, Liu G, Yang LJ, Chang LJ, Lue TF *et al.* Treatment of type 1 diabetes with adipose tissue-derived stem cells expressing pancreatic duodenal homeobox 1. *Stem Cells Dev* 2009; **18**(10)**:** 1399-1406.

199. Miyazaki S, Yamato E, Miyazaki J-i. Regulated Expression of pdx-1 Promotes In Vitro Differentiation of Insulin-Producing Cells From Embryonic Stem Cells. *Diabetes* 2004; **53**(4)**:** 1030-1037.

200. Lavon N, Yanuka O, Benvenisty N. The effect of overexpression of Pdx1 and Foxa2 on the differentiation of human embryonic stem cells into pancreatic cells. *STEM CELLS* 2006; **24**(8)**:** 1923-1930.

201. Vincent R, Treff N, Budde M, Kastenberg Z, Odorico J. Generation and characterization of novel tetracycline-inducible pancreatic transcription factor-expressing murine embryonic stem cell lines. *Stem Cells Dev* 2006; **15**(6)**:** 953-962.

202. Raikwar SP, Zavazava N. PDX1-engineered embryonic stem cell-derived insulin producing cells regulate hyperglycemia in diabetic mice. *Transplant Res* 2012; **1**(1)**:** 2047-1440.

203. Kaneto H, Nakatani Y, Miyatsuka T, Matsuoka TA, Matsuhisa M, Hori M *et al.* PDX-1/VP16 fusion protein, together with NeuroD or Ngn3, markedly induces insulin gene transcription and ameliorates glucose tolerance. *Diabetes* 2005; **54**(4)**:** 1009-1022.

204. Wang AY, Ehrhardt A, Xu H, Kay MA. Adenovirus transduction is required for the correction of diabetes using Pdx-1 or Neurogenin-3 in the liver. *Molecular therapy : the journal of the American Society of Gene Therapy* 2007; **15**(2)**:** 255-263.

205. Song YD, Lee EJ, Yashar P, Pfaff LE, Kim SY, Jameson JL. Islet cell differentiation in liver by combinatorial expression of transcription factors neurogenin-3, BETA2, and RIPE3b1. *Biochem Biophys Res Commun* 2007; **354**(2)**:** 334-339.

206. Heremans Y, Van De Casteele M, in't Veld P, Gradwohl G, Serup P, Madsen O *et al.* Recapitulation of embryonic neuroendocrine differentiation in adult human pancreatic duct cells expressing neurogenin 3. *J Cell Biol* 2002; **159**(2)**:** 303-312.

207. Yechoor V, Liu V, Espiritu C, Paul A, Oka K, Kojima H *et al.* Neurogenin3 is sufficient for transdetermination of hepatic progenitor cells into neo-islets in vivo but not transdifferentiation of hepatocytes. *Developmental cell* 2009; **16**(3)**:** 358-373.

208. Yatoh S, Akashi T, Chan PP, Kaneto H, Sharma A, Bonner-Weir S *et al.* NeuroD and reaggregation induce β-cell specific gene expression in cultured hepatocytes. *Diabetes/Metabolism Research and Reviews* 2007; **23**(3)**:** 239-249.

209. Blyszczuk P, Czyz J, Kania G, Wagner M, Roll U, St-Onge L *et al.* Expression of Pax4 in embryonic stem cells promotes differentiation of nestin-positive progenitor and insulin-producing cells. *Proceedings of the National Academy of Sciences* 2003; **100**(3)**:** 998-1003.

210. Liew CG, Shah NN, Briston SJ, Shepherd RM, Khoo CP, Dunne MJ *et al.* PAX4 enhances beta-cell differentiation of human embryonic stem cells. *PLoS ONE* 2008; **3**(3).

211. Gefen-Halevi S, Rachmut IH, Molakandov K, Berneman D, Mor E, Meivar-Levy I *et al.* NKX6.1 promotes PDX-1-induced liver to pancreatic beta-cells reprogramming. *Cell Reprogram* 2010; **12**(6)**:** 655-664.

212. Duarte S, Carle G, Faneca H, Lima MCPd, Pierrefite-Carle V. Suicide gene therapy in cancer: Where do we stand now? *Cancer Letters* 2012; **324**(2)**:** 160-170.

213. Bondanza A, Hambach L, Aghai Z, Nijmeijer B, Kaneko S, Mastaglio S *et al.* IL-7 receptor expression identifies suicide gene-modified allospecific CD8+ T cells capable of self-renewal and differentiation into antileukemia effectors. *Blood* 2011; **117**(24)**:** 6469-6478.

214. Freytag SO, Movsas B, Aref I, Stricker H, Peabody J, Pegg J *et al.* Phase I trial of replication-competent adenovirus-mediated suicide gene therapy combined with IMRT for prostate cancer. *Molecular Therapy* 2007; **15**(5)**:** 1016-1023.

215. Pandha HS, Martin LA, Rigg A, Hurst HC, Stamp GWH, Sikora K *et al.* Genetic prodrug activation therapy for breast cancer: A phase I clinical trial of erbB-2-directed suicide gene expression. *Journal of Clinical Oncology* 1999; **17**(7)**:** 2180-2189.

216. Wang J, Lu XX, Chen DZ, Li SF, Zhang LS. Herpes simplex virus thymidine kinase and ganciclovir suicide gene therapy for human pancreatic cancer. *World Journal of Gastroenterology* 2004; **10**(3)**:** 400-403.

217. Ketola A, Määttä AM, Pasanen T, Tulimäki K, Wahlfors J. Osteosarcoma and chondrosarcoma as targets for virus vectors and herpes simplex virus thymidine kinase/ganciclovir gene therapy. *International journal of molecular medicine* 2004; **13**(5)**:** 705-710.

218. Fischer U, Steffens S, Frank S, Rainov NG, Schulze-Osthoff K, Kramm CM. Mechanisms of thymidine kinase/ganciclovir and cytosine deaminase/5-fluorocytosine suicide gene therapy-induced cell death in glioma cells. *Oncogene* 2005; **24**(7)**:** 1231-1243.

219. Khatri A, Zhang B, Doherty E, Chapman J, Ow K, Pwint H *et al.* Combination of cytosine deaminase with uracil phosphoribosyl transferase leads to local and distant bystander effects against RM1 prostate cancer in mice. *The Journal of Gene Medicine* 2006; **8**(9)**:** 1086-1096.

220. Kanai F, Kawakami T, Hamada H, Sadata A, Yoshida Y, Tanaka T *et al.* Adenovirus-mediated transduction of Escherichia coli uracil phosphoribosyltransferase gene sensitizes cancer cells to low concentrations of 5-fluorouracil. *Cancer Research* 1998; **58**(9)**:** 1946-1951.

221. Freeman SM, Abboud CN, Whartenby KA, Packman CH, Koeplin DS, Moolten FL *et al.* The "Bystander Effect": Tumor Regression When a Fraction of the Tumor Mass Is Genetically Modified. *Cancer Research* 1993; **53**(21)**:** 5274-5283.

222. Hu YL, Fu YH, Tabata Y, Gao JQ. Mesenchymal stem cells: A promising targeted-delivery vehicle in cancer gene therapy. *Journal of Controlled Release* 2010; **147**(2)**:** 154-162.

223. Kim SU. Neural Stem Cell-based Gene Therapy for Brain Tumors. *Stem Cell Reviews and Reports* 2011; **7**(1)**:** 130-140.

224. Kucerova L, Altanerova V, Matuskova M, Tyciakova S, Altaner C. Adipose tissue-derived human mesenchymal stem cells mediated prodrug cancer gene therapy. *Cancer Research* 2007; **67**(13)**:** 6304-6313.

225. Chang DY, Yoo SW, Hong Y, Kim S, Kim SJ, Yoon SH *et al.* The growth of brain tumors can be suppressed by multiple transplantation of mesenchymal stem cells expressing cytosine deaminase. *International Journal of Cancer* 2010; **127**(8)**:** 1975-1983.

226. Friedenstein AJ, Deriglasova UF, Kulagina NN, Panasuk AF, Rudakowa SF, Luria EA *et al.* Precursors for fibroblasts in different populations of hematopoietic cells as detected by the in vitro colony assay method. *Exp Hematol* 1974; **2**(2)**:** 83-92.

227. Vija L, Farge D, Gautier JF, Vexiau P, Dumitrache C, Bourgarit A *et al.* Mesenchymal stem cells: Stem cell therapy perspectives for type 1 diabetes. *Diabetes Metab* 2009; **35**(2)**:** 85-93.

228. Augello A, Kurth TB, De Bari C. Mesenchymal stem cells: a perspective from in vitro cultures to in vivo migration and niches. *Eur Cell Mater* 2010; **20:** 121-133.

229. Dominici M, Le Blanc K, Mueller I, Slaper-Cortenbach I, Marini F, Krause D *et al.* Minimal criteria for defining multipotent mesenchymal stromal cells. The International Society for Cellular Therapy position statement. *Cytotherapy* 2006; **8**(4)**:** 315-317.

230. Tyndall A, Walker UA, Cope A, Dazzi F, De Bari C, Fibbe W *et al.* Immunomodulatory properties of mesenchymal stem cells: a review based on an interdisciplinary meeting held at the Kennedy Institute of Rheumatology Division, London, UK, 31 October 2005. *Arthritis Res Ther* 2007; **9**(1)**:** 301.

231. Abdi R, Fiorina P, Adra CN, Atkinson M, Sayegh MH. Immunomodulation by mesenchymal stem cells: a potential therapeutic strategy for type 1 diabetes. *Diabetes* 2008; **57**(7)**:** 1759-1767.

232. Bassi EJ, Aita CA, Camara NO. Immune regulatory properties of multipotent mesenchymal stromal cells: Where do we stand? *World J Stem Cells* 2011; **3**(1)**:** 1-8.

233. De Ugarte DA, Morizono K, Elbarbary A, Alfonso Z, Zuk PA, Zhu M *et al.* Comparison of multi-lineage cells from human adipose tissue and bone marrow. *Cells Tissues Organs* 2003; **174**(3)**:** 101-109.

234. Campagnoli C, Roberts IAG, Kumar S, Bennett PR, Bellantuono I, Fisk NM. Identification of mesenchymal stem/progenitor cells in human first-trimester fetal blood, liver, and bone marrow. *Blood* 2001; **98**(8)**:** 2396-2402.

235. In't Anker PS, Scherjon SA, Kleijburg-Van Der Keur C, De Groot-Swings GMJS, Claas FHJ, Fibbe WE *et al.* Isolation of mesenchymal stem cells of fetal or maternal origin from human placenta. *Stem Cells* 2004; **22**(7)**:** 1338-1345.

236. Noort WA, Kruisselbrink AB, In't Anker PS, Kruger M, Van Bezooijen RL, De Paus RA *et al.* Mesenchymal stem cells promote engraftment of human umbilical cord blood-derived CD34+ cells in NOD/SCID mice. *Experimental Hematology* 2002; **30**(8)**:** 870-878.

237. Wang HS, Hung SC, Peng ST, Huang CC, Wei HM, Guo YJ *et al.* Mesenchymal stem cells in the Wharton's jelly of the human umbilical cord. *Stem Cells* 2004; **22**(7)**:** 1330-1337.

238. Fan CG, Tang FW, Zhang QJ, Lu SH, Liu HY, Zhao ZM *et al.* Characterization and neural differentiation of fetal lung mesenchymal stem cells. *Cell Transplantation* 2005; **14**(5)**:** 311-321.

239. Sato T, Hidaka K, Iwanaga A, Ito M, Asano M, Nakabeppu Y *et al.* Impairment of cardiomyogenesis in embryonic stem cells lacking scaffold protein JSAP1. *Biochemical and Biophysical Research Communications* 2005; **338**(2)**:** 1152-1157.

240. Rasmusson I. Immune modulation by mesenchymal stem cells. *Experimental cell research* 2006; **312**(12)**:** 2169-2179.

241. Gebler A, Zabel O, Seliger B. The immunomodulatory capacity of mesenchymal stem cells. *Trends in Molecular Medicine* 2012; **18**(2)**:** 128-134.

242. Ben-Ami E, Berrih-Aknin S, Miller A. Mesenchymal stem cells as an immunomodulatory therapeutic strategy for autoimmune diseases. *Autoimmunity Reviews* 2011; **10**(7)**:** 410-415.

243. Han KH, Ro H, Hong JH, Lee EM, Cho B, Yeom HJ *et al.* Immunosuppressive mechanisms of embryonic stem cells and mesenchymal stem cells in alloimmune response. *Transplant Immunology* 2011; **25**(1)**:** 7-15.

244. da Silva Meirelles L, Fontes AM, Covas DT, Caplan AI. Mechanisms involved in the therapeutic properties of mesenchymal stem cells. *Cytokine & growth factor reviews* 2009; **20**(5)**:** 419-427.

245. Le Blanc K, Tammik L, Sundberg B, Haynesworth SE, Ringdén O. Mesenchymal Stem Cells Inhibit and Stimulate Mixed Lymphocyte Cultures and Mitogenic Responses Independently of the Major Histocompatibility Complex. *Scandinavian Journal of Immunology* 2003; **57**(1)**:** 11-20.

246. Devine SM, Cobbs C, Jennings M, Bartholomew A, Hoffman R. Mesenchymal stem cells distribute to a wide range of tissues following systemic infusion into nonhuman primates. *Blood* 2003; **101**(8)**:** 2999-3001.

247. Benvenuto F, Ferrari S, Gerdoni E, Gualandi F, Frassoni F, Pistoia V *et al.* Human Mesenchymal Stem Cells Promote Survival of T Cells in a Quiescent State. *STEM CELLS* 2007; **25**(7)**:** 1753-1760.

248. Xue Q, Luan XY, Gu YZ, Wu HY, Zhang GB, Yu GH *et al.* The negative co-signaling molecule b7-h4 is expressed by human bone marrow-derived mesenchymal stem cells and mediates its T-cell modulatory activity. *Stem Cells Dev* 2010; **19**(1)**:** 27-38.

249. Augello A, Tasso R, Negrini SM, Amateis A, Indiveri F, Cancedda R *et al.* Bone marrow mesenchymal progenitor cells inhibit lymphocyte proliferation by activation of the programmed death 1 pathway. *Eur J Immunol* 2005; **35**.

250. Chamberlain G, Fox J, Ashton B, Middleton J. Concise Review: Mesenchymal Stem Cells: Their Phenotype, Differentiation Capacity, Immunological Features, and Potential for Homing. *STEM CELLS* 2007; **25**(11)**:** 2739-2749.

251. Shi M, Liu ZW, Wang FS. Immunomodulatory properties and therapeutic application of mesenchymal stem cells. *Clinical & Experimental Immunology* 2011; **164**(1)**:** 1-8.

252. Nauta AJ, Kruisselbrink AB, Lurvink E, Willemze R, Fibbe WE. Mesenchymal Stem Cells Inhibit Generation and Function of Both CD34+-Derived and Monocyte-Derived Dendritic Cells. *The Journal of Immunology* 2006; **177**(4)**:** 2080-2087.

253. Glennie S, Soeiro I, Dyson PJ, Lam EWF, Dazzi F. Bone marrow mesenchymal stem cells induce division arrest anergy of activated T cells. *Blood* 2005; **105**(7)**:** 2821-2827.

254. Corcione A, Benvenuto F, Ferretti E, Giunti D, Cappiello V, Cazzanti F *et al.* Human mesenchymal stem cells modulate B-cell functions. *Blood* 2006; **107**(1)**:** 367-372.

255. Deng W, Han Q, Liao L, You S, Deng H, Zhao RCH. Effects of allogeneic bone marrow-derived mesenchymal stem cells on T and B lymphocytes from BXSB mice. *DNA and Cell Biology* 2005; **24**(7)**:** 458-463.

256. Traggiai E, Volpi S, Schena F, Gattorno M, Ferlito F, Moretta L *et al.* Bone marrow-derived mesenchymal stem cells induce both polyclonal expansion and differentiation of B cells isolated from healthy donors and systemic lupus erythematosus patients. *Stem Cells* 2008; **26**(2)**:** 562-569.

257. Krampera M, Cosmi L, Angeli R, Pasini A, Liotta F, Andreini A *et al.* Role for Interferon-γ in the Immunomodulatory Activity of Human Bone Marrow Mesenchymal Stem Cells. *STEM CELLS* 2006; **24**(2)**:** 386-398.

258. Rasmusson I, Ringden O, Sundberg B, Le Blanc K. Mesenchymal stem cells inhibit the formation of cytotoxic T lymphocytes, but not activated cytotoxic T lymphocytes or natural killer cells. *Transplantation* 2003; **76**(8)**:** 1208-1213.

259. Sotiropoulou PA, Perez SA, Gritzapis AD, Baxevanis CN, Papamichail M. Interactions between human mesenchymal stem cells and natural killer cells. *STEM CELLS* 2006; **24**(1)**:** 74-85.

260. Spaggiari GM, Capobianco A, Abdelrazik H, Becchetti F, Mingari MC, Moretta L. Mesenchymal stem cells inhibit natural killer-cell proliferation, cytotoxicity, and cytokine production: role of indoleamine 2,3-dioxygenase and prostaglandin E2. *Blood* 2008; **111**(3)**:** 1327-1333.

261. Jiang XX, Zhang Y, Liu B, Zhang SX, Wu Y, Yu XD *et al.* Human mesenchymal stem cells inhibit differentiation and function of monocyte-derived dendritic cells. *Blood* 2005; **105**(10)**:** 4120-4126.

262. Zhang W, Ge W, Li C, You S, Liao L, Han Q *et al.* Effects of mesenchymal stem cells on differentiation, maturation, and function of human monocyte-derived dendritic cells. *Stem Cells Dev* 2004; **13**(3)**:** 263-271.

263. Lazarus HM, Koc ON, Devine SM, Curtin P, Maziarz RT, Holland HK *et al.* Cotransplantation of HLA-Identical Sibling Culture-Expanded Mesenchymal Stem Cells and Hematopoietic Stem Cells in Hematologic Malignancy Patients. *Biology of blood and marrow transplantation : journal of the American Society for Blood and Marrow Transplantation* 2005; **11**(5)**:** 389-398.

264. Le Blanc K, Samuelsson H, Gustafsson B, Remberger M, Sundberg B, Arvidson J *et al.* Transplantation of mesenchymal stem cells to enhance engraftment of hematopoietic stem cells. *Leukemia* 2007; **21**(8)**:** 1733-1738.

265. Ende N, Chen R, Reddi AS. Effect of human umbilical cord blood cells on glycemia and insulitis in type 1 diabetic mice. *Biochem Biophys Res Commun* 2004; **325**(3)**:** 665-669.

266. Bassi EJ, Moraes-Vieira PM, Moreira-Sa CS, Almeida DC, Vieira LM, Cunha CS *et al.* Immune regulatory properties of allogeneic adipose-derived mesenchymal stem cells in the treatment of experimental autoimmune diabetes. *Diabetes* 2012; **61**(10)**:** 2534-2545.

267. Madec AM, Mallone R, Afonso G, Abou Mrad E, Mesnier A, Eljaafari A *et al.* Mesenchymal stem cells protect NOD mice from diabetes by inducing regulatory T cells. *Diabetologia* 2009; **52**(7)**:** 1391-1399.

268. Klinker MW, Wei C-H. Mesenchymal stem cells in the treatment of inflammatory and autoimmune diseases in experimental animal models. *World Journal of Stem Cells* 2015; **7**(3)**:** 556-567.

269. Hess D, Li L, Martin M, Sakano S, Hill D, Strutt B *et al.* Bone marrow-derived stem cells initiate pancreatic regeneration. *Nature biotechnology* 2003; **21**(7)**:** 763-770.

270. Lee RH, Seo MJ, Reger RL, Spees JL, Pulin AA, Olson SD *et al.* Multipotent stromal cells from human marrow home to and promote repair of pancreatic islets and renal glomeruli in diabetic NOD/scid mice. *Proc Natl Acad Sci U S A* 2006; **103**(46)**:** 17438-17443.

271. Urbán VS, Kiss J, Kovács J, Gócza E, Vas V, Monostori Ė *et al.* Mesenchymal Stem Cells Cooperate with Bone Marrow Cells in Therapy of Diabetes. *STEM CELLS* 2008; **26**(1)**:** 244-253.

272. Ezquer FE, Ezquer ME, Parrau DB, Carpio D, Yanez AJ, Conget PA. Systemic administration of multipotent mesenchymal stromal cells reverts hyperglycemia and prevents nephropathy in type 1 diabetic mice. *Biol Blood Marrow Transplant* 2008; **14**(6)**:** 631-640.

273. Boumaza I, Srinivasan S, Witt WT, Feghali-Bostwick C, Dai Y, Garcia-Ocana A *et al.* Autologous bone marrow-derived rat mesenchymal stem cells promote PDX-1 and insulin expression in the islets, alter T cell cytokine pattern and preserve regulatory T cells in the periphery and induce sustained normoglycemia. *Journal of autoimmunity* 2009; **32**(1)**:** 33-42.

274. Sohni A, Verfaillie CM. Mesenchymal Stem Cells Migration Homing and Tracking. *Stem Cells International* 2013; **2013**.

275. Rombouts WJC, Ploemacher RE. Primary murine MSC show highly efficient homing to the bone marrow but lose homing ability following culture. *Leukemia* 2003; **17**(1)**:** 160-170.

276. Zhao Y, Lin B, Darflinger R, Zhang Y, Holterman MJ, Skidgel RA. Human Cord Blood Stem Cell-Modulated Regulatory T Lymphocytes Reverse the Autoimmune-Caused Type 1 Diabetes in Nonobese Diabetic (NOD) Mice. *PLoS ONE* 2009; **4**(1)**:** 4226.

277. Yoshimatsu G, Sakata N, Tsuchiya H, Minowa T, Takemura T, Morita H *et al.* The Co-Transplantation of Bone Marrow Derived Mesenchymal Stem Cells Reduced Inflammation in Intramuscular Islet Transplantation. *PLoS ONE* 2015; **10**(2)**:** e0117561.

278. Rackham CL, Chagastelles PC, Nardi NB, Hauge-Evans AC, Jones PM, King AJ. Co-transplantation of mesenchymal stem cells maintains islet organisation and morphology in mice. *Diabetologia* 2011; **54**(5)**:** 1127-1135.

279. Dor Y, Brown J, Martinez OI, Melton DA. Adult pancreatic beta-cells are formed by self-duplication rather than stem-cell differentiation. *Nature* 2004; **429**(6987)**:** 41-46.

280. Teta M, Rankin MM, Long SY, Stein GM, Kushner JA. Growth and regeneration of adult beta cells does not involve specialized progenitors. *Developmental cell* 2007; **12**(5)**:** 817-826.

281. Carlsson PO, Schwarcz E, Korsgren O, Le Blanc K. Preserved beta-cell function in type 1 diabetes by mesenchymal stromal cells. *Diabetes* 2015; **64**(2)**:** 587-592.

282. Cai J, Wu Z, Xu X, Liao L, Chen J, Huang L *et al.* Umbilical Cord Mesenchymal Stromal Cell With Autologous Bone Marrow Cell Transplantation in Established Type 1 Diabetes: A Pilot Randomized Controlled Open-Label Clinical Study to Assess Safety and Impact on Insulin Secretion. *Diabetes Care* 2016; **39**(1)**:** 149-157.

283. Gimble JM, Katz AJ, Bunnell BA. Adipose-derived stem cells for regenerative medicine. *Circulation research* 2007; **100**(9)**:** 1249-1260.

284. Hu J, Yu X, Wang Z, Wang F, Wang L, Gao H *et al.* Long term effects of the implantation of Wharton's jelly-derived mesenchymal stem cells from the umbilical cord for newly-onset type 1 diabetes mellitus. *Endocrine journal* 2013; **60**(3)**:** 347-357.

285. Hasegawa Y, Ogihara T, Yamada T, Ishigaki Y, Imai J, Uno K *et al.* Bone marrow (BM) transplantation promotes beta-cell regeneration after acute injury through BM cell mobilization. *Endocrinology* 2007; **148**(5)**:** 2006-2015.

286. Milanesi A, Lee J-W, Li Z, Da Sacco S, Villani V, Cervantes V *et al.* Beta-Cell Regeneration Mediated by Human Bone Marrow Mesenchymal Stem Cells. *PLoS ONE* 2012; **7**(8)**:** e42177.

287. Zhao Y. Stem cell educator therapy and induction of immune balance. *Current diabetes reports* 2012; **12**(5)**:** 517-523.

288. Zhao Y, Jiang Z, Zhao T, Ye M, Hu C, Yin Z *et al.* Reversal of type 1 diabetes via islet beta cell regeneration following immune modulation by cord blood-derived multipotent stem cells. *BMC medicine* 2012; **10:** 3.

289. Zhao Y, Jiang Z, Zhao T, Ye M, Hu C, Zhou H *et al.* Targeting insulin resistance in type 2 diabetes via immune modulation of cord blood-derived multipotent stem cells (CB-SCs) in stem cell educator therapy: phase I/II clinical trial. *BMC medicine* 2013; **11:** 160.

290. Zhao Y, Mazzone T. Human cord blood stem cells and the journey to a cure for type 1 diabetes. *Autoimmunity Reviews* 2010; **10**(2)**:** 103-107.

291. Mesples A, Majeed N, Zhang Y, Hu X. Early immunotherapy using autologous adult stem cells reversed the effect of anti-pancreatic islets in recently diagnosed type 1 diabetes mellitus: preliminary results. *Medical science monitor : international medical journal of experimental and clinical research* 2013; **19:** 852-857.

292. Wu H, Wen D, Mahato RI. Third-party mesenchymal stem cells improved human islet transplantation in a humanized diabetic mouse model. *Molecular therapy : the journal of the American Society of Gene Therapy* 2013; **21**(9)**:** 1778-1786.

293. Scuteri A, Donzelli E, Rodriguez-Menendez V, Ravasi M, Monfrini M, Bonandrini B *et al.* A Double Mechanism for the Mesenchymal Stem Cells' Positive Effect on Pancreatic Islets. *PLoS ONE* 2014; **9**(1)**:** e84309.

294. Berman DM, Willman MA, Han D, Kleiner G, Kenyon NM, Cabrera O *et al.* Mesenchymal stem cells enhance allogeneic islet engraftment in nonhuman primates. *Diabetes* 2010; **59**(10)**:** 2558-2568.

295. Fiorina P, Jurewicz M, Augello A, Vergani A, Dada S, La Rosa S *et al.* Immunomodulatory function of bone marrow-derived mesenchymal stem cells in experimental autoimmune type 1 diabetes. *Journal of immunology (Baltimore, Md. : 1950)* 2009; **183**(2)**:** 993-1004.

296. Xie Q-P, Huang H, Xu B, Dong X, Gao S-L, Zhang B *et al.* Human bone marrow mesenchymal stem cells differentiate into insulin-producing cells upon microenvironmental manipulation in vitro. *Differentiation* 2009; **77**(5)**:** 483-491.

297. Pagliuca FW, Millman JR, Gurtler M, Segel M, Van Dervort A, Ryu JH *et al.* Generation of functional human pancreatic beta cells in vitro. *Cell* 2014; **159**(2)**:** 428-439.

298. Oh S-H, Muzzonigro TM, Bae S-H, LaPlante JM, Hatch HM, Petersen BE. Adult bone marrow-derived cells trans-differentiating into insulin-producing cells for the treatment of type I diabetes. *Laboratory Investigation* 2004; **84**(5)**:** 607-617.

299. Tang DQ, Cao LZ, Burkhardt BR, Xia CQ, Litherland SA, Atkinson MA *et al.* In vivo and in vitro characterization of insulin-producing cells obtained from murine bone marrow. *Diabetes* 2004; **53**(7)**:** 1721-1732.

300. Wu XH, Liu CP, Xu KF, Mao XD, Zhu J, Jiang JJ *et al.* Reversal of hyperglycemia in diabetic rats by portal vein transplantation of islet-like cells generated from bone marrow mesenchymal stem cells. *World J Gastroenterol* 2007; **13**(24)**:** 3342-3349.

301. Cheung AT, Dayanandan B, Lewis JT, Korbutt GS, Rajotte RV, Bryer-Ash M *et al.* Glucose-Dependent Insulin Release from Genetically Engineered K Cells. *Science* 2000; **290**(5498)**:** 1959-1962.

302. Kirk K, Hao E, Lahmy R, Itkin-Ansari P. Human embryonic stem cell derived islet progenitors mature inside an encapsulation device without evidence of increased biomass or cell escape. *Stem Cell Research* 2014; **12**(3)**:** 807-814.

303. Wang N, Adams G, Buttery L, Falcone FH, Stolnik S. Alginate encapsulation technology supports embryonic stem cells differentiation into insulin-producing cells. *Journal of Biotechnology* 2009; **144**(4)**:** 304-312.

304. Weir GC. Islet encapsulation: advances and obstacles. *Diabetologia* 2013; **56**(7)**:** 1458-1461.

305. Sun Y, Chen L, Hou XG, Hou WK, Dong JJ, Sun L *et al.* Differentiation of bone marrow-derived mesenchymal stem cells from diabetic patients into insulin-producing cells in vitro. *Chin Med J* 2007; **120**(9)**:** 771-776.

306. Abouzaripour M, Pasbakhsh P, Atlasi N, Shahverdi AH, Mahmoudi R, Kashani IR. In Vitro Differentiation of Insulin Secreting Cells from Mouse Bone Marrow Derived Stage-Specific Embryonic Antigen 1 Positive Stem Cells. *Cell Journal (Yakhteh)* 2016; **17**(4)**:** 701-710.

307. Moshtagh PR, Emami SH, Sharifi AM. Differentiation of human adipose-derived mesenchymal stem cell into insulin-producing cells: an in vitro study. *Journal of physiology and biochemistry* 2013; **69**(3)**:** 451-458.

308. Khorsandi L, Khodadadi A, Nejad-Dehbashi F, Saremy S. Three-dimensional differentiation of adipose-derived mesenchymal stem cells into insulin-producing cells. *Cell and tissue research* 2015; **361**(3)**:** 745-753.

309. Timper K, Seboek D, Eberhardt M, Linscheid P, Christ-Crain M, Keller U *et al.* Human adipose tissue-derived mesenchymal stem cells differentiate into insulin, somatostatin, and glucagon expressing cells. *Biochemical and Biophysical Research Communications* 2006; **341**(4)**:** 1135-1140.

310. Tsai P-J, Wang H-S, Shyr Y-M, Weng Z-C, Tai L-C, Shyu J-F *et al.* Transplantation of insulin-producing cells from umbilical cord mesenchymal stem cells for the treatment of streptozotocin-induced diabetic rats. *Journal of Biomedical Science* 2012; **19**(1)**:** 1-9.

311. Wang H-w, Lin L-m, He H-y, You F, Li W-z, Huang T-h *et al.* Human umbilical cord mesenchymal stem cells derived from Wharton's jelly differentiate into insulin-producing cells in vitro. *Chinese Medical Journal-Beijing* 2011; **124**(10)**:** 1534.

312. Sun B, Roh K-H, Lee S-R, Lee Y-S, Kang K-S. Induction of human umbilical cord blood-derived stem cells with embryonic stem cell phenotypes into insulin producing islet-like structure. *Biochemical and Biophysical Research Communications* 2007; **354**(4)**:** 919-923.

313. Siegel G, Kluba T, Hermanutz-Klein U, Bieback K, Northoff H, Schäfer R. Phenotype, donor age and gender affect function of human bone marrow-derived mesenchymal stromal cells. *BMC medicine* 2013; **11**(1)**:** 1-20.

314. Heathman TRJ, Rafiq QA, Chan AKC, Coopman K, Nienow AW, Kara B *et al.* Characterization of human mesenchymal stem cells from multiple donors and the implications for large scale bioprocess development. *Biochemical Engineering Journal* 2016; **108:** 14-23.

315. Gerace D, Martiniello-Wilks R, Nassif NT, Lal S, Steptoe R, Simpson AM. CRISPR-targeted genome editing of mesenchymal stem cell-derived therapies for type 1 diabetes: a path to clinical success? *Stem Cell Research & Therapy* 2017; **8**(1)**:** 62.

316. Siddappa R, Licht R, van Blitterswijk C, de Boer J. Donor variation and loss of multipotency during in vitro expansion of human mesenchymal stem cells for bone tissue engineering. *Journal of orthopaedic research : official publication of the Orthopaedic Research Society* 2007; **25**(8)**:** 1029-1041.

317. Alvarez-Viejo M, Menendez-Menendez Y, Blanco-Gelaz MA, Ferrero-Gutierrez A, Fernandez-Rodriguez MA, Gala J *et al.* Quantifying mesenchymal stem cells in the mononuclear cell fraction of bone marrow samples obtained for cell therapy. *Transplant Proc* 2013; **45**(1)**:** 434-439.

318. Baer PC, Geiger H. Adipose-Derived Mesenchymal Stromal/Stem Cells: Tissue Localization, Characterization, and Heterogeneity. *Stem Cells International* 2012; **2012:** 11.

319. François M, Copland IB, Yuan S, Romieu-Mourez R, Waller EK, Galipeau J. Cryopreserved mesenchymal stromal cells display impaired immunosuppressive properties as a result of heat-shock response and impaired interferon-γ licensing. *Cytotherapy* 2012; **14**(2)**:** 147-152.

320. Francois M, Romieu-Mourez R, Li M, Galipeau J. Human MSC suppression correlates with cytokine induction of indoleamine 2,3-dioxygenase and bystander M2 macrophage differentiation. *Molecular therapy : the journal of the American Society of Gene Therapy* 2012; **20**.

321. Moll G, Alm JJ, Davies LC, von Bahr L, Heldring N, Stenbeck-Funke L *et al.* Do Cryopreserved Mesenchymal Stromal Cells Display Impaired Immunomodulatory and Therapeutic Properties? *STEM CELLS* 2014; **32**(9)**:** 2430-2442.

322. Khatri A, Husaini Y, Ow K, Chapman J, Russell PJ. Cytosine deaminase-uracil phosphoribosyltransferase and interleukin (IL)-12 and IL-18: a multimodal anticancer interface marked by specific modulation in serum cytokines. *Clinical cancer research : an official journal of the American Association for Cancer Research* 2009; **15**(7)**:** 2323-2334.

323. Van Vlasselaer P, Falla N, Snoeck H, Mathieu E. Characterization and purification of osteogenic cells from murine bone marrow by two-color cell sorting using anti-Sca-1 monoclonal antibody and wheat germ agglutinin. *Blood* 1994; **84**(3)**:** 753-763.

324. Eslaminejad MB, Nadri S. Murine mesenchymal stem cell isolated and expanded in low and high density culture system: Surface antigen expression and osteogenic culture mineralization. *In Vitro Cellular and Developmental Biology - Animal* 2009; **45**(8)**:** 451-459.

325. Baddoo M, Hill K, Wilkinson R, Gaupp D, Hughes C, Kopen GC *et al.* Characterization of mesenchymal stem cells isolated from murine bone marrow by negative selection. *Journal of Cellular Biochemistry* 2003; **89**(6)**:** 1235-1249.

326. Soleimani M, Nadri S. A protocol for isolation and culture of mesenchymal stem cells from mouse bone marrow. *Nature Protocols* 2009; **4**(1)**:** 102-106.

327. Siclari VA, Zhu J, Akiyama K, Liu F, Zhang X, Chandra A *et al.* Mesenchymal progenitors residing close to the bone surface are functionally distinct from those in the central bone marrow. *Bone* 2013; **53**(2)**:** 575-586.

328. Council NHaMR. Australian code for the care and use of animals for scientific purposes. In. 8th Edition ed: Canbera: National Health and Medical Research Council, 2013.

329. Rostovskaya M, Anastassiadis K. Differential Expression of Surface Markers in Mouse Bone Marrow Mesenchymal Stromal Cell Subpopulations with Distinct Lineage Commitment. *PLOS ONE* 2012; **7**(12)**:** e51221.

330. Baustian C, Hanley S, Ceredig R. Isolation, selection and culture methods to enhance clonogenicity of mouse bone marrow derived mesenchymal stromal cell precursors. *Stem Cell Research & Therapy* 2015; **6**(1)**:** 151.

331. Lee T-C, Lee T-H, Huang Y-H, Chang N-K, Lin Y-J, Chien P-WC *et al.* Comparison of Surface Markers between Human and Rabbit Mesenchymal Stem Cells. *PLoS ONE* 2014; **9**(11)**:** e111390.

332. Hass R, Kasper C, Böhm S, Jacobs R. Different populations and sources of human mesenchymal stem cells (MSC): A comparison of adult and neonatal tissue-derived MSC. *Cell Communication and Signaling* 2011; **9**(1)**:** 12.

333. Boxall SA, Jones E. Markers for Characterization of Bone Marrow Multipotential Stromal Cells. *Stem Cells International* 2012; **2012:** 12.

334. Bonab MM, Alimoghaddam K, Talebian F, Ghaffari SH, Ghavamzadeh A, Nikbin B. Aging of mesenchymal stem cell in vitro. *BMC Cell Biology* 2006; **7**(1)**:** 14.

335. Peffers MJ, Collins J, Fang Y, Goljanek-Whysall K, Rushton M, Loughlin J *et al.* Age-related changes in mesenchymal stem cells identified using a multi-omics approach. *Eur Cell Mater* 2016; **31:** 136-159.

336. Stolzing A, Jones E, McGonagle D, Scutt A. Age-related changes in human bone marrow-derived mesenchymal stem cells: consequences for cell therapies. *Mechanisms of ageing and development* 2008; **129**(3)**:** 163-173.

337. Lee MW, Kim DS, Ryu S, Jang IK, Kim HJ, Yang JM *et al.* Effect of Ex Vivo Culture Conditions on Immunosuppression by Human Mesenchymal Stem Cells. *BioMed Research International* 2013; **2013:** 10.

338. Kim J-H, Lee H-S, Choi H-K, Kim J-A, Chu I-S, Leem S-H *et al.* Heterogeneous Niche Activity of Ex-Vivo Expanded MSCs as Factor for Variable Outcomes in Hematopoietic Recovery. *PLOS ONE* 2016; **11**(12)**:** e0168036.

339. Churchman SM, Boxall SA, McGonagle D, Jones EA. Predicting the Remaining Lifespan and Cultivation-Related Loss of Osteogenic Capacity of Bone Marrow Multipotential Stromal Cells Applicable across a Broad Donor Age Range. *Stem Cells International* 2017; **2017:** 10.

340. Turinetto V, Vitale E, Giachino C. Senescence in Human Mesenchymal Stem Cells: Functional Changes and Implications in Stem Cell-Based Therapy. *International Journal of Molecular Sciences* 2016; **17**(7)**:** 1164.

341. Nawrocka D, Kornicka K, Szydlarska J, Marycz K. Basic Fibroblast Growth Factor Inhibits Apoptosis and Promotes Proliferation of Adipose-Derived Mesenchymal Stromal Cells Isolated from Patients with Type 2 Diabetes by Reducing Cellular Oxidative Stress. *Oxidative Medicine and Cellular Longevity* 2017; **2017:** 22.

342. Yu JM, Wu X, Gimble JM, Guan X, Freitas MA, Bunnell BA. Age-related changes in mesenchymal stem cells derived from rhesus macaque bone marrow. *Aging cell* 2011; **10**(1)**:** 66-79.

343. Marędziak M, Marycz K, Tomaszewski KA, Kornicka K, Henry BM. The Influence of Aging on the Regenerative Potential of Human Adipose Derived Mesenchymal Stem Cells. *Stem Cells International* 2016; **2016:** 2152435.

344. Kretlow JD, Jin Y-Q, Liu W, Zhang WJ, Hong T-H, Zhou G *et al.* Donor age and cell passage affects differentiation potential of murine bone marrow-derived stem cells. *BMC Cell Biology* 2008; **9**(1)**:** 60. doi: 10.1186/1471-2121-9-60

345. Pons J, Huang Y, Arakawa-Hoyt J, Washko D, Takagawa J, Ye J *et al.* VEGF improves survival of mesenchymal stem cells in infarcted hearts. *Biochem Biophys Res Commun* 2008; **376**(2)**:** 419-422.

346. Tokunaga A, Oya T, Ishii Y, Motomura H, Nakamura C, Ishizawa S *et al.* PDGF receptor beta is a potent regulator of mesenchymal stromal cell function. *Journal of bone and mineral research : the official journal of the American Society for Bone and Mineral Research* 2008; **23**(9)**:** 1519-1528.

347. Tamama K, Fan VH, Griffith LG, Blair HC, Wells A. Epidermal growth factor as a candidate for ex vivo expansion of bone marrow-derived mesenchymal stem cells. *Stem Cells* 2006; **24**(3)**:** 686-695.

348. Lee S, Jeong S, Lee C, Oh J, Kim S-C. Mesenchymal Stem Cells Derived from Human Exocrine Pancreas Spontaneously Express Pancreas Progenitor-Cell Markers in a Cell-Passage-Dependent Manner. *Stem Cells International* 2016; **2016:** 2142646.

349. Baertschiger RM, Bosco D, Morel P, Serre-Beinier V, Berney T, Buhler LH *et al.* Mesenchymal stem cells derived from human exocrine pancreas express transcription factors implicated in beta-cell development. *Pancreas* 2008; **37**(1)**:** 75-84.

350. Bianco P, Cao X, Frenette PS, Mao JJ, Robey PG, Simmons PJ *et al.* The meaning, the sense and the significance: translating the science of mesenchymal stem cells into medicine. *Nat Med* 2013; **19**(1)**:** 35-42.

351. Eggenhofer E, Luk F, Dahlke MH, Hoogduijn MJ. The Life and Fate of Mesenchymal Stem Cells. *Frontiers in Immunology* 2014; **5:** 148.

352. Fischer UM, Harting MT, Jimenez F, Monzon-Posadas WO, Xue H, Savitz SI *et al.* Pulmonary passage is a major obstacle for intravenous stem cell delivery: the pulmonary first-pass effect. *Stem Cells Dev* 2009; **18**(5)**:** 683-692.

353. Karimi MA, Lee E, Bachmann MH, Salicioni AM, Behrens EM, Kambayashi T *et al.* Measuring Cytotoxicity by Bioluminescence Imaging Outperforms the Standard Chromium-51 Release Assay. *PLOS ONE* 2014; **9**(2)**:** e89357.

354. Aluigi M, Fogli M, Curti A, Isidori A, Gruppioni E, Chiodoni C *et al.* Nucleofection is an efficient nonviral transfection technique for human bone marrow-derived mesenchymal stem cells. *Stem Cells* 2006; **24**(2)**:** 454-461.

355. Haleem-Smith H, Derfoul A, Okafor C, Tuli R, Olsen D, Hall DJ *et al.* Optimization of high-efficiency transfection of adult human mesenchymal stem cells in vitro. *Molecular biotechnology* 2005; **30**(1)**:** 9-20.

356. Halim NSSA, Fakiruddin KS, Ali SA, Yahaya BH. A Comparative Study of Non-Viral Gene Delivery Techniques to Human Adipose-Derived Mesenchymal Stem Cell. *International Journal of Molecular Sciences* 2014; **15**(9)**:** 15044-15060.

357. Nakashima S, Matsuyama Y, Nitta A, Sakai Y, Ishiguro N. Highly efficient transfection of human marrow stromal cells by nucleofection. *Transplant Proc* 2005; **37**(5)**:** 2290-2302.

358. Kay MA, Glorioso JC, Naldini L. Viral vectors for gene therapy: the art of turning infectious agents into vehicles of therapeutics. *Nat Med* 2001; **7**(1)**:** 33-40.

359. Kobinger GP, Weiner DJ, Yu Q-C, Wilson JM. Filovirus-pseudotyped lentiviral vector can efficiently and stably transduce airway epithelia in vivo. *Nat Biotech* 2001; **19**(3)**:** 225-230.

360. Escors D, Breckpot K. Lentiviral Vectors in Gene Therapy: Their Current Status and Future Potential. *Archivum Immunologiae et Therapiae Experimentalis* 2010; **58**(2)**:** 107-119.

361. Xing L, Deng X, Kotedia K, Ackerstaff E, Ponomarev V, Ling CC *et al.* Non-invasive molecular and functional imaging of cytosine deaminase and uracil phosphoribosyltransferase fused with red fluorescence protein. *Acta oncologica (Stockholm, Sweden)* 2008; **47**(7)**:** 1211-1220.

362. Koyama F, Sawada H, Hirao T, Fujii H, Hamada H, Nakano H. Combined suicide gene therapy for human colon cancer cells using adenovirus-mediated transfer of escherichia coli cytosine deaminase gene and Escherichia coli uracil phosphoribosyltransferase gene with 5-fluorocytosine. *Cancer gene therapy* 2000; **7**(7)**:** 1015-1022.

363. Longley DB, Harkin DP, Johnston PG. 5-Fluorouracil: mechanisms of action and clinical strategies. *Nat Rev Cancer* 2003; **3**(5)**:** 330-338.

364. Polak A, Eschenhof E, Fernex M, Scholer HJ. Metabolic Studies with 5-Fluorocytosine-C in Mouse, Rat, Rabbit, Dog and Man. *Chemotherapy* 1976; **22**(3-4)**:** 137-153.

365. Harrell RL, Rajanayagam S, Doanes AM, Guzman RJ, Hirschowitz EA, Crystal RG *et al.* Inhibition of vascular smooth muscle cell proliferation and neointimal accumulation by adenovirus-mediated gene transfer of cytosine deaminase. *Circulation* 1997; **96**(2)**:** 621-627.

366. Strohschein K, Radojewski P, Winkler T, Duda GN, Perka C, von Roth P. In Vivo Bioluminescence Imaging – A Suitable Method to Track Mesenchymal Stromal Cells in a Skeletal Muscle Trauma. *The Open Orthopaedics Journal* 2015; **9:** 262-269.

367. Geuze RE, Prins HJ, Oner FC, van der Helm YJ, Schuijff LS, Martens AC *et al.* Luciferase labeling for multipotent stromal cell tracking in spinal fusion versus ectopic bone tissue engineering in mice and rats. *Tissue engineering. Part A* 2010; **16**(11)**:** 3343-3351.

368. Bai ZM, Deng XD, Li JD, Li DH, Cao H, Liu ZX *et al.* Arterially transplanted mesenchymal stem cells in a mouse reversible unilateral ureteral obstruction model: in vivo bioluminescence imaging and effects on renal fibrosis. *Chinese medical journal* 2013; **126**(10)**:** 1890-1894.

369. Ankrum JA, Ong JF, Karp JM. Mesenchymal stem cells: immune evasive, not immune privileged. *Nature biotechnology* 2014; **32**(3)**:** 252-260.

370. Podetz-Pedersen KM, Vezys V, Somia NV, Russell SJ, McIvor RS. Cellular immune response against firefly luciferase after sleeping beauty-mediated gene transfer in vivo. *Human gene therapy* 2014; **25**(11)**:** 955-965.

371. Yin Y, Takahashi Y, Hamana A, Nishikawa M, Takakura Y. Effects of transgene expression level per cell in mice livers on induction of transgene-specific immune responses after hydrodynamic gene transfer. *Gene Ther* 2016; **23**(7)**:** 565-571.

372. Spees JL, Gregory CA, Singh H, Tucker HA, Peister A, Lynch PJ *et al.* Internalized antigens must be removed to prepare hypoimmunogenic mesenchymal stem cells for cell and gene therapy. *Molecular therapy : the journal of the American Society of Gene Therapy* 2004; **9**(5)**:** 747-756.

373. Rosova I, Dao M, Capoccia B, Link D, Nolta JA. Hypoxic preconditioning results in increased motility and improved therapeutic potential of human mesenchymal stem cells. *Stem Cells* 2008; **26**(8)**:** 2173-2182.

374. Meyerrose TE, De Ugarte DA, Hofling AA, Herrbrich PE, Cordonnier TD, Shultz LD *et al.* In vivo distribution of human adipose-derived mesenchymal stem cells in novel xenotransplantation models. *Stem Cells* 2007; **25**(1)**:** 220-227.

375. Meyerrose TE, Roberts M, Ohlemiller KK, Vogler CA, Wirthlin L, Nolta JA *et al.* Lentiviral-transduced human mesenchymal stem cells persistently express therapeutic levels of enzyme in a xenotransplantation model of human disease. *Stem Cells* 2008; **26**(7)**:** 1713-1722.

376. Kim I, Bang SI, Lee SK, Park SY, Kim M, Ha H. Clinical Implication of Allogenic Implantation of Adipogenic Differentiated Adipose-Derived Stem Cells. *Stem Cells Translational Medicine* 2014; **3**(11)**:** 1312-1321.

377. Hare JM, Fishman JE, Gerstenblith G, DiFede Velazquez DL, Zambrano JP, Suncion VY *et al.* Comparison of allogeneic vs autologous bone marrow-derived mesenchymal stem cells delivered by transendocardial injection in patients with ischemic cardiomyopathy: the POSEIDON randomized trial. *Jama* 2012; **308**(22)**:** 2369-2379.

378. Makela T, Takalo R, Arvola O, Haapanen H, Yannopoulos F, Blanco R *et al.* Safety and biodistribution study of bone marrow-derived mesenchymal stromal cells and mononuclear cells and the impact of the administration route in an intact porcine model. *Cytotherapy* 2015; **17**(4)**:** 392-402.

379. Nystedt J, Anderson H, Tikkanen J, Pietila M, Hirvonen T, Takalo R *et al.* Cell surface structures influence lung clearance rate of systemically infused mesenchymal stromal cells. *Stem Cells* 2013; **31**(2)**:** 317-326.

380. Choi EW, Shin IS, Park SY, Yoon EJ, Kang SK, Ra JC *et al.* Characteristics of mouse adipose tissue-derived stem cells and therapeutic comparisons between syngeneic and allogeneic adipose tissue-derived stem cell transplantation in experimental autoimmune thyroiditis. *Cell Transplant* 2014; **23**(7)**:** 873-887.

381. Liang J, Li X, Zhang H, Wang D, Feng X, Wang H *et al.* Allogeneic mesenchymal stem cells transplantation in patients with refractory RA. *Clinical rheumatology* 2012; **31**(1)**:** 157-161.

382. Hardikar AA, Marcus-Samuels B, Geras-Raaka E, Raaka BM, Gershengorn MC. Human pancreatic precursor cells secrete FGF2 to stimulate clustering into hormone-expressing islet-like cell aggregates. *Proc Natl Acad Sci U S A* 2003; **100**(12)**:** 7117-7122.

383. Dodson BP, Levine AD. Challenges in the translation and commercialization of cell therapies. *BMC Biotechnology* 2015; **15**(1)**:** 70.

384. Heathman TRJ, Nienow AW, McCall MJ, Coopman K, Kara B, Hewitt CJ. The translation of cell-based therapies: clinical landscape and manufacturing challenges. *Regenerative Medicine* 2015; **10**(1)**:** 49-64.

385. Li VC, Kirschner MW. Molecular ties between the cell cycle and differentiation in embryonic stem cells. *Proceedings of the National Academy of Sciences of the United States of America* 2014; **111**(26)**:** 9503-9508.

386. Lin P, Lin Y, Lennon DP, Correa D, Schluchter M, Caplan AI. Efficient Lentiviral Transduction of Human Mesenchymal Stem Cells That Preserves Proliferation and Differentiation Capabilities. *Stem Cells Translational Medicine* 2012; **1**(12)**:** 886-897.

387. Zhang X-Y, La Russa VF, Reiser J. Transduction of Bone-Marrow-Derived Mesenchymal Stem Cells by Using Lentivirus Vectors Pseudotyped with Modified RD114 Envelope Glycoproteins. *Journal of Virology* 2004; **78**(3)**:** 1219-1229.

388. Ricks DM, Kutner R, Zhang X-Y, Welsh DA, Reiser J. Optimized Lentiviral Transduction of Mouse Bone Marrow-Derived Mesenchymal Stem Cells. *Stem Cells and Development* 2008; **17**(3)**:** 441-450.

389. O'Han M, Meyers G, Rasko J, Martiniello-Wilks R. Nucleofection is an efficient method for the genetic modification of murine mesenchymal stem cells. *Journal of Gene Medicine* 2009; **11**(9)**:** 848.

390. McMahon JM, Conroy S, Lyons M, Greiser U, O'Shea C, Strappe P *et al.* Gene transfer into rat mesenchymal stem cells: a comparative study of viral and nonviral vectors. *Stem Cells Dev* 2006; **15**(1)**:** 87-96.

391. Yuan H, Li J, Xin N, Zhao Z, Qin G. Expression of Pdx1 mediates differentiation from mesenchymal stem cells into insulin-producing cells. *Molecular Biology Reports* 2010; **37**(8)**:** 4023-4031.

392. Pataskar A, Jung J, Smialowski P, Noack F, Calegari F, Straub T *et al.* NeuroD1 reprograms chromatin and transcription factor landscapes to induce the neuronal program. *The EMBO Journal* 2016; **35**(1)**:** 24-45.

393. Qing-Song G, Ming-Yan Z, Lei W, Xiang-Jun F, Yu-Hua L, Zhi-Wei W *et al.* Combined Transfection of the Three Transcriptional Factors, PDX-1, NeuroD1, and MafA, Causes Differentiation of Bone Marrow Mesenchymal Stem Cells into Insulin-Producing Cells. *Experimental Diabetes Research* 2012; **2012:** 10.

394. Srinivasan P, Huang GC, Amiel SA, Heaton ND. Islet cell transplantation. *Postgraduate Medical Journal* 2007; **83**(978)**:** 224-229.

395. D'Amour KA, Bang AG, Eliazer S, Kelly OG, Agulnick AD, Smart NG *et al.* Production of pancreatic hormone-expressing endocrine cells from human embryonic stem cells. *Nature biotechnology* 2006; **24**(11)**:** 1392-1401.

396. Gruenloh W, Kambal A, Sondergaard C, McGee J, Nacey C, Kalomoiris S *et al.* Characterization and In Vivo Testing of Mesenchymal Stem Cells Derived from Human Embryonic Stem Cells. *Tissue Engineering. Part A* 2011; **17**(11-12)**:** 1517-1525.

397. Karussis D, Karageorgiou C, Vaknin-Dembinsky A, et al. Safety and immunological effects of mesenchymal stem cell transplantation in patients with multiple sclerosis and amyotrophic lateral sclerosis. *Archives of Neurology* 2010; **67**(10)**:** 1187-1194.

398. Freitag J, Bates D, Boyd R, Shah K, Barnard A, Huguenin L *et al.* Mesenchymal stem cell therapy in the treatment of osteoarthritis: reparative pathways, safety and efficacy – a review. *BMC Musculoskeletal Disorders* 2016; **17:** 230.

399. Aguilar S, Nye E, Chan J, Loebinger M, Spencer-Dene B, Fisk N *et al.* Murine but Not Human Mesenchymal Stem Cells Generate Osteosarcoma-Like Lesions in the Lung. *STEM CELLS* 2007; **25**(6)**:** 1586-1594.

400. Miura M, Miura Y, Padilla-Nash HM, Molinolo AA, Fu B, Patel V *et al.* Accumulated chromosomal instability in murine bone marrow mesenchymal stem cells leads to malignant transformation. *Stem Cells* 2006; **24**(4)**:** 1095-1103.

401. Tolar J, Nauta AJ, Osborn MJ, Panoskaltsis Mortari A, McElmurry RT, Bell S *et al.* Sarcoma derived from cultured mesenchymal stem cells. *Stem Cells* 2007; **25**(2)**:** 371-379.

402. Friedenstein AJ, Latzinik NV, Gorskaya Yu F, Luria EA, Moskvina IL. Bone marrow stromal colony formation requires stimulation by haemopoietic cells. *Bone and mineral* 1992; **18**(3)**:** 199-213.

403. Kuznetsov SA, Friedenstein AJ, Robey PG. Factors required for bone marrow stromal fibroblast colony formation in vitro. *Br J Haematol* 1997; **97**(3)**:** 561-570.

404. De Schauwer C, Goossens K, Piepers S, Hoogewijs MK, Govaere JLJ, Smits K *et al.* Characterization and profiling of immunomodulatory genes of equine mesenchymal stromal cells from non-invasive sources. *Stem Cell Research & Therapy* 2014; **5**(1).

405. Phinney DG, Kopen G, Isaacson RL, Prockop DJ. Plastic adherent stromal cells from the bone marrow of commonly used strains of inbred mice: variations in yield, growth, and differentiation. *J Cell Biochem* 1999; **72**(4)**:** 570-585.

406. Peister A, Mellad JA, Larson BL, Hall BM, Gibson LF, Prockop DJ. Adult stem cells from bone marrow (MSCs) isolated from different strains of inbred mice vary in surface epitopes, rates of proliferation, and differentiation potential. *Blood* 2004; **103**(5)**:** 1662-1668.

407. Hsu PD, Lander ES, Zhang F. Development and applications of CRISPR-Cas9 for genome engineering. *Cell* 2014; **157**(6)**:** 1262-1278.

408. Kabadi AM, Gersbach CA. Engineering synthetic TALE and CRISPR/Cas9 transcription factors for regulating gene expression. *Methods (San Diego, Calif.)* 2014; **69**(2)**:** 188-197.

409. Kabadi AM, Ousterout DG, Hilton IB, Gersbach CA. Multiplex CRISPR/Cas9-based genome engineering from a single lentiviral vector. *Nucleic Acids Research* 2014; **42**(19)**:** e147-e147.

410. Konermann S, Brigham MD, Trevino AE, Joung J, Abudayyeh OO, Barcena C *et al.* Genome-scale transcriptional activation by an engineered CRISPR-Cas9 complex. *Nature* 2015; **517**(7536)**:** 583-588.

411. Wei S, Zou Q, Lai S, Zhang Q, Li L, Yan Q *et al.* Conversion of embryonic stem cells into extraembryonic lineages by CRISPR-mediated activators. *Scientific reports* 2016; **6:** 19648.

412. Black Joshua B, Adler Andrew F, Wang H-G, D'Ippolito Anthony M, Hutchinson Hunter A, Reddy Timothy E *et al.* Targeted Epigenetic Remodeling of Endogenous Loci by CRISPR/Cas9-Based Transcriptional Activators Directly Converts Fibroblasts to Neuronal Cells. *Cell Stem Cell* 2016; **19**(3)**:** 406-414.

413. Jusiak B, Cleto S, Perez-Pinera P, Lu TK. Engineering Synthetic Gene Circuits in Living Cells with CRISPR Technology. *Trends Biotechnol* 2016; **34**(7)**:** 535-547.

414. Gimenez CA, Ielpi M, Mutto A, Grosembacher L, Argibay P, Pereyra-Bonnet F. CRISPR-on system for the activation of the endogenous human INS gene. *Gene Ther* 2016; **23**(6)**:** 543-547.

415. Gong M, Bi Y, Jiang W, Zhang Y, Chen L, Hou N *et al.* Immortalized mesenchymal stem cells: an alternative to primary mesenchymal stem cells in neuronal differentiation and neuroregeneration associated studies. *Journal of Biomedical Science* 2011; **18**(1)**:** 87.

416. Bourgine P, Le Magnen C, Pigeot S, Geurts J, Scherberich A, Martin I. Combination of immortalization and inducible death strategies to generate a human mesenchymal stromal cell line with controlled survival. *Stem Cell Research* 2014; **12**(2)**:** 584-598.

417. Santos FD, Andrade PZ, da Silva CL, Cabral JMS. Scaling-up Ex Vivo Expansion of Mesenchymal Stem/Stromal Cells for Cellular Therapies. In: Chase LG, Vemuri MC (eds). *Mesenchymal Stem Cell Therapy*. Humana Press: Totowa, NJ, 2013, pp 1-14.

418. Panchalingam KM, Jung S, Rosenberg L, Behie LA. Bioprocessing strategies for the large-scale production of human mesenchymal stem cells: a review. *Stem Cell Research & Therapy* 2015; **6**(1)**:** 225.